Optimisation of 405 nm HINS-light Technology for the Development of Patient-Safe Decontamination in Arthroplasty Surgery

Praveen Ramakrishnan

In partial fulfilment of the requirements
for the degree of Doctor of Engineering

2015

University of Strathclyde
Biomedical Engineering:
Doctoral Training Centre in Medical Devices
and
Department of Electronic and Electrical Engineering
The Robertson Trust Laboratory for Electronic Sterilisation Technologies

DECLARATION OF AUTHORS RIGHTS

This thesis is the result of the author's original research. It has been composed by the author and has not been previously submitted for examination which has led to the award of a degree.

Signed:

Date:

ACKNOWLEDGEMENTS

I would like to thank my supervisors Professor M. Helen Grant, Dr. Michelle Maclean and Professor Scott J. MacGregor for their continuous guidance, support and encouragement throughout the course of this study.

I would like to extend my thanks to Professor John G. Anderson for his invaluable input and advice provided throughout the research.

Thanks are also due to Mrs. Catherine Henderson for limitless and patient advice in the cell lab. I would like to express my gratitude to Dr. Catherine Lawrence, Mrs. Olga Maria Posada Estefan and Mrs. Carlota Cunha Matos for their valuable help with the FACS.

I am grateful to Dr. Dominic Meek and Dr. Jon Clarke for helping us out in collecting hospital data from Southern General hospital and Golden Jubilee Hospital.

It would have been impossible to complete this thesis without the encouragement and support from family, friends and fellow colleagues from our department, for which I am eternally grateful.

This research has been funded by the Engineering and Physical Sciences Research Council.

ABSTRACT

Healthcare associated infections (HAI) pose a major threat to patients admitted to hospitals and infection rates following orthopaedic arthroplasty surgery are as high as 4%, while the infection rates are even higher after revision surgery. 405 nm high-intensity narrow spectrum (HINS) light has been proven to reduce environmental contamination in hospital isolation rooms, and there is potential to develop this technology for application in orthopaedic surgery.

Cultured rat osteoblasts were exposed to 405 nm light to investigate if bactericidal doses of the light could be used safely in the presence of mammalian cells. Cell viability was measured by MTT reduction and microscopy techniques, function by alkaline phosphatase activity, and proliferation by the BrdU assay. 405 nm light exposures of up to a dose of 36 J/cm^2 had no significant effect on osteoblast cell viability while exposure of a variety of clinically related bacteria, to 36 J/cm^2 resulted in up to 100% kill. High irradiance 405 nm light exposures (54 J/cm^2) significantly affected the osteoblast cell viability indicating dose dependency.

405 nm light exposure involved reactive oxygen species (ROS) production in both mammalian and bacterial cells, as shown by fluorescence generated from 6-carboxy-2',7'-dichlorodihydrofluorescein diacetate dye. Light treated osteoblast cells showed a decrease in intracellular reduced glutathione content and a corresponding increase in the efflux of oxidised glutathione, both indicating oxidative damage. The mammalian cells were significantly protected from dying at 54 J/cm^2 by catalase, which detoxifies H_2O_2. Bacterial cells were significantly protected by sodium

pyruvate (H_2O_2 scavenger) and by a combination of free radical scavengers (sodium pyruvate, dimethyl thiourea (·OH scavenger), catalase) at 162 and 324 J/cm^2. Thus the cytotoxic mechanism of 405 nm light in mammalian cells and bacteria could be oxidative stress involving predominantly H_2O_2 generation, with other ROS contributing to the damage.

The cell viability and cytotoxicity results suggest that 405 nm light could be used for continual patient safe decontamination during orthopaedic replacement surgeries and further development of this light technology is encouraged.

TABLE OF CONTENTS

CHAPTER 1

INTRODUCTION 1

1.1 Healthcare associated infections 1

1.1.1 Incidence of HAI in the UK 2

1.1.2 Risk factors contributing to HAI and its impact 4

1.1.3 Morbidity, Mortality, length and cost of stay of patients in hospitals due to HAI 7

1.2 Types of HAI and causative micro-organisms 10

1.3 Incidence of infections in orthopaedics i.e: joint replacement surgery 16

1.4 Causes of HAI 18

1.4.1 Environmental survival of bacteria resulting in infections 21

1.5 Airborne transmission and preventive measures taken to maintain sterility in an operating theatre 24

1.5.1 Methods of fighting and preventing implant associated infections using silver coated implants and hydrogels 28

1.5.2 Bacterial inactivation using Ultraviolet (UV) light 30

1.6 Bacterial inactivation using visible light 31

1.6.1 Electromagnetic spectrum of light 32

1.6.2 Porphyrins 35

1.6.3 Photodynamic Inactivation 39

1.6.4 Bacterial cell inactivation by stimulation of exogenous/ endogenous porphyrins using blue light 43

1.6.5 Mammalian cell susceptibility to blue light 48

1.7 Environmental Decontamination system (EDS) using 405 nm High Intensity Narrow Spectrum (HINS) violet-blue light for bacterial inactivation 50

1.8 Summary 51

1.9 Research objectives 52

CHAPTER 2

MATERIALS AND METHODS 54

2.1 405 nm HINS light system 54

2.1.1 405 nm light system set-up 54

2.1.2 Irradiance distribution across culture plates 56

2.1.3 Irradiance/Exposure regimes – Calculation of light dose 60

2.2 Mammalian cell studies 60

2.2.1 Preparation of standard stock solutions 60

2.2.2 Cell line culture 61

2.2.2.1 Mammalian cell passage and 2-D cell culture 61

2.2.2.2 Cell counting and 405 nm light exposure 62

2.3 Bacterial cell studies 64

2.3.1 Preparation of standard growth media and diluents 64

2.3.2 Bacterial strains used 65

2.3.3 Bacterial cell culture 66

2.3.4 Preparation of bacteria for exposure to 405 nm light 66

2.3.5 Enumeration of viable bacteria 68

CHAPTER 3

DIFFERENTIAL SENSITIVITY OF OSTEOBLASTS AND BACTERIAL PATHOGENS TO 405-NM LIGHT HIGHLIGHTING POTENTIAL FOR DECONTAMINATION APPLICATIONS IN ORTHOPAEDIC SURGERY 70

3.1 Introduction 70

3.1.1 Detection of apoptosis *in-vitro* 74

3.2 Methods and Materials 85

3.2.1 Effect of different doses of 405 nm light on mammalian cells 85

3.2.1.1 Measurement of cell viability after exposure to 405 nm light 85

3.2.1.1.1 Crystal Violet assay 86

3.2.1.1.2 Lowry assay 86
3.2.1.2 Survivability of mammalian cells for extended periods of time in buffer 88
3.2.1.3 405 nm light-dose dependent study 89
3.2.1.4 Establishing a damage threshold for exposing cells to 405 nm light 90
3.2.1.4.1 MTT assay 91
3.2.1.4.2 Alkaline Phosphatase assay 91
3.2.1.4.3 BrdU assay 92
3.2.1.4.4 Qualitative analysis 93
3.2.1.5 Detection of apoptosis in-vitro 95
3.2.1.5.1 Western blotting 95
3.2.1.5.2 Flow cytometry by Fluorescence-Activated Cell Sorting (FACS) 100
3.2.2. Effects of different doses of 405 nm light on a range of bacteria 101
3.2.3 Statistical analysis 102
3.3 Results 103
3.3.1 Measurement of mammalian cell viability after exposure to 405 nm light 103
3.3.2 Survivability of mammalian cells for extended periods of time in buffer 105
3.3.3 Study of the dose dependent effects of 405 nm light 107
3.3.4 MTT, ALP and BrdU assay 109
3.3.5 Live/Dead cell staining of cells after exposure to 405 nm light 111
3.3.6 Phalloidin/DAPI staining 113
3.3.7 Western blotting (PARP analysis) 115
3.3.8 Flow cytometry 116
3.3.9 Effects of different doses of 405 nm light on a range of bacteria 119

3.4 Discussion 121

CHAPTER 4

CYTOTOXIC RESPONSES TO 405 NM LIGHT EXPOSURE IN MAMMALIAN AND BACTERIAL CELLS: INVOLVEMENT OF REACTIVE OXYGEN SPECIES 128

4.1 Introduction 128

4.2 Materials and Methods 134

4.2.1 Culture and 405 nm light exposure of mammalian cells 134

4.2.1.1 ROS detection and measurement in mammalian cells 135

4.2.1.2 Extracellular oxidised glutathione (GSSG) and intracellular reduced glutathione (GSH) measurement 136

4.2.1.3 Measurement of mammalian cell viability in the presence and absence of scavengers 138

4.2.2 Culture and 405 nm light treatment of bacterial cells 139

4.2.2.1 ROS detection and measurement in bacterial cells 140

4.2.2.2 Measurement of bacterial cell viability in the presence and absence of ROS scavengers 140

4.2.2.3 Detection and measurement of bacterial ROS in the presence of scavengers 141

4.2.3 Statistical analysis 142

4.3 Results 143

4.3.1 ROS detection in mammalian cells using carboxy-H_2DCFDA 143

4.3.2 Measurement of GSH/GSSG content in mammalian cells 146

4.3.3 Mammalian cell viability in the presence and absence of ROS scavengers 148

4.3.4 ROS detection in bacterial cells using carboxy-H_2DCFDA 152

4.3.5 Bacterial cell viability in the presence and absence of ROS scavengers 155

4.3.6 ROS detection and measurement in bacterial cells in the presence of scavengers using carboxy-H_2DCFDA 157
4.4 Discussion 160
CHAPTER 5
ASSESSMENT OF LIGHT SPECTRA OBTAINED FROM SURGICAL LIGHTS USED IN OPERATING THEATRES IN HOSPITALS AND OPTICAL ANALYSIS OF 405 NM LED ARRAYS 167
5.1 Introduction 167
5.2 Existing OT light spectrum measurement in hospitals 170
5.2.1 Southern General Hospital (SGH) 170
5.2.2 Golden Jubilee National Hospital (GJNH) 180
5.3 Optical Analysis of 405 nm LED sources 189
5.3.1 99-DIE LED array 189
5.3.2 High Power 405 nm LED array 193
5.3.3 405 nm GE LED array 196
5.4 Combination of surgical light spectra obtained from hospitals with high power 405 nm LED array (Photonstar) 199
5.4.1 Combination of surgical light spectra obtained from Golden Jubilee National Hospital with high power 405 nm LED array (Photonstar) 199
5.4.2 Combination of surgical light spectra obtained from Southern General Hospital with high Power 405 nm LED array (Photonstar) 202
5.5 Proposed 3D models of a 405 nm light system for use in Operating theatres for decontamination during surgery 205
5.5.1 Surgical light system integrated with 405 nm LEDs 206
5.5.2 Laminar flow chamber integrated with 405 nm LEDs for environmental decontamination 207
5.5.3 Tray tables integrated with 405 nm LEDs for surgical device decontamination 208

5.5.4 Conclusion 210

CHAPTER 6

SUMMARY AND FUTURE WORK 212

6.1 A summary of the research findings 214

6.1.1 Effect of 405 nm HINS light on osteoblast cell line 214

6.1.2 Cytotoxic responses to 405 nm light exposure in mammalian and bacterial cells 218

6.1.3 Assessment of light spectra obtained from surgical lights used in operating theatres in hospitals and optical analysis of 405 nm LED arrays 223

6.2 Limitations, future work and conclusions 226

6.2.1 Study of the effects of 405 nm light on primary cell types and on *in-vivo* animal models 226

6.2.2 Study of the effects of 405 nm light on implant materials 228

6.2.3 Study of the effects of 405 nm light on different bacterial species 229

6.2.4 Study of the effects of 405 nm light on mammalian-bacterial cell *in-vitro* co-culture models 232

6.2.5 Designing a 405 nm light system for continual decontamination during arthroplasty surgery 233

6.2.6 Other areas of 405 nm light application 234

6.2.6.1 Endoscope storage 234

6.2.6.2 Food and drinks industry 235

PUBLICATIONS 236

REFERENCES 237

APPENDIX 265

LIST OF FIGURES

FIGURE 1.1: Poster from the Health Protection Scotland and Healthier Scotland "Global hand hygiene campaign", 2014. 2

FIGURE 1.2: The rates of contamination/100 arthroplasty surgeries, caused due to contamination of different medical devices and accessories used at the time of surgery. 20

FIGURE 1.3: Laminar air flow in an operating theatre. 27

FIGURE 1.4: The Electromagnetic spectrum. 33

FIGURE 1.5: Molecular structure of a hematoporphyrin IX molecule that is commonly used in cancer therapy. 34

FIGURE 1.6: Molecular structure of a pyrrole subunit and porphyrin molecule. 35

FIGURE 1.7: Molecular structure of protoporphyrin IX molecule. 36

FIGURE 1.8: Typical porphyrin absorption spectrum. 37

FIGURE 1.9: Light penetration into the skin by different wavelengths of light. 39

FIGURE 1.10: The schematic illustration of photodynamic therapy including the Jablonski diagram. 41

FIGURE 1.11: Formation of different reactive oxygen species at different stages of the free radical chain reaction. 41

FIGURE 2.1: 405 nm HINS light system. 55

FIGURE 2.2: Emission spectrum of 3 X 3 array of uncapped 405 nm LEDs for (a) device 1 and (b) device 2. 55

FIGURE 2.3: The 3 X 3 grid pattern of (a) 405 nm LEDs off and (b) 405 nm LEDs on used for exposure of mammalian and bacterial cells to 405 nm HINS light. 56

FIGURE 2.4: Average irradiance distribution across a 12 well plate when positioned 8 cm below the 405 nm HINS light treatment system. 57

FIGURE 2.5: Average irradiance distribution across a 24-well plate when positioned 8 cm below the 405 nm HINS light treatment system. 58

FIGURE 2.6: Average irradiance distribution across a 96-well plate when positioned 8 cm below the 405 nm HINS light treatment system. 59

FIGURE 2.7: The experimental set up for exposure of mammalian cells to 405 nm HINS light. 64

FIGURE 2.8: The experimental set up involving the exposure of bacterial cells on agar plates to 405 nm HINS light at room temperature. 68

FIGURE 3.1: Extrinsic and Intrinsic pathways of apoptosis. 76

FIGURE 3.2: Principle of TUNEL assay. 80

FIGURE 3.3: Principle of the comet assay. 83

FIGURE 3.4: Studies assessing viability of rat osteoblasts for A) 30 h in DMEM and DPBS, B) every 10 h up until 30 h in DMEM and DPBS. 89

FIGURE 3.5: Preparation of transfer cassettes for transfer of protein bands from gel to membrane. 98

FIGURE 3.6: Viability of osteoblasts following exposure to 5 mW/cm^2 405 nm light for 1, 2 and 3 h. 104

FIGURE 3.7: Viability of osteoblasts in DMEM and DPBS for A, B) a 30 h and C), D) up to a 30 h time point, while adding fresh growth medium to plates after every 10 h. 106

FIGURE 3.8: Crystal Violet staining and Protein content of osteoblasts exposed to 18 and 54 J/cm^2 of 405 nm light using different irradiance/exposure time regimes. 108

FIGURE 3.9: MTT reduction, ALP activity and cell proliferation in osteoblasts exposed to 18, 27, 36 and 45 J/cm^2 of 405 nm light. 110

FIGURE 3.10: The viability of osteoblast cells after exposure to 5mW/cm^2 of 405 nm light. 112

FIGURE 3.11: The cell morphology of osteoblast cells after exposure to 5mW/cm^2 of 405 nm light. 114

FIGURE 3.12: Western blotting of homogenates prepared from 2 x 10^6 cells/cm^2 exposed to 405 nm light for 1, 2 and 3 h at 15 mW/cm^2 and unexposed samples. 115

FIGURE 3.13: The % of live cells (Q4), early apoptotic cells (Q1), late apoptotic cells(Q2) and dead cells (Q3) for both unexposed and 405 nm light exposed for 1, 2 and 2.5 h using PE-Annexin V and 7-AAD. 117

FIGURE 3.14: Survival of a range of surface seeded clinically-relevant bacterial pathogens exposed to 405 nm HINS-light at doses ranging from 4.5 J/cm^2 – 36 J/cm^2. 120

FIGURE 4.1: The conversion of hydrogen peroxide to water molecules in the presence of glutathione peroxidase. 131

FIGURE 4.2: Schematic illustration of the generation of green fluorescence by carboxy-H$_2$DCFDA. 132

FIGURE 4.3: Pathways of ROS production and clearance. 133

FIGURE 4.4: Visual detection of ROS production in immortalised rat osteoblasts upon exposure to 5 mW/cm^2 405 nm light using carboxy-H$_2$DCFDA and using fluorescence microscopy. 144

FIGURE 4.5: Measurement of ROS fluorescence intensity in immortalised rat osteoblasts upon exposure to 5 mW/cm^2 405 nm light, using carboxy-H$_2$DCFDA. 145

FIGURE 4.6: Intracellular GSH concentration and extracellular GSSG concentration of rat osteoblasts exposed to 5 mW/cm^2 405 nm light 147

FIGURE 4.7: Protein concentration of rat osteoblasts exposed to 5 mW/cm^2 405 nm light at a dose of 54 J/cm^2, in the absence (DPBS alone) and presence of ROS scavengers. 149

FIGURE 4.8: % of cellular MTT reduction of rat osteoblasts exposed to 5 mW/cm^2 405 nm light at a dose of 54 J/cm^2, in the absence (DPBS alone) and presence of ROS scavengers. 151

FIGURE 4.9: Visual detection of ROS production using carboxy-H$_2$DCFDA in the bacterium *Staphylococcus epidermidis*, upon exposure to 15 mW/cm^2 405 nm light for 1, 3 and 6 h and using fluorescence. 153

FIGURE 4.10: Measurement of ROS fluorescence intensity in the bacterium *Staphylococcus epidermidis*, upon exposure to 15 mW/cm^2 405 nm light for 1, 3 and 6 h using carboxy-H$_2$DCFDA. 154

FIGURE 4.11: Viability of *Staphylococcus epidermidis* exposed to 15 mW/cm^2 405 nm light for 3 and 6 h in the absence (in PBS) and presence of ROS scavengers. 156

FIGURE 4.12: Visual detection of ROS production in *Staphylococcus epidermidis,* exposed to 162 J/cm^2 405 nm light in the absence (in PBS) and presence of ROS scavengers, using carboxy-H_2DCFDA and using fluorescence microscopy. 158

FIGURE 4.13: Measurement of % increase in fluorescence intensity in *Staphylococcus epidermidis,* exposed to 162 J/cm^2 405 nm light in the absence (in PBS) and presence of ROS scavengers, using carboxy-H_2DCFDA. 159

FIGURE 5.1: An operating theatre environment including the operating theatre table and surgical light system. 168

FIGURE 5.2: The spectra obtained from A) Halogen lamp, B) White LED lamp (Gallium Nitride (or) Indium Gallium nitride LEDs peaking at about 465 nm combined with Cerium-doped Yttrium Aluminium Garnet phosphor which emits at about 500-700 nm. 169

FIGURE 5.3: A) The spectrum measured at 1.3 m height from one light source highlighting the UV, Visible-405 nm, Visible and IR components B) spectral distribution of Visible -405 nm component between 400 - 420 nm. 171

FIGURE 5.4: A) The spectrum measured at 1.3 m height from two light sources combined at the focal point (highlighting the UV, Visible-405 nm, Visible and IR components B) spectral distribution of Visible-405 nm component between 400 - 420 nm. 173

FIGURE 5.5: A) The spectrum measured at 2 m height from one light source combined highlighting the UV, Visible-405 nm, Visible and IR components B) spectral distribution of Visible-405 nm component between 400 -420 nm. 175

FIGURE 5.6: A) The spectrum measured at 2 m height from two light sources combined at the focal point, highlighting the UV, Visible-405 nm, Visible and IR components B) spectral distribution of Visible-405 nm component between 400 -420 nm. 177

FIGURE 5.7: The spectrum measured at ground level at an approximate distance of 2.2 m with surgical lights turned off and room lights ON, highlighting the UV, Visible-405 nm, Visible and IR components 179

FIGURE 5.8: A) The spectrum measured at 1.3 m height from one light source highlighting the UV, Visible-405 nm, Visible and IR components B) spectral distribution of Visible-405 nm component between 400 -420 nm. 181

FIGURE 5.9: A) The spectrum measured at 1.3 m height from two light sources combined at the focal point highlighting the UV, Visible-405 nm, Visible and IR components B) spectral distribution of Visible-405 nm component between 400 -420 nm. 183

FIGURE 5.10: A) The spectrum measured at 2 m height from one light source highlighting the UV, Visible-405 nm, Visible and IR components B) spectral distribution of Visible-405 nm component between 400 -420 nm. 185

FIGURE 5.11: A) The spectrum measured at 2 m height from two light sources combined including the UV, Visible-405 nm, Visible and IR components B) spectral distribution of Visible-405 nm component between 400 -420 nm. 187

FIGURE 5.12: The 99 DIE -LED array (Optodiode) powered by a SMPS giving a peak output at 405 nm (14 nm FWHM). 190

FIGURE 5.13: Spectral graphs of absolute intensities (µW/cm^2) obtained from the 99-DIE- LED array (Optodiode) at different distances using a HR4000, Ocean Optics spectrometer. 191

FIGURE 5.14: The high power 405 nm LED array (Photonstar) giving a peak output at 405 nm (14 nm FWHM). 193

FIGURE 5.15: Spectral graphs of absolute intensities (µW/cm^2) obtained from the high power 405 nm LED array (Photonstar) at different distances using a HR4000, Ocean Optics spectrometer. 194

FIGURE 5.16: Spectral graphs of absolute intensities (µW/cm^2) obtained from the 405 nm GE LEDs at different distances using a HR4000, Ocean Optics spectrometer. 197

FIGURE 5.17: The spectral graphs of 405 nm spectrum obtained from A) one 405 nm Photonstar LED array combined with one surgical light source, B) two 405 nm Photonstar LED array combined with two surgical light sources, measured at 1.3 m height from the light source at Golden Jubilee National Hospital. 200

FIGURE 5.18: The spectral graphs of 405 nm spectrum obtained from A) one 405 nm Photonstar LED array combined with one surgical light source, B) two 405 nm Photonstar LED array combined with two surgical light sources, measured at 1.3 m height from the light source at Southern General Hospital. 203

FIGURE 5.19: Surgical light system integrated with 405 nm LEDs to promote surgical site decontamination in an operating theatre environment. 206

FIGURE 5.20: Laminar flow system integrated with 405 nm LEDs to promote environmental decontamination in an operating theatre environment. 207

FIGURE 5.21: The integration of 405 nm LEDs with tray tables enabling A) complete enclosure of tables B) use of stands on tray tables with 405 nm LEDs to facilitate easy handling of devices. 209

LIST OF TABLES

TABLE 1.1: Comparison of HAI prevalence across the UK and Republic of Ireland (excluding Scotland) in acute hospitals between February 2006 and May 2006, and Scotland between 2005 & 2006. 4

TABLE 1.2: Incidence of HAI in adult patients in NHS acute and non-acute hospitals by intrinsic risk factors; sex and age. 6

TABLE 1.3: Findings of studies of the costs of HAI by type of infection, length of stay and extra hospital costs or charges 1977-2000. 9

TABLE 1.4: MRSA and *Clostridium difficile* related deaths in Scotland from 2000 – 2010. 11

TABLE 1.5: Number and percentage of HAI in NHS acute hospitals, by HAI group. 13

TABLE 1.6: Number and percentage of SSI in NHS acute hospitals, by site and type of SSI. 14

TABLE 1.7: Number and percentage of HAI in NHS acute hospitals during the 2005/2006 and 2011 surveys, by HAI group. 15

TABLE 1.8: Survival of different bacterial species on inanimate surfaces. 22

TABLE 1.9: The absorption peaks of different porphyrin molecules. 38

TABLE 1.10: Examples of bacterial species susceptible to blue light irradiation in the absence of exogenous photosensitisers. 46

TABLE 2.1: Bacterial strains used throughout the study. 66

TABLE 3.1: Different methods for detection of apoptosis in cells, with their advantages and disadvantages. 77

TABLE 3.2: The different periods of osteoblast cell exposure to 405 nm light, irradiance levels and the corresponding applied doses 85

TABLE 3.3: Protein standards prepared at different concentrations. 87

TABLE 3.4: Irradiance levels and exposure times used to apply low dose (18 J/cm^2) and high dose (54 J/cm^2) 405 nm light to osteoblasts. 90

TABLE 3.5: Preparation of gels for performing electrophoresis. 97

TABLE 3.6: Mean % of live, early apoptotic, late apoptotic and dead cells for each time point tested for A) 1st run, B) 2nd run. 118

TABLE 4.1: The different periods of osteoblast cell exposure to 405 nm light,

irradiance levels and the corresponding applied doses. 135
TABLE 4.2: The different concentrations of GSSG standards. 136
TABLE 4.3: The different concentrations of GSH standards. 137
TABLE 4.4: The different periods of bacterial cell exposure to 405 nm irradiance levels and the corresponding applied doses. 140
TABLE 4.5: The half-life periods of various ROS. 161
TABLE 5.1: Absolute intensities of different light components present in the spectrum measured at 1.3 m from one light source. 172
TABLE 5.2: Absolute intensities of different light components present in the spectrum measured at 1.3 m from two light sources combined at the focal point. 174
TABLE 5.3: Absolute intensities of different light components present in the spectrum measured at 2 m from one light source. 176
TABLE 5.4: Absolute intensities of different light components present in the spectrum measured at 2 m from two light sources combined at the focal point. 178
TABLE 5.5: Absolute intensities of different light components present in the fluorescent spectrum measured at ground level at an approximate distance of 2.2 m from the ceiling. 179
TABLE 5.6: Absolute intensities of different light components present in the spectrum measured at 1.3 m from one light source. 182
TABLE 5.7: Absolute intensities of different light components present in the spectrum measured at 1.3 m from two light sources combined at the focal point. 184
TABLE 5.8: Absolute intensities of different light components present in the spectrum measured at 2 m from one light source. 186
TABLE 5.9: Absolute intensities of different light components present in the spectrum measured at 2 m from two light sources combined at the focal point. 188
TABLE 5.10: The absolute intensities (mW/cm^2) measured at different wavelengths and at different distances from the 99-DIE- LED array (Optodiode). 192

TABLE 5.11: The absolute intensities (mW/cm^2) measured at different wavelengths and at different distances from the high power 405 nm LED array (Photonstar). 195

TABLE 5.12: The absolute intensities (mW/cm^2) measured at different wavelengths and at different distances from the 405 nm GE LEDs. 198

TABLE 5.13: The absolute intensities (mW/cm^2) of 405 nm Photonstar LED array, measured for different spectral regions at a distance of 1.3 m from A) one surgical LED light source and B) two surgical LED light sources. 201

TABLE 5.14: The absolute intensities (mW/cm^2) of 405 nm Photonstar LED array, measured for different spectral regions at a distance of 1.3 m from A) one surgical halogen light source and B) two surgical halogen light sources. 204

LIST OF ABBREVIATIONS

7-AAD	7-Aminoactinomycin D
ACGIH	American Conference of Governmental Industrial Hygienists
ADP	Adenosine diphosphate
AgNP	Silver nanoparticle
ALA	5 –aminolevulinic acid
ALP	Alkaline phosphate activity
ANOVA	One-way analysis of variance
AO	Acridine orange
APAF1	Apoptotic protease activating factor 1
APS	Ammonium persulfate
ATP	Adenosine triphosphate
BrdU	5-bromo-2'-deoxyuridine
BSA	Bovine serum albumin
Carboxy-H_2DCFDA	6-carboxy-2',7'-dichlorodihydrofluorescein diacetate
Ce-YAG	Cerium-doped Yttrium Aluminium Garnet
CFDA	Carboxyfluorescein diacetate
CFU	Colony forming units
d.H_2O	distilled water
DAB	Diaminobenzidine
DAC	Disposable antibacterial coating
DAPI	4',6-diamidino-2-phenylindole
DMEM	Dulbecco’s modified eagle’s media
DMSO	Dimethyl sulfoxide
DMTU	Dimethyl thiourea
DNA	Deoxyribonucleic acid
DPBS	Dulbecco’s phosphate- buffered saline
dUTP	2´-Deoxyuridine, 5´-Triphosphate
EDS	Environmental decontamination system

EDTA	Ethylenediaminetetraacetic acid
ELISA	Enzyme Linked Immuno Sorbent Assay
FACS	Fluorescence-activated cell sorting
FADD	FAS- associated death domain
FCS	Foetal calf serum
FITC	Fluorescein isothiocyanate
FPCL	Fibroblast-populated collagen lattice
FWHM	Full-width half-maximum
GaN	Gallium Nitride
GE	General Electric
GI	Gastrointestinal infection
GJNH	Golden Jubilee National Hospital
GRI	Glasgow Royal Infirmary
GSH	Reduced glutathione
GSSG	Glutathione disulfide or oxidized glutathione
H_2DCFDA	Dichlorodihydrofluorescein diacetate
HAI	Healthcare associated infection
HEPA	High-efficiency particulate arrestance
HINS	High-intensity narrow spectrum
HPS	Health Protection Scotland
HRP	Horseradish peroxidase
ICU	Intensive Care Unit
ICNIRP	International Commission on Non-Ionizing Radiation Protection
IHC	Immunohistochemical detection
IngaN	Indium Gallium Nitride
LED	Light emitting diode
LMG	Laboratorium voor Microbiologie
LRTI	Lower respiratory tract infection
MLAF	Mobile laminar airflow
MRSA	Methicillin resistant *Staphylococcus aureus*

MTT	3-(4,5-Dimethylthiazol-2-yl)-2,5-diphenyltetrazolium bromide
NA	Nutrient agar
NADH	Nicotinamide adenine dinucleotide
NADPH	Nicotinamide adenine dinucleotide phosphate
NB	Nutrient broth
NCTC	National Collection of Type Cultures
NEM	N-Ethylmaleimide
NHS	National Health Service
OPT	O-Phthalaldehyde
OT	Operating theatre
PACT	Photodynamic Antimicrobial Chemotherapy
PARP	poly ADP ribose polymerase
PBS	Phosphate buffered saline
PDI	Photodynamic inactivation
PDT	Photodynamic therapy
PE	Phycoerythrin
PEI-c_{e6}	Polyethylenimine chlorine (e6)
PerCP	Peridinin chlorophyll
PI	Propidium Iodide
PLGA	Poly (lactic-co-glycolic acid)
pNPP	p-nitrophenyl phosphate
PS	Phosphatidylserine
PVDF	Polyvinylidene fluoride
ROLEST	The Robertson Trust Laboratory for Electronic Sterilisation Technologies
ROS	Reactive oxygen species
SCGE	Single cell gel electrophoresis
SDS	Sodium dodecyl sulfate
SDS-PAGE	Sodium dodecyl sulfate polyacrylamide gel electrophoresis
SEM	Scanning electron microscopy

SGH	Southern General Hospital
SMPS	Switch mode power supply
SSI	Surgical site infection
TBO	Toluidine blue O
TBS	Tris buffered saline
TCA	Trichloroacetic acid
TdT	Deoxynucleotidyl transferase
TEM	Transmission electron microscopy
TEMED	Tetramethylethylenediamine
TiAlNb	Titanium aluminium niobium
TKA	Total knee arthroplasty
TRADD	TNFR-associated death domain
TTBS	Tween tris buffered saline
TUNEL	Terminal deoxynucleotidyl transferase dUTP nick end labelling
UTI	Urinary tract infection
UV	Ultraviolet

Chapter 1

INTRODUCTION

1.1 Healthcare associated infections

Healthcare Associated Infections (HAIs) or nosocomial infections are infections acquired by patients in a hospital or any other healthcare setting (e.g. care homes, general practice and dental surgeries) that are not present at the time of admission. HAI affects approximately 10% of patients admitted to hospital, and is responsible for over 5000 deaths in the UK annually (Improving Patient Care by Reducing the Risk of Hospital Acquired Infection: A Progress Report, National Audit Office 2004). In order to reduce the incidence and spread of HAIs, performing hand hygiene has been quoted by Health Protection Scotland and Healthier Scotland (Figure 1.1) as the single most important thing to do to improve hygiene in a hospital environment or a healthcare setting. Despite advancements in public health and hospital care, these infections continue to pose a threat to hospitalized patients.

Fig. 1.1: Poster from the Health Protection Scotland and Healthier Scotland "Global hand hygiene campaign", 2014.

1.1.1 Incidence of HAI in the UK

The incidence of HAI is a useful measure as it illustrates the number of patients that acquire a HAI during a defined time period such as a year, and rates may be expressed as a percentage of total discharges. The first Scottish National HAI Prevalence Survey was conducted by Health Protection Scotland (HPS) between October 2005 and October 2006 on 13,574 inpatients and included all acute hospitals and a 25% sample of non-acute hospitals. The survey reported that 9.5% and 7.3% of patients in acute and non-acute hospitals, respectively, had a HAI at the time of survey (NHS Scotland National HAI Prevalence survey, 2007). The highest prevalence of HAI in acute hospital inpatients was found in the specialities including Care of the Elderly (11.9%), Surgery (11.2%), Medicine (9.6%) and Orthopaedics (9.2%) (NHS Scotland National HAI Prevalence survey, 2007). HPS conducted a second national HAI prevalence survey in 2011 on 13,558 inpatients in 75 hospitals

including all independent (n=7), acute (n=42), paediatric hospitals (n=3) and 25% of NHS non-acute hospitals (n=23), because of the changing epidemiology of HAI in Scotland (Scottish National Point Prevalence Survey of Healthcare Associated Infection and Antimicrobial Prescribing 2011). The prevalence of HAI was recorded to be present in 4.9 % and 2.5 % of patients in acute and non-acute hospitals respectively. In Paediatric and Independent hospitals, the HAI incidence was not significantly different to that in acute care. Several factors that contributed to the risk of HAI included ageing population (Strausbaugh, 2001), and emerging and re-emerging antimicrobial resistant microorganisms (European Centre for Disease Prevention and Control, 2011). According to HAI prevalence surveys conducted in acute hospitals in the UK and Republic of Ireland (excluding Scotland) between February 2006 to May 2006 (Smyth *et al*., 2008) and Scotland between 2005 – 2006 (Reilly *et al*., 2007), the % HAI prevalence rate in Scotland was 9.5 %, quite high compared to England (8.2 %), Wales (6.3%) and Northern Ireland (5.5 %) (Table 1.1).

Table 1.1: Comparison of HAI prevalence across the UK and Republic of Ireland. Based on HAI prevalence surveys conducted in acute hospitals in the UK and Republic of Ireland (excluding Scotland) between February 2006 and May 2006 (Smyth *et al*., 2008), and Scotland between 2005 & 2006 (Reilly *et al*., 2007).

Country	Number of hospitals	Number of patients	Infection prevalence rate
England	190	58,795	8.2%
Wales	23	5,825	6.3%
Northern Ireland	15	3,625	5.5%
Republic of Ireland	45	7,518	4.9%
Scotland	45	11,608	9.5%

1.1.2 Risk factors contributing to HAI and its impact

Intrinsic risk factors that contribute to the existence of HAIs among patients include: • patients who are immunocompromised because of age (elderly, infants), • patients having a medical condition, • severity of the underlying illness, • suppression of the immune system (treatments for leukaemias and cancers, transplant patients, recurrent blood transfusions) and • surgical/medical treatments. According to a study carried out by Weinstein in 1998, the HAI rates in paediatric and adult Intensive Care Units (ICU) were roughly three times higher than elsewhere in hospitals in U.S.A (Weinstein, 1998). Extrinsic risk factors include:• surgical or other invasive procedures (Meddings *et al*, 2013) (and it is a pertinent point that improving patients survival leaves them more vulnerable to infections), • diagnostic or therapeutic interventions (e.g., invasive devices, implanted foreign bodies, immunosuppressive medications, organ transplantations), • extensive use of antibiotics and the emergence

of several antibiotic-resistant micro-organisms (e.g. *Acinetobacter baumannii*), • increased movement of patients between wards due to limited number of beds in hospitals, • excessive nursing overload (Daud-Gallotti RM *et al*, 2012).

HAIs not only affect the patients leading to severe illness, pain and depression, but also directly affect the caretakers and employers in several ways such as longer stay in the hospital (Plowman *et al*., 1999), longer recovery time, reduced quality of life and more money being spent towards patient treatment and infection control measures (Coello *et al*., 1993). More expensive antibiotics will be required to treat patients suffering from HAI caused due to antibiotic resistant micro-organisms.

Table 1.2 shows the % of incidence of HAI rates in NHS acute and non-acute hospitals in 2011, based on sex and age.

Table 1.2: Incidence of HAI in adult patients in NHS acute and non-acute hospitals by intrinsic risk factors; sex and age. (Scottish National Point Prevalence Survey of Healthcare Associated Infection and Antimicrobial Prescribing 2011).

Intrinsic risk factor	Category	NHS acute hospitals			NHS non-acute hospitals		
		Sample size	Number of infections reported	% of Incidence	Sample size	Number of infections reported	% of Incidence
Sex	Male	4661	267	5.7	838	20	2.4
	Female	6238	277	4.4	797	20	2.5
Age	16-29	668	21	3.1	677	5	0.7
	30-49	1511	59	3.9			
	50-64	1891	118	6.2			
	64-79	3575	200	5.6	417	11	2.6
	80+	3284	148	4.5	545	25	4.6

When looking specifically at HAI arising from surgical procedures, other risk factors include:• the duration of surgery, • number of staff present at the time of surgery, • presence of foreign material, and • pre-operative hair removal. The duration of surgery is defined as the time between skin incision and skin closure (Leong *et al*., 2006). During surgery, bacteria carried on airborne particles can settle in the wound, surgical instruments or on the hands of operating staff. The staff present in the theatre disperse the majority of the organisms and the dispersal of these micro-organisms increases with the speed of staff movement thereby representing the biggest risk in joint replacement surgery. According to a study by Howorth in 1985, it has been estimated that each person sheds 10,000 micro-organisms every minute

increasing to 50,000 per minute during periods of activity (Howorth, 1985). Hence the number of staff present at the time of surgery also poses as a risk factor for the incidence of HAI. Sutures, drains and prosthetic implants have been reported to increase the risk of post-operative infection. To cause an infection in the absence of a suture, approximately 6.5 million bacteria would be required, while just 100 bacteria can cause an infection in the presence of one suture (Wilson, 2006). Prosthetic implants used in orthopaedic or cardiac surgeries attract coagulase-negative staphylococci which in turn can form biofilms and adhere to implanted material. Cruse & Ford in 1973, and Tkach *et al*., in 1979, identified that pre-operative shaving with a razor contributes to wound infection as cuts on the surface of the skin reduce the integrity of the skin and release dermal bacteria into the operative field making the skin environment favourable for bacterial proliferation (McIntyre and McCloy, 1994).

1.1.3 Morbidity, Mortality, length and cost of stay of patients in hospitals due to HAI

HAI was believed to cost the NHS at least £1bn annually and caused at least 5,000 deaths and are a contributing factor in over 1,500 deaths (The Management and Control of Hospital Acquired Infection in Acute NHS Trusts in England: National Audit Office 2000, Improving Patient Care by Reducing the Risk of Hospital Acquired Infection: A Progress Report, National Audit Office 2004). HAIs are the most common complication seen in hospitalized patients. Digiovine and his co-workers found that HAI increased the length of Intensive Care Unit stay of patients by an extra 10 days and costs by an extra $34,508 when compared to uninfected patients (Digiovine *et al*., 1999). According to a study conducted by Graves and his

team in Australia, it was reported that 38 patients were diagnosed for HAI out of 4,488 admissions and lower respiratory tract infection (LRTI) was associated with an increase of 2.58 days stay in the hospital and variable costs of AU$24.04 (AU$10.15-$43.46) per LRTI (Graves *et al*., 2007). Plowman and co-workers (2001) reported that out of roughly 4,000 adult patients admitted to a district general hospital in England, 309 patients presented with one or more HAI during the in-patient period which in turn incurred hospital costs of an additional £3,154 and an increase in length of stay from 8 to 22 days when compared with the uninfected patients.

In 2000, Plowman's study found that infected patients were 7.1 times more likely to die in hospital than uninfected patients and infected patients may spend on average an extra 11 days in hospital (Plowman *et al*., 2000). However, the Scottish HAI prevalence report calculates the average increased length of stay as 6.6 days (Reilly *et al*., 2007). The report also notes the length of stay and cost associated with HAIs can vary depending on the hospital speciality the patient is being treated in. Care of the elderly has the longest increase of additional acute hospital stay (13.7 days) at a cost of £187 per added day and therefore an average total cost of case treatment of £2,562. Whereas obstetrics has the shortest increase in length of stay due to patient HAI contraction (3.2 days) but the highest cost per added day at £596, resulting in a total cost of £1,907 per case. According to a 2006 review, it was concluded that the costs of HAIs are underestimated and that Methicillin Resistant *Staphylococcus aureus* (MRSA) alone results in annual costs to the UK economy of between £3-11 billion (Gould, 2006). An outbreak of MRSA in Kettering, for example, was estimated to cost the individual hospital involved approximately £400,000

(Department of Health, UK, 1995). Table 1.3 shows the additional costs and length of stay of patients with different type of HAIs recorded between 1977 and 2000.

Table 1.3 - Findings of studies of the costs of HAI by type of infection, length of stay and extra hospital costs or charges 1977-2000.

Study	Country	Type of Infection (Number of HAIs)	Additional length of stay (days)	Additional cost per case (£)
Rubertstein *et al*., 1982	US	Surgical Wound Infections (19)	12.9	1,912
Guard *et al*., 1983	France	All infections (61)	6.7	1,294
Mugford *et al*., 1989	UK	Surgical Wound Infections (41)	2.1	1,170
Liu-yi and Shu-qun, 1990	China	Multiple (43)	25	1,254
Kappstein *et al*., 1992	Germany	Pneumonia (34)	10.13	6,405
Coello *et al*., 1993	UK	Surgical Wound Infections (12)	10.2	1,798
Plowman *et al*., 1999	UK	Lower Respiratory Tract Infections (48)	8	2,080
Plowman *et al*., 1999	UK	Urinary Tract Infections (107)	5	1,122
Plowman *et al*., 1999	UK	Blood Stream Infections (4)	4	6,209
Plowman, 2000	UK	All infections (309)	11	3,000
Reilly *et al*., 2007	UK	All infections (1103)	6.6	2,548
Tarricone *et al*., 2010	Italy	Central Line-associated Blood Stream Infection (43)	8.46	~ 6,580

The most recent surveillance of HAIs in Scottish ICUs was conducted between the period of January till December 2013 by Health Protection Scotland. Data from 6,775 patients admitted to 23 Scottish ICUs were collected and 224 infections were reported. HAIs were found to increase the length of stay of patients from 5 to 19 days; an increased stay of 14 days (Surveillance of Healthcare Associated Infections in Scottish Intensive Care Units, Annual report of data from January - December 2013: Health Protection Scotland, 2014). The annual cost of HAIs to NHS Scotland is estimated to be £183 million (Reilly *et al*., 2007).

1.2 Types of HAI and causative micro-organisms

Most HAIs are caused by bacteria that exist harmlessly in the general population. However, in a healthcare environment these micro-organisms have a high incidence of causing infections in patients admitted to hospital as they already have poor health or an underlying condition and lack immunity to fight against these micro-organisms. The most common types of HAI occurring in acute hospital inpatients in Scotland were urinary tract infections (UTI - 17.9% of all HAI), surgical site infections (SSI - 15.9%), gastrointestinal infections (GI - 15.4%), followed by eye, ear, nose, throat and mouth infections (12.5%) (Reilly *et al*., 2007). In non-acute hospitals, patients with UTI were frequent (28.1% of all HAI), as were skin and soft tissue infections (26.8%). The majority of organisms responsible for HAI in non-acute care were identified as *Escherichia coli* (22.2 %), *Clostridium difficile* (18.5 %) and *Staphylococcus aureus* (11.1 %), while in acute care incidences were identified to be *Staphylococcus aureus* (24.5%), *Escherichia coli* (20.8%) and *Clostridium difficile* (7.7%) (Scottish National Point Prevalence Survey of Healthcare Associated Infection and Antimicrobial Prescribing 2011: Health Protection Scotland, 2012).

Table 1.4 shows the number of deaths reported in Scotland between 2000 and 2010, where MRSA or *Clostridium difficile* was responsible for the deaths.

Table 1.4: MRSA and *Clostridium difficile* related deaths in Scotland from 2000 – 2010 where MRSA, and *Clostridium difficile* were: (a) recorded as the underlying cause of death; or (b) described as a contributory factor; Source: The General Register Office for Scotland.

Year	Number of Deaths reported where,					
	MRSA was :			*Clostridium difficile* was :		
	(a) An underlying cause	(b) Contributing factor	Either (a) or (b)	(a) An underlying cause	(b) Contributing factor	Either (a) or (b)
2000	35	74	109	38	78	116
2001	36	100	136	57	113	170
2002	46	109	155	70	94	164
2003	39	130	169	73	115	188
2004	42	148	190	98	141	239
2005	38	174	212	102	211	313
2006	51	162	213	164	253	417
2007	56	174	230	220	377	597
2008	48	166	214	248	517	765
2009	24	137	161	139	326	465
2010	25	93	118	65	205	270

In the last 5 years, UTI was identified as the most prevalent type of HAI (22.6% of all HAI) in Scotland, many of these occurred in patients who had been catheterised and the risk of acquiring a UTI increases with prolonged catheterisation time (Scottish National Point Prevalence Survey of Healthcare Associated Infection and Antimicrobial Prescribing 2011: Health Protection Scotland, 2012). The most commonly identified bacteria in UTI infections are *Escherichia coli*, *Klebsiella*

species, and enterococci that are the endogenous intestinal flora. Maki and Tambyah reported that common skin bacteria like *Staphyloccocus* species and *Cornybacterium* might be introduced into the body following insertion of the urinary catheter due to contaminated equipment or from the hands of healthcare workers (Maki & Tambyah, 2001). von Eiff and his co-workers stated that with increasing technological advancements in implanting vascular grafts and orthopaedic implants, there is an increase in the incidence of implanted device-associated infections (von Eiff *et al*., 2005). SSI was found to remain as a large proportion of all HAI (18.6%), particularly in orthopaedic, vascular and gastrointestinal surgery in acute care (Scottish National Point Prevalence Survey of Healthcare Associated Infection and Antimicrobial Prescribing 2011: Health Protection Scotland, 2012). Table 1.5 shows the number of inpatients in NHS acute hospitals affected with different types of HAI in 2011, and Table 1.6 shows the number and percentage of SSI in NHS acute hospitals, by site and type of SSI (Scottish National Point Prevalence Survey of Healthcare Associated Infection and Antimicrobial Prescribing 2011: Health Protection Scotland, 2012).

Table 1.5: Number and percentage of HAI in NHS acute hospitals, by HAI group. (Scottish National Point Prevalence Survey of Healthcare Associated Infection and Antimicrobial Prescribing 2011: Health Protection Scotland, 2012)

HAI type	Number of inpatients with HAI	% of inpatients with HAI
Urinary tract infection	136	22.6
Surgical site infection	112	18.6
Eye, ear and nose, throat and mouth infection	55	9.2
Gastrointestinal tract infection	41	6.8
Skin and soft tissue	24	4.0
Bone/joint infection	3	0.5
Reproductive tract infection	3	0.5
Cardiovascular system infection	1	0.2

Table 1.6: Number and percentage of SSI in NHS acute hospitals, by site and type of SSI. (Scottish National Point Prevalence Survey of Healthcare Associated Infection and Antimicrobial Prescribing 2011: Health Protection Scotland, 2012).

Surgical procedure category	Superficial SSI		Deep SSI		Organ Space SSI		All SSI	
	N	%	N	%	N	%	N	%
Orthopaedic surgery	11	26.8	19	46.3	11	26.8	41	99.9
General surgery	14	50.0	7	25.0	7	25.0	28	100
Vascular surgery	9	60.0	5	33.3	1	6.7	15	100
Cardiac surgery	7	77.8	1	11.1	1	11.1	9	100
Neurosurgery	3	50.0	2	33.3	1	16.7	6	100
Obstetrics and Gynaecology	4	100	0	0	0	0	4	100
ENT surgery	3	100	0	0	0	0	3	100

Table 1.7 describes the distribution of HAI types reported during the 2005/2006 and 2011 surveys. The percentage of HAI for each type of HAI in both the surveys has been calculated from the total number of HAI. The percentage of all HAI that were Bloodstream infection (BSI), pneumonia and UTI is higher in 2011 than 2005/2006.The percentage of SSI though lower (18.7 %) in 2011 than in the 2005/2006 survey (21.4 %) is still high in terms of the number of patients being infected.

Table 1.7: Number and percentage of HAI in NHS acute hospitals during the 2005/2006 and 2011 surveys, by HAI group.

Type of HAI	2005/2006 survey		2011 survey	
	Number of HAI	% of HAI	Number of HAI	% of HAI
Urinary tract infection	130	15.6	117	23.8
Surgical site infection	179	21.4	92	18.7
Pneumonia	78	9.3	89	18.1
Bloodstream infection	32	3.8	52	10.6
Eye, ear, nose, throat or mouth infection	114	13.6	49	10.0
Gastrointestinal infection	168	20.1	28	5.7
Skin and soft tissue infection	81	9.7	18	3.7
Lower respiratory infection other than pneumonia	19	2.3	17	3.5
Systemic infection	12	1.4	16	3.3
Cardiovascular system infection	4	0.5	6	1.2
Reproductive system infection	11	1.3	3	0.6
Central Nervous System infection	2	0.2	3	0.6
Bone and joint	6	0.7	2	0.4
Total	**836**	**100**	**492**	**100**

1.3 Incidence of infections in orthopaedics i.e: joint replacement surgery

Joint arthroplasty is one of the commonly performed successful surgeries in orthopaedics. In England and Wales, approximately 160,000 total hip and knee replacement surgeries are carried out every year (National joint registry; http://www.njrcentre.org.uk). In Scotland, 7,609 primary hip and 7,169 primary knee arthroplasty surgeries were carried out in 2013 (Scottish Arthroplasty Project – Biennial report, 2014). However, infections occurring post-surgery by bacteria, commonly *Staphylococcus aureus* (Geipel, 2009) still remain the most morbid complications arising and are difficult and expensive to treat (Eron & Lipsky, 2006; Joshi *et al*., 2010; Meehan *et al*., 2009; Pulido *et al*., 2008). SSIs associated with medical implants still remain a common and serious complication in arthroplasty surgery. They not only contribute to increased rates of patient morbidity and mortality but also result in increased duration hospitalisation post-surgery and patient dissatisfaction (Jenks *et al*., 2014).

Jamsen and co-workers (2010) stated that infections after knee and hip replacement surgeries are critical and that several preventive measures need to be taken to reduce the HAI incident rates among patients. Deep prosthetic joint infection is a serious complication of hip replacement and if left untreated can result in severe pain, persistent dislocation and death (Hunter & Dandy, 1977). Infection rates following primary total hip replacement surgeries is about 2.2 % (Ridgeway *et al*., 2005) while the infection rates post spinal surgeries is about 2 % (Olsen *et al*., 2008). It has also been found that infection rates following endoprosthetic replacement of large bone defects after tumor resection is about 13 % while infections arising from external fixation occurs in up to 70 % of cases treated (Malawer & Chou, 1995; Mahan *et al*.,

1991). The incidence of infection (almost always caused by *Staphylococcus aureus* and *Staphylococcus epidermidis*) rates in revision surgery (where the existing artificial joint needs to be replaced) is even higher and it is about 3.2 – 5.6 % for both hips and knees (Montanaro *et al*., 2011). Bozic and co-workers (2010) reviewed and analysed the clinical, demographic and economic data of a total of 60, 355 revision total knee arthroplasty (TKA) procedures performed in the US, between October 1, 2005 and December 31, 2006. They found that the most common causes of revision TKA were infection (25.2 %) followed by loosening of the implant (16.1 %). According to the 10th Annual report, 2013, conducted in England and Wales, it was recorded in the National Joint registry that infection accounted for 12 % of indications for revision hip arthroplasty and 22 % for revision knee arthroplasty (10th Annual Report 2013).

Kurtz and co-workers (2007) have estimated a rise in the occurrence of infections between 2005 and 2030 by 4 % for both primary and revision hip and knee arthroplasties in the Unites States. Cahill and co-workers (2008) showed that the infections occurring post total joint replacement surgeries among patients reduced patient satisfaction and severely impaired functional health status and health-related quality of life, while treating patients suffering from these infections is considered an economic burden for hospitals (Sculco, 1993).

1.4 Causes of HAI

Some of the factors that are responsible for increasing the opportunity for people to acquire HAI are • failure to wash hands by medical personnel between medical procedures and between patients, • an extended hospital stay, • use of indwelling catheters, • existence of antibiotic resistant bacteria, and • any type of invasive procedure including surgery and the dressing or drainage of surgical wounds (Encyclopedia of Surgery, 2009).

HAI can be transferred into the body by three methods • contact transmission, • airborne transmission and • droplet transmission (Wong & Leung, 2004). Contact transmission occurs either directly or indirectly. Direct contact transmission occurs through direct physical transfer of bacteria from medical personnel, other patients or visitors to the patient. Indirect contact transmission occurs when a contaminated or improperly cleaned medical device is used on a patient that transfers the HAI causing bacteria to the surgical site. Airborne transmission occurs via coughing, sneezing, talking, laughing or exhaling and during body movement (e.g., bacterial shed from the body during general movement, bandage changing, bed changing) that suspends particles (< 5 μm) in the air which become aerosolized and spread over an entire room eventually reaching the surgical site of patient during surgery. Dust particles containing bacteria can also be spread by airborne transmission. Droplet transmission involves the suspension and spread of HAI causing bacteria in the warm, moist droplets as a result of coughing, talking or sneezing. Other modes of transmission include common vehicle transmission involving contamination of food sources or water supplies, vector borne transmission involving the spread of HAI causing microorganisms through vectors like mosquitoes and flies.

Our human body, especially skin and mucosal surfaces is inhabited by populations of microbes including bacteria (e.g., *Escherichia coli* in colon) that play an important role in maintaining a normal and healthy physiology. However, if the bacteria populate in areas not naturally colonized (injury) or sterile (blood, abdominal cavity), infections occur. Invasive surgical procedures provide bacteria with a way to get into normally sterile areas of the body thereby increasing a patient's risk of getting an infection. Following surgery, contaminated dressings or the hands of medical personnel who change the dressing can contribute to the occurrence of surgical wound infections. Other wounds caused by burns, trauma, or pressure sores can also become easily infected often as a result of prolonged bed rest or prolonged use of a wheelchair.

According to a study conducted by Davis *et al*., 1999, who was an orthopaedic surgeon from the Bone Infection Group, University of Manchester, considerable numbers of surgical devices used during arthroplasty surgery were found to be contaminated with bacteria (Figure 1.2).

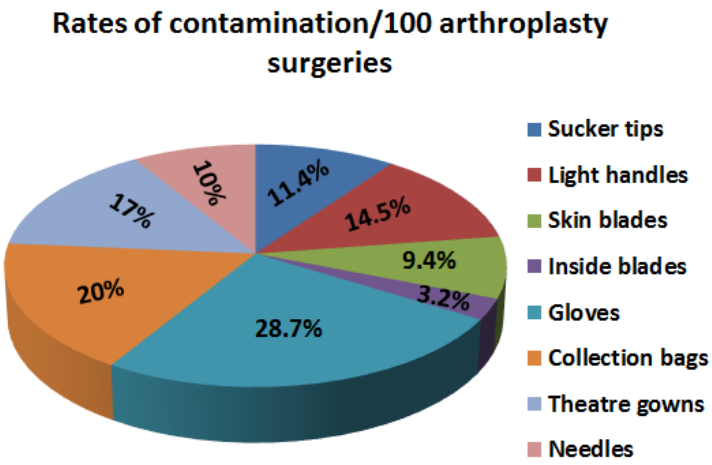

Fig 1.2: The rates of contamination/ 100 arthroplasty surgeries, caused due to contamination of different medical devices and accessories used at the time of surgery. Davis *et al*, 1999; From the Bone Infection Group, University of Manchester, North Manchester General Hospital, Manchester, England.

Millions of medical devices are used every year and despite many advances in the field of biomaterials, the use of a significant number of each type of device results in bacterial colonisation and leads to implant-related infection (Alexander *et al*., 2004). The most commonly identified bacteria responsible for causing surgical site infections in vascular, orthopaedic and trauma surgeries were found to be *Staphylococcus aureus* and *Staphylococcus epidermidis* (Campoccia *et al*., 2006, Misteli *et al*., 2011; Owens & Stossel, 2008).

1.4.1 Environmental survival of bacteria resulting in infections

Bacteria not only survive in/on the human body as mentioned earlier but according to Kramer and co-workers (2006), they also survive on inanimate surfaces for prolonged time periods. Different bacterial species (both gram positive and gram negative) and their survival on dry inanimate surfaces such as steel, plastic etc has been summarised in Table 1.8. Due to their survivability for longer time periods, the chances of them being transferred from surfaces to patients are quite high resulting in the spread of HAI among patients in a hospital environment. A case involving a MRSA outbreak among 12 patients admitted in a burns unit and plastic surgery department was reported by Embil and co-workers (2001) and this outbreak also spread to another community hospital (the bacterial species were tested to be identical using pulsed-field gel electrophoresis) resulting from the transfer of a patient from the burns unit. The source of the outbreak was identified to be a hand held shower unit and a contaminated stretcher used by the patient in the burns unit and replacing both pieces of equipment terminated the outbreak (Embil *et al*., 2001).

Table 1.8: Survival of different bacterial species on inanimate surfaces adapted from Kramer at al., 2006.

Bacterial species	Duration of existence
Acinetobacter spp.	3 days – 5 months
Bordetella pertussis	3-5 days
Campylobacter jejuni	up to 6 days
Clostridium difficile (spores)	5 months
Chlamydia pneumoniae, C. trachomatis	≤ 30 hours
Chlamydia psittaci	15 days
Corynebacterium diphtheriae	7 days – 6 months
Corynebacterium pseudotuberculosis	1-8 days
Escherichia coli	1.5 hours – 16 months
Enterococcus spp. (Including Vancomycin Resistant and Vancomycin sensitive)	5 days – 4 months
Haemophilus influenzae	12 days
Helicobacter pylori	≤ 90 minutes
Klebsiella spp.	2 hours - > 30 months
Listeria spp.	1 day – months
Mycobacterium bovis	> 2 months
Mycobacterium tuberculosis	1 day – 4 months
Neisseria gonorrhoeae	1 – 3 days
Proteus vulgaris	1- 2 days
Pseudomonas aeruginosa	6 hours – 16 months; on floor - 5 weeks
Salmonella typhi	6 hours – 4 weeks
Salmonella typhimurium	10 days – 4.2 years
Salmonella spp.	1 day
Serrartia marcescens	3 days – 2 months; on dry floor - 5
Shigella spp.	2 days – 5 months
Staphylococcus aureus, including MRSA	7 days – 7 months
Streptococcus pneumoniae	1 – 20 days
Streptococcus pyogenes	3 days – 6.5 months
Vibrio cholerae	1 - 7 days

Landis and co-workers (2008) identified that bacterial populations in the range of 10^5 – 10^6 colony forming units (CFU) can increase the incidence of HAI among patients and can also inhibit wound healing in healthy individuals. In 1964, Bendy and co-workers showed that decubitis ulcers could not be healed without bringing the bacterial counts to below 10^6 CFU/ml of wound fluid (Bendy *et al*., 1964). Similarly, fatal sepsis occurred in visceral cultures containing bacterial populations of more than 10^6 CFU/g of tissue (Krizek & Davis. 1966). In another study, conducted by Murphy and co-workers, they showed that successful closure of wounds in goats with pedicled flaps could not be achieved when the wounds were contaminated with more than 10^5 CFU per gram of tissue (Murphy *et al*., 1986).

The number of bacteria required to cause an infection in patients is greatly reduced with the use of indwelling medical equipment such as catheters, needles etc. In 1956, Elek carried out a comparative study between the number of bacteria required to cause an infection in human volunteers injected with *Staphylococcus pyogenes* under the skin and in volunteers who were sutured through the skin with *Staphylococcus aureus* coated suture material that was tied in place. It was found that 7.5×10^6 CFU of *Staphylococcus pyogenes* was required to cause swelling, redness and pus formation when injected under the skin while just 100 CFU of *Staphylococcus aureus* was sufficient to cause infection around the stitched area of skin (Elek, 1956). Charnley and Eftekhar (1969) projected that as low as 10 CFU of *staphylococci* is sufficient to induce an infection in patients post total hip replacement surgery (Charnley & Eftekhar, 1969). In 1982, Lidwell and co-workers demonstrated that even 1 CFU/m^3 of *Staphyloccocus aureus* in air achieved through the use of ultra

clean air and whole-body exhaust ventilate suits can still cause sepsis post total knee or hip replacement surgery (Lidwell *et al*., 1982).

1.5 Airborne transmission and preventive measures taken to maintain sterility in an operating theatre

Improvements in hand hygiene could reduce the incidence of HAI rates by up to 50% (Pittet *et al*., 2000; Larson, 2004). However, one of the main sources of infection occurring during surgery, is the presence of higher populations of airborne contaminants. Lidwell and co-workers (1983) identified that the number of airborne bacteria measured within an area of 30 cm encircling the wound correlated with the number of infections occurring after orthopaedic implant surgery. Whyte and co-workers (1982) found out that airborne transmission was the main mode of transmitting 98 % of microorganisms to the wound area. They also identified that, out of the total number of bacteria being cleared out during surgery in comparison with the airborne bacterial populations, 35 % of these bacteria were thought to have reached the wound directly, while the remaining 65 % to have fallen on gloves of medical personnel or on surgical devices used at the time of surgery, resulting in an indirect contamination of the surgical site. Namdari and co-workers (2011) found that there is a small risk of patients getting infected with a known microorganism of the preceding ‘dirty cases’ (cases involving the removal of an infected implant scheduled before ‘clean’ procedures). It is well known that the operating theatre staff are the prime source of airborne bacteria as they disseminate around 10^4 skin scales/minute while walking, out of which 10 % contain bacteria (Hambraeus, 1988). Clark and de CalcinaGoff (2009) found that 10^7 bacteria carrying skin fragments were released from the body within a 24 hour period. The release was caused due to

the abrasive action of fabrics worn by the staff, upon the skin (Benediktsdottir & Hambraeus, 1982).

However, it is not only the operating staff who have direct contact with the patient during surgery that pose a risk of infection. Clark and co-workers (1985) identified that mechanical cleaning methods and movement of people also contribute to the airborne particles, as settled particles get disturbed and get resuspended in the air. Ayliffe and Collins (1967) carried out an investigation following 3 cases of post-operative *Staphylococcus aureus* wound infections in the same ward and found out that a medical orderly (ward or nurse assistant) was the source of infection. Bacteriological reports discovered an unusual strain of *Staphylococcus aureus* that was resistant to tetracycline and novobiocin, but sensitive to penicillin. Large numbers of this unusual strain of bacteria were not only isolated from the skin and hair of the orderly, who suffered from eczema, but also from the air samples collected from ward areas visited by the orderly. It was therefore concluded that though the orderly was not in direct contact with the patient, they still contributed to the infection owing to their presence during the surgical procedure (Ayliffe & Collins, 1967).

One of the possible reasons for infection in this example is lack of use of a laminar flow ventilation system as it only came into regular use in orthopaedic theatres in the 1980s. A laminar flow ventilation system involves blowing a continuous flow of highly filtered ‘bacteria-free’ air downstream, which is recirculated using positive pressure back into the operating environment such that the air contaminants that are produced during the surgery are removed from the surgical site periodically (Figure

1.3). Alexakis and co-workers (1976) showed that the use of a laminar flow system resulted in 95 % reduction in the airborne bacterial levels, measured by slit-sampling. In spite of the use of modern laminar airflow systems in operating theatres, contaminants still tend to persist in the air during surgery. Owers and co-workers (2004) reported a high number of bacterial isolates during orthopaedic surgery even with the use of laminar flow ventilation. Pastuszka and co-workers (2005) measured the bacterial concentrations to be as high as 236 CFU/m^3 during cardiac surgeries. In another study, airborne bacterial populations of around 100 CFU/m^3 were measured in fully vented operating theatre rooms during cardiac surgery, with counts of 45 CFU/m^3 present in surface swabs (Qudiesat *et al*., 2009). In the UK, for conventionally vented operating theatre rooms, a limit of 180 CFU/m^3 for an average period of 5 minutes has been set, and a limit of < 1 CFU/m^3 encircling the wound area has been set, with the use of ultra-clean air together with the total body exhaust gowns (UK Department of Health document, Health Technical Memorandum 2025).

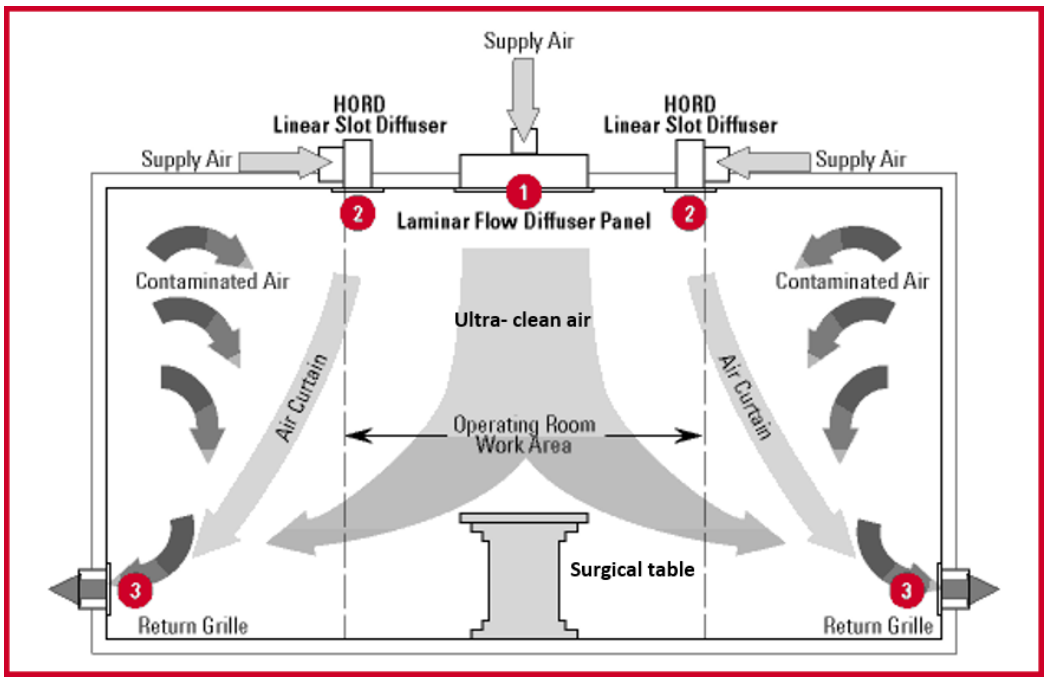

Figure 1.3: Laminar air flow in an operating theatre adapted from (http://www.sagomed.com.vn/en/product.php?id=75&cid=78).

Though the use of laminar airflow is the most efficient operating room ventilation system currently in use ((Memarzadeh & Manning, 2002; Evans, 2011), indoor obstacles such as medical lamps, medical devices and surgical staff can affect the unidirectional airflow pattern of a vertical laminar airflow system (Chow and Yang, 2005; Chow *et al*., 2006). Hence, a study on whether the use of a conventional turbulent-mixing mobile laminar airflow (MLAF) screen could reduce the bacterial contamination in an operating room and at the same time overcome the above mentioned issues associated with the vertical laminar airflow system, using computational fluid dynamics technique was conducted by Sadrizadeh and co-workers (2014). They found that the airborne and sedimenting counts of bacteria-carrying particles downstream of the operating team were reduced to 1 CFU/m^3 acceptable for orthopaedic/implant surgery when the MLAF units (one placed at the

foot of the operating table and the other at the end of the instrument table) were added to conventional operating room ventilation and they were functioning at a velocity of 0.4 m/s (Sadrizadeh *et al*., 2014). However, the installation of these units would occupy more space in the surgical environment than the conventional laminar flow system and limit easy mobility of operating staff. Gastmeier and co-workers (2012) suggest that the efficacy of laminar flow is debatable and it has been implicated as a risk factor for surgical site infections. Brandt and co-workers (2008) also showed that operating room ventilation with high-efficiency particulate arrestance (HEPA) filtered (vertical) laminar airflow had no protective effect on the rate of surgical site infection in orthopaedic and abdominal surgery, but significantly increased the risk of occurrence of SSI after hip prosthesis implantation compared to the conventional turbulent ventilation with high-efficiency particulate air-filtered air.

1.5.1 Methods of fighting and preventing implant associated infections using silver coated implants and hydrogels

With advances in medical technology and the increase in life expectancy worldwide, the need for medical implants has grown to a great extent (Hetrick & Schoenfisch, 2006). Nevertheless, this demand for medical implants has also resulted in continual problems of bacterial infections in patients (Darouiche, 2004; Nablo *et al*., 2005). The bacterial strains responsible for causing these implant infections include gram-positive *Staphylococcus aureus* and gram-negative *Escherichia coli* (An & Friedman, 1996). In earlier studies, silver nanoparticles (AgNPs) were shown to possess strong antimicrobial properties against these strains of bacteria and drug resistance did not develop (Kvitek *et al*., 2008; Kim *et al*., 2007; Sondi *et al*., 2003).

Hence, Wang and co-workers (2013) investigated the toxicity of AgNPs based coating materials *in vitro* and *in vivo*. They identified that a poly (lactic-co-glycolic acid) (PLGA) electrospun membrane embedded with optimised silver nanoparticles at a dose of 0.5 wt % of AgNPs was safe and effective in prevention of implant associated infections. In another study conducted by Kuehl and co-workers (2015), they showed that silver coated titanium aluminium niobium (TiAlNb) alloys in combination with pre-operative antibiotic prophylaxis using daptomycin resulted in 100 % prevention and using vancomycin resulted in a 33 % prevention rate in a perioperative infection with MRSA. Logoluso and co-workers (2015) conducted a single blind study in 98 patients (19 in Austria, 32 in Greece and 37 in Italy) undergoing osteosynthesis for closed fractures. The patients received vancomycin-loaded disposable antibacterial coating (DAC – antibacterial-loaded hydrogel coating) while the control group did not receive the coating. Pre- and post- operative assessment of laboratory tests, clinical score (SF-12 score), wound healing (ASEPSIS score) and x-rays were performed at regular time intervals. It was found that there was no significant difference in wound healing and clinical scores, laboratory tests or in x-rays between the control group and the group that received vancomycin-loaded DAC at a mean of 6 months follow up. However, two cases of surgical site infections were reported in the control group that did not receive the coating (Logoluso *et al*., 2015). Lorenzo and co-workers (2014) also showed that implant coating with an antibacterial- loaded DAC hydrogel reduces bacterial populations and biofilm formation in vitro (Drago *et al*., 2014). Despite all these promising results, some of the shortcomings of these proposed techniques include limited chemical stability, local inflammatory reactions owing to the composition of

materials and lack of controlled release kinetics from the coatings (Crabtree *et al*., 2003; Walder *et al*., 2002; Kraft *et al*., 2000; Masse *et al*., 2000; Riley *et al*., 1995).

1.5.2 Bacterial inactivation using Ultraviolet (UV) light

The germicidal UV or UV-C light (100 – 280 nm), primarily at 254 nm which is the peak output of the mercury vapor lamps, is mutagenic to bacteria, viruses and other organisms (Kowalski *et al*., 2000) and hence is being regularly used for UV-sterilisation. The concept of airborne disinfection by UV light was first pioneered by William F. Wells in 1935. He irradiated aerosolized *Balantidium coli* with 254 nm radiation and showed that the airborne infectious organism was effectively killed in a short span of time (Wells, 1935). In 1960, Hart irradiated higher amounts of the bactericidal UV around the surgical site and instrument/supply tables at the Duke University hospital and reported a reduction in post-operative wound infections in clean cases from 11.62 % to 0.24 % (Hart, 1960). Owing to the initial successes, several studies have been reported since then with the use of germicidal UV (Lowell *et al*., 1980; Berg *et al*., 1991; Ritter *et al*., 2007).

In 1980, Lowell and co-workers demonstrated that the use of UV lamps reduced the infection rates post total hip replacement surgery from 3.06 % to 0.53 %. Berg and co-workers reported a reduction in bacterial CFU/m^3 from 7.67 resulting from laminar flow ventilation to 2.96 CFU/m^3 using 254 nm UV-C radiation. Ritter and co-workers (2007) conducted a detailed study over a period of 19 years taking into account 5980 joint replacement procedures and found that the use of UV light reduced the risk of infections following surgeries from 1.77 to 0.57 %. Although the use of UV light reduced bacterial burden and the risk of incidence of HAI among patients, it caused several other problems to exposed patients and medical personnel.

The exposed people developed erythema of the skin and conjunctivitis which led to the introduction of the use of fully covered protective clothing, eye protection wear and sun screen to be applied on any exposed areas, to protect against the light.

Lidwell and co-workers (1994) introduced safety limits in the use of UV light intensities; 30 $\mu W/cm^2$ is used though 300 $\mu W/cm^2$ did not show any adverse side effects. Although UV light shows remarkable reductions in airborne bacterial burden and incidence rates of infection, it is not widely accepted in the UK due to the requirement of protective accessories to be worn by the exposed medical personnel, including fully covering protective clothing that is too hot, heavy and uncomfortable for regular use, and protective eye wear (Gosden *et al*., 1998; Taylor *et al*., 1995). However, UV light systems are regularly used in operating theatres for disinfection purposes in the US and in Sweden (Ritter *et al*., 2007; Berg *et al*., 1991).

1.6 Bacterial inactivation using visible light

Although UV light has been successfully used to reduce the populations of airborne bacteria in an operating theatre, there have been several problems associated with the use of UV light in the presence of medical personnel and patients as explained in the previous section. Use of visible light of different wavelengths has also been shown to cause bacterial inactivation (Maclean *et al*., 2009) and the mechanisms involved in bacterial cell death are described below.

1.6.1 Electromagnetic spectrum of light

The electromagnetic spectrum consists of different components with different wavelengths and frequencies. These components are gamma rays, X-rays, ultraviolet light, visible light, infrared light, microwaves and radio waves (Figure 1.4). Gamma rays are high energy photons of shorter wavelength ranging between 0.00001 nm – 0.001 nm. These rays are commonly used for sterilising medical devices due to their bactericidal properties and also for diagnostic purposes in nuclear medicine imaging techniques. X-rays of wavelength approximately ranging between 0.001 – 10 nm are extensively used for medical imaging especially in generating radiographs, in computed tomography and radiotherapy. Since gamma rays and x-rays are ionising radiations, they are not often used for patient exposure.

The sunlight reaching the surface of the earth comprises a portion of the electromagnetic spectrum including ultraviolet, visible and infrared light. UV light of wavelength ranging from 100 – 400 nm is split into 3 components, UV-C (100 ~ 280 nm), UV-B (280 ~ 315 nm) and UV-A (315 ~ 400 nm). UV light (especially UV-A and UV-B) reaching the surface of the earth from the sun plays an important role in conditions like premature skin aging, skin cancers (damaging the cellular deoxyribonucleic acid (DNA) of the skin producing genetic mutations) and eye damage (cataracts). It also suppresses the immune system, reducing its ability to react to the above mentioned conditions.

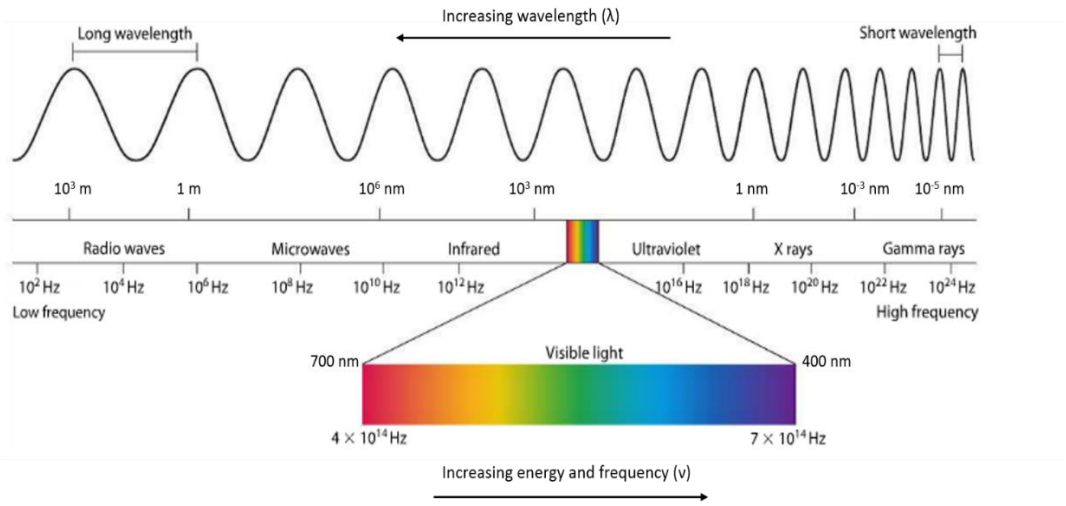

Fig 1.4: The Electromagnetic spectrum adapted from https://www.studyblue.com/notes /note/n/module-3-waves-and-the-electromagnetic-spectrum/deck/8054719)

Light of wavelength 400 – 700 nm is known as visible light. Wavelengths of 400 – 700 nm are visible to the human eye, hence the name visible light. Visible light (non-ionising radiation) has a variety of medicinal therapeutic applications. Phototherapy using high intensity blue-green light (~ 450 nm) is used to treat jaundice in new-born infants through the process of isomerisation of trans-bilirubin into the water-soluble cis-bilirubin isomer (Stokowski, 2006, Ennever *et al*., 1984). Blue light (peaks at 407 – 420 nm) has been shown to have anti-inflammatory and antibacterial properties, and has been used in the treatment of acne (Kawada *et al*., 2002; Sigurdsson *et al*., 1990). Narrow bandwidth blue light has also been proven to effectively reverse the symptoms of depression with a seasonal pattern in the case of seasonal affective disorder (Glickman *et al*., 2006). Red light of wavelength 630 nm, in combination with the systemic injection of a hematoporphyrin derivative, has resulted in normal

reepithelialisation in patients with psoriasis (Berns *et al*., 1984). Visible red light of wavelength 635 nm is also used in the treatment of cancer cells, and is known as photodynamic therapy (PDT), where the area of interest is targeted with the light in combination with a photosensitising agent. The photosensitising molecule first tested in humans and being commonly used in cancer therapy is a hematoporphyrin derivative (Figure 1.5) that is well retained by tumour tissues (Cao *et al*., 2009; Kessel, 1982). PDT is also used for treating arthritis, psoriasis, atherosclerosis, age-related macular degeneration and restenosis in veins and arteries (Hamblin & Hasan, 2004). PDT can also be used to inactivate microorganisms and is termed Photodynamic inactivation (PDI) or Photodynamic Antimicrobial Chemotherapy (PACT).

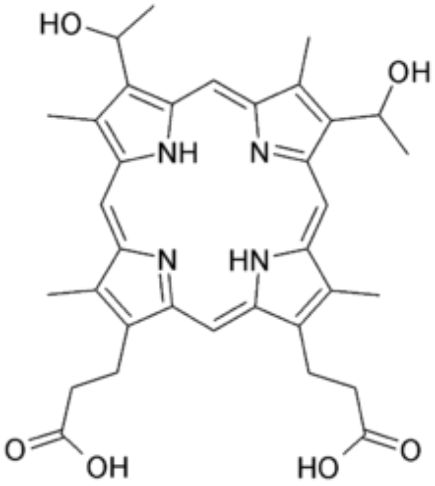

Fig. 1.5: Molecular structure of a hematoporphyrin IX molecule that is commonly used in cancer therapy. (Source: http:// www.sigmaaldrich.com /catalog /product/aldrich/258334?lang=en&region=GB)

1.6.2 Porphyrins

One of the main types of photosensitisers that can be used in PDT/PDI are porphyrins. Porphyrins are a group of naturally occurring heterocyclic macrocycle organic compounds composed of 4 pyrrole subunits, that are interconnected at their α-carbon atoms via methine bridges, and unsaturated =CH- groups (Figure 1.6). Porphyrins play a vital role in a variety of biological processes such as pigmentation changes, photosynthesis and catalysis (Goldoni, 2002). Each pyrrole subunit consists of one nitrogen atom and four carbon atoms, each of which is bonded to a hydrogen atom. The parent and the simplest form of porphyrin is called porphin, and substituted porphines are known as porphyrins. This structure provides a vacant site at its centre which can incorporate metal ions forming metalloporphyrins. The function of each porphyrin is decided by the type of metal ion incorporated and any additional side chains.

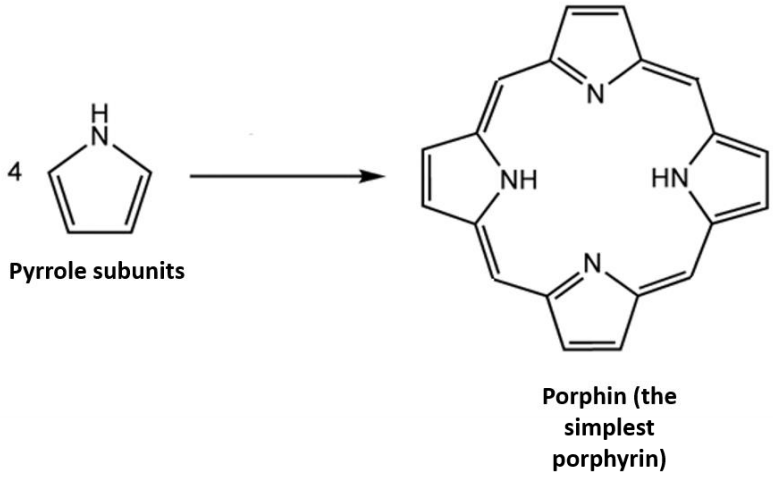

Fig. 1.6: Molecular structure of a pyrrole subunit and porphin molecule adapted from https://en.wikipedia.org/wiki/Porphyrin.

Haem (protoporphyrin IX) (Figure 1.7), the pigment in red blood cells, involves the incorporation of an iron atom in the middle, is one of the best known porphyrins and is responsible for transportation of oxygen throughout the entire body. The incorporation of a magnesium atom forms chlorophyll and is responsible for photosynthesis.

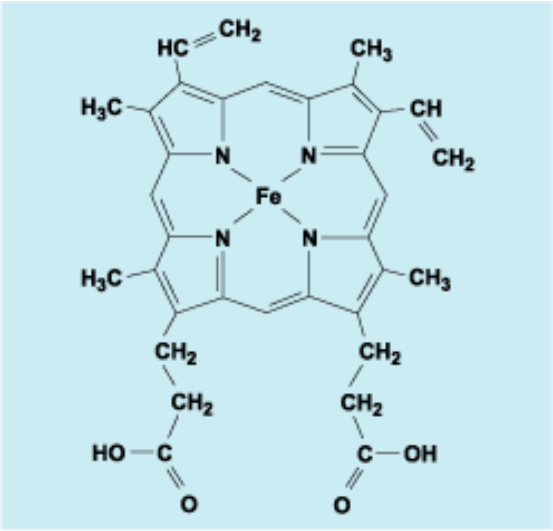

Fig. 1.7: Molecular structure of protoporphyrin IX molecule (specific porphyrin present in Haem B group of haemoglobin) containing an iron (Fe) atom in the middle bonded to four interior nitrogen atoms. (Source: http://www.glogster.com/ctilley93/the-dracula-gene/g-6nadsiedoo6culk0plql9a0)

Krasnovskii and co-workers (1982) found that the metalloporphyrins were not effective in photodynamic inactivation, since the metal atom quenches the production of reactive oxygen species (ROS) rapidly, which would otherwise induce cell damage and death. Later, Evensen (1995) identified that the free base porphyrin molecules (precursors to metalloporphyrins) present in organisms (Wijesekera and Dolphin, 1985) took part in photodynamic inactivation.

The typical absorption spectrum of a porphyrin (Figure 1.8) consists of a Soret band and 4 Q-bands. If activation of naturally occurring porphyrins such as haem, cytochromes and melanin present in tissues is required, longer wavelengths of light are necessary (increasing penetration with increasing wavelength) which would activate the outermost Q-band. It is clear from the absorption spectrum that the peak absorbance (Soret band) of a porphyrin molecule exists around 405 nm. Hence, the light that will cause most porphyrin excitation, generation of ROS and therefore effective bacterial kill, would be blue light. Table 1.9 shows the Soret bands (absorption peaks) of some of the porphyrin molecules studied. Though the peaks vary slightly, they still lie around the 405 nm range.

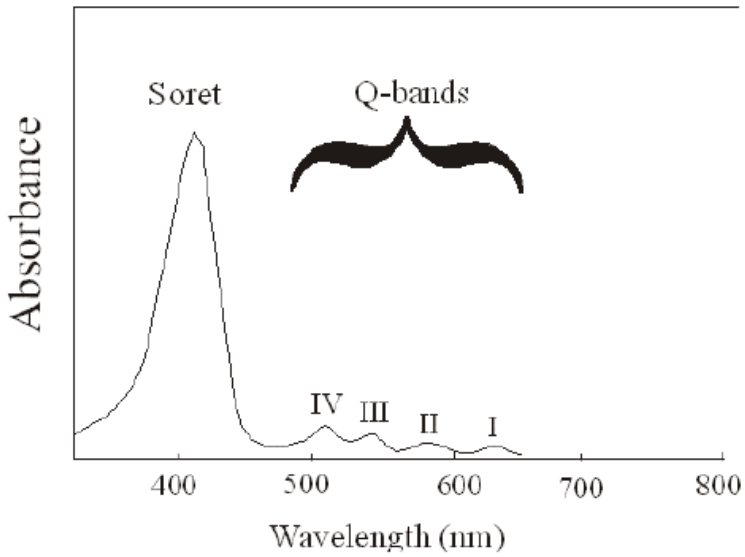

Fig. 1.8: Typical porphyrin absorption spectrum adapted from 'Photosensitisers in medicine, Kristian Berg, Norway, http://www.photobiology.info/Berg.html'.

Table 1.9: The absorption peaks of different porphyrin molecules (Rimington, 1960)

Porphyrin	Absorption peak (Soret max) (nm)
Aetioporphyrin I	399.5
Coproporphyrin III tetramethyl ester	399.5
Deuteroporphyrin dimethyl ester	399
Haematoporphyrin dimethyl ester	402
Porphin	396.5
Phylloerythrin methyl ester	415
Protoporphyrin dimethyl ester	407.5
Uroporphyrin I octamethyl ester (natural.)	406
Uroporphyrin III octamethyl ester (synthesised.)	405-406

The 4 Q-bands present in the spectrum are smaller absorption peaks ranging from wavelengths of approximately 500 to 650 nm and light in this region has been used previously for bacterial inactivation of bacteria (Wilson, 2004; Nussbaum *et al*., 2003). The most commonly used light for PDT in the presence of exogenous photosensitisers, is red light as it penetrates deeper into tissues (Figure 1.9) compared to other wavelengths in the visible spectrum. However, the intensity required to cause bacterial kill using red light will be higher than blue light as energy of light increases with decreasing wavelength.

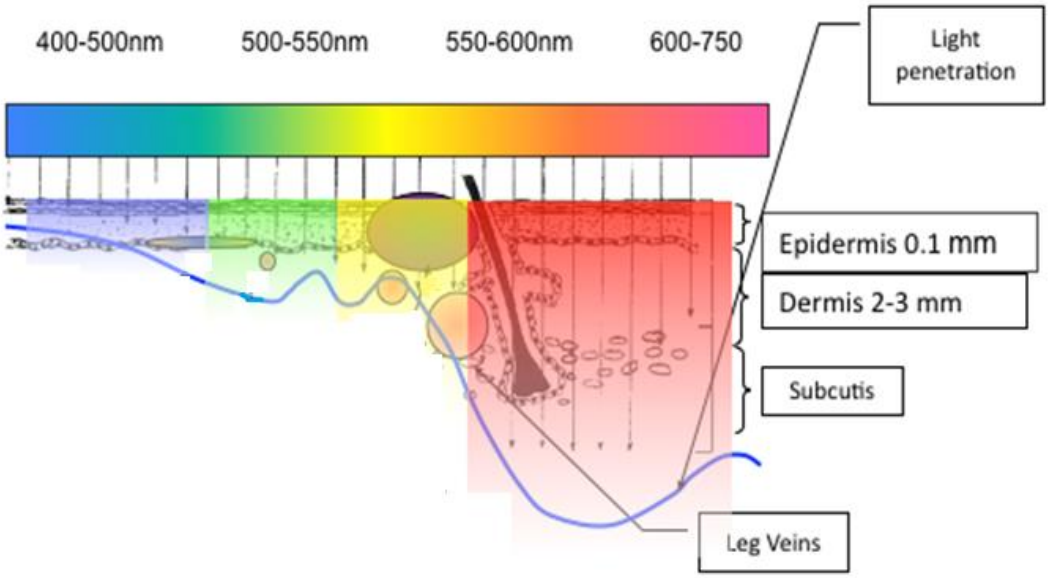

Fig. 1.9: Light penetration into the skin by different wavelengths of light adapted from http://porcelainfacespa.com/blog/ipl-a-solution-to-acne-pigmentation/.

1.6.3 Photodynamic Inactivation

PDI involves the administration of a photosensitising agent, oxygen, and subsequent irradiation of the photosensitising molecule by light of specific wavelength depending on the photosensitiser used. This results in a sequence of photochemical and photobiological processes within the targeted cells producing a variety of ROS. The ROS then interacts with the surrounding biomolecules within cells leading to cellular damage and eventually cell death via oxidative reactions (Dougherty *et al*., 1998; Hamblin & Hasan, 2004). The photosensitiser is excited from the steady ground state to an excited state when illuminated by light of a specific wavelength. This excited singlet state refers to a state where all the electrons present in the molecule are spin-paired, a measure of the angular momentum of the particle. The photosensitiser can either loose energy in the form of light producing fluorescence

and return to the ground state from the excited state, or can undergo intersystem crossing to a lesser energy but long lived triplet state (Figure 1.10). Only a small proportion of the excited photosensitiser molecules (~5%) return to the ground state, while the remaining molecules undergo intersystem crossing to the photosensitised triplet state (Perun *et al*., 2008).

The triplet state photosensitised photosensitiser molecules can enter into two different pathways, commonly known as type I and type II reactions (Figure 1.10). Type 1 reactions involve the interaction of excited triplet state photosensitiser molecules with the substrate molecule (amino acids present in the cell) to produce a variety of ROS, including superoxide and hydrogen peroxide. Type II reactions involve the interaction of excited triplet state photosensitiser molecules with the ground state triplet molecular oxygen ($^3O_2$) resulting in the production of highly reactive singlet oxygen ($^1O_2$) (Wijesekera & Dolphin, 1985). The type of ROS produced at different stages of the free radical chain reaction is shown in Figure 1.11, and these ROS eventually disrupt the cell membrane causing cell death (Schafer & Buettner, 1999; Thomas & Girotti, 1989). Examples of photosensitisers include porphyrins, dyes such as rose Bengal, methylene blue etc depending on the wavelength of light being used for inactivation.

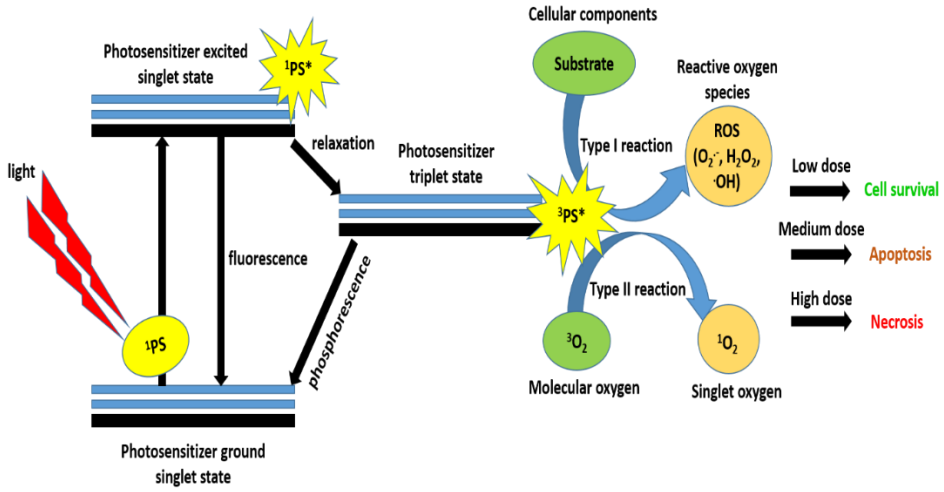

Fig 1.10: The schematic illustration of photodynamic therapy including the Jablonski diagram (Jablonski, 1933) adapted from Tegos *et al*., 2012.

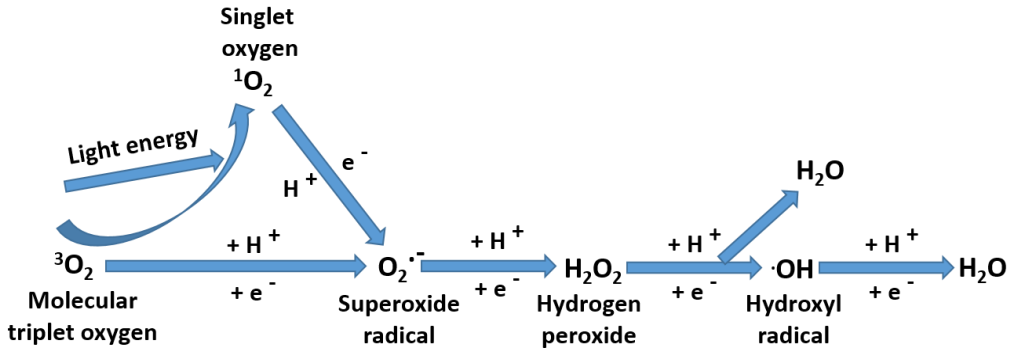

Fig. 1.11: Formation of different reactive oxygen species at different stages of the free radical chain reaction, adapted from Peter & Edward, 1984.

Singlet oxygen, a highly reactive oxygen species can interact with a variety of biomolecules (Fuchs & Thiele, 1998). The damage caused by PDI to cells is thought to be mainly through interactions between singlet oxygen and the cell membrane. Malik and Lugaci in 1987, exposed Friend erythroleukaemia cells pre-treated with 5 –aminolevulinic acid (ALA) (to enhance the endogenous porphyrin content of cells) to 380 nm light for 2 min and studied the effects after a few days, using scanning electron microscopy (SEM) and flow cytometry. Cells incubated with 5-ALA, after exposure to the light and a 2 day post-treatment period, showed membrane deformations and irregularities, while after a 5 day post-treatment period, severe membrane damage was observed. Flow cytometry results showed a rapid increase in cell volume (in response to membrane damage) and sudden influx of water into the damaged cell. SEM results showed no significant nuclear damage (Malik & Lugaci, 1987).

In another study by Ahn and co-workers (2004), SEM and transmission electron microscopy (TEM) were employed to study the PDT (630 nm light) effects on CaSki human cervical squamous cell carcinoma cells using a hematoporphyrin derivative as the photosensitiser. After one hour of treatment, disruption of the plasma membrane, cell shrinkage and cytoplasm leakage were observed, while the plasma membrane seemed to have undergone complete disintegration after a 6 hour treatment period. However, there was no evidence of nuclear membrane damage (Ahn *et al*., 2004). Recently, Nakanishi-Ueda and co-workers (2013) studied the effects of blue light emitting diode (LED) light exposure on retinal pigment epithelial cells to detect any cellular damage occurring in the cells and to understand the mechanism. It was found that blue light of wavelength 470 nm significantly reduced the cellular viability by

the generation of intracellular ROS as determined by confocal laser microscope image analysis. The ROS generation measured immediately after exposure, increased to 395 % of control at 50 J/cm^2 (Nakanishi-Ueda *et al*., 2013).

Albrecht and Gitter (2005) described an effective PDI approach for bacterial kill in which they utilised Safranin O as the photosensitiser and irradiated it with light at 530 nm to kill Gram-positive and Gram-negative bacteria present in the areas surrounded by complex media such as blood serum, saliva or blood. In another study, Hamblin and Demidova (2006) described the use of toluidine blue O (TBO), a non-porphyrin based photosensitiser for inactivating *Bacillus cereus* spores. In this study, *Bacillus cereus* spores were incubated with TBO for 10 minutes and irradiated with 635 nm light to achieve a killing ratio of more than 99.9% of these spores. Dai and co-workers (2009) studied the PDT of Gram-negative *Acinetobacter baumannii* in a burn wound infection using polyethylenimine chlorine (e6) (PEI-c_{e6}) conjugate and red light at wavelength 660 nm.

1.6.4 Bacterial cell inactivation by stimulation of exogenous/endogenous porphyrins using blue light

The bacterial photo-inactivation induced by different light sources decreases with increasing illumination wavelength (Nitzan & Ashkenazi, 1999; Nitzan & Ashkenazi, 2001). Nitzan and Ashkenazi (1999) studied the effects of blue light (400 – 450 nm), green light (480 -550 nm) and red light (600 – 700 nm) on *Deinococcus radiodurans* using two different porphyrin derivatives, the cationic 20a and the natural derivative 14a. Strong photodynamic bacterial effects on *D. radiodurans* were achieved for both photosensitisers, e.g for cationic 20a

photosensitiser, 5 J/cm^2 blue light resulted in a 7 log reduction in cell viability, while 35 J/cm^2 of green light and 85 J/cm^2 of red light were required to obtain similar reductions. Blue, green and red light were also tested on antibiotic-resistant bacteria including *Acinetobacter baumannii* and *Escherichia coli* using cationic photosensitiser 20a and total eradication of both bacteria was obtained (7 J/cm^2 for *A.baumannii* and 9 J/cm^2 for *E.coli)* using a 407 nm blue light, while a 8 or 16 -20-fold higher light intensity, respectively, was required for total eradication of both bacteria using green or red light (Nitzan and Ashkenazi, 2001).

Guffey and Wilborn (2006) studied the effects of 470 nm blue light of doses 1, 3, 5, 10 and 15 J/cm^2 on *Pseudomonas aeruginosa* and *Staphylococcus aureus*. They found that blue light killed *Pseudomonas aeruginosa* effectively (96.5 % reduction) at all doses administered, while being effective at 10 and 15 J/cm^2 for *Staphylococcus aureus* (62 % reduction). In another study conducted by Lipovsky and co-workers, the effects of 415 nm and 455 nm blue light on *S.aureus* and *E.coli* (Lipovsky *et al*., 2010) were investigated. They found that exposing *S.aureus* to 415 nm blue light for 20 minutes at a dose of 120 J/cm^2 resulted in a 90 % reduction in viability while a dose of 60 J/cm^2 resulted in 50 % reduction. They also showed that blue light of wavelength 455 nm at 120 J/cm^2 caused only a 50 % reduction in *S.aureus* viability. A 98 – 99.9 % reduction in *E.coli* viability was achieved with 415 nm after 10 minutes of illumination, while a 90 % reduction was achieved with 455 nm blue light after 20 minutes of illumination (Lipovsky *et al*., 2010). In 2013, Dai and co-workers demonstrated that blue light of wavelength 415 nm rescued mice from potentially fatal *Pseudomonas aeruginosa* burn infection. In their study they first created burns on the dorsal surface of adult 7 – to – 8 week old female BALB/c

mice weighing 17 – 21g, with a preheated brass block, resulting in third degree burns. Then, 3×10^6 CFU of bacterial suspension was topically applied to the eschar of the burn. After bacterial inoculation onto the burn, the burnt region was exposed to 415 nm blue light at 55.8 J/cm^2 (14.6 mW/cm^2 for 30 minutes). They found a complete elimination of bacterial luminescence after exposure to 55.8 J/cm^2 of 415 nm blue light. Though the mouse skin exposed to 55.8 J/cm^2 of 415 nm blue light showed swelling of basal cell nuclei and slight oedema in the upper dermis after immediate exposure, after 48 h post-treatment period, the epithelium returned to its normal composition. In addition to these results, it was also found, using the terminal deoxynucleotidyl transferase dUTP nick end labelling (TUNEL) assay that no DNA damage was observed up to 48 h post light treatment and that intracellular coproporphyrin III and/or uroporphyrin III was associated with the blue light inactivation of *Pseudomonas aeruginosa*, as the fluorescence spectra of the bacterial cells dissolved in NaOH-SDS, peaked at 613 and 667 nm, which are very close to the typical florescence emissions of coproporphyrin III and uroporphyrin III, when excited at 405 nm (Dai *et al*., 2013).

Inducing bacterial cell damage through light exposure does not necessarily require the use of external photosensitising agents such as 5-ALA or hematoporphyrins as several bacterial strains contain high levels of porphyrins, naturally. These naturally produced porphyrins can be stimulated to generate highly reactive singlet oxygen and other ROS similar to the stimulation with external photosensitisers. Ashkenazi and co-workers successfully demonstrated the inactivation of *Propionibacterium acnes* involving the illumination of endogenous coproporphyrin using blue light of wavelength 407- 420 nm at 75 J/cm^2. This blue light exposure resulted in a decrease

of two orders of magnitude in cell viability (Ashkenazi *et al*., 2003). Several species of bacteria have been shown to be inactivated using blue light illumination involving the excitation of endogenous porphyrins and are summarised in Table 1.10.

Table 1.10: Examples of bacterial species susceptible to blue light irradiation in the absence of exogenous photosensitisers.

Bacterial species	Wavelength (nm)	Dose (J/cm^2)	log_{10} reduction	Reference
Acinetobacter baumannii	405 (± 5)	108	4.2	Maclean *et al*., 2009
Acinetobacter baumannii	415 (± 10)	70.2	4	Zhang *et al*., 2014
Clostridium perfringens	405 (± 5)	45	4.4	Maclean *et al*., 2009
Enterococcus faecalis	405 (± 5)	216	2.6	Maclean *et al*., 2009
Escherichia coli	407 - 420	75	2	Ashkenazi *et al*., 2003
Fusobacterium nucleatum	450 - 480	94	6	Feuerstein *et al*., 2005
Helicobacter pylori	405 (± 2)	32	5	Ganz *et al*., 2005
Helicobacter pylori	405 (± 5)	30	5	Hamblin *et al*., 2005
Klebsiella pneumoniae	405 (± 5)	180	4.2	Maclean *et al*., 2009
Methicillin resistant staphylococcus aureus	405 (± 5)	45	5	Maclean *et al*., 2009
Methicillin resistant staphylococcus aureus	415 (± 10)	170	4.75	Dai *et al*., 2013
Porphyromanas gingivalis	450 - 480	62	6	Feuerstein *et al*., 2005
Prevotella spp.	488 -514	80	4	Henry *et al*., 1996
Prevotella intermedia	380 -520	4.2	5	Soukos *et al*., 2005
Prevotella nigrescens	380 -520	4.2	5	Soukos *et al*., 2005
Propionibacterium acnes	407 – 420	75	2	Ashkenazi *et al*., 2003
Proteus vulgaris	405 (± 5)	144	4.7	Maclean *et al*., 2009
Pseudomonas aeruginosa	405 (± 5)	180	3.9	Maclean *et al*., 2009
Pseudomonas aeruginosa	415 (± 10)	109.9	7.64	Dai *et al*., 2013
Staphylococcus aureus	405 (± 5)	36	5	Maclean *et al*., 2009
Staphylococcus epidermidis	405 (± 5)	42	4.6	Maclean *et al*., 2009
Streptococcus pyogenes	405 (± 5)	54	5	Maclean *et al*., 2009

Complete inactivation of different species of bacteria requires different intensities of light and this could be due to the fact that different bacteria contain different concentrations of porphyrins (Lipovsky *et al*., 2009). Lipovsky and co-workers exposed two different clinical isolates of *Staphylococcus aureus* (Methicillin-resistant and Methicillin-sensitive) to wavelengths of 400 – 800 nm broadband visible light at 300 mW/cm^2. They found that a dose of 180 J/cm^2 for an exposure period of 10 minutes resulted in 99.8 % reduction in cell viability in methicillin-sensitive strain of *Staphylococcus aureus*, while the same dose resulted in just a 55. 5 % reduction in cell viability in methicillin-resistant strain of *Staphylococcus aureus.* The experiments of Maclean *et al* involved the exposure of *Staphylococcus aureus* to 630 J/cm^2 (350 mW/cm^2 for 30 minutes) broadband visible light and achieved a 5-log reduction in cell population. They identified that the highest $\log_{10}$ reductions were achieved in the 405 ± 5 nm region, using narrow band pass filters to identify the effective bactericidal wavelength to within 10 nm (Maclean *et al*., 2008).

Maclean and co-workers later established that a range of bacterial species was susceptible to inactivation by blue light at 405 nm wavelength. Of the range investigated, methicillin –sensitive *Staphylococcus aureus* was demonstrated to be the most susceptible followed by methicillin-resistant *Staphylococcus aureus* and *Staphylococcus epidermidis* (Maclean *et al*., 2009). Nitzan and co-workers (2004) identified higher production of coporphyrin in gram-positive bacteria (six times higher concentrations in *Staphylococcus aureus* and *Staphylococcus epidermidis* compared to gram-negative species) and this could be a possible reason for the visible-light inactivation being more effective in gram-positive bacteria than in gram-negative bacteria. For example, *E.coli*, a common cause of gastrointestinal infections

has been demonstrated to be less susceptible to visible light inactivation (Maclean *et al*., 2009).

The gram-negative species did not show a predominant porphyrin, but rather produced approximately equal concentrations of different porphyrins including coporphyrin, protoporphyrin, uroporphyrin, and 5- and 7- carboxy porphyrin (Nitzan *et al*., 2004). Since each different porphyrin exhibits a slightly different absorption peak, lack of a predominant porphyrin in gram-negative bacteria is possible and this could result in the requirement of higher doses of blue light exposure to induce effective bacterial inactivation in gram-negative bacteria.

1.6.5 Mammalian cell susceptibility to blue light

The doses of blue light required to kill the less susceptible bacterial species is high and the effect that these doses have on mammalian cells is not fully understood. Mammalian cells have shown susceptibility to visible light induced damage in earlier studies. McDonald and co-workers (2011) exposed fibroblast-populated collagen lattices (FPCL) to 405 nm light at 0.5, 1.8 and 15 mW/cm^2 for 1 h during the lag phase of the cells (day 0), the active phase (day 3) and the slow contraction phase (day 5), to study the effects of light on wound healing. They found that FPCLs exposed to 0.5 and 1.8 mW/cm^2 during day 0 and day 3, continued contracting without any inhibitory effects while FPCLs exposed to 15 mW/cm^2, stopped contracting. Exposure of FPCLs to 15 mW/cm^2 on day 5 after FPCLs had reached maximum contraction, maintained ~ 72% contracted size (McDonald *et al*., 2011). The MTT assay results showed that there was no significant difference in cell numbers in FPCLs compared to unexposed controls, for up to 24, 72 and 120 h post

treatment, when exposed to 0.5 and 1.8 mW/cm^2 of 405 nm light on day 0, 3 and 5 respectively. However, FPCLs upon exposure to 15 mW/cm^2 on day 0, 3 and 5 showed a 73%, 23% and 84% decrease in viable cell number respectively, when compared to untreated controls (McDonald *et al*., 2011).

Godley and co-workers found that blue light of wavelength (380 – 550 nm) induced mitochondrial DNA damage in human primary retinal epithelial cells when exposed at 2.8 mW/cm^2 for up to 3 h (Godley *et al*., 2005). Taoufik and co-workers studied the effect of blue light on proliferation of human gingival fibroblasts and found a mild inhibition in the proliferation of cells (Taoufik *et al*., 2008). Similarly, hepatocytes (Malik and Lugaci, 1987) and keratinocytes (Pflaum *et al*., 1998) have also shown their susceptibility to blue light induced damage. Despite their susceptibility, mammalian cells possess strong protective defense mechanisms to withstand higher levels of oxidative stress compared to bacteria (Bouillaguet *et al*., 2008). The singlet oxygen produced upon excitation of a porphyrin based photosensitiser, interacts with unsaturated lipids present in the membrane forming lipid hydroperoxides (LOOH), and this ultimately disrupts the cell membrane. Wang and co-workers showed that phospholipid hydroperoxide glutathione peroxidase eliminates the LOOH preventing membrane damage (Wang *et al*., 2001). Enzymes and antioxidants including superoxide dismutase, peroxiredoxins, ascorbic acid and α-tocopherol play an important role in preventing cellular damage in mammalian cells either alone or in combination with β-carotene (Bohm *et al*., 2001; Marin-Garcia, 2005; Pflaum *et al*., 1998).

1.7 Environmental Decontamination system (EDS) using 405 nm High Intensity Narrow Spectrum (HINS) violet-blue light for bacterial inactivation

Maclean and co-workers (2010) studied the performance efficacy of a HINS light environmental decontamination system (HINS-light EDS) installed in a hospital isolation room used to treat burn patients, in Glasgow Royal Infirmary (GRI), Glasgow, UK. Two ceiling-mounted HINS-light EDS emitting 405 nm violet blue light at 0.5 mW/cm^2 were used to permit continuous environmental disinfection throughout the day. They demonstrated that the use of HINS-light EDS over a 24 h period, resulted in ~ 90% reduction in surface bacterial levels including *Staphylococcus aureus* and methicillin-resistant *Staphylococcus aureus*, when the room was unoccupied, and between 56 – 86 % reductions were achieved for over a six-day period when the room was occupied by an MRSA-infected burns patient (Maclean *et al*, 2010). The reductions achieved were found to be greater than the reductions achieved by normal infection control and cleaning activities alone. Bache and co-workers (2012) also studied the efficacy of HINS-light EDS for continuous disinfection of the inpatient isolation rooms and the outpatient clinic in the burn unit in GRI. The inpatient studies showed a significant 27 – 75 % reduction in bacterial levels, while the outpatient studies during clinics demonstrated a 61 % reduction of bacterial contamination on surfaces throughout the room. In GRI, HINS-light EDS systems installed in an isolation room within the vascular ward occupied by a MRSA +ve patient, resulted in a significant 58% reduction of total *staphylocooci* in the room area while in an ICU resulted in an average 53% reduction of total viable bacteria across the whole room (Booth *et al*., 2010).

1.8 Summary

From earlier studies and statistics, it is clear that HAI in patients is an expensive and significant problem in spite of the use of modernised equipment in hospitals for sterilisation and cleaning purposes. HAI in patients post orthopaedic surgeries is identified as one of the serious complications to be treated in hospitals. Bacterial airborne contamination seems to be one of the prime sources for the incidence of HAI. It has been successfully demonstrated that exposure to blue light can cause significant reductions in bacterial counts in both gram positive and gram negative bacteria that are responsible for causing these infections. Previous studies involving the exposure of bacterial strains to low intensity 405 nm HINS violet – blue light using an environmental decontamination system, have shown significant bacterial inactivation in hospital wards. Hence, the use of 405 nm light could potentially lower the bacterial burden in operating rooms, thereby reducing the incidence of HAI in patients resulting from SSI. It is desirable to reduce the risk of HAI occurring post orthopaedic surgeries, but if the intensities and doses of 405 nm light required for quicker bacterial inactivations are high, then significant damage may occur to the exposed mammalian tissues as well, thereby limiting the use of 405 nm light in an operating environment.

Hence, the aim of this research is to find out if higher intensities/ doses of 405 nm HINS violet-blue light could be used in a hospital environment i.e. operating theatres, especially during orthopaedic surgeries in the presence of medical personnel and patients, for safe decontamination. Identifying a threshold dose of 405 nm HINS light that is bactericidal to a variety of HAI causing bacterial strains, as well as safe

for mammalian cell exposure would be essential for facilitating a safer decontamination procedure.

1.9 Research objectives

As previously described, a common mode of HAI is surgical site infection, especially infections occurring post implantation of medical devices e.g. post joint replacement surgeries. The use of 405 nm HINS-light during implantation surgeries may lower the bacterial burden in an operating environment, thereby reducing the risk of HAI. The use of light during these joint replacement procedures, however, involves the exposure of mammalian cells, especially osteoblasts, cells involved in bone growth and development and any harmful effects on the function of osteoblasts would affect the integration of implant into the hip/knee joint thereby affecting the stability of hip/knee replacement.

The main aim of this study is to find a safe threshold dose of 405 nm HINS light that does not induce any significant damage to mammalian cells, i.e.; osteoblasts (bone cells), but is still bactericidal to a variety of clinically related bacteria responsible for causing HAI, and hence could have the potential to be developed for continual decontamination during arthroplasty surgery.

The research objectives are as follows.

- Investigate whether the adverse effects of 405 nm HINS light on mammalian cells are dose dependent.

- Establish a safe threshold dose for use of 405 nm light in an operating environment by studying (i) the cell alkaline phosphate activity (ALP), (ii) the cell metabolic activity and (iii) the cell proliferation rate
- Evaluate inactivation of different strains of HAI causing bacteria by exposure to 405 nm light
- Quantify the reduced glutathione (GSH) and oxidised glutathione (GSSG) content of the osteoblasts post different exposure periods to 405 nm light to find out if there is any oxidative damage to cells.
- Quantify the production of ROS using carboxy-H_2DCFDA in osteoblasts and bacterial cells exposed to 405 nm light at different exposure periods/doses
- Determine the viability and metabolic activity of the osteoblasts in the presence of various scavengers of ROS, for different doses of 405 nm light exposure
- Quantify the viability and ROS production of bacterial cells at different doses in the presence of the same ROS scavengers
- Measure the 405 nm light component that is already present in the orthopaedic operating theatre light spectra at different heights from the surgical table.
- Investigate the 405 nm light spectra of different 405 nm LEDs, to identify the best array among those available.
- Propose 3D models showing the ideal positioning of 405 nm LEDs in an operating theatre to facilitate efficient decontamination of different areas.

Chapter 2

MATERIALS AND METHODS

The following chapter explains the materials and methods that are common throughout this research work. Alterations, if any, to the general methods are explained in the appropriate chapters. Methods explicit to each chapter are detailed in the materials and methods section of that appropriate chapter.

2.1 405 nm HINS light System

2.1.1 405 nm light system set-up

The light systems used in this study (Figure. 2.1) emitted high intensity 405 nm violet blue light from the visible spectrum. Each device consisted of an array of nine 405-nm light-emitting diodes (LEDs) (GE Illumination – Vio GE-VHD-1A-3D8), with a peak wavelength of 405 nm and full-width half-maximum (FWHM) of 14 nm. The optical emission spectra of the systems were measured using a spectrometer (model HR4000, Ocean Optics) and Originpro 2015 software, and are shown in Figure 2.2. Two identical systems (termed ‘device 1’and ‘device 2’) were constructed in order to allow simultaneous experiments to be conducted.

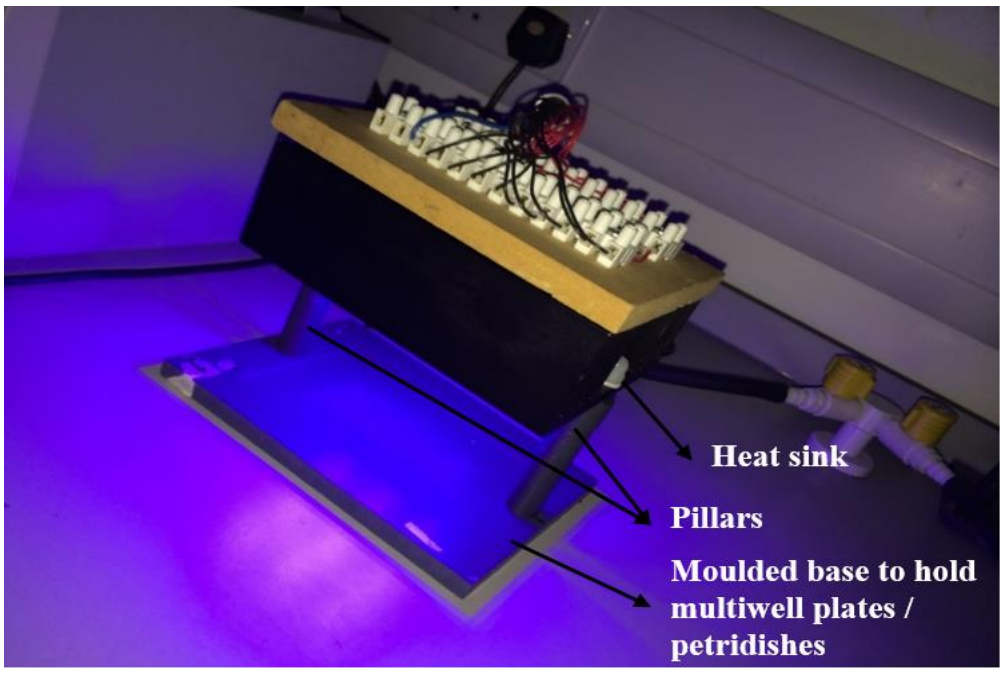

Fig. 2.1: 405 nm HINS light system

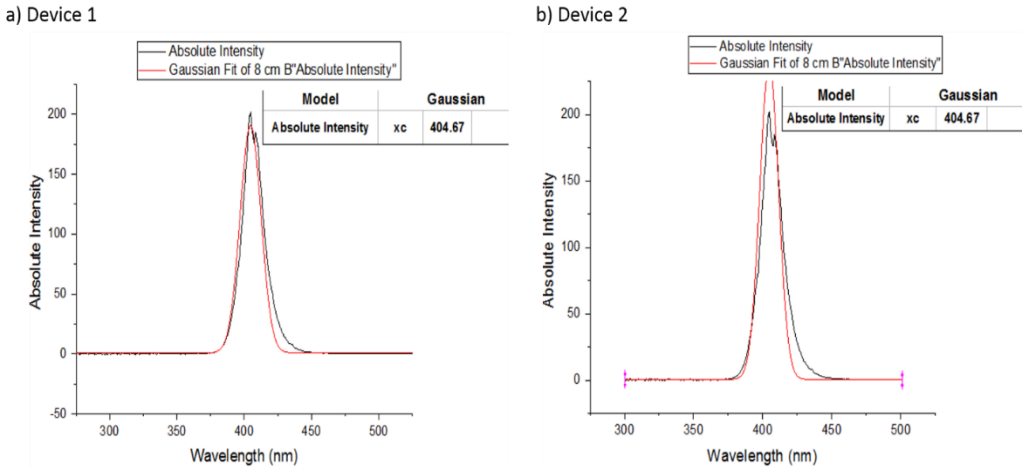

Fig. 2.2: Emission spectrum of 3 × 3 array of uncapped 405 nm LEDs for (a) device 1 and (b) device 2 at a distance of 8 cm from the light source. The term 'Model' refers to the parameter 'Absolute Intensity' that is recorded and the graph of 'Guassian' refers to the normalized symmetric bell curve measuring the peak output at the centre of the curve.

The LEDs used in these systems were purchased as warm white LEDs, however the hemispherical phosphor coated caps were carefully removed to expose three 405 nm diodes. The uncapped LEDs were arranged in a 3 × 3 grid pattern (6 cm× 6 cm) (Figure 2.3), and bonded to a heat sink for thermal management, thus preventing sample heating during light exposure. The heat sink was supported by two pillars above a moulded base designed to fit a multiwell plate in order to fix the position of the sample plates directly below the LEDs. Preliminary experiments suggested that a distance of 8 cm between the samples and the light source, produced the optimal intensity across the central wells of the culture plate. This was manufactured in the Electronic and Electrical Engineering department of the University of Strathclyde. The 405 nm LEDs were powered by Switch Mode Power Supply (SMPS; Rapid Electronics model number 85-1901, UK).

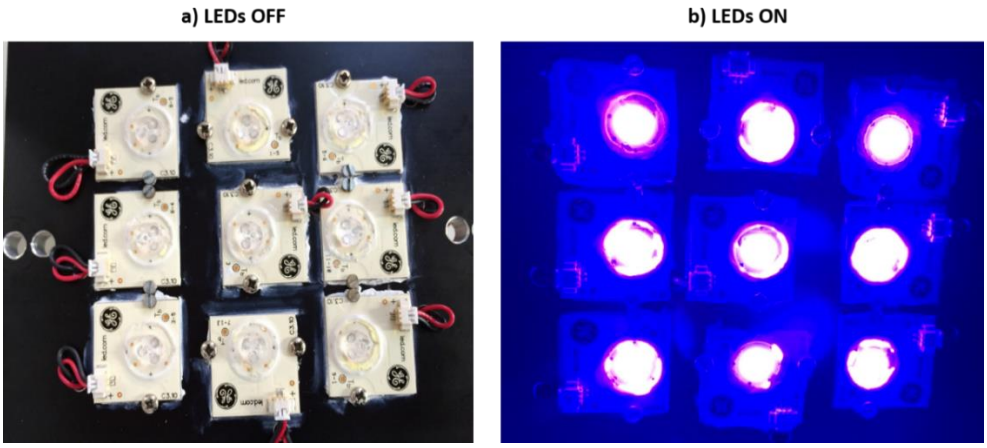

Fig. 2.3 The 3 × 3 grid pattern of (a) 405 nm LEDs off and (b) 405 nm LEDs on, used for exposure of mammalian and bacterial cells to 405 nm HINS light.

2.1.2 Irradiance distribution across culture plates

The light source was set at a height of 8 cm above the base plate (where the multiwell sample plate would be positioned) based on previous work (McDonald *et*

al., 2011), and the LEDs were set at a current of 0.550 A and a voltage of 9.24 V. The irradiance distribution across multiwell plates was measured using a radiant power meter (Model 70260, Oriel Instruments) and photodiode detector (model 1Z02413, Ophir), calibrated at 405 nm. Using these values, 3-dimensional profiles of the light irradiance achieved across 12-, 24- and 96-well plates were plotted (Figure 2.4, 2.5 & 2.6, respectively). It was found that the middle 2 wells, middle 4 wells and the middle 16 wells in a 12 well, 24 well and 96 well plate, respectively, received uniform irradiance, therefore these wells were selected for use in the cell exposure experiments.

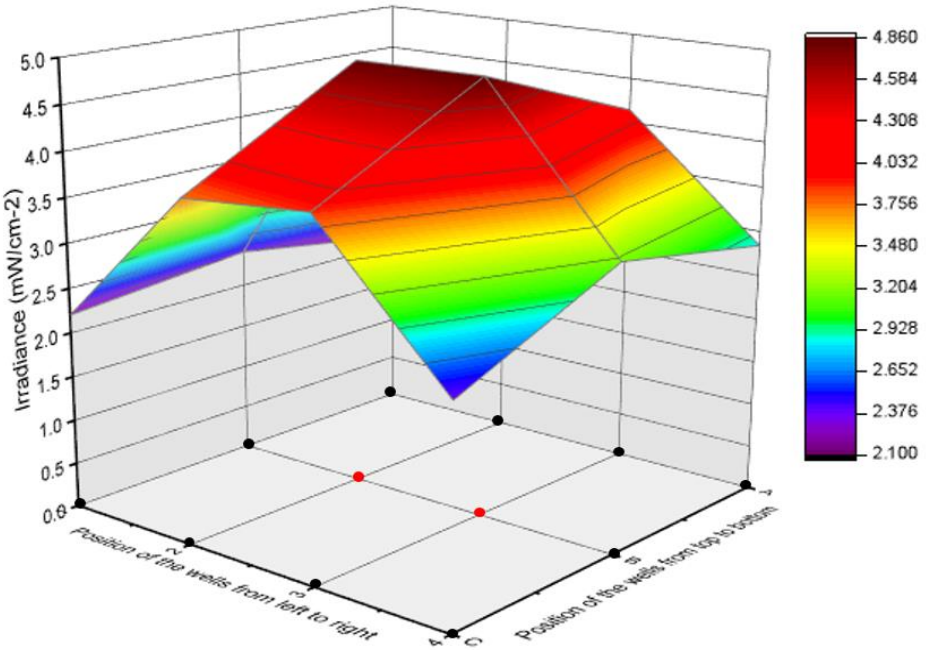

Fig.2.4 Average irradiance distribution across a 12-well plate when positioned 8 cm below the 405 nm HINS light treatment system. The LEDs were run using 0.550 A and 9.24 V. The black dots represent the unused wells and the red dots represent the 2 central wells that will be seeded with mammalian or bacterial cells for 405 nm light exposure. The intensity scale (on the right) refers to different power intensities received at different regions of the multi-well plate.

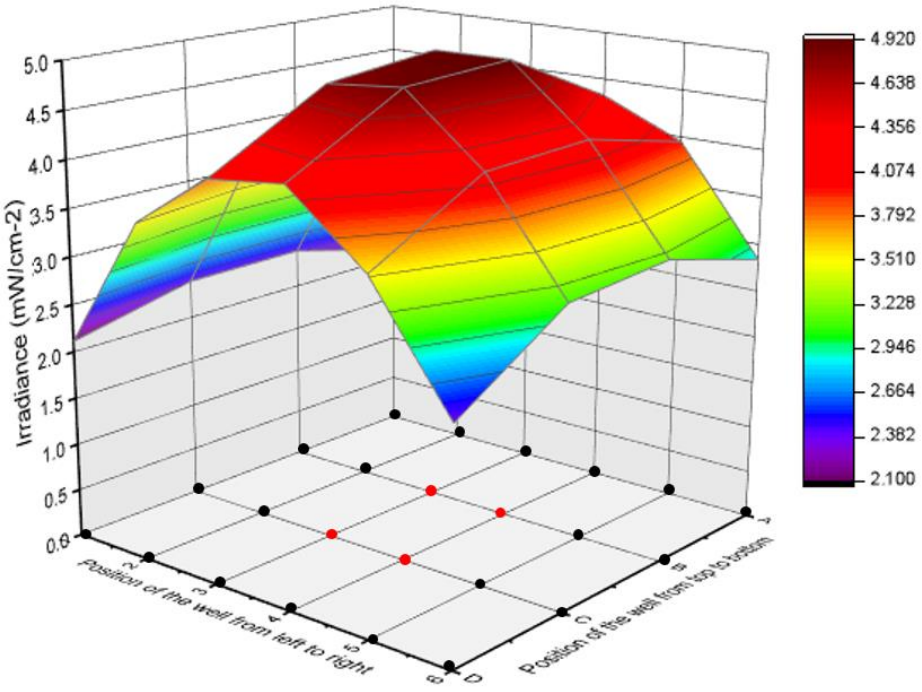

Fig.2.5 Average irradiance distribution across a 24-well plate when positioned 8 cm below the 405 nm HINS light treatment system. The LEDs were run using 0.550 A and 9.24 V. The black dots represent the unused wells and the red dots represent the 4 central wells that will be seeded with mammalian or bacterial cells for 405 nm light exposure. The intensity scale (on the right) refers to different power intensities received at different regions of the multi-well plate.

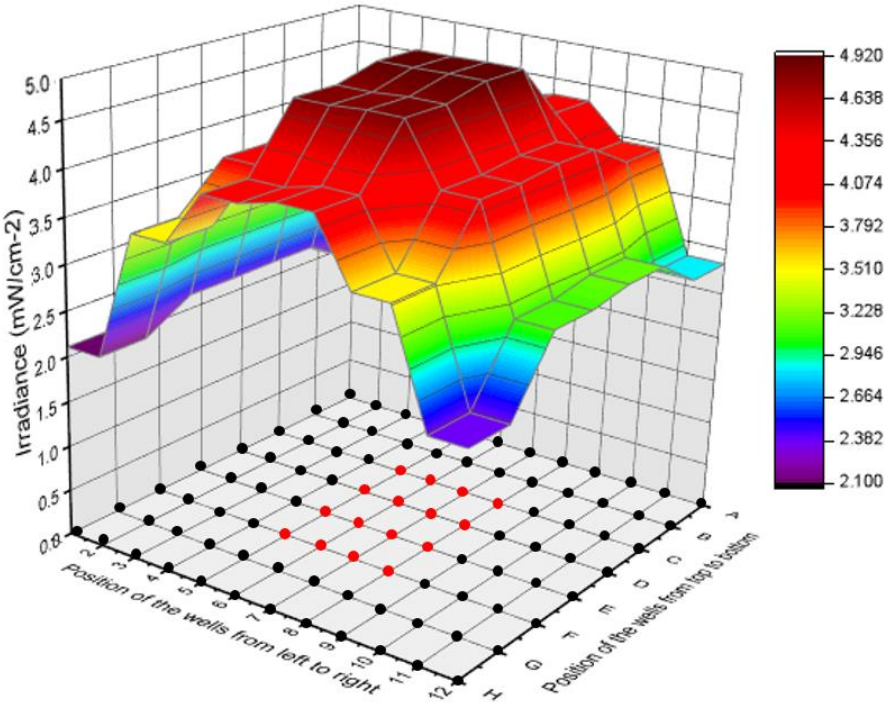

Fig.2.6 Average irradiance distribution across a 96-well plate when positioned 8 cm below the 405 nm HINS light treatment system. The LEDs were run using 0.550 A and 9.24 V. The black dots represent the unused wells and the red dots represent the 16 central wells that will be seeded with mammalian or bacterial cells for 405 nm light exposure. The intensity scale (on the right) refers to different power intensities received at different regions of the multi-well plate.

2.1.3 Irradiance/Exposure regimes – Calculation of Light dose

The 405 nm light doses used for mammalian and bacterial cell exposures were calculated using the formula,

$$\mathbf{E = P \times t}$$

where, E = Dose, measured in Joules/unit area (J/cm^2)

P – Power / Irradiance of light/unit area (W/cm^2)

t – Time of exposure (seconds)

2.2 Mammalian cell studies

2.2.1 Preparation of standard stock solutions

1) Versene

Versene was prepared by dissolving 12g of NaCl, 0.3g of KCl, 1.73g of anhydrous Na_2HPO_4, 0.3g of KH_2PO_4, 0.3g of EDTA and 4.5 ml of 0.5% solution of Phenol Red in 1.5 litres of distilled water. The solution was then sterilised in an autoclave at 121°C, 15 psi for 30 minutes and aliquoted into 20 ml universal bottles and stored at room temperature for use.

2) Tris Buffered Saline (TBS) for Trypsin stock

TBS was prepared by dissolving 4g of NaCl, 0.05g of Na_2HPO_4, 0.5g of glucose, 1.5g of Tris, 0.19g of KCl and 1.5 ml of 0.5% solution of Phenol Red in 500 ml of distilled water. The pH was set to 7.7 at room temperature with approximately 0.94 ml of concentrated HCl. Trypsin solution was then sterilised in an autoclave at 121°C, 15 psi for 30 minutes and added to give a final concentration of 0.25% (w/v),

50 ml of 2.5% stock. Later the solution was aliquoted into 20 ml universal bottles and stored at -20˚C.

3) Complete Dulbecco's Medium

To 500 ml of Dulbecco's Modified Eagle's Media (DMEM) ((Lonza, catalogue number BE12-604F), 10% (v/v) sterile Foetal Calf Serum (FCS) (PAA Laboratories, catalogue number A15-101), penicillin (50 units/ml), streptomycin (50 μg/ml) and 1% (v/v) of non-essential amino acids were added to be used for the cell growth.

2.2.2 Cell line culture

2.2.2.1 Mammalian cell passage and 2-D cell culture

Immortalised rat osteoblasts (OST 5) cells (isolated by SV40 transfection of neonatal rat calvarial osteoblasts in our laboratory by Prof H.Grant in the Department of Biomedical Engineering) were chosen to conduct the experiments with HINS light due to the robust nature of cells and in order to identify the potential of using 405 nm light for safe mammalian cell exposures during orthopaedic surgeries. These mammalian cells were cultured as monolayers in 25 cm^2 and 75 cm^2 rectangular tissue culture flasks in DMEM in a humidified atmosphere of 5% CO_2 in air at 37˚C. When the flasks were confluent after 4 days in culture, the medium was removed and 5 ml of the chelating agent, versene (0.02 % w/v) for a 25 cm^2 flask, or 10 ml for a 75 cm^2 flask, was added twice to wash the cell monolayer and remove any traces of serum. After removing the solution of versene from the flask, 1 ml (25 cm^2 flask) or 2 ml (75 cm^2 flask) of 0.05 % trypsin in versene (w/v) was added - just enough to cover the cell layer. The flask was left undisturbed for 2-3 minutes allowing the cells to detach themselves from the surface. Later 5 ml (25 cm^2 flask) or 9 ml (75 cm^2

flask) of complete DMEM was added to inhibit the action of trypsin, and pipetted up and down to break up any cell clumps using a 10 ml pipette. Later, the entire solution was transferred to a new 20 ml bottle. The bottle was gently shaken to ensure that the cells were evenly suspended throughout the solution. The volume of the solution was measured using a pipette and the cells were reseeded at the split ratio 1:10 in a 25 cm^2 small flask and 1:15 in a 75 cm^2 large flask. The flasks were then kept in the incubator set at 37˚C and 5 % CO_2 for 4 days. The small flasks were used for cell passage and large flasks were used for conducting experiments.

2.2.2.2 Cell counting and 405 nm light exposure

For 405 nm light exposures, cells from a 75 cm^2 large flask were trypsinised and counted using a haemocytometer before seeding at a seeding density of 5×10^3 cells/cm^2 in a 24-well plate and 2×10^4 cells/cm^2 in a 96-well plate. After the seeding process, the plates were left in the incubator overnight at 37°C. The following day, the medium was removed and replaced with Dulbecco's Phosphate- Buffered Saline (DPBS) (Lonza, UK) buffer (1 ml/ well for a 24 well plate and 200 µl/ well for a 96 well plate) before the seeded multiwell plates were exposed to set durations and irradiances of 405 nm light, using the treatment systems (Figure 2.1).

The medium was replaced with DPBS buffer for light exposure to avoid any possible generation of ROS facilitated by the components of the culture medium. It has been previously shown by Smith, in 2009 that the cell viability on exposure to visible and near-UV radiation was significantly reduced when exposed in culture medium when compared to phosphate buffered saline (PBS) (Sigma, UK). Tyrosine, folic acid and riboflavin were found to be some of the components present in the culture medium

that are responsible for generating ROS in the presence of 405 nm light (Grzelak *et al*., 2001).

Control plates were set up for all experiments, and were held under identical conditions but were non-light exposed. All experiments were carried out in an incubator at 37°C & 5% CO_2 (Figure 2.7) for defined time points. After exposure, the plates were removed, cells washed twice with DPBS, culture medium was added and the plates returned to the incubator for defined post treatment periods (48 h and 72 h) before conducting qualitative and quantitative studies.

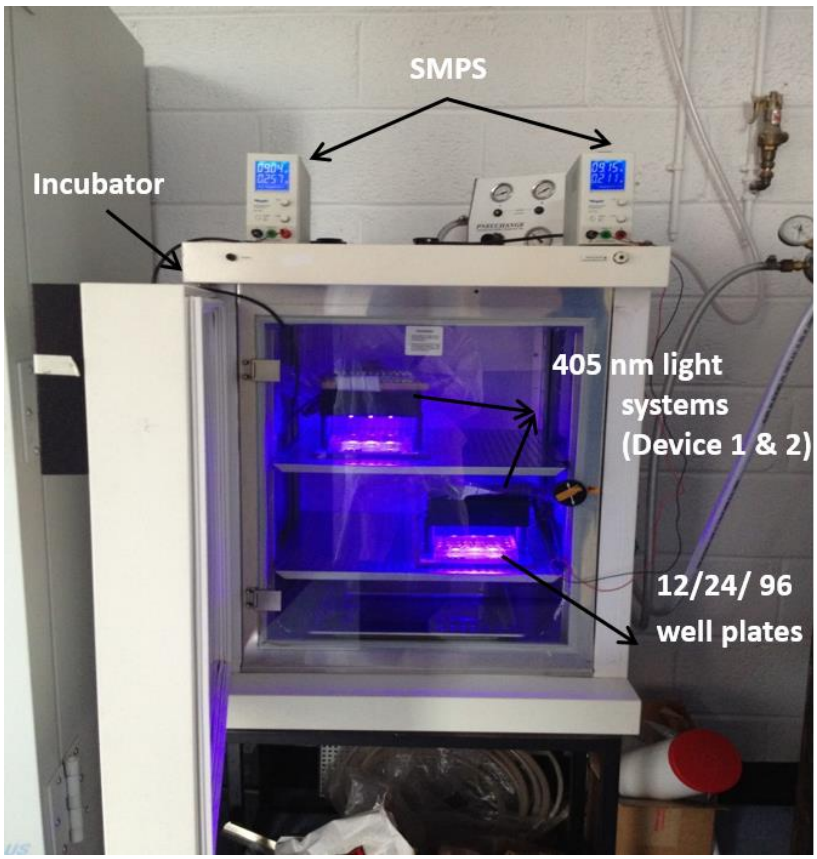

Fig. 2.7 shows the experimental set up for exposure of mammalian cells to 405 nm HINS light. The set up consists of 405 nm light systems each powered by a separate SMPS, placed inside an incubator maintained at 37°C and 5 % CO_2 with the multi-well plates placed underneath the light source. The unexposed controls were placed in another incubator under identical conditions without light exposure.

2.3 Bacterial cell studies

2.3.1 Preparation of standard growth media and diluents

1) Nutrient broth (CM0001, Oxoid Ltd, UK)

1.3 g of Nutrient broth was dissolved in 100 ml of distilled water in 250 ml flasks. The opening of the flasks was closed with cotton wool bungs which were then

covered with aluminium foil and labelled before autoclaving at 121°C for 15 minutes.

2) Nutrient agar (CM0003, Oxoid Ltd, UK)

7 g of Nutrient agar was dissolved in 250 ml of distilled water in 250 ml bottles. The bottles were then autoclaved at 121°C for 15 minutes. Immediately after autoclaving, the bottles of molten agar were held in a water bath at 48°C until cool enough to handle. The molten agar was then poured into sterile 55 mm diameter Petri dishes and allowed to set.

3) Phosphate Buffered Saline (PBS) Diluent (BR0014G, Oxoid Ltd, UK)

PBS was prepared by dissolving 1 PBS tablet per 100 ml distilled water, and sterilised by autoclaving at 121°C for 15 minutes. PBS diluent was prepared in volumes of 100 ml for re-suspension of bacterial cultures, and 9 ml for serial dilution of bacterial suspensions.

2.3.2 Bacterial strains used

The bacterial strains used in this study are listed in Table 2.1. The strains were all supplied from the bacterial culture collection held within The Robertson Trust Laboratory for Electronic Sterilisation Technologies (ROLEST) at the University of Strathclyde, and were purchased from either the National Collection of Type Cultures (NCTC), Collindale, UK, or the Laboratorium voor Microbiologie (LMG), Universiteit Gent, Belgium.

Table 2.1: Bacterial strains used throughout the study

Bacterium	Source and Type Culture Ref No	Gram Status
Staphylococcus aureus	NCTC 4135	Gram positive
Staphylococcus epidermidis	LMG 10474	Gram positive
Escherichia coli	NCTC 9001	Gram negative
Pseudomonas aeruginosa	LMG 9009	Gram negative
Klebsiella pneumonia	NCTC 09633	Gram negative
Acinetobacter baumannii	LMG 1041	Gram negative

2.3.3 Bacterial Cell culture

Bacterial strains are stored on frozen MicroBank beads at -20°C. To cultivate a stock bacterial culture, a bead was streaked onto an agar plate and incubated at 37°C for 24-hr. After incubation, a loopful of the resultant culture was streaked onto an agar slope and incubated at 37°C for 24-hr before storing at 4°C for use as the stock culture. To cultivate bacteria for experimental use, a sterile inoculation loop was used to transfer a small inoculum from the stock culture to 100 ml nutrient broth. The nutrient broth was then incubated at 37°C for 18 h under rotary conditions (120 rpm).

2.3.4 Preparation of bacteria for exposure to 405 nm light

a) Preparation of Bacteria:

Post-incubation, the resultant broth culture was dispensed into 2 × sterile 50 ml centrifuge tubes. The tubes were centrifuged at 4300 rpm for 10 minutes. After

centrifuging, the supernatant (liquid) was discarded, leaving the pellet of bacterial cells at the bottom of the tube. A sterile 100 ml bottle of PBS was taken and 2 ml of this was pipetted into each of the centrifuge tubes. A vortex was used to mix the pellet/PBS mixture so as to fully re-suspend the pellet in the PBS. The suspension was transferred back to the 100 ml bottle of PBS to achieve a starting population of approximately 10^9 colony forming units (CFU)/ml.

b) Exposure of Bacteria on Agar Surfaces:

Using serial10-fold dilutions, the cell suspension was then diluted to give a starting population of 10^3 CFU/ml (10^{-6} dilution). Samples (100 µl) were then pipetted onto 55 mm nutrient agar plates and spread evenly over the surface using L shaped spreaders, giving approximately 150 to 300 CFU/plate. Seeded agar plates were then exposed to 405-nm light for different periods of time at room temperature as shown in Figure 2.8. The control plates were left on the bench with no 405 nm light exposure.

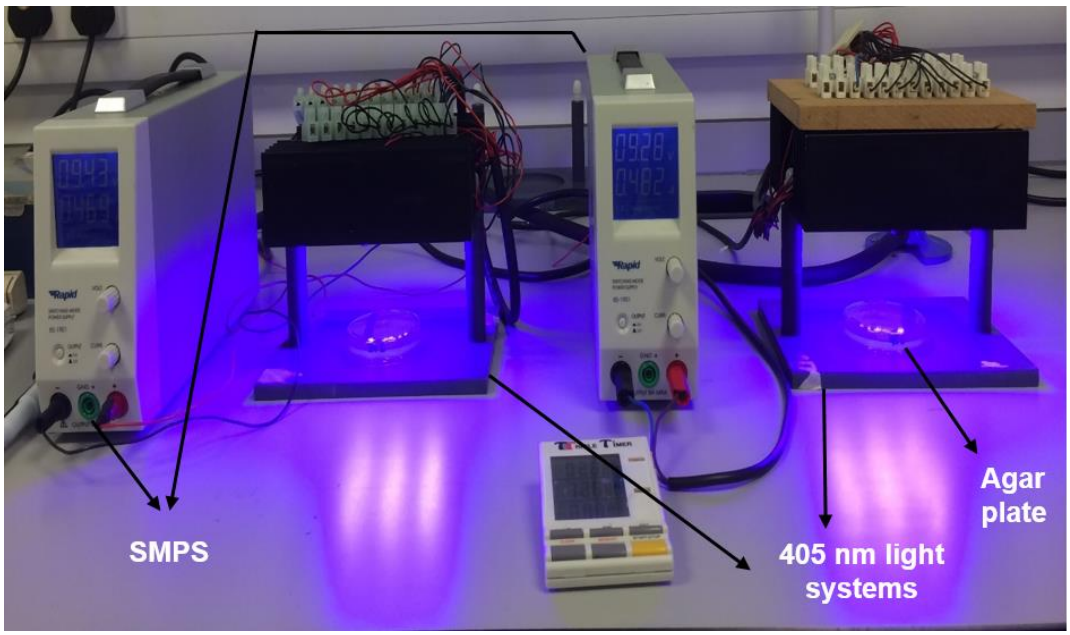

Fig. 2.8 The experimental set up involving the exposure of bacterial cells on agar plates to 405 nm HINS light at room temperature.

c) Exposure of Bacteria in Liquid Suspension:

For exposure of bacterial suspensions, population density of 10^9 CFU/ml (neat cell suspension) was prepared. Samples (2 ml) were then pipetted into the two central wells of a 12-well plate and exposed to 405-nm light for different periods of time at room temperature. The control plates were left on the bench with no 405 nm light exposure.

2.3.5 Enumeration of viable bacteria

Manual counting

After exposing the seeded agar plates to 405 nm light for defined time periods, the devices were turned off and the plates were incubated at 37°C for 24 hours. The number of surviving bacterial colony forming units (CFU) were manually counted

the following day using a colony counter (Stuart Scientific Colony counter). Results were then reported as the number of surviving CFU/plate.

2.3.5.2 Spiral plating

Spiral plating using a WASP 2 automatic plater (Don Whitley Scientific, UK), was performed as an alternative to manual spreading and as a method to enumerate higher populations of bacteria, as used in the bacterial suspension experiments. The spiral plater methodology involves logarithmic plating of 50 µl of bacterial suspension onto agar plates before and after exposure to 405 nm light for stipulated times. After incubation at 37°C for 24 hours, a counting grid was centred over the contact plates to enumerate bacterial colonies. The bacterial colony count per segment was then converted to its corresponding CFU/ml values by reference to supplied charts. Later, the values were multiplied by their respective dilution factors to give the number of CFU/ml of the original sample.

Chapter 3

Differential sensitivity of osteoblasts and bacterial pathogens to 405-nm light highlighting potential for decontamination applications in orthopaedic surgery

3.1 Introduction

HAI affects approximately 10% of patients admitted to hospital, and is responsible for over 5000 deaths in the UK annually (Improving Patient Care by Reducing the Risk of Hospital Acquired Infection: A Progress Report, National Audit Office 2004). HAI can be caused by airborne and environmental bacterial contamination which can be transmitted to surgical site wounds either directly from the environment or indirectly via vectors such as healthcare worker's hands (Albrecht *et al*., 2009 & Loftus *et al*., 2011). 405-nm HINS light has antimicrobial activity against HAI-related bacterial pathogens including methicillin-resistant *Staphylococcus aureus* (McLean *et al*., 2009) and, due to the use of visible light wavelengths, this does not pose the same health concerns as those associated with using ultraviolet light. This 405-nm light technology has already been used to develop an environmental decontamination system for the disinfection of air and environmental surfaces, which has been successfully clinically evaluated within isolation rooms at Glasgow Royal Infirmary (MacLean *et al*., 2010; Bache *et al*., 2012).

Infection rates following orthopaedic arthroplasty surgery are as high as 4%, while the infection rates are even higher after revision surgery (Hamilton & Jamieson.,

2008), and the environment and surgical devices have been highlighted as sources of bacterial contamination (Davis *et al*., 1999) (see figure 1.2).

The bactericidal properties of 405-nm light suggest that this may aid in reducing the incidence of infections that arise from environmental contamination during arthroplasty surgery. The toxic effect of 405-nm light on bacterial cells is not replicated to the same extent in mammalian cells, and this has been successfully demonstrated in previous studies (McDonald *et al*., 2011 & Smith *et al*., 2009). If 405-nm light technology was to be promoted for localized disinfection during arthroplasty surgery, the bone would likely be exposed to 405-nm light during the course of surgery and any inhibitory effects on the function of osteoblasts may affect the integration of the orthopaedic implant into the bone post-surgery. It is therefore essential to consider the duration of an orthopaedic surgical procedure and establish the effects of 405 nm light on osteoblast function during this potential exposure. Discussion with surgeons has revealed that the duration of routine arthroplasty surgeries was between 1 and 2 h, although a complex revision may take up to 4 h (Mr. Dominic Meek, Consultant Orthopaedic Surgeon, Southern General Hospital, 1345 Govan Rd, Govan, Glasgow G51 4TF, personal communication) . Previous studies on fibroblasts for wound healing have shown that 405 nm light had no significant effect on cell viability when exposed to a dose of 18 J/cm^2 (5 mW/cm^2 for 1 h), while a substantial decline in cell viability was observed at a dose of 54 J/cm^2 (15 mW/cm^2 for 1 h) (McDonald *et al*., 2011). Hence, the aim of this study was,

(i) to establish whether the adverse effects of 405-nm light seen on mammalian cells were dose dependent.

(ii) to determine a damage threshold of exposure of osteoblasts to 405-nm light.
(iii) to find out whether doses below the damage threshold can exert a bactericidal effect on clinically relevant pathogenic bacteria.

Demonstration of these key parameters would be an essential step toward assessing whether this novel technology could be developed and applied for localized decontamination of the patient environment during arthroplasty surgeries. To achieve these aims, experiments were carried out on the viability, proliferation and presence of apoptosis in osteoblasts treated with the 405 nm light sources.

A cell viability assay is an assay that is carried out to determine the ability of the cells or tissues to maintain their normal function or to recover their viability post treatment (after exposing them to a particular radiation for a particular period of time or treating them with chemicals etc.). There are several dyes being used to assess the viability of cells. The most commonly used dyes for labelling live cells are Acridine Orange, Calcein, Carboxyfluorescein Diacetate (CFDA) and some of the dyes used for labelling dead cells are Propidium Iodide and Ethidium Bromide.
Acridine Orange (AO) / Propidium Iodide (PI) is one of the most commonly used fluorescent dye combinations to differentiate live cells, apoptotic and necrotic cells from each other, and was the combination used in the present work.

AO (Excitation wavelength – 502 nm, Emission wavelength – 525 nm) is considered to be an inclusion stain that crosses the plasma membrane of live cells and early apoptotic cells due to its high permeable nature, and it stains the nucleus which, when viewed by fluorescence microscopy, appears green (Fan *et al.*, 2006). Live cells appear to have green nucleus with intact cell structure, while early apoptotic

cells appear to have bright green nucleus due to chromatin condensation and fragmented DNA (dense green areas). PI (Excitation wavelength – 540 nm, Emission wavelength – 610 nm) on the other hand is considered to be an exclusion stain that is impermeable to intact plasma membranes (live cells). Late apoptotic cells and necrotic cells will stain with both AO and PI. Comparatively, PI produces the highest intensity emission. Hence, late apoptotic cells that are smaller in size, exhibit an orange red nucleus showing intense condensation of chromatin whilst necrotic cells appear to have a large red nucleus with intact nuclear structure (Moore *et al*., 1998). The fluorescent colour of the stains is obtained by specific chemical properties of different staining dyes, and the distribution of fluorescence is controlled by the ability of the stains to cross the plasma membrane of viable cells and dead cells (Mishell *et al*., 1980).

Eukaryotic cells contain three main kinds of cytoskeletal filaments namely microfilaments, intermediate filaments, and microtubules. These cytoskeletal structures play an important role in providing the mechanical support that enables the cells to carry out important functions like intracellular transport (the movement of vesicles and organelles), and cellular division and they maintain the structure of the cells. However, during apoptosis, the distribution of actin filaments changes in cells including the accumulation of actin around the edge of apoptotic cells indicating cell rounding (Rosenblatt *et al.*, 2001; Desouza *et al*., 2012).

Phalloidin is a heat-stable, toxic, hexapeptide produced by *Amanita phalloides* that acts by binding to F-actin filaments disrupting the depolymerisation process (Cooper, 1987). This property makes Phalloidin a useful tool to study the distribution of F-

actin in cells by labelling the actin filaments with green fluorescence, generated by FITC-labelled phalloidin; this can be observed using fluorescence microscopy. DAPI is an effective fluorescent stain that crosses the plasma membrane of the cells and binds strongly to A-T rich regions in DNA emitting a blue fluorescence. DAPI stains both live and dead cells because of its ability to cross the intact plasma membrane (Kapuscinski, 1995). The combination of phalloidin-FITC and DAPI was used in the present work to study the distribution of actin in cells.

3.1.1. Detection of apoptosis *in-vitro*

Cell death occurs mainly either by necrosis or apoptosis. Necrosis, a pathological process, occurs when cells are exposed to extreme variance from physiological conditions (e.g., hypoxia, hypothermia) or chemical insult. The insult damages the plasma membrane, results in lysis of intracellular organelles leading to inflammation that can cause further distress or injury within the adjacent tissues and cells eventually causing widespread cell death. *In vivo* necrotic cell death is often associated with extensive tissue damage resulting in an intense inflammatory response (Zou *et al*., 1997). In contrast, apoptosis is a process involving the occurrence of a series of biochemical events within the cell leading to characteristic cell changes (morphology) and eventually secondary necrosis. These morphological changes include membrane blebbing, cell shrinkage, nuclear fragmentation, chromatin condensation and chromosomal DNA fragmentation **(**Elmore, 2007).

The apoptotic cell appears as a round oval mass with dense cytoplasm and tightly packed organelles. The separation of cell fragments into apoptotic bodies occurs during the ‘budding’ process and these apoptotic bodies consist of cytoplasm with

tightly packed organelles with or without a nuclear fragment within an intact plasma membrane. These bodies are consequently phagocytosed by macrophages, parenchymal cells or neoplastic cells and degraded within phagolysosomes, preventing the occurrence of an inflammatory reaction thereby inhibiting widespread cell death. Apoptosis occurs either via the intrinsic or extrinsic pathway (Figure 3.1). Caspases (cysteine-aspartic proteases) are a family of cysteine proteases that play crucial roles in apoptosis, necrosis and inflammation (Alnemri *et al*, 1996). The two different types of apoptotic caspases are i) initiator caspases and ii) effector or executioner caspases. The initiator caspases (-2, -8, -9, -10) cleave the inactive pro-forms of effector caspases and activate them. The executioner caspases (-3, -6, -7) in turn cleave other protein substrates within the cell triggering the apoptotic process.

The extrinsic pathway is triggered through the binding of a ligand to a death receptor, which in the presence of adapter proteins ((FAS- associated death domain (FADD)/TNFR-associated death domain (TRADD)), results in dimerization and activation of procaspase-8. Active caspase-8 then initiates apoptosis either directly by cleaving and activating executioner caspases (-3, -6, -7), or indirectly via activating the intrinsic or mitochondrial pathway through cleavage of BID (pro-apoptotic protein) to induce efficient cell death. Several cellular stresses activate the intrinsic pathway that cause the mitochondria to release cytochrome c, forming apoptosome ((comprised of APAF1 (apoptotic protease activating factor 1), cytochrome c, ATP, and caspase- 9)). The apoptosome in turn activates caspase-9 which then initiates apoptosis by cleaving and thereby activating executioner caspases which in turn initiate apoptotic processes within the cell via cleaving protein substrates.

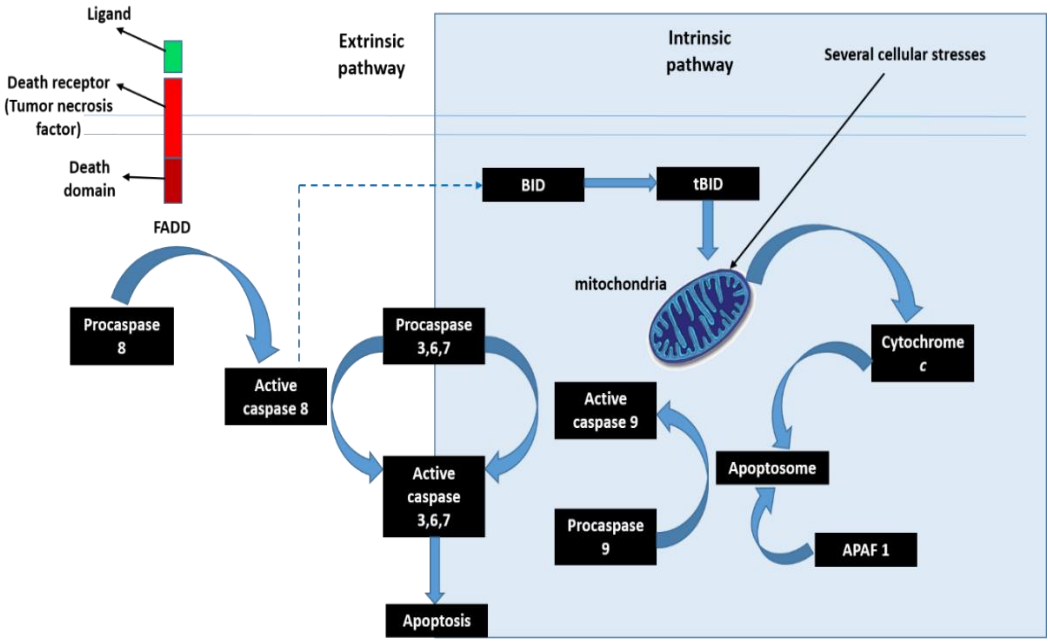

Fig. 3.1: Extrinsic and Intrinsic pathways of apoptosis. (Adapted from David *et al*., 2013).

Currently used methods to detect apoptosis, their advantages and disadvantages are discussed below (Table 3.1).

Table 3.1: Different methods for detection of apoptosis in cells, with their advantages and disadvantages

Method	Description	Advantages	Disadvantages
Morphological imaging			
Light microscopy	During early stages of apoptosis, morphological changes including cell shrinkage and chromatin condensation occur (Fadeel et al., 1999 & Elmore, 2007). An apoptotic cell appears round or oval shaped with dense purple nuclear fragments and dark eosinophilic cytoplasm using haematoxylin and eosin stain (Lynch et al., 1969).	Simple, cost effective method for detecting apoptotic cells	Cell fixation required. Lack of reproducibility and objectivity during qualitative measurements. Less sensitive and prone to human error.
Electron microscopy	Using a scanning electron microscope (SEM), cell shrinkage, and membrane blebbing can be visualised (Archana et al., 2013). Transmission electron microscope (TEM) shows chromatin condensation around the nuclear membrane and convolutions in the nuclear membrane preceding nuclear fragmentation (Shiraishi et al., 2006).	TEM analysis is qualitative. SEM studies (qualitative/semi-quantitative) provide information on the cell surface, cell-cell interactions, cell-substrate interaction.	Difficult to evaluate apoptotic features by SEM. Time consuming procedure (5-6 days for TEM and 24 h for SEM). Requires laborious sample preparation. Expensive method as it requires special equipment.

Fluorescent microscopy	Staining procedure includes adding fluorescent dyes like AO, CFDA, and Calcein to stain live cells green. PI, Ethidium Bromide to stain dead cells red. Phalloidin-FITC stain actin filaments of cells green and DAPI stains nucleus of both live and dead cells blue. These dyes make cells visible under the fluorescent microscope using the appropriate colour filters corresponding to the dye.	Simple, rapid and accurate. Differentiates live cells from dead cells. No cell fixation required. Allows discrimination between apoptotic and necrotic cells using combinations such as AO/PI.	More expensive than light microscopy. Qualitative rather than quantitative. Difficult to visualise the extent of apoptosis due to small area coverage.
Immuno-histochemistry based methods			
Flow cytometry (Annexin V – FITC staining)	Phosphatidylserine (PS), an important cell membrane phospholipid, is located facing the cytosolic side of the cell membrane in healthy cells, while the PS molecules flip towards the extracellular surface of the cell in apoptotic cells. Agents like Annexin-V, a cellular protein labelled with FITC (a fluorescent substance) when added to cells can be used to determine this translocation of PS molecules occurring during apoptosis (Vermes et al., 1995), which when	Quantitative, accurate and reproducible assay. Most sensitive method to detect ongoing apoptosis (Petrovsky et al., 2003). Annexin V with PI or 7-AAD can be used to monitor the progression of apoptosis: from viable cells, to early	Time consuming. Annexin V binds to apoptotic cells even in conditions of excess necrosis. Suspension cells required, but use of adherent cells involves extensive trypsinization to produce suspensions, repeated centrifugations and each process

	used in conjunction with PI (or) 7-aminoactinomysin (7-AAD) can be used to determine the percentage of apoptotic and necrotic cells present in the sample using flow cytometry.	apoptosis, to late apoptosis and finally necrosis (cell death). Well suited for automation. Measures the results in 10s of thousands of cells.	can make healthy non-apoptotic cells stain Annexin V positive.
TUNEL assay (Figure 3.2)	TUNEL (**T**dT-mediated d**U**TP-biotin **n**ick **e**nd-**l**abeling) is a common method used for detecting the fragmentation of DNA in a cell *in situ* during apoptosis by labelling the terminal end of nucleic acids (Ansari et al., 1993). The assay involves the identification of nicks present in the DNA using an enzyme deoxynucleotidyl transferase (TdT) which in turn catalyzes the addition of modified dUTPs that are secondarily labelled with a marker. Cells with severely damaged DNA are also labelled using TUNEL. The nuclei are visualized by either fluorometric or colorimetric methods.	Sensitive. Commonly used method for apoptosis detection. Healthy cells appear green with methylene green dye or appear red-bluish with haematoxylin. Apoptotic cells appear fragmented and/or condensed and stained in brown using diaminobenzidine (DAB) (a colorimetric dye).	Qualitative. Expensive method. Some of the nuclei labelled by the TUNEL assay may represent proliferating cells. Requires fixation and permeabilisation and hence cannot be performed on live cells. TdT concentration and duration of proteolytic treatment greatly affects results (Kochx et al., 1998).

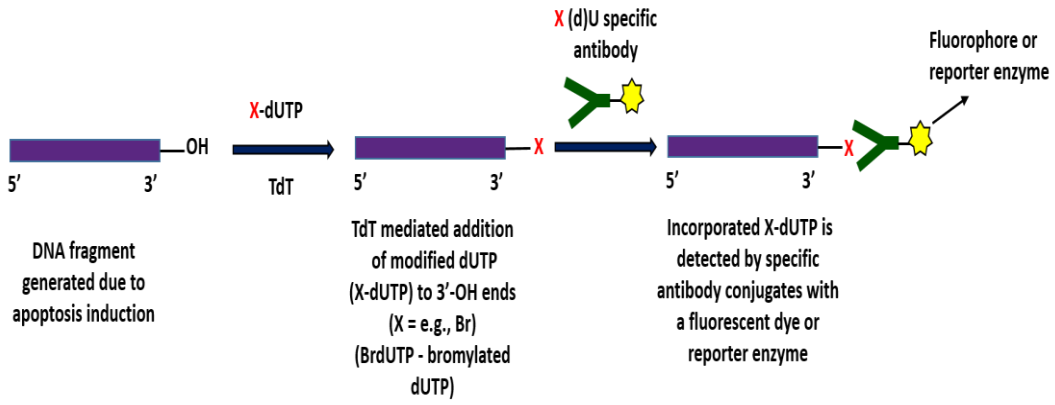

Fig. 3.2: Principle of TUNEL assay.

Active Caspase-3 detection	Caspase 3 belongs to the family of cysteine proteases that cleave their target proteins at aspartic acid residues in a defined sequence (Logue and Martin, 2008). Different stimuli that induce apoptosis in cells, activate the initiator caspases 8, 9 which then cleave inactive procaspase 3 (one of the executioner caspase) resulting in cleaved or activated caspase 3, thereby resulting in apoptosis. Neo-epitopes, generated as a result of enzymatic activation of procaspases are used as antigens for producing antibodies specific for immunodetection of the cleaved product.	Activated caspase-3 Immunohisto--chemical detection (IHC) is an easy, sensitive, and reliable method for detecting and quantifying apoptosis (Haupt et al., 2003).	Preparing adherent cell types for flow cytometry-based caspase assays can initiate early apoptotic responses. Another potential disadvantage is that the cells need to be permeabilised for detection, and hence additional controls need to be included for other processes like necrosis, which causes the cell membrane to become permeable.

Western blotting	Used to determine the presence or absence of expression of certain proteins (e.g poly ADP ribose polymerase (PARP) antigen) that are specific for apoptosis as well as to identify whether those expressed proteins are lysed or not. During apoptosis, PARP protein (116 kDa) is broken down to ~ 85 kDa and ~ 25 kDa by caspase -3, -7 (Kaufmann et al., 1993). This method is also used to determine the location of cytochrome c in the cell which is released from mitochondria into the cytoplasm during apoptosis (Kluck et al., 1997). A clean fractionation is required to differentiate cytoplasmic fraction of cells from the mitochondrial fraction to detect the release of cytochrome c.	Easy to perform.	Non quantitative. Risk of contamination of cytoplasmic fraction with mitochondrial fraction is possible leading to false results with the detection of cytochrome c. Requires mitochondrial marker (cytochrome c oxidase) to detect any mitochondrial contamination present in the cytoplasm.

Agarose gel electrophoresis and Comet assay (Figure 3.3)	In early apoptosis, the genomic DNA is broken down into ~ 180 base pairs or its multiples at internucleosomal regions and hence during electrophoresis gives a ladder like pattern of discontinuous DNA fragments (Oberhammer et al., 1993) in the range of 20 – 300 kb. However, a smear pattern is obtained on the gel for necrotic cells due to random DNA fragmentation.	SCGE is quantitative. Sensitive and easy to perform. Comet assay has higher sensitivity than TUNEL staining. Determines the extent of cell death and DNA damage more accurately.	Multiple steps involved and hence time consuming. Often tedious and might damage the cell membrane during the process thereby affecting the results.
	In Single cell gel electrophoresis (SCGE) or comet assay (Collins, 2002) (Figure 3.5), the extent of DNA damage is measured at an individual cell level. The degraded DNA appears as comet shaped structures on the electrophoregrams. The comet formed estimates the DNA content (head) present in the nucleus as well as the amount and pattern of fragmented/damaged DNA that has migrated from the nucleus (tail) in the agarose gels during electrophoresis. Healthy	More feasible and accessible than Electron microscopy.	Only measures result in single cells.

	viable cells appear with large heads and minute tails behind while apoptotic cells appear with small heads and large tails behind. Necrotic cells show large nuclear remnants and lack tails.	The comet assay is used to detect different forms of DNA strand breakage (single, double-stranded breakage) depending on the pH level used during electrophoresis .	

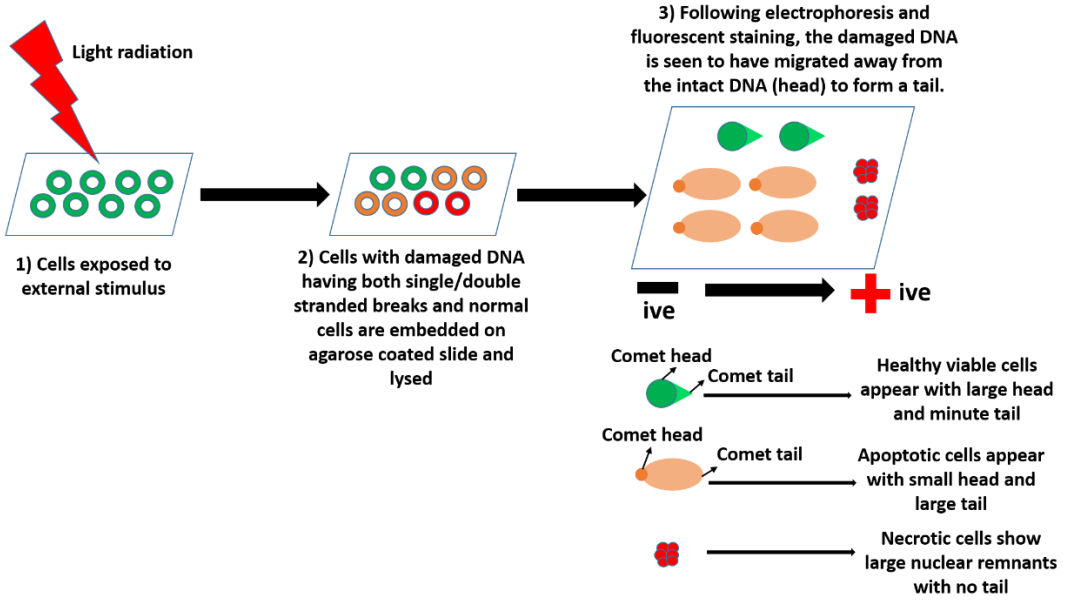

Fig. 3.3: Principle of the comet assay

Immunology based methods			
ELISA	The internucleosomal DNA fragmentation can be detected in both cell culture and human serum/plasma by Enzyme Linked Immuno Sorbent Assay (ELISA) (Salgamme et al., 1997). M30 antigen also known as caspase cleaved cytokeratin 18 can be measured together with DNA fragmentation in cell culture or plasma/serum by ELISA (Apoptosense ELISA assay, Peviva, Sweden).	High sensitivity and accurate. Highly specific.	Time consuming.

In this study, the methods that were chosen to study apoptosis in mammalian cells exposed to 405 nm light were Western Blotting and Flow cytometry. PARP analysis by western blotting to detect the activation of caspases, was carried out in this study due to its, i) easy performance and, ii) availability in our laboratory. Fluorescence-activated cell sorting (FACS) using Annexin V (stains apoptotic cells) and 7-AAD (stains dead cells) was performed i) due its accuracy and ii) to quantify the % of apoptotic cells and necrotic cells present in samples of 10s of thousands of cells after exposing them to 405 nm light for increasing periods of time.

3.2 Methods and Materials

3.2.1 Effect of different doses of 405 nm light on mammalian cells

Immortalised osteoblast (OST 5) cells were used for cell exposures in the central wells of 24-well plates and 96 well plates. Cells were seeded at a density of 5×10^3 cells/cm^2 in 24-well plates, and 2×10^4 cells/cm^2 in 96-well plates, and left in the incubator overnight at 37°C. The 405 nm light dose applied to cells was calculated as the product of the respective irradiance (W/cm^2) × time (s) (Table 3.2). For microscopy, cells were seeded on glass coverslips (13-mm diameter) at 5×10^3 cells /cm^2 in 24 well plates.

Table 3.2: The different periods of osteoblast cell exposure to 405 nm light, irradiance levels and the corresponding applied doses.

Period of exposure (minutes)	Irradiance (mW/cm^2)	Dose (J/cm^2)
60	5	18
90	5	27
120	5	36
150	5	45
180	5	54

3.2.1.1 Measurement of cell viability after exposure to 405 nm light

Cells seeded at a density of 5×10^3 cells/cm^2 in 24-well plates were exposed to 405 nm light in 1 ml Dulbecco's phosphate-buffered saline (DPBS) at doses of 18, 36 and 54 J/cm^2 using the light systems (refer to figure 2.1), inside an incubator at 37°C and in an atmosphere of 5% CO_2. Unexposed controls were held under the same conditions but in a separate incubator (to avoid any effects of the light on the

control).

After the stipulated exposure periods, the DPBS solution was removed, 1 ml of Dulbecco's modified Eagle's medium (DMEM) was added to the wells and the cells were incubated for 48 and 72 h at 37°C and in an atmosphere of 5% CO_2. The following assays were performed on both the light-exposed and non-exposed control cell populations after the incubation periods.

3.2.1.1.1 Crystal Violet assay

After the 48 and 72 h post treatment periods, the growth medium was removed and the cells were washed twice with DPBS at pH 7.4 at room temperature. 200 µl of 4 % formalin was added to all the samples (both unexposed and 405 nm light treated) inside a fume hood and they were left undisturbed for 30 minutes. The formalin solution was then removed and the cells were washed 3 times with DPBS at pH 7.4 to remove any traces of formalin left on the sample. Following the wash, 200 µl of Crystal Violet (1 mg/ml in distilled water (d.H_2O)) was added to the cells and they were left at room temperature for 20 minutes. The Crystal Violet solution was then removed and the cells were washed 3 times with DPBS at pH 7.4 to remove traces of dye. 1 ml of Triton-x 100 (0.1 % in PBS) was then added to the samples and they were left on a rotary plate for 24 hours before reading the absorbance using a spectrophotometer (Shimazdu, model UV-2101PC) at 540 nm.

3.2.1.1.2 Lowry assay

The total protein content of the osteoblasts was determined 2 and 3 days after 405 nm light exposure by Lowry assay (Lowry *et al*., 1951).

After the post-treatment periods, medium was removed and cells washed twice with

DPBS to removes traces of medium, before solubilizing the cells in 200 µl/well of 0.5 M NaOH overnight. Next day, the standards (Table 3.3), Solution A containing 2 % w/v Na_2CO_3, 1 % w/v $CuSO_4$, 1 % w/v NaKtartrate and Solution B containing 1:4 dilution of Folin's reagent in d.H_2O, were prepared.

Table 3.3: Protein standards prepared at different concentrations.

Protein Concentration (µg/ml)						
	0	**25**	**50**	**100**	**150**	**200**
Bovine Serum Albumin (BSA) (ml)	0.000	0.125	0.250	0.500	0.750	1.000
0.5 M NaOH (ml)	1.000	0.875	0.750	0.500	0.250	0.000

50 µl of the samples and standards were pipetted into clean test tubes and diluted with 950 µl of 0.5 M NaOH. To the samples and standards 5 ml of Solution A was added, the samples mixed and left for 10 minutes. Later, 0.5 ml of Solution B was added, samples mixed well immediately and left for up to 90 minutes at room temperature before reading the absorbance at 725 nm against a dH_2O blank using a spectrophotometer (Shimazdu, model UV-2101PC). The protein concentrations of the samples were calculated from the BSA standards. A standard curve was obtained for every independent experiment.

3.2.1.2 Survivability of mammalian cells for extended periods of time in buffer

Studies were carried out in order to find out if the cells could survive at 54 J/cm^2 by lowering the 405 nm light intensity from 5 mW/cm^2 to 0.5 mW/cm^2 (10 - fold reduction) and extending the period of exposure to 30 h from 3 h, thereby maintaining the dose constant. 0.5 mW/cm^2 was the approximate light intensity used in the previous hospital studies (Bache *et al*., 2012; Maclean *et al*., 2010; Booth *et al*., 2010). In order to detect the survivability of cells after being left in DPBS buffer alone (no light exposure) for 30 hours, cells seeded at a density of 5×10^3 cells/cm^2 in 24-well plates were left in growth medium (Plate A) as well as in DPBS buffer (Plate B) for 30 hours inside an incubator at 37°C and in an atmosphere of 5% CO_2. After the 30 hour incubation period, buffer and growth medium were removed, samples washed twice with DPBS and fresh growth medium was added to both plates (Plate A and Plate B) (Figure 3.4A). The plates were left for a 48 and 72 h recovery period. Another set of experiments involved leaving the cells in DPBS (Plate C) and growth medium (Plate D) for up to a 30 h time point, while adding fresh growth medium to both plates (C & D) for an overnight period after every 10 h point. This is explained on Figure 3.4B. After the 30 h time period, fresh medium was added to Plate C and Plate D and they were left for a 48 and 72 h recovery period (Figure 3.4B). Later, the following assays were carried out to study the cell viability.

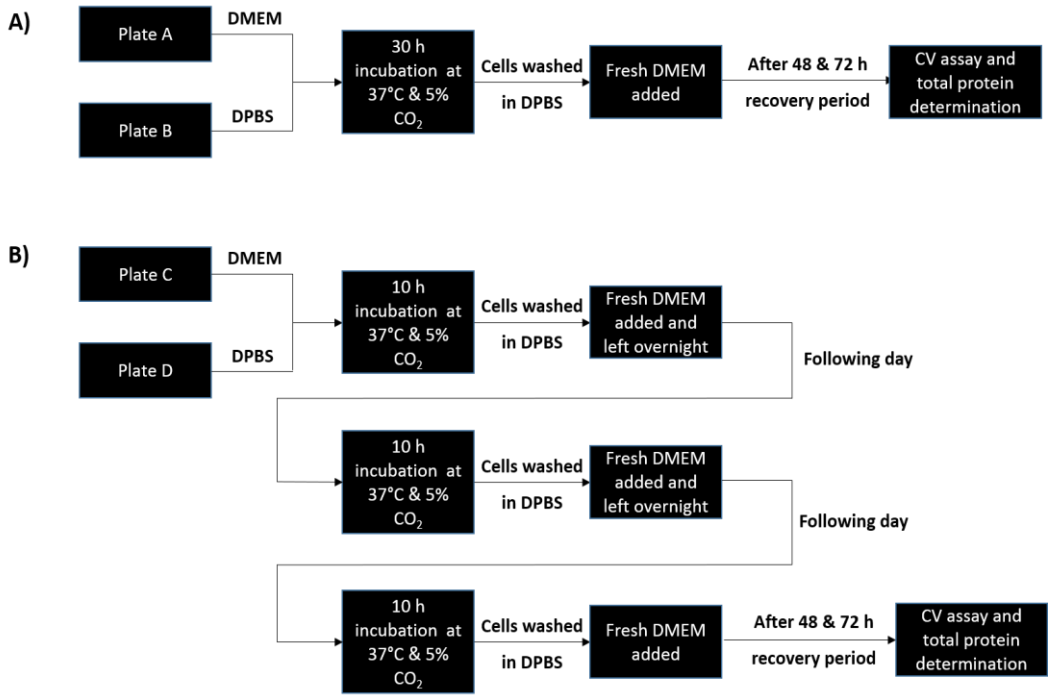

Fig 3.4: Studies assessing cell viability of rat osteoblasts for A) 30 h in DMEM and DPBS, B) every 10 h up until 30 h in DMEM and DPBS.

After the 48 and 72 h post treatment periods, crystal violet staining of cellular DNA in attached cells was quantified as described earlier. The total protein content of the osteoblasts was determined 2 and 3 days post 405 nm light exposure by Lowry assay (Lowry *et al*., 1951) as described earlier.

3.2.1.3 405 nm light-dose dependent study

To investigate the dose-dependent effects of 405-nm light on the osteoblasts, growth medium was removed and the samples exposed to 405 nm light using the light systems (Figure 2.1), in 1 ml DPBS, inside an incubator at 37°C and in an atmosphere of 5% CO_2, at a low dose of 18 J/cm^2 and a high dose of 54 J/cm^2 using varying irradiance/exposure regimes (Table 3.4). Unexposed controls were held

under the same conditions but in a separate incubator (to avoid any effects of the light on the control).

Table 3.4: Irradiance levels and exposure times used to apply low dose (18 J/cm^2) and high dose (54 J/cm^2) 405 nm light to osteoblasts.

Low Dose Exposures			High Dose Exposures		
Period of exposure (minutes)	Irradiance (mW/cm^2)	Dose (J/cm^2)	Period of exposure (minutes)	Irradiance (mW/cm^2)	Dose (J/cm^2)
60	5	18	60	15	54
120	2.5	18	120	7.5	54
180	1.7	18	180	5	54
240	1.25	18	240	3.75	54

After the stipulated exposure periods, the DPBS solution was removed, 1 ml of DMEM was added to the wells and the cells were incubated for 48 and 72 h at 37°C and in an atmosphere of 5% CO_2. The following assays were performed on both the light-exposed and non-exposed control cell populations after the incubation periods. After the 48 and 72 h post treatment periods, crystal violet staining of cellular DNA and the total protein content of attached cells were quantified as described earlier.

3.2.1.4 Establishing a damage threshold for exposing cells to 405 nm light

To establish a damage threshold for osteoblast cells, growth medium was removed post overnight incubation and the samples exposed to 405 nm light at an irradiance of 5 mW/cm^2 in 1 ml DPBS for increasing time periods (60, 90, 120, and 150 min corresponding to doses of 18, 27, 36, and 45 J/cm^2) inside an incubator at 37°C and in an atmosphere of 5% CO_2. Unexposed controls were held under the same

conditions but in a separate incubator (to avoid any effects of the light on the control). After the stipulated exposure time, the DPBS was removed, 1 ml DMEM was added to wells, and the cells were incubated for 48 and 72 h before carrying out the following assays.

3.2.1.4.1 MTT assay

Cell metabolism was measured using the MTT (3-(4,5-dimethylthiazol-2-yl)-2,5-diphenyltetrazolium bromide) assay as described previously (Ho *et al*., 2004). 10 mM solution of MTT in PBS was prepared at 6.75 pH. After the 48 and 72 h post treatment periods, medium was removed and cells washed twice with DPBS to removes traces of medium. Then, 50 µl of MTT solution was added per well and samples incubated at 37°C for 4 h. Later, the MTT solution was removed and 200 µl of dimethyl sulfoxide (DMSO) was added per well to dissolve the formazan product. The samples were mixed well before measuring the absorbance at 540 nm using 96 well plate reader (Multiskan Ascent).

3.2.1.4.2 Alkaline Phosphatase assay

Alkaline Phosphatase (ALP) is an enzyme that plays a crucial role in osteoid formation and mineralisation, and is commonly used to measure osteoblast activity *in vitro*. Osteoblast cell function using ALP assay was measured, as described by McDonald *et al*, 2011. After the 48 and 72 h post treatment periods, growth medium was removed and cells washed twice with DPBS to removes traces of medium. 200 µl of p-nitrophenyl phosphate (pNPP) in glycine buffer (1 mg/ml) was then added to each well. pNPP was then dephosphorylated to p-nitrophenol and phosphate in the presence of ALP. The absorbance of p-nitrophenol was measured at 405 nm

immediately and at 15 minutes after addition using a 96 well plate reader (Multiskan Ascent). The ALP activity, measured in IU/l, was given by:

$$\text{ALP activity} = \frac{(OD_{15} - OD_0) \times 1000}{t \times \varepsilon}$$ (Bowers & McComb, 1966)

where, OD_{15} and OD_0 are the optical densities measured at 15 and 0 minutes.

1000 is the conversion factor to convert ml to l.

t is the incubation time

ε is the extinction coefficient of p-nitrophenol (18.75 mM/cm)

3.2.1.3.3 BrdU assay

The bromodeoxyuridine (BrdU) ELISA assay was carried out to measure the cell proliferation rate post 405 nm light exposure using QIA 58 BrdU cell proliferation assay kit (Calbiochem—Merckmillipore). The assay was used for quantification of BrdU (a thymidine analog) incorporation into newly synthesised DNA strands of actively proliferating cells. A working stock solution of BrdU was prepared by diluting the BrdU label 1:2000 into freshly prepared DMEM. 20 µl of the working stock solution was pipetted into each well of cells to be labelled, 4 h prior to the completion of 48 h and 72 h post treatment periods. The plates were then left in the incubator at 37°C and 5 % CO_2 for 4 h. The medium was removed by inverting the plates over the sink and blotting them gently on paper towels. 200 µl of the Fixative/Denaturing solution was added to each well and samples incubated at room temperature for 30 minutes. 100 × Anti-BrdU Antibody (1:100) was diluted in the Antibody Dilution Buffer. 100 µl of this solution was added to each well and samples

incubated at room temperature for 1 h. A working solution (1 ×) of Wash Buffer was prepared and the wells were washed 3 times with Wash Buffer. The plates were dried by tapping on paper towels.

The conjugate was prepared by diluting the reconstituted (in 1 × PBS) Peroxidase Goat Anti-Mouse IgG HRP Conjugate in the Conjugate Diluent and syringe filtering through a 0.2-micron filter. 100 µl of this solution was pipetted into each well and samples incubated at room temperature for 30 minutes. After the incubation period, the wells were washed 3 times with 1 × Wash Buffer and the plates dried on paper towels. The plates were then flooded with d.H_2O and the liquid contents of wells removed by inverting the plates over the sink and tapping them on paper towels. 100 µl of Substrate Solution was added to each well and samples incubated in the dark at room temperature for 15 minutes. Following the incubation period, 100 µl of Stop solution was added to each well in the same order as the Substrate Solution had been previously added, to stop the reaction. The absorbance was measured in each well using a 96 well plate reader (Multiskan Ascent) at dual wavelengths of 450 – 540 nm, within 30 minutes of adding the Stop Solution.

3.2.1.3.4 Qualitative analysis

(i) Live/ dead cell staining

AO / PI staining (Sigma Aldrich Company Ltd., UK**)**

After the 48 and 72 h post treatment periods, the growth medium was removed and the cell monolayer (grown on coverslips) washed twice with DPBS (pH 7.4). 2 ml of PI (20 µg/ml in PBS, pH 7.4) was added to each well and samples incubated in the dark for 1 minute. After the incubation period, PI solution was removed, discarded to

a waste bottle and cells washed 3 times with DPBS (pH 7.4) to remove extracellular traces of dye. 2 ml of Acridine orange (100 µg/ml in PBS at pH7.4) was added and samples incubated in the dark for another 1 minute. Later, the dye was removed, discarded into a waste bottle and the cells washed 3 times with DPBS (pH 7.4). The coverslips were transferred into 4 cm^2 petridishes and 3 ml of DPBS was added. The samples were viewed immediately under a Zeiss AxioImager Z1 fluorescent microscope using a 20× wet lens (NA = 0.5).

(ii) Staining for Actin

Phalloidin-FITC / DAPI staining

After the 48 and 72 h post treatment periods, the growth medium was removed and the cell monolayer (grown on coverslips) was washed twice with warm DPBS (37°C). The cells were fixed with 4% formalin in PBS for 20 minutes inside a fume hood. After the 20-minute period, the cells were washed 3 times with DPBS. The following steps were carried out in the dark (under tin-foil) as FITC is light sensitive. 125 µl of Phalloidin-FITC (Sigma Aldrich Company Ltd., UK) (final dilution 1:500 in PBS) was added to cells and samples incubated in a moist chamber for 1 h. Later, the cells were washed 3 times with DPBS and 300 nM 4′,6-diamidino-2-phenylindole dihydrochloride (DAPI) (Life technologies, Paisley, Scotland, UK) was added to cells for 30 seconds. The DAPI solution was removed, cells washed 3 times with DPBS and the coverslips were placed into 4 cm^2 petridishes. 3 ml of DPBS was added and the samples were viewed immediately under a Zeiss AxioImager Z1 fluorescent microscope using a 20× wet lens (NA = 0.5).

3.2.1.5 Detection of apoptosis *in-vitro*

3.2.1.5.1 Western blotting

Initial blotting experiments were carried out seeding 1×10^6 cells in 12 well plates and leaving them overnight inside an incubator at 37°C and in an atmosphere of 5% CO_2. Following incubation and 405 nm light exposures, both the unexposed and 405 nm exposed samples produced less dense optical bands that were almost invisible on the blot paper, due to low protein content. In order to achieve denser optical bands on the blot paper, 2×10^6 cells were seeded into the central wells of 12 well plates and left overnight inside an incubator at 37°C and in an atmosphere of 5% CO_2. Following incubation, the plates were exposed to 405 nm light at 54, 108, 162 J/cm^2 doses in DPBS. Higher doses of 405 nm light were applied due to the use of higher cell population. Unexposed controls were held under the same conditions but in a separate incubator (to avoid any effects of the light on the control).

Preparation of cell homogenates

After exposure, the cells were washed twice with DPBS and 500 µl of 0.1M Sodium Phosphate buffer (NaPi) at pH 7.6 was added to the wells. Later, the cells were scraped out and 500 µl of cell suspension (containing NaPi buffer and scraped cells) were then transferred into clean test tubes and homogenised using a Black & Decker, UK electric drill as motor-driven homogeniser. The homogenates were split into three 150 µl aliquots for western blotting, one 50 µl for protein measurement (mg/ml) for each sample and transferred into clean eppendorf tubes. The samples were stored at -80°C up until the day of performing western blotting.

Protein measurement

The total protein content of the osteoblast homogenates was determined by Lowry assay (Lowry *et al*., 1951) as described earlier (refer to Section 3.2.1.1.2).

Sodium dodecyl sulfate polyacrylamide gel electrophoresis (SDS-PAGE)

The stock solutions were prepared as follows.

a) Stacking gel buffer – **0.5 M Tris Buffer at pH 6.8**

6 g of Tris was dissolved in 40 ml of distilled water and titrated to pH 6.8 with 1M HCl. The buffer was made up to 100 ml with distilled water and stored in cold room at 4°C until use.

b) Separating gel buffer – 1.5M Tris buffer at pH 8.8

36.33 g of Tris was dissolved in 48 ml of distilled water and titrated to pH 8.8 with 1M HCl. The buffer was made up to 200 ml with distilled water and stored in cold room at 4°C until use.

c) Reservoir buffer (10 ×) – Tris/Glycine/SDS buffer (0.25M Tris/ 1.92M Glycine/ 1% SDS pH 8.3**)**

Purchased from Sigma.

d) Laemmli buffer (2 ×) – (d.H_2O/ 0.5M Tris pH 6.8/Glycerol/ 10% SDS/ β-mercaptoethanol/ 0.05% (w/v) bromophenol blue).

` Purchased from Sigma.

Methodology

The glass plates of size 10 × 10 cm were cleaned with 70% (v/v) ethanol and assembled in the cast chamber. The gels were prepared as shown in Table 3.5. The comb was inserted into plates prior to casting gels and 1 cm below the bottom of the

comb was marked using a marker pen. The gels were poured to just above this mark. The resolution gel was cast first and allowed to set. 300 µl of distilled water was pipetted on top of the gel to prevent the top of the gel from drying out. The gels were allowed to set for 25 minutes and then the water was removed. The stacking gel was then poured on top of the set resolution gel. Combs were inserted into the stacking gel and it was allowed to set.

Table 3.5: Preparation of gels for performing electrophoresis.

Solutions	Stacking gel	10% Resolution gel
Acrylamide/bis acrylamide (40% stock)	1 ml	5.625 ml
Stacking gel buffer	2.5 ml	-
Resolving gel buffer	-	5.625 ml
1.5% Ammonium persulfate (APS)	0.5 ml	1.125 ml
Distilled water	6 ml	10.125 ml
Tetramethylethylenediamine (TEMED)	10 µl	17.5 µl

The samples (unexposed and 405 nm light treated cell homogenates) were prepared at 1 mg/ml in Laemmli buffer and boiled for 2 minutes in surelock eppendorffs. The combs were removed and the gel sandwiches were clicked into the electrode. Electrophoresis buffer (Tris/Glycine/SDS) was poured to fill the upper chamber making sure the buffer filled the wells and the system was checked for any leaks. After checking for leaks, the set up was placed in the electrophoresis tank (Model

No: TV100, Fisherbrand, UK) and filled with buffer until approximately 1 cm above the bottom of the plates. The molecular weight standards (ColorBurst™ Electrophoresis Marker, Sigma, UK) at 10 µg/well and samples at 20 µg/well were loaded into the wells. The electrophoresis was allowed to proceed at 50 mA until the molecular standards and the samples ran almost to the bottom of the gel.

While the gels were running, the transfer buffer (Towbin's buffer) was prepared to a volume of 1.5 l by mixing 1050 ml of distilled water, 300 ml methanol and 150 ml of 10 × Tris/Glycine transfer buffer. The Scotch Brite pads and filter paper were soaked in transfer buffer for 15 minutes. The polyvinylidene fluoride (PVDF) membrane was soaked in methanol before placing it in transfer buffer for 15 minutes. Once the gels had run, the power was turned off, gel sandwiches were removed from the tank and placed in the transfer buffer for a few minutes. The transfer cassettes were prepared as shown in Figure 3.5.

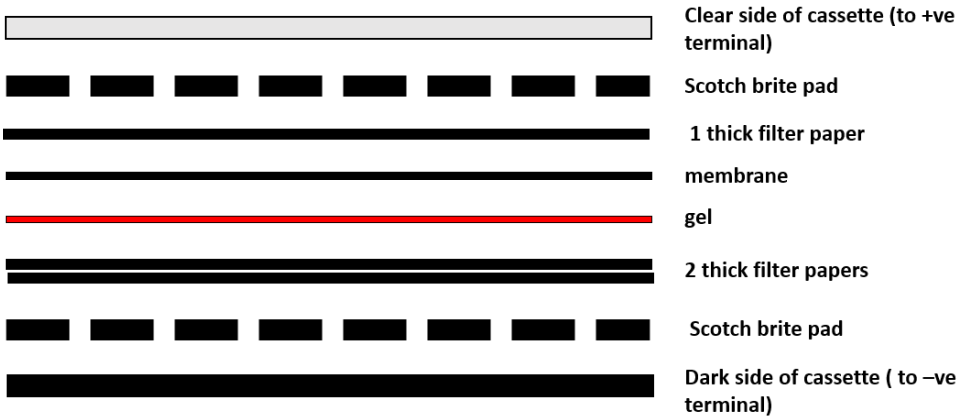

Fig. 3.5: Preparation of transfer cassettes for transfer of protein bands from gel to membrane.

The cassettes were placed into the tank (Model No: EB10, Fisherbrand, UK) which was partially filled with transfer buffer, with the black side of the cassette at the black of the tank. The tank was filled up with transfer buffer, attached to a cooling unit and ran overnight at 200 mA.

3 % gelatin (Fish gelatin) was prepared in 1 × Tween Tris Buffered Saline ((TTBS prepared by adding 0.5 ml of Tween 20 to 1 l of 1 × Tris Buffered Saline (TBS)) and placed in warm water to dissolve. The membranes were placed in 3 % gelatin solution for 1 h at 37°C in a rotary shaker. Later, the gelatin was poured off and membranes washed 3 times in TTBS (shaking) for 5 minutes each wash. The primary antibody, anti – PARP in 1 % (w/v) gelatin at 1:2000 dilution in TTBS was prepared, added to the membranes and shaken for 1 h at 37°C in a rotary shaker. The antibody was poured off and membranes were washed 3 times in TTBS for 5 minutes each wash (shaking). The secondary antibody, anti-rabbit IgG-ALP (Bio-Rad; Hertfordshire, UK) in 1 % (w/v) gelatin at 1:10000 dilution in TTBS was prepared, added to the membranes and shaken for 1 h at 37°C in a rotary shaker. The secondary antibody solution was poured off and the membranes washed twice with TTBS for 5 minutes each wash (shaking) and once with TBS (shaking). The bands on the membranes were visualised using the alkaline phosphatase detection system (Bio-Rad) [BCIP/NBT]. The membranes were dried between 2 sheets of filter paper and scanned within a CanoScan N670U scanner using the software CanoScan toolbox 4.1 (Canon; Middlesex, UK). The bands of samples (both unexposed and 405 nm treated) were identified and quantified using the molecular weight standards.

3.2.1.5.2 Flow cytometry by Fluorescence-Activated Cell Sorting (FACS)

Cells were seeded at 5×10^3 cells/ cm^2 in the central wells of 12 well plates and left overnight inside an incubator at 37°C and in an atmosphere of 5% CO_2. Following incubation, the plates were exposed to 405 nm light at 18, 36 and 45 J/cm^2 doses in DPBS. Unexposed controls were held under the same conditions but in a separate incubator (to avoid any effects of the light on the control). Post 405 nm light exposures, DPBS was removed and 2 ml of fresh DMEM was added to wells for both unexposed and light exposed samples and left inside an incubator at 37°C and in an atmosphere of 5% CO_2 for 48 h.

After the 48 h post treatment period, 2 ml of the medium was transferred into micro-centrifuge tubes. The adherent cells were washed twice with versene, and TrypLE (cell dissociation agent) (Thermo Fisher Scientific, UK) was added to wells, and they were left in the incubator at 37°C and in an atmosphere of 5% CO_2 for a couple of minutes until the cells detached. The cell suspensions were transferred into the corresponding micro-centrifuge tubes holding the medium that was transferred earlier. The tubes were centrifuged for 5 minutes at 350 × g. The supernatant was aspirated and the cells were re-suspended in 200 µl of FACS buffer. Following this, the cells were centrifuged for 5 minutes at 350 × g and the supernatant discarded. The cells were then re-suspended in 100 µl of Annexin binding buffer ((0.01M HEPES, 0.14M NaCl and 2.5 mM $CaCl_2$; Sigma-Aldrich; Dorset, UK) in distilled water (pH 7.4)). 5 µl/sample of Annexin V- phycoerythrin (PE) and 0.25 µg/ 5 µl of 7- Aminoactinomycin D (7-AAD) (both BD Bioscience; Oxford, UK) were then added to each tube. Tubes were vortexed and incubated at room temperature for 15 minutes in the dark. Following this incubation period, the samples were transferred

into FACS tubes, and 200 µl of Annexin binding buffer and 200 µl of FACS flow (BD Bioscience; Oxford, UK) were added to each tube. Calibrite^{TM} beads (BD Bioscience; Oxford, UK) were used to adjust the instrument settings, set fluorescence compensation and check instrument sensitivity. The data were recorded (at least 20,000 events for unexposed and 405 nm light exposed samples) using a FACS Canto flow cytometer and using FACS Diva software. The graphs were reproduced using Flowjo V.10 software.

3.2.2 Effects of different doses of 405 nm light on a range of bacteria

The bacteria used in this study were *Staphylococcus aureus* NCTC 4135, *Escherichia coli* NCTC 9001, *Pseudomonas aeruginosa* LMG 9009, *Klebsiella pneumoniae* NCTC 09633, *Staphylococcus epidermidis* LMG 10474, and *Acinetobacter baumannii* LMG 1041 (NCTC, National Collection of Type Cultures, Collindale, UK; LMG, Laboratorium voor Microbiologie, Universiteit Gent, Belgium). Bacteria were cultured in nutrient broth (Oxoid, UK) at 37°C for 18 h under rotary conditions (120 rpm). Broths were centrifuged at 4300 rpm for 10 min, and the cell pellet was re-suspended in PBS. The cell suspension was then diluted in PBS to obtain a concentration of 10^3 colony forming units (CFU)/ml. Samples (100 µl) were then spread onto 55 mm agar plates, giving approximately 150 to 300 CFU/plate, and these seeded agar plates were then exposed to 405-nm light at an irradiance of 5 mW/cm^2 for increasing time periods (15, 30, 60, 90, and 120 min corresponding to doses of 4.5, 9, 18, 27, and 36 J/cm^2). Post-exposure, plates were incubated at 37°C for 24 h before enumeration of the viable CFU/plate. Results are reported as % surviving CFU/plate as compared to non-exposed control samples.

3.2.3 Statistical analysis

Number of samples used for each study are provided for their respective graph/table of results. Results are expressed as mean ± standard error of the mean. Significance has been established by Student's t test, which compares the mean of each 405 nm light exposed group against their respective unexposed group.

3.3 Results

3.3.1 Measurement of mammalian cell viability after exposure to 405 nm light

In order to establish the maximum duration that 5 mW/cm^2 irradiance of 405 nm light could be used safely for mammalian cell exposure, viability of the cells in culture was measured 48 and 72 h post- 1, 2 and 3 h exposure by both total protein content and DNA staining with Crystal Violet in attached cells. Data in Fig. 3.6 show that cells tolerated exposure to 5 mW/cm^2 405 nm light for up to 2 h (36 J/cm^2) without significant loss of viability, but 3 h exposure (54 J/cm^2) resulted in a significant decrease in the number of viable attached cells (Fig. 3.6A) and protein concentration (Fig. 3.6B) compared with their respective unexposed samples. There seemed to be a decrease in protein content of unexposed cells after 1 h at the 48 and 72 h recovery period, however, this was not significant compared to the 2 and 3 h unexposed samples.

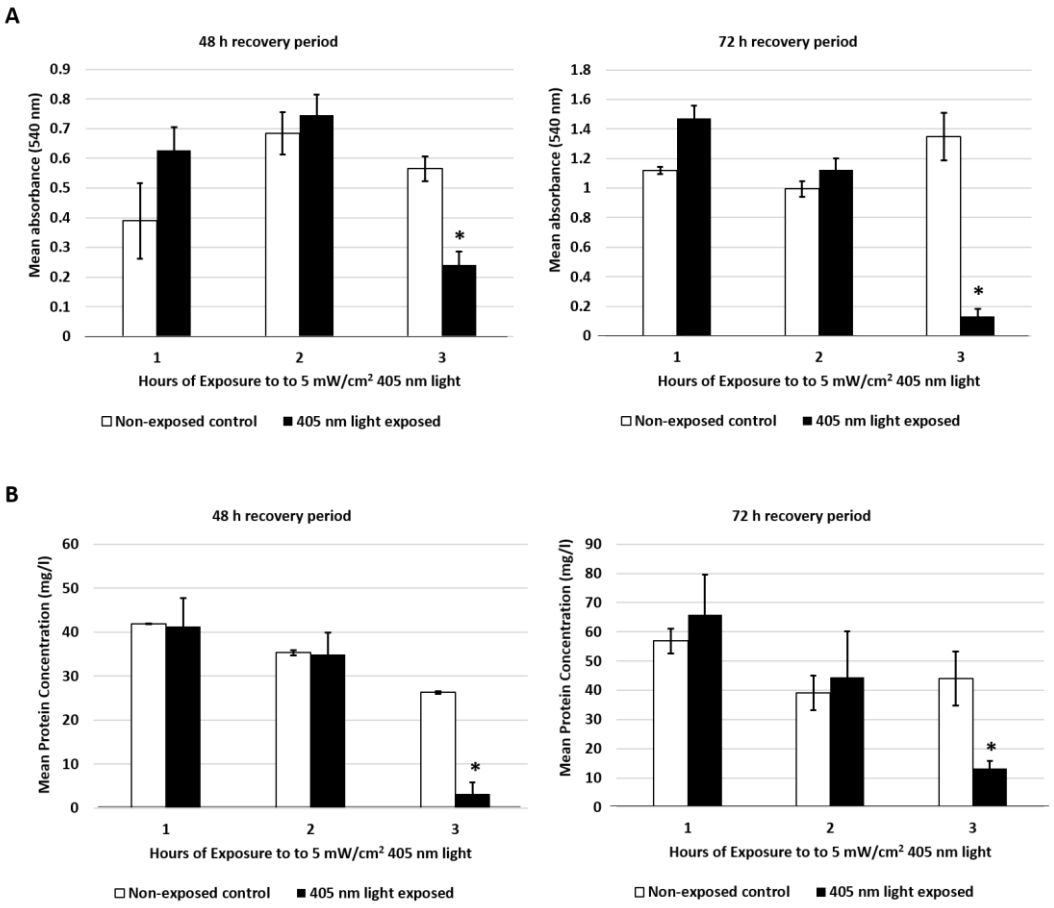

Fig.3.6: Viability of osteoblasts following exposure to 5 mW/cm^2 405 nm light for 1, 2 and 3 h. **A** shows the Crystal Violet staining of cultures incubated in the presence of 5 mW/cm^2 405 nm light, and control cultures incubated in the absence of 405 nm light. **B** shows the protein content of cultures incubated in the presence of 5 mW/cm^2 405 nm light, and control cultures incubated in the absence of 405 nm light. (*p < 0.05, unpaired student t-test, comparing the controls and 405 nm light treated samples after the same exposure time, n = 8 ± SEM.

3.3.2 Survivability of mammalian cells for extended periods of time in buffer

In order to find out whether the mammalian cells could survive a dose of 54 J/cm^2, if the light was applied over a prolonged period of time by reducing the irradiance level (from 5 mW/cm^2 to 0.5 mW/cm^2) but increasing the time duration (3 h to 30 h), preliminary experiments were carried out measuring cell survival in buffer (DPBS) alone for the entire duration. It was found that there was a significant loss of cell viability after a 48 and 72 h incubation period for cell cultures left in DPBS after a period of 30 h when compared to samples left in DMEM (Fig. 3. 7A, B). It was also found that there was a significant difference in cell viability after a 48 and 72 h incubation period for samples left in DPBS for every 10 h for up to a 30 h period (Fig.3.7 C, D). Therefore, experiments using the light under these conditions (0.5 mW/cm^2 for 30 h) were not able to be carried out.

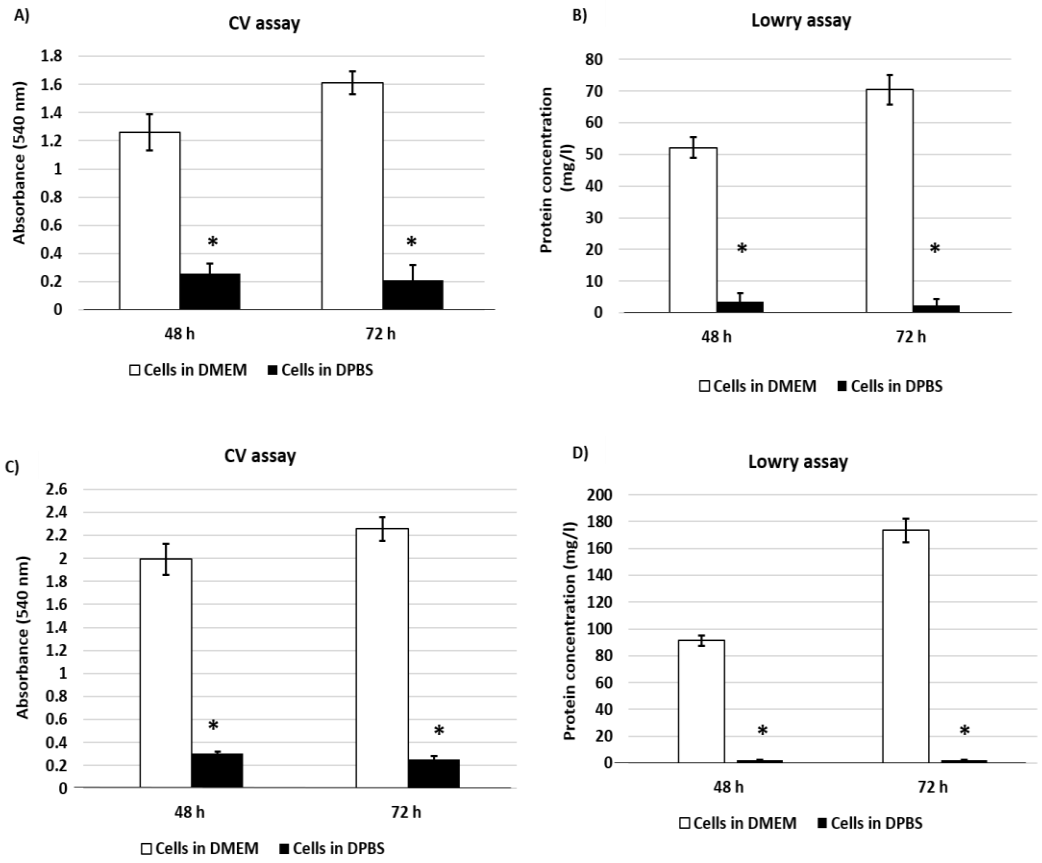

Fig.3.7: Viability of osteoblasts in DMEM and DPBS for A, B) a 30 h and C), D) up to a 30 h time point, while adding fresh growth medium to plates after every 10 h point allowing the cells to recover, and after 48 and 72 h post –incubation periods (see Fig 3.4, page 91, for experimental design). (*$p < 0.05$, unpaired student *t*-test, comparing the controls in DMEM and controls in DPBS after the same duration of time, $n = 6 \pm$ SEM)

3.3.3 Study of the dose dependent effects of 405 nm light

Data in Fig. 3.8 show that exposure of cells to 18 J/cm^2 405-nm light using different irradiance/exposure period regimes caused no significant difference in the crystal violet staining or protein concentration between the control and the treated samples after 48- and 72-h post-treatment periods. In contrast, a significant difference was evident between the control and the 405 nm treated samples exposed to higher doses of 54 J/cm^2 irrespective of how the dose was administered.

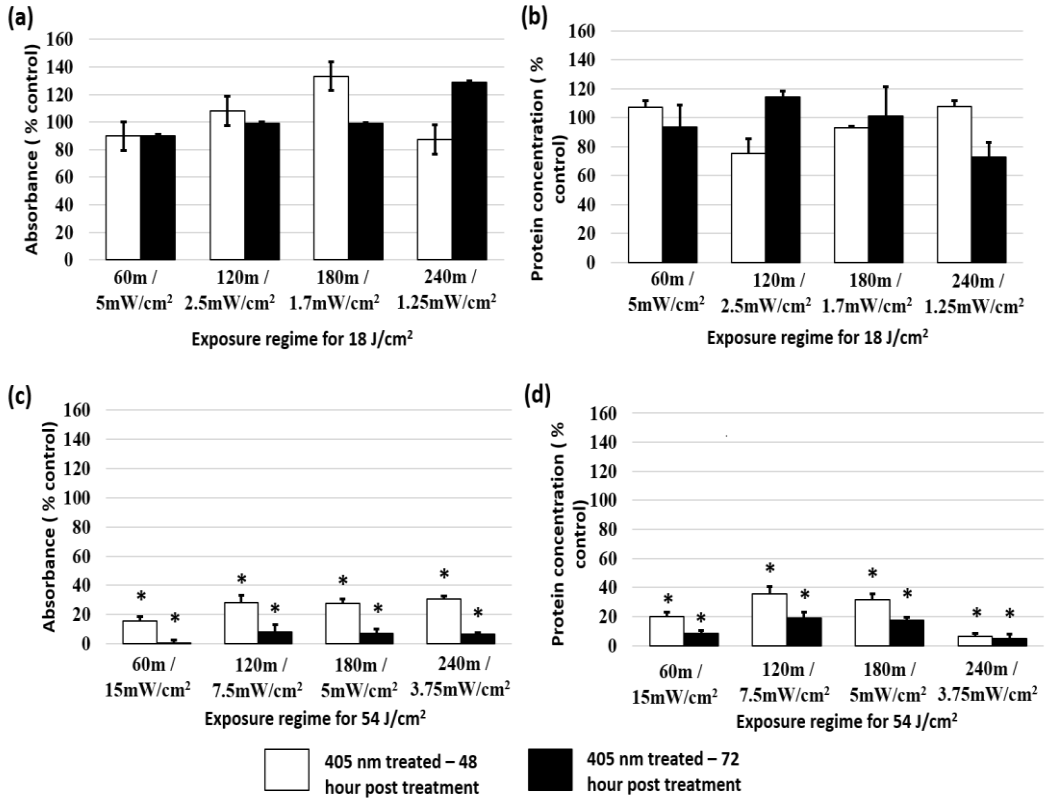

Fig. 3.8: Crystal Violet staining and Protein content of osteoblasts exposed to different doses of 405 nm light. (a), Crystal Violet Absorbance (% control), (b) Protein concentration (% control) of rat osteoblasts exposed to 405 nm light at a low dose of 18 J/cm^2 and (c), Crystal Violet Absorbance (% control), (d) Protein concentration (% control) of rat osteoblasts exposed to a high dose of 54 J/cm^2. Doses were achieved using different irradiance/exposure time regimes, and were followed by either 48 or 72-hour post treatment periods. Results are means of $n = 8 \pm$ SEM. Statistically different using unpaired Student's t-test comparing control and light treated samples, * $p < 0.05$.

3.3.4 MTT, ALP and BrdU assay

Data in Fig. 3.9 show that cells exposed to doses of 18, 27, and 36 J/cm^2 (5 mW/cm^2 for 60, 90, and 120 min, respectively) exhibited no significant effect on the MTT reduction, the ALP activity or the cell proliferation rate as measured by the BrdU method. In contrast, cells exposed to doses above 36 J/cm^2 (5 mW/cm^2 for more than 120 min) showed a significant decrease in all the parameters of cell function measured.

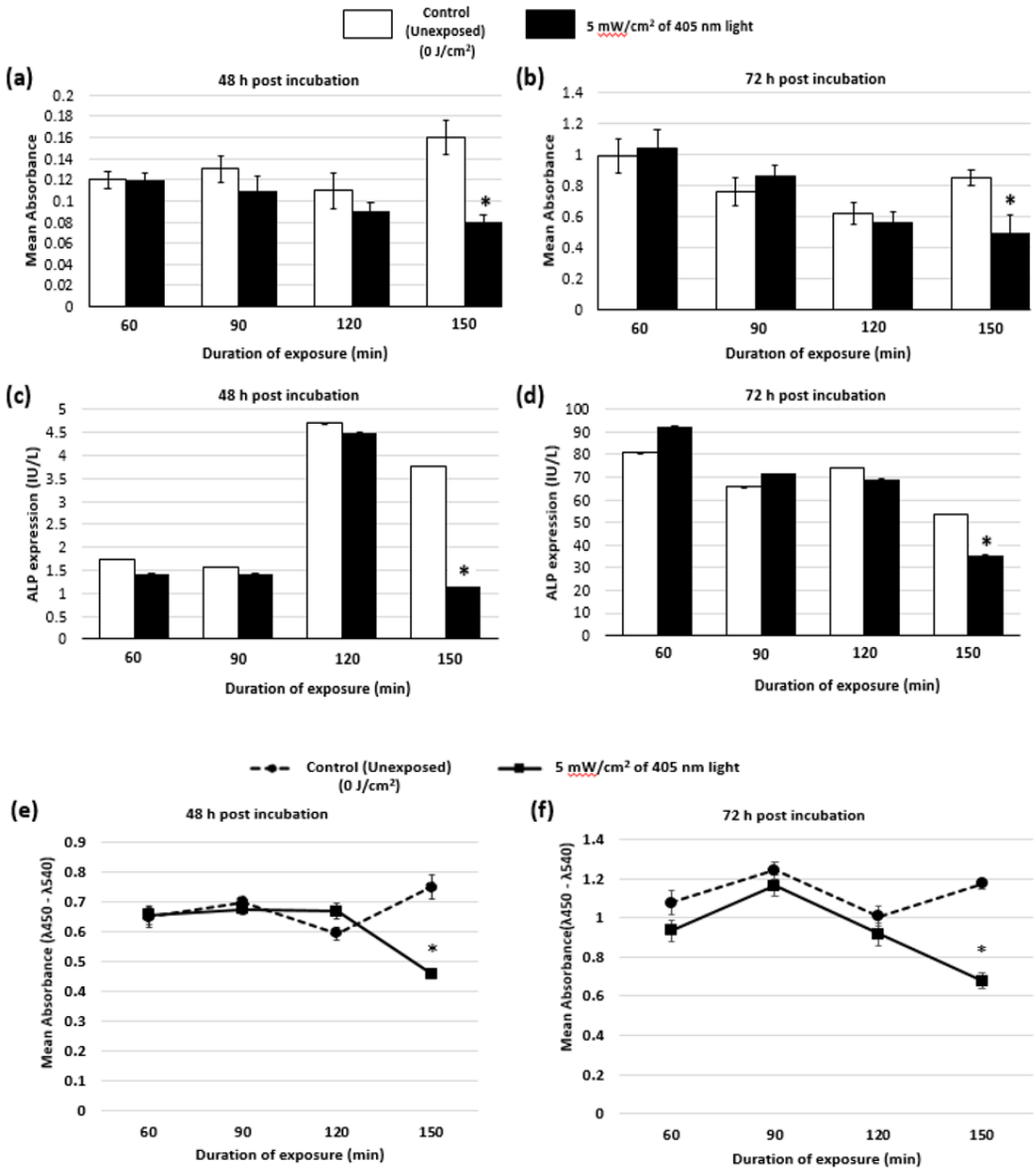

Fig. 3.9: MTT reduction, ALP activity and cell proliferation in osteoblasts exposed to different doses of 405 nm light. (a) & (b), MTT reduction (Mean Absorbance ± SEM, *n* = 8); (c) & (d) ALP activity (IU/L ± SEM, *n* = 8) and ; (e) & (f) BrdU responses (Mean ± SEM, *n* = 8) of rat osteoblasts exposed to 405 nm light doses of 18, 27, 36 and 45 J/cm^2 (5 mW/cm^2 for 60, 90, 120 and 150 min respectively) followed by 48 (left) and 72 hours (right) post treatment period. * Statistically different, using unpaired Student's t-test comparing control and light treated samples, $p < 0.05$.

3.3.5 Live/Dead cell staining of cells after exposure to 405 nm light

After both 48- and 72-h culture post exposure to light, similar levels of live cells were observed following 60, 90 and 120 min exposure to 5 mW/cm^2 405 nm light when compared to their respective unexposed controls. On the contrary, more apoptotic and dead cells were observed following 150 min (45 J/cm^2) exposure to 405-nm light (Fig. 3.10) compared to its respective unexposed sample. These results are qualitative.

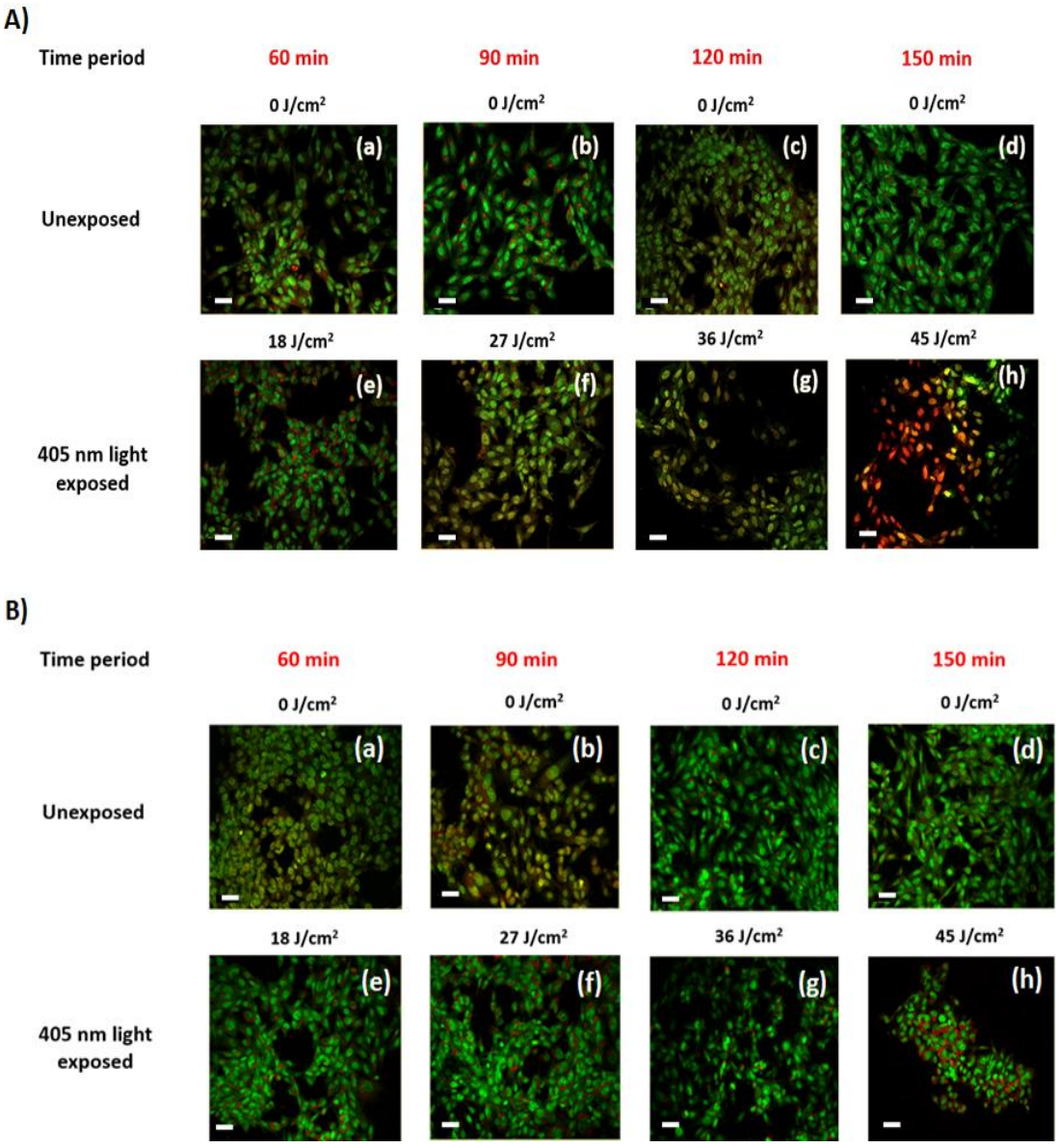

Fig. 3.10: The viability of osteoblast cells after exposure to 5mW/cm^2 of 405 nm light. (**A (a-h)** – Unexposed and 405 nm light exposed samples (18, 27, 36 & 45 J/cm^2) after a 48 hour post incubation period), **B** (**a-h**) – Unexposed and 405 nm light exposed samples (18, 27, 36 & 45 J/cm^2) after a 72 hour post incubation period). Acridine Orange stains live cells green, early and late apoptotic cells bright green and orange respectively and, Propidium Iodide stains dead cells red. Scale bars are 40 µm.

3.3.6 Phalloidin/DAPI staining

Staining of the actin with phalloidin-FITC showed that after exposure to 45 J/cm^2 light, the actin formed a ring around the cell membrane, and more cells rearranged themselves into a circular shape, when compared with the respective unexposed samples for both 48- and 72-h post treatment periods. Samples exposed to 18, 27 and 36 J/cm^2 of 405 nm light, however, showed no ring formation of actin around the cell membrane when compared with their respective unexposed samples for both 48- and 72-h post treatment periods (Fig. 3.11) (see appendix Fig A.3 for larger images of actin rings formed in samples exposed to 45 J/cm^2).

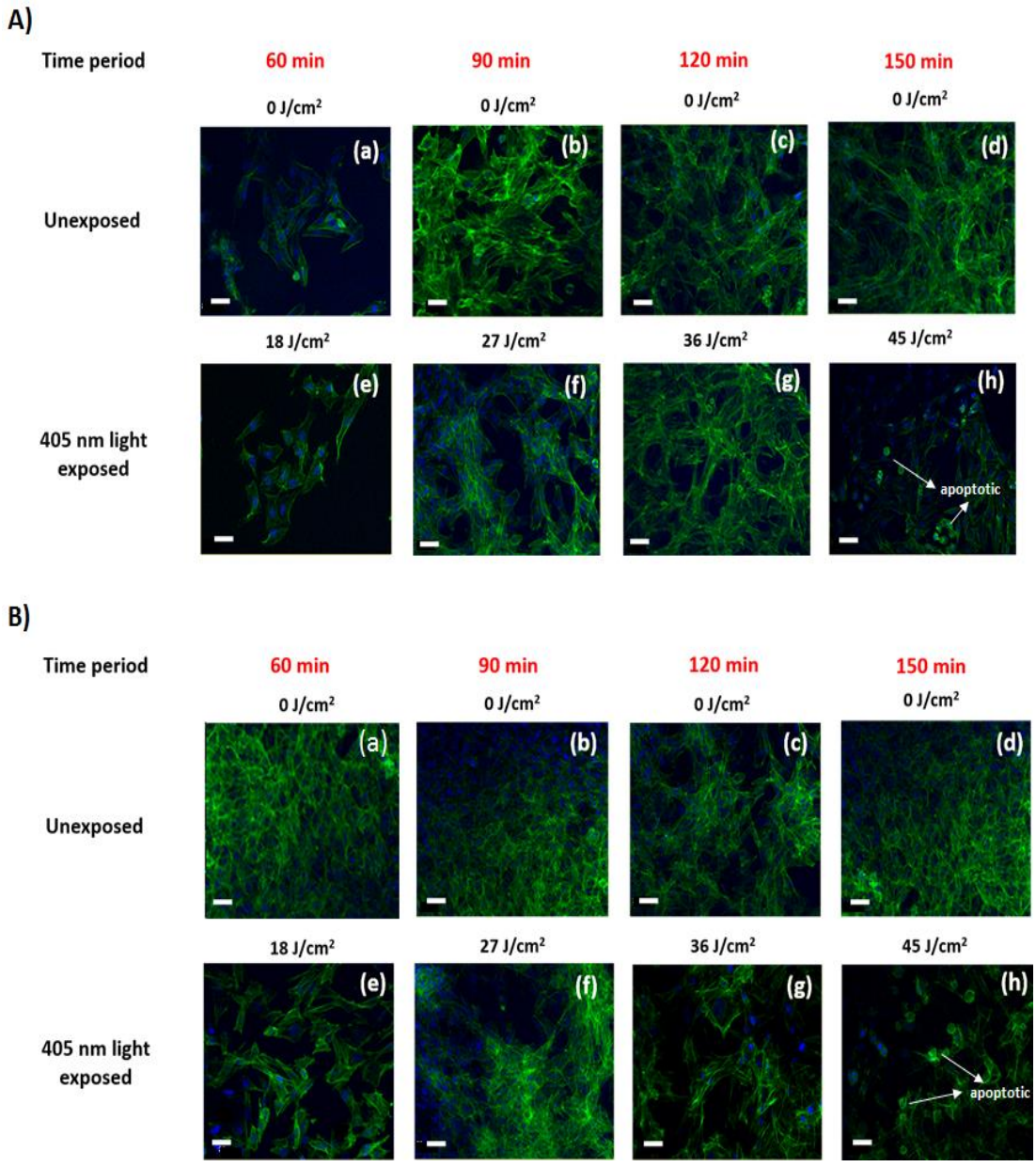

Fig. 3.11: The morphology of osteoblast cells after exposure to 5mW/cm^2 of 405 nm light (**A (a-h)** – Unexposed and 405 nm light exposed samples (18, 27, 36 & 45 J/cm^2) after a 48 hour post incubation period), **B** (**a-h**) – Unexposed and 405 nm light exposed samples (18, 27, 36 & 45 J/cm^2) after a 72 hour post incubation period). Phalloidin -FITC stains the cytoskeleton green and DAPI stains the nucleus blue. Scale bars are 40 μm.

3.3.7 Western Blotting (PARP analysis)

Initial blotting experiments using 1×10^6 cells produced less dense optical bands that were almost invisible on the blot paper, due to low protein content and hence 2×10^6 cells were used. At this cell population, it was found that there was no detectable PARP cleavage seen on the membrane for samples analysed immediately after exposure to 405 nm light for 1, 2 and 3 h at 15 mW/cm^2 compared to their respective unexposed samples (Figure 3.12). The molecular weight of the protein was identified by comparing the position of the band with the known molecular standard bands.

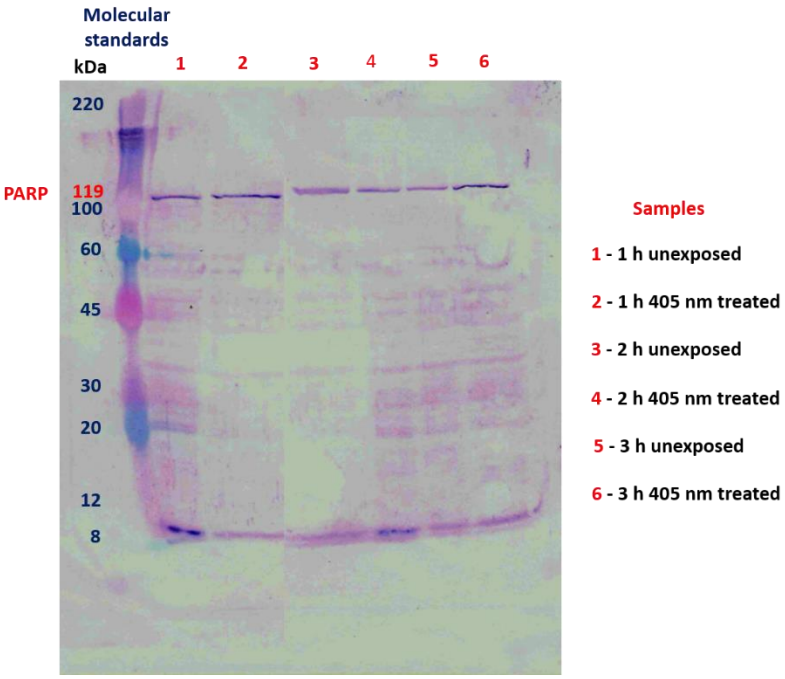

Fig. 3.12: Western blotting of homogenates prepared from 2 x 10^6 cells/cm^2 exposed to 405 nm light for 1, 2 and 3 h at 15 mW/cm^2 and unexposed samples.

3.3.8 Flow cytometry

Out of the 20,000 cells analysed, it was found that the % of early apoptotic cells was between 55 – 65 % for both the unexposed and 405 nm light exposed samples while the % of late apoptotic cells were between 30 – 40 % for both the unexposed and 405 nm light exposed samples, for up to a period of 2 h (Figure 3.13) (Table 3.6). A higher percentage of cells (50.6 % cells) were identified in the late apoptotic phase for the 2.5 h unexposed sample compared with the cells exposed to the 405 nm light (13.3%) for the same time point (Table 3.6). No evidence for a greater % apoptosis was seen in samples following exposure to 405 nm light when compared with the unexposed controls. In fact, the % apoptosis in the control untreated cells was very high and this could probably be because of the manipulation required to obtain the cells in suspension for flow cytometry. Calibrite beads (BD Bioscience, Oxford, UK) were used to adjust instrument settings, set fluorescence compensation, and check instrument sensitivity before the cells were analysed.

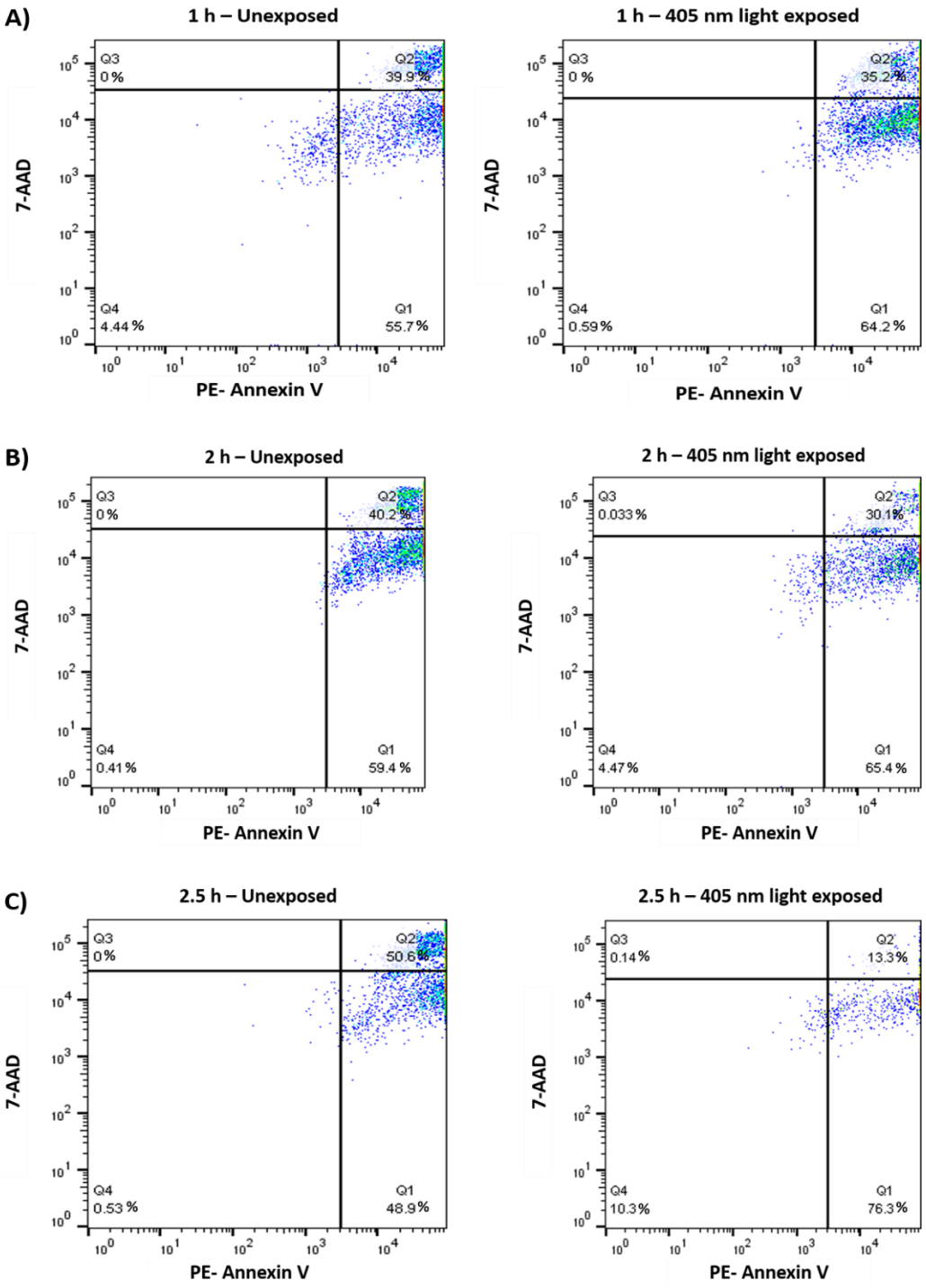

Fig. 3.13: shows the % of live cells (Q4), early apoptotic cells (Q1), late apoptotic cells(Q2) and dead cells (Q3) for all the samples (both unexposed and 405 nm light exposed for 1, 2 and 2.5 h) using PE-Annexin V and 7-AAD.

Table. 3.6: Mean % of live, early apoptotic, late apoptotic and dead cells after exposure to 405 nm light for each time point tested for A) 1st run, B) 2nd run.

A)

	Q4 (% of live cells)	Q1 (% of early apoptotic cells)	Q2 (% of late apoptotic cells)	Q3 (% of dead cells)
1 h				
Unexposed	4.44	55.7	39.9	0
405 nm exposed	0.59	64.2	35.2	0
2 h				
Unexposed	0.41	59.4	40.2	0
405 nm exposed	4.47	65.4	30.1	0.033
2.5 h				
Unexposed	0.53	48.9	50.6	0
405 nm exposed	10.3	76.3	13.3	0.14

B)

	Q4 (% of live cells)	Q1 (% of early apoptotic cells)	Q2 (% of late apoptotic cells)	Q3 (% of dead cells)
1 h				
Unexposed	1.40	56.5	42.1	0.015
405 nm exposed	1.11	66.5	32.4	0
2 h				
Unexposed	1.06	66.5	32.3	0.11
405 nm exposed	0.64	60.5	38.8	0.078
2.5 h				
Unexposed	0.29	63.3	36.3	0.031
405 nm exposed	6.21	74.0	17.7	0.012

3.3.9 Effects of different doses of 405 nm light on a range of bacteria

Results in Figure 3.14 highlight the inactivation kinetics of a range of Gram-positive (*S. aureus, S. epidermidis*) and Gram-negative (*P. aeruginosa, A. baumannii, E. coli, K. pneumoniae*) bacteria. The susceptibility of the organisms varied with *A. baumannii* proving most susceptible with > 98% kill achieved after exposure to 4.5 J/cm^2 ($p < 0.001$) compared to the non-treated sample. Significant inactivation of all organisms was achieved by exposure to 18 J/cm^2 and between 99.5% and 100% inactivation of all species was shown after application of 36 J/cm^2.

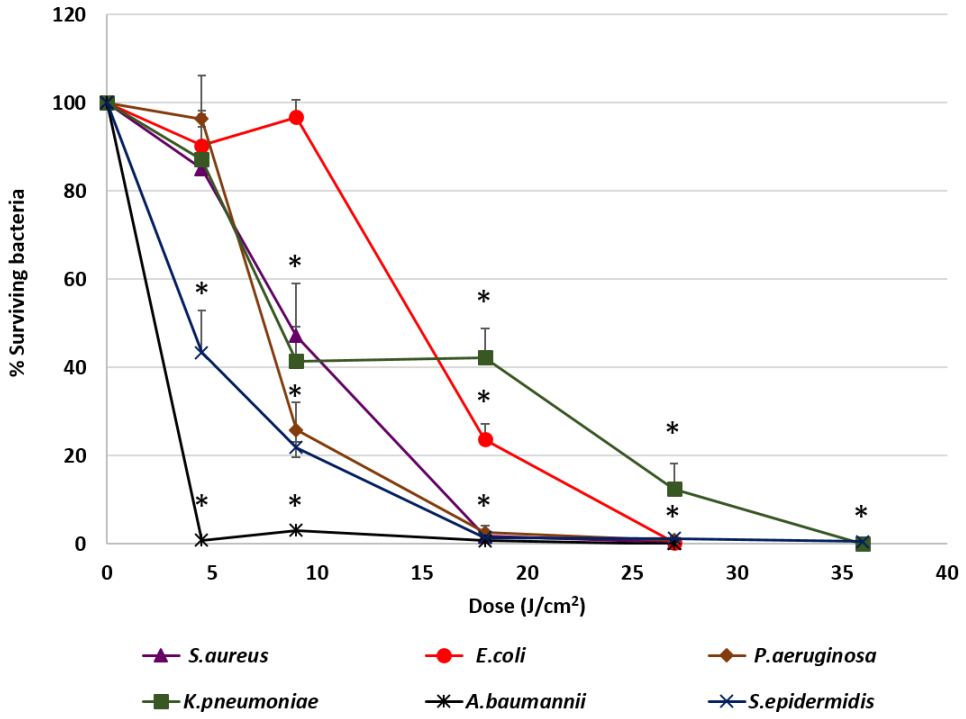

Fig. 3.14 Survival of a range of surface seeded clinically-relevant bacterial pathogens exposed to 405 nm light at doses ranging from 4.5 J/cm^2 – 36 J/cm^2 compared to their respective unexposed controls. Results are means of $n = 4 \pm$ SEM, ***** statistically different, using unpaired Student's t-test comparing control and light treated samples, $p < 0.05$.

3.4 Discussion

The mammalian cell studies show that cell exposures to 405 nm light for up to a dose of 36 J/cm^2 (5 mW/cm^2 for 2 h) cause no observable effects on the cell viability, function, proliferation rate, and morphology using the techniques employed in this study (Fig. 3.9, 3.10 and 3.11). However, at higher doses i.e., 54 J/cm^2, 405 nm light had a detrimental effect on mammalian cell viability (Fig. 3.6, 3.8, 3.9, 3.10 and 3.11). Studies were undertaken to find out if cells could survive 54 J/cm^2 of 405 nm light when delivered at a lower irradiance of 0.5 mW/cm^2 (10 fold less) for 30 h. However, these studies could not be continued as initial experiments revealed that the cells did not survive in DPBS buffer for 30 h due to lack of supply of nutrients for the 30 h period. (Fig. 3.7). The dose dependency study results (Fig. 3.8) suggest that irrespective of how the 405 nm light doses were administered, the cells showed no loss in cell viability at 18 J/cm^2 while there was a significant loss in viability at 54 J/cm^2 for all irradiance/exposure period regimes used, indicating that the effect of 405 nm light on mammalian cells is dose dependent, within the range of irradiances utilised in this study.

AO and PI dyes were used in this study to differentiate between live cells, apoptotic and necrotic cells, and study the viability of osteoblasts after 48- and 72-h post light exposure periods. After both 48- and 72-h culture periods post treatment, more apoptotic and dead cells were observed following 150 min (45 J/cm^2) exposure compared to 120 min (36 J/cm^2) exposure to 5 mW/cm^2 405-nm light (Fig. 3.10A & B), confirming the findings with MTT. Phalloidin-FITC and DAPI staining of the cells showed that most of the cells exposed to 405 nm light at 45 J/cm^2 rearranged into circular shapes with their actin forming a ring around the cell membrane when

compared with the samples exposed to 36 J/cm^2 for both 48- and 72-h post treatment period (Fig. 3.11A & B). Accumulation of actin around the outer-cell perimeter is indicative of membranes being strengthened and crosslinked to prevent leakage of the cell contents and is a sign of apoptosis. This phenomenon helps to ensure that apoptosis occurs in single cells, as strengthening the cell membrane prevents toxic cytokines and inflammatory mediators from leaking out to affect neighbouring cells.

At 48 h in culture post-exposure to light, the cells show early apoptosis (Fig. 3.10A (g)), but this damage appears to be repaired at 72 h in culture post-exposure to light (Fig. 3.10B (g)). To confirm induction of apoptosis, experiments were carried out to determine if caspases were activated following exposure to 405 nm light. This was performed by PARP analysis by western blotting. PARP, a nuclear enzyme found in the nucleus of the cell plays a crucial role in DNA repair, DNA integrity and cell death (Herceg & Wang, 2001). During apoptosis, proteolytic cleavage of PARP-1 into a 85- and a 24 kDa fragment occurs by caspase -3 and -7 (Kaufmann *et al*.,1993 & Lazebnik *et al*., 1994). In the present study, it was found that there was no detectable PARP cleavage occurring at any of the applied 405 nm light doses when compared with their respective unexposed samples (Fig. 3.12) indicating that the doses applied did not induce detectable activation of the caspases. It would have been ideal to conduct PARP analysis with the cell densities and doses of 405 nm light shown in previous experiments to induce damage (refer to Section 3.3.4), however higher cell seeding densities were required due to lack of sensitivity of this method, and therefore higher doses of 405 nm light were used in order to induce cell damage in such high cell populations. Because of difficulties with the sensitivity of

this method, the results of the experiments on cleavage of PARP are not conclusive; a more sensitive method to detect apoptosis was required.

To obtain further evidence for the occurrence of apoptosis, post treatment cells exposed to 405 nm light were analysed by FACS to identify the presence of PS on the external surface of the cell membranes by annexin-PE binding. FACS results revealed that there were too many cells in the early and late stages of apoptosis present in the control unexposed samples (Fig. 3.14). FACS analysis requires a suspension of cells and one of the possible reasons for the occurrence of apoptosis in control cells could be due to the use of an adherent cell type for this study. Since a cell dissociation agent was used to detach cells, it could have triggered an apoptotic event in cells. Thus we were not able to confirm the occurrence of apoptosis in cells exposed to 405 nm light by either of the methods used. These experiments to detect apoptosis were carried out at the end of the doctorate period, and time did not allow the investigation of alternative methods for detecting apoptosis.

When investigating the comparative effects of 405-nm light exposure on bacterial and mammalian cells, results demonstrated that doses up to 36 J/cm^2, which were found to have no impact on the mammalian cells, induced significant bactericidal effects (Fig.3.15). A previously published study reported the antibacterial effects of 405-nm light against these clinically relevant organisms, demonstrating their susceptibility at population densities of up to 9-log$_{10}$ CFU/ml in liquid suspension (MacLean *et al*., 2009). However, the present study uses light doses and surface-seeded bacterial cells at population densities (~10^2 CFU/plate) that are more relevant to practical clinical environmental decontamination applications, (MacLean *et al*.,

2010) as has been demonstrated in a previous work (McDonald *et al*., 2013). The present study confirms, by direct comparison, the selective detrimental effect that light of this wavelength can have on infection-causing organisms in comparison to mammalian osteoblasts. The antibacterial effect of 405-nm light is not thought to be mediated through direct DNA crosslinking, unlike that of UV light (Oguma *et al*., 2001). Instead, the 405 nm violet-blue light inactivation effect is considered to be caused by the excitation of intracellular photosensitive porphyrin molecules, which results in the production of reactive oxygen species (ROS), inducing oxidative damage and, consequently, cell death (MacLean *et al*., 2009; Lubart *et al*., 2011; Dai *et al*., 2013; Lipovsky *et al*., 2010). Indeed, previous studies have detected endogenous porphyrins within *S. aureus* (Lipovsky *et al*., 2010), *P. aeruginosa* (Dai *et al*., 2013), and *A. baumannii* (Zhang *et al*, 2014), and implicated these violet-blue light sensitive molecules in the inactivation mechanism. In addition, a study by Lipovsky *et al*., 2010, compared the sensitivity of two strains of *S. aureus* and found that the more light-sensitive strain contained 10-fold more endogenous porphyrins than the more resilient strain.

Further evidence of the involvement of porphyrins in the inactivation process was provided by Nitzan *et al*., who demonstrated that bacterial susceptibility to violet-blue light inactivation can be increased when exogenous 5-aminolevulinic acid (ALA), the precursor of the porphyrin biosynthesis pathway, was added in order to amplify the levels of endogenous porphyrins within the bacterial cells (Nitzan *et al*., 2004; Nitzan and Kauffman, 1999). Since ROS are considered to cause widespread oxidative damage to bacterial cells and the mechanism of action is not site specific, as is the case with many antibiotics, this explains not only the broad spectrum

antimicrobial efficacy of 405-nm light but also why highly antibiotic resistant species such as *Acinetobacter baumannii* show no greater resistance to 405-nm light than non-antibiotic resistant bacteria. Bacterial cells have also been shown to have much greater sensitivity than mammalian cells to violet-blue light in the region of 405 nm (McDonald *et al*., 2013; Dai *et al*., 2013). Low levels of antioxidant defence enzymes in certain bacteria have been implicated as a possible reason for this (Halliwell and Gutteridge, 2001). In contrast, most mammalian cells are well equipped to survive in high oxygen conditions, and contain ample cytoprotective mechanisms such as superoxide dismutase, catalase, and glutathione peroxidase (Halliwell and Gutteridge, 2001).

These findings thus highlight the potential for development of 405-nm light for inactivation of bacterial contaminants around surgical sites. Exposure to 405-nm light has also been proven to cause no adverse effects on wound healing (McDonald *et al*., 2011), thus providing further evidence for potential clinical application of this disinfection technology. Environmental decontamination systems installed in Glasgow Royal Infirmary uses low intensity (0.5 mW/cm^2) for continual decontamination of hospital isolation rooms (MacLean *et al*., 2010). However, if 405 nm light is to be used for decontamination during arthroplasty surgeries which are carried out for about 1-2 h, quicker bacterial inactivation is required. The present study thus involved exposing mammalian and bacterial cells to higher intensity of 405 nm light (5mW/cm^2). McDonald, 2011 conducted 1 h exposure studies to 405 nm light at different intensities (e.g. 0.5, 1.8, 5 and 15 mW/cm^2) and established that no detrimental effects were observed in the viability of osteoblasts upon exposure to 5 mW/cm^2 for 1 h compared to 15 mW/cm^2 for 1 h. However, the experiments

conducted in this present study determined the viability of osteoblasts upon exposure to 5 mW/cm^2 for different time periods (1, 2 & 3 h) and a safe threshold dose of 36 J/cm^2 (5 mW/cm^2 for 2 h) for mammalian cell exposure, yet bactericidal was identified. Importantly, the dose-dependent effects of 405-nm light on osteoblast cells, were established from this current study, suggest that the dose of 36 J/cm^2, which may be achieved by applying different irradiances for varying time periods (e.g., 10 mW/cm^2 for 1 h, 5 mW/cm^2 for 2 h, 3.3 mW/cm^2 for 3 h, and 2.5 mW/cm^2 for 4 h), does not cause detectable damage to mammalian cells, regardless of how the dose is applied. These findings are significant, and should provide a basis for the development of light sources which could be applied practically within operating theatres at levels appropriate for the typical operating times relevant to arthroplasty surgery.

Further safety advantages of light of this wavelength compared with UV light relate to the photon energy of 405-nm light. The depth of penetration of visible light into tissue increases with wavelength (Sternberg and D. Dolphin, 1998) and the penetration of 405-nm light, which although greater than that of UV light, is low and it will not penetrate deeply into bone; particularly when compared to light of a longer wavelength, e.g., 690-nm laser light that penetrates 0.16 ± 0.4 cm at an intensity of 4.3 mW/cm^2 into the porcine trabecular bone (Bisland and Burch, 2006). Also, the 405-nm intensities suggested for use during surgical exposures would be low; therefore, theatre personnel are unlikely to require protection from these visible violet-blue light wavelengths. This is unlike UV light which, due to the high photon energy and associated detrimental health effects, is normally only used in the absence of people. There have been limited attempts to utilize UV light during surgical

procedures but these have required operating staff to wear protective clothing during exposure (Taylor *et al*., 1995; Gosden *et al*., 1998). This is not comfortable, and so was not popular with the staff.

In summary, 405 nm light has proven to have strong antimicrobial effects against a variety of medically significant bacteria at a dose level of 36 J/cm^2. Conversely, mammalian cell studies found that the osteoblasts appear healthy when exposed to doses up to 36 J/cm^2; at higher doses, there is a negative impact on cell viability, function, and proliferation rate. The results obtained from the application of low dose and high dose light using a range of irradiance/exposure time regimes have demonstrated that the effects of 405-nm light on osteoblast cells are dose dependent. This study has established a dose level at which there is a differential sensitivity to the effects of 405-nm light between osteoblasts and bacteria; exposure of mammalian cells up to a dose of 36 J/cm^2 does not cause any observable effect on osteoblast viability. At this dose, the 405-nm light is still bactericidal indicating that there is potential to develop the technology for decontamination of the environment around patients during arthroplasty surgery.

Chapter 4

Cytotoxic responses to 405 nm light exposure in mammalian and bacterial cells: involvement of reactive oxygen species

4.1 Introduction

Violet-blue light in the region of 405 nm has antimicrobial activity against a variety of medically-relevant bacterial species (Bache et al., 2012; Maclean et al., 2015, 2013, 2009; McKenzie et al., 2014) and studies have demonstrated the increased susceptibility of bacterial cells compared to their mammalian counterparts – potentially providing the ability to preferentially inactivate microbial contamination in wound and tissue environments (Dai et al., 2013; Zhang et al., 2014).

The mechanism of the bactericidal action, and the occurrence of mammalian cell toxicity beyond a threshold exposure level (36 J/cm^2), have not been fully elucidated, but it is thought to involve the photo-excitation of endogenous porphyrin molecules, a process which generates reactive oxygen species (ROS). ROS, including singlet oxygen ($^1O_2$), superoxide anion ($O_2^{\cdot -}$), hydrogen peroxide (H_2O_2) and hydroxyl groups ($^{\cdot}OH$), are chemically reactive free radicals that play a crucial role in cell signalling and homeostasis, but overproduction becomes toxic to cells and alters redox balance causing significant damage to cell structures via oxidation of cellular macromolecules such as proteins, lipids, nucleic acids, NADH/NADPH and soluble thiols (Devasagayam et al., 2004). Since mammalian and bacterial cells contain intracellular porphyrins, during violet-blue light exposure, these porphyrins may become photosensitized leading to an overproduction of ROS (Kotelevets et al.,

2004; Lavi et al., 2004.Lubart et al., 2011).

As with traditional photodynamic inactivation reactions (Figure 1.6), which involve the use of exogenous photosensitive dyes or porphyrins (Gayl, 2001), photosensitization using violet-blue light is thought to cause cellular damage via two different pathways: Type I and Type II. With the Type I mechanism, the electronically excited sensitizer (e.g. endogenous porphyrin) reacts directly with the cellular component resulting in free radical formation (e.g. $O_2^{\cdot -}$ and $\cdot OH$). These free radicals propagate further free radical chain reactions (Figure 1.7). In the Type II process, the excited photosensitizer reacts directly with molecular oxygen resulting in the formation of $^1O_2$ (Davies and Pattison, 2006). Both pathways culminate in significant oxidative damage to exposed cells.

The experiments described in this chapter were carried out to investigate and compare the inactivation mechanism which occurs within mammalian and bacterial cells upon exposure to toxic levels of 405 nm violet-blue light. The study aimed to demonstrate ROS generation in mammalian and bacterial cells as a consequence of 405 nm violet-blue light exposure, and also to determine whether these ROS contributed to its cytotoxicity. With 405 nm light being highlighted in a number of recent studies as having potential applications for patient-safe environmental decontamination and wound decontamination, determining the mechanism(s) responsible for the effects induced in mammalian and bacterial cells upon exposure is important (Maclean et al., 2010; McDonald et al., 2011).

Osteoblasts, and the bacterium *Staphylococcus epidermidis*, were selected for use in this study as an example of a robust mammalian cell type, and a component of the natural skin microflora and common cause of hospital infection, respectively (Cogen et al., 2008; Lawrence and Waugh, 2013; Otto, 2009). In the present study, cells were exposed to increasing doses of 405 nm light to study how this affected the production of intracellular ROS in both the mammalian and bacterial cells. Glutathione, one of the important antioxidants present in plants, animals and a few bacteria, plays a crucial role in preventing cellular damage caused due to excess production of ROS including free radicals and peroxides (Couto *et* al., 2013). When glutathione peroxidase reduces peroxides, glutathione (GSH) is converted to its oxidised form (GSSG) (Figure 4.1), and the GSSG formed, is recycled and converted back to GSH in the presence of glutathione reductase (Figure 4.1). Oxidation (dimerization) of GSH to GSSG by various ROS has been widely utilised as an indicator of oxidative stress in mammalian cells (for example, Engelmann et al., 2005).

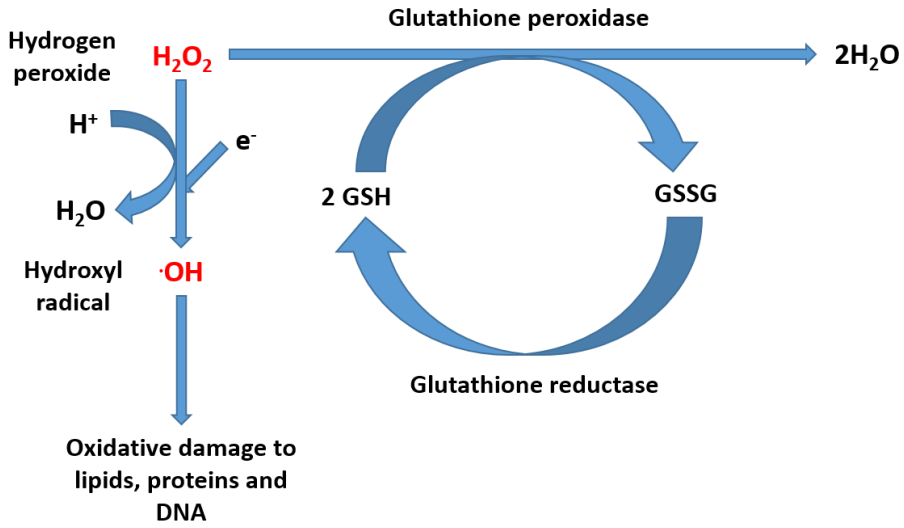

Fig. 4.1: The conversion of hydrogen peroxide to water molecules in the presence of glutathione peroxidase as adapted from Lehninger Principles of Biochemistry, Fifth edition, 2008, W.H Freeman and Company.

Dichlorodihydrofluorescein Diacetate (H_2DCFDA) dye has been commonly used to detect the generation of various ROS in neutrophils and macrophages (Johnson and Spence, 2010). Though the dye is insensitive to singlet oxygen directly, the singlet oxygen can indirectly contribute to the oxidation of the dye through its reaction with cellular components that yield peroxy radicals and peroxy products (Bilski et al., 2002). In order to detect and measure the production of intracellular ROS in mammalian and bacterial cells, 6-carboxy-2', 7'-dichlorodihydrofluorescein diacetate dye (carboxy-H_2DCFDA)(Invitrogen, catalogue no: C 400) was chosen as it is an improved version of H_2DCFDA dye that enables retention of the fluorescent product inside cells for a longer time period. Carboxy- H_2DCFDA is a chemically reduced, acetylated form of fluorescein used as an indicator for ROS in cells including cancer cells, astrocytes and phagocytes (Bols and Brubacher, 2001; Testa

et al., 2011; Trifunovic et al., 2005; Wu and Yotnda, 2011). This non-fluorescent molecule is readily converted to a green-fluorescent form when the acetate groups are removed by intracellular esterases, and oxidation by interaction with ROS occurs within the cell (Figure 4.2). The generation of green fluorescence from carboxy-H_2DCFDA following de-acetylation and oxidation is indicative of the presence of oxidative stress (Johnson and Spence, 2010). The cytotoxic response to the 405 nm light exposure was monitored by the reduction of MTT, which correlates cell metabolic activity with viability. The osteoblasts are an adherent cell line, and the number of viable cells adhering to the culture dishes after exposure to the light was also monitored by total cell protein.

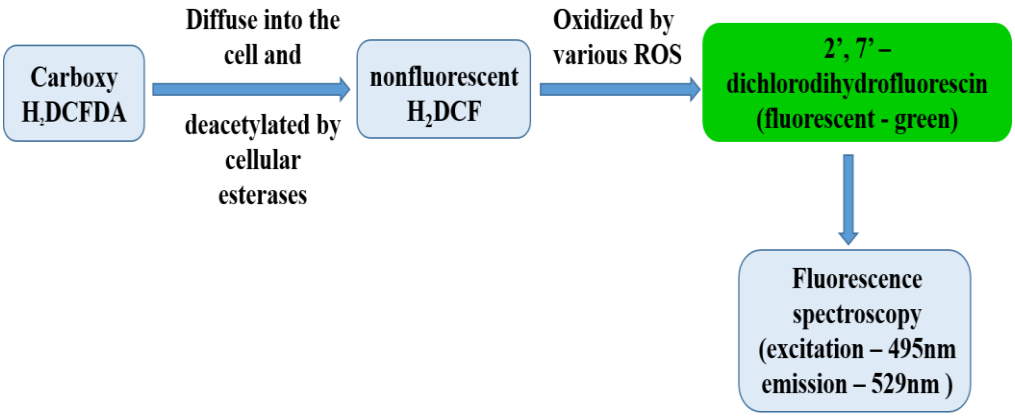

Fig.4.2: Schematic illustration of the generation of green fluorescence by carboxy-H_2DCFDA.

ROS scavengers play an important role in dealing with over production of ROS in the cell during oxidative stress conditions (Figure 4.3), thereby preventing cell death (Wulf Dröge., 2002). In order to further evaluate the role of ROS in the cytotoxic mechanism, different ROS scavengers, which can aid in cell protection by either preventing or removing the excess ROS produced during oxidative stress situations, were used (Sies, 1997).

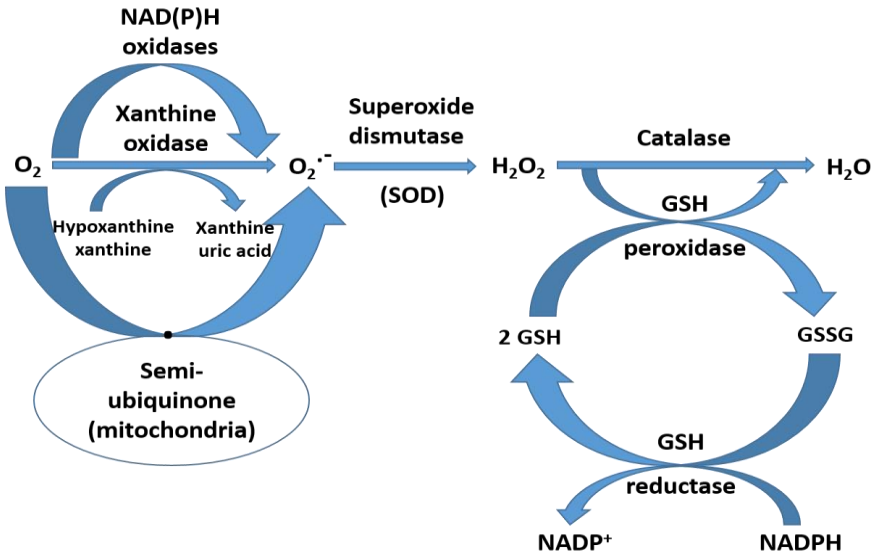

Fig. 4.3: Pathways of ROS production and clearance adapted from Wulf Dröge., 2002

Sodium pyruvate (an intracellular H_2O_2 scavenger), dimethyl thiourea (DMTU, an intracellular ·OH scavenger) and catalase (detoxifies extracellular H_2O_2) were added to mammalian and bacterial cell samples, both singly and in combination, during 405 nm light exposure, and the effect on the cells monitored. These scavenging chemicals were chosen based on their successful use in a previous study by MacLean and co-workers (Maclean et al., 2008). Sodium pyruvate has previously been shown to

protect human neuroblastoma cells at concentrations ≥ 1 mM against H_2O_2 insult (Wang et al., 2007), and DMTU, a ·OH scavenger, effectively protects renal cells and human bronchial epithelial cells at concentrations of 1 mM (Linas et al., 1987) and 10 mM (Rappeneau et al., 2000) respectively. Preliminary experiments with each of the scavengers were carried out to determine the effective dose, and ascertain that they were not toxic to the cells at that dose. The study results are discussed in terms of the cellular mechanisms involved in 405 nm violet-blue light cellular inactivation, and factors influencing the differing susceptibility of mammalian and bacterial cells to the light.

4.2 Materials and Methods

4.2.1 Culture and 405 nm light exposure of mammalian cells

Immortalised osteoblast (OST 5) cells were used for cell exposures in 24-well plates and 96 well plates. Cells were seeded at a density of 5×10^3 cells/cm^2 in 24-well plates, and 2×10^4 cells/cm^2 in 96-well plates, and left in the incubator overnight at 37°C and in an atmosphere of 5 % CO_2.

Post-incubation, growth medium was removed and 1 ml Dulbecco's Phosphate Buffered Saline (DPBS) solution was added to the central wells. The plates were transferred to an incubator at 37˚C in an atmosphere of 5% CO_2 where the samples were exposed to increasing doses of 405 nm light (Table 4.1), with dose (J/cm^2) calculated as the product of the irradiance (W/cm^2) × time (s). Unexposed controls were held under the same conditions but in a separate incubator (to avoid any effects of the light on the control). After the stipulated exposure periods, the following assays were performed on both the light-exposed and non-exposed control samples.

Table 4.1: The different periods of osteoblast cell exposure to 405 nm light, irradiance levels and the corresponding applied doses.

Exposure Period (hours)	Irradiance (mW/cm^2)	Dose (J/cm^2)
1	5	18
1.5	5	27
2	5	36
2.5	5	45
3	5	54

4.2.1.1 ROS detection and measurement in mammalian cells

ROS detection and measurement in adherent osteoblast cells was carried out using carboxy-H_2DCFDA dye (Invitrogen, UK: C400, Lot 28351W). After 405 nm light treatments at 5 mW/cm^2 for 1, 1.5, 2, 2.5 and 3 h (18, 27, 36, 45 and 54 J/cm^2 respectively), the DPBS solution was removed from the wells, and the cell monolayer washed twice with DPBS. The washing step was used to remove any cell debris present in the sample after 405 nm light exposure. The samples were immediately treated with 200 µl of 25 µM carboxy-H_2DCFDA and incubated in the dark at 37°C and 5 % CO_2 for 30 minutes to allow the probe to accumulate within the cells. After incubation, the cells were washed twice with DPBS. 1 ml 0.1% (v/v) Triton X-100 was then added to each well, and the cells incubated in the dark at room temperature for 20 minutes to allow the fluorochrome to leach out of the cells. Fluorescence was measured immediately using a RF-5001PC spectrofluorophotometer at an excitation wavelength of 495 nm and emission wavelength of 525 nm as described previously (Smith et al., 1992).

For microscopic imaging, cells (5×10^3 cells/cm^2) were grown on coverslips placed in the wells of 24-well plates. Post light treatment, cells were washed twice with DPBS, 200 µl of 25 µM carboxy-H_2DCFDA was added to the cells and they were then incubated in the dark at 37°C and 5 % CO_2 for 30 minutes. Post-incubation, excess dye was removed and cells were washed twice with DPBS. Coverslips were then placed onto microscopic slides and the samples viewed under a Axio Imager Z1 fluorescent microscope (Zeiss, Hertfordshire, UK) for green fluorescence at an excitation wavelength of 450-490 nm and emission wavelength of 515-565 nm using a 20× water lens (NA = 0.5).

4.2.1.2 Extracellular oxidised glutathione (GSSG) and intracellular reduced glutathione (GSH) measurement

(i) Preparation of GSSG standards: -

The following set of GSSG standards (Table 4.2) were prepared by adding set volumes of 1mM GSSG to set volumes of 25 % w/v Trichloroacetic acid (TCA) and DPBS.

Table 4.2: The different concentrations of GSSG standards.

	Concentration GSSG (µM)					
	0	**0.25**	**0.5**	**1**	**2.5**	**5**
1mM GSSG (µl)	0	2.5	5	10	25	50
25% TCA (ml)	2	2	2	2	2	2
DPBS (ml)	8	7.997	7.995	7.99	7.975	7.95

After 405 nm light treatment at 5 mW/cm^2 for 0, 1, 1.5, 2, 2.5 and 3 h (0, 18, 27, 36, 45 and 54 J/cm^2 respectively), 800 µl of DPBS buffer was removed from the wells without detaching the cells. The buffer was centrifuged at 10,000 ×g for 2 minutes to remove cell debris. 200 µl of 25% (w/v) TCA was then immediately added to the centrifuged supernatants (to prevent any further oxidation of GSH to GSSG). 200 µl of standards and samples were pipetted into clean test tubes, 100 µl of N-Ethylmaleimide (NEM) solution added and the tubes incubated for 30 minutes. After the incubatory period 2.1 ml of 0.2M NaOH and 100 µl of 1 mg/ml O-Phthalaldehyde (OPT) was added, mixed well and stored in the dark for 15 minutes. The fluorescence was read at 350 nm excitation and 420 nm emission using a RF-5001PC spectrofluorophotometer (Shimadzu, Japan) as described previously by Hilf and Hissin, 1976**.** The standard curve was obtained for every independent experiment.

(ii) Preparation of GSH standards: -

The following set of GSH standards (Table 4.3) were prepared by adding set volumes of 1 mM GSH to set volumes of 10 % TCA.

Table 4.3: The different concentrations of GSH standards.

	Concentration GSH (µM)					
	0	**0.25**	**0.5**	**1**	**2.5**	**5**
1mM GSH (µl)	0	2.5	5	10	25	50
10% TCA (ml)	10	9.997	9.995	9.99	9.975	9.950

After 405 nm light treatment at 5 mW/cm^2 for 0, 1, 1.5, 2, 2.5 and 3 h (0, 18, 27, 36, 45 and 54 J/cm^2 respectively), 200 µl of 10 % (w/v) TCA was added to the cells and the plates were placed on ice for 10 minutes. Thereafter, GSH was measured in the cellular acidic extracts by pipetting 25 µl of samples into clean test tubes. 2.3 ml of the phosphate buffer at pH 8.0 was added, lights were switched off and 100 µl of 1 mg/ml OPT was added. The samples were mixed well and stored in the dark for 15 minutes before reading the fluorescence at 350 nm excitation and 420 nm emission using a RF-5001PC spectrofluorophotometer, as described previously by Hilf and Hissin, 1976**.** The standards were treated the same way and the standard curve was obtained for every independent experiment.

The loss in intracellular GSH (nmoles) was correlated with the gain in extracellular GSSG (nmoles) in the buffer (taking into account differences in the volumes of the samples), between samples treated with 45 and 54 J/cm^2 to determine whether GSH loss was due to oxidation.

4.2.1.3 Measurement of mammalian cell viability in the presence and absence of scavengers

(i) Lowry assay

Cells were seeded at 5 × 10^3 cells/cm^2 in 24 well plates prior to exposure. The osteoblasts were exposed to 54 J/cm^2 405 nm light treatment (5 mW/cm^2 for 3 h) in the absence and presence of reactive oxygen species (ROS) scavengers: sodium pyruvate (1 mM,), dimethyl thiourea (1 mM,) and catalase (50 U/ml). The total protein content of the osteoblasts attached to the plate was determined 2 days after exposure as described previously in section 3.2.1.1.2.

(ii) MTT assay

Mammalian cell viability was measured using the MTT assay as described previously (Ho et al., 2004) and section 3.2.1.4.1. After exposing the osteoblasts in 96 well plates to 54 J/cm^2 of 405 nm light in the absence and presence of reactive oxygen species (ROS) scavengers: (1 mM sodium pyruvate, 1 mM dimethyl thiourea and 50 U/ml catalase), the MTT reduction was measured post a 48 h incubatory period (section 3.2.1.4.1).

4.2.2 Culture and 405 nm light treatment of bacterial cells

Staphylococcus epidermidis LMG 10474 (Laboratorium voor Microbiologie, Universiteit Gent, Belgium) was inoculated in 100 ml nutrient broth (NB) and incubated at 37°C for 18 hours under rotary conditions (120 rpm). Post-incubation, the broth was centrifuged at 3939 × g for 10 minutes, and the pellet re-suspended in 100 ml PBS, giving a population density of approximately 10^9 colony forming units (CFU)/ml. Two ml volumes of bacterial suspension were transferred to the middle 2 wells of a 12-well plate and exposed, at room temperature, to increasing doses of 405 nm light (Table 4.5). Unexposed controls were held under the same conditions but without 405 nm light exposure. A higher population density of 10^9 CFU/ml was used to enable the detection of ROS under the fluorescent microscope. Due to the use of this higher population density, the samples were exposed to higher doses of 405 nm light treatment (Table 4.4) than those used for inactivation of lower population densities, as detailed in Chapter 3.

Table 4.4: The different periods of bacterial cell exposure to 405 nm light, irradiance levels and the corresponding applied doses.

Exposure Period (hours)	Irradiance (mW/cm^2)	Dose (J/cm^2)
1	15	54
3	15	162
6	15	324

4.2.2.1 ROS detection and measurement in bacterial cells

After 405 nm light treatments at 15 mW/cm^2 for 0, 1, 3 and 6 h (0, 54, 162 and 324 J/cm^2 respectively), the bacterial cell suspensions were removed from the wells, and centrifuged at 3939 × g for 10 minutes to achieve a cell pellet. 200 µl 25 µM carboxy-H_2DCFDA was then added to the pellet, mixed, and left in the dark for 30 minutes at room temperature. Post-incubation, 195 µl of the aliquot was made up to 1 ml with PBS, and the fluorescence measured as described for the mammalian cells, directly in the cell suspension.

For microscopic imaging, 5 µl of the undiluted pellet with dye was pipetted onto a microscope slide and viewed for green fluorescence as described for the mammalian cells, but using a 100 × oil immersion lens (NA = 0.5).

4.2.2.2 Measurement of bacterial cell viability in the presence and absence of ROS scavengers

After exposure of bacterial suspensions to 15 mW/cm^2 405 nm light for 3 and 6 h (162 and 324 J/cm^2 respectively), bacterial samples were diluted in PBS (10^{-5}

dilution for unexposed samples and 10^{-1} up to 10^{-6} dilutions for 405 nm light exposed samples), plated onto nutrient agar (NA), and incubated at 37°C overnight before enumeration of the viable CFU/ml. To assess the effect of ROS scavengers on the inactivation kinetics, exposures were repeated in the presence of a range of scavengers: 100 mM Sodium pyruvate; 100 mM Dimethyl thiourea (DMTU); and 200 U/ml catalase, both individually, and combined (at the same concentrations). Higher concentrations of all the above mentioned scavengers were used for the bacterial cell studies (compared to those used for the mammalian cell studies) due to the use of higher bacterial cell densities and thus administration of higher 405 nm light doses. For each scavenger used, appropriate non-exposed controls were included in each experiment.

4.2.2.3 Detection and measurement of bacterial ROS in the presence of scavengers

The bacterial cell suspensions were exposed to 162 J/cm^2 405 nm light (15 mW/cm^2 for 3 h) in the presence of the ROS scavengers (100 mM Sodium pyruvate; 100 mM Dimethyl thiourea; 200 U/ml catalase). After light treatment, the bacterial cell suspensions were removed from the wells, and the fluorescence measured fluorimetrically and detected microscopically using carboxy-H_2DCFDA as described earlier. For each scavenger used, appropriate non-exposed controls were included in each experiment.

4.2.3 Statistical analysis

Number of samples used for each study are provided for their respective graph/table of results. Results are expressed as mean ± standard error of the mean. Significance has been established by either Student's t test, which compares the mean of each 405 nm light exposed group against their respective unexposed group, or one-way ANOVA followed by Dunnett's post hoc test which compares the means of each group against the mean of the reference group, using Minitab software.

4.3 Results

4.3.1 ROS detection in mammalian cells using carboxy-H_2DCFDA

The green fluorescence generated from carboxy-H_2DCFDA was detected by both fluorescence microscopy (Fig. 4.4), and by quantitative fluorescence measurement by spectrofluorimetry of the lysed cells (Fig. 4.5). The fluorescence intensity measurement for the unexposed cells (Fig. 4.4) was averaged over all exposure time points. This procedure was justified because there was no significant difference between the unexposed samples at all time points ($p>0.05$), using one-way ANOVA plus Tukey post hoc test. Data in Fig. 4.4 and Fig. 4.5 show a significant increase ($p<0.05$) in intracellular green fluorescence for 405 nm light treated samples for up to a period of 2 h (36 J/cm^2) when compared with the respective unexposed samples, using one-way ANOVA plus Dunnett's post-hoc test. The intracellular fluorescence of the 405 nm treated cells decreased at 2.5 and 3 h exposures (45 and 54 J/cm^2) compared to 2 h exposed samples.

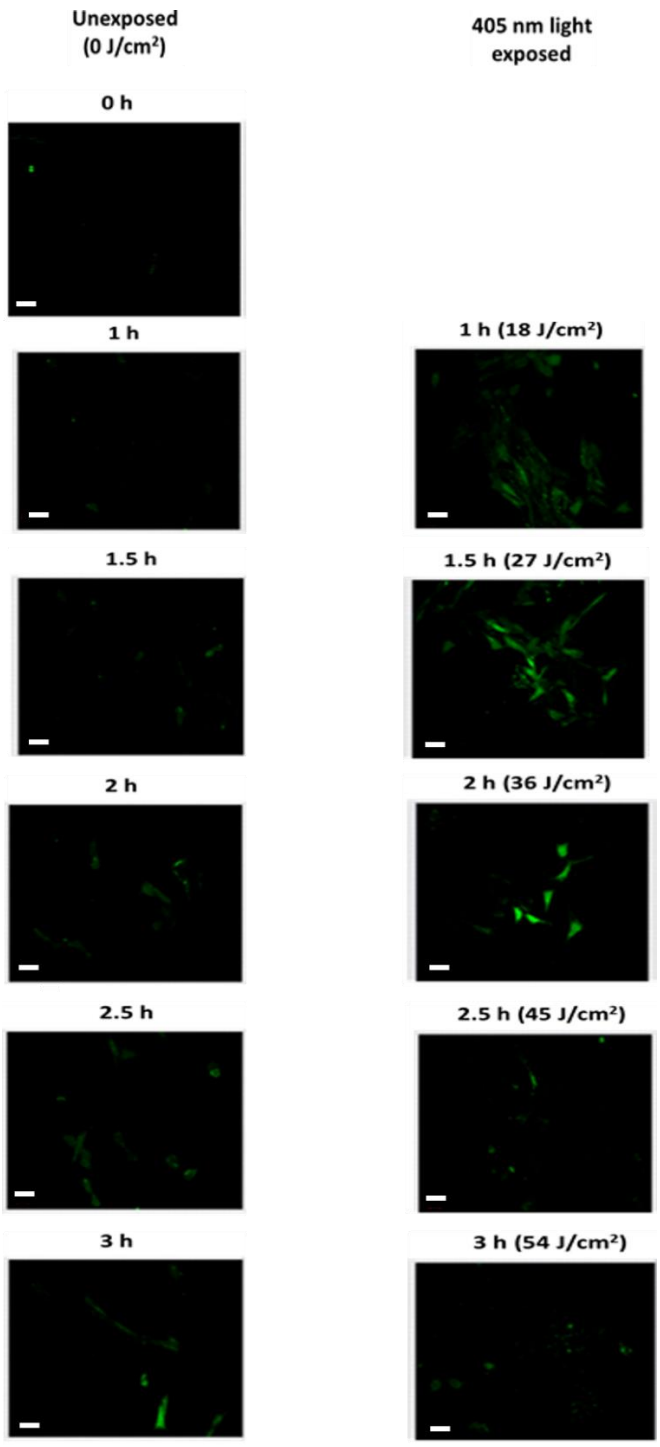

FIG. 4.4: Visual detection of ROS production in immortalised rat osteoblasts upon exposure to 5 mW/cm^2 405 nm light for 1, 1.5, 2, 2.5 and 3 h (18, 27, 36, 45 & 54 J/cm^2 respectively), using carboxy-H_2DCFDA and using fluorescence microscopy at an excitation wavelength of 450-490 nm and emission wavelength of 515-565 nm. Scale bars are 40 µm.

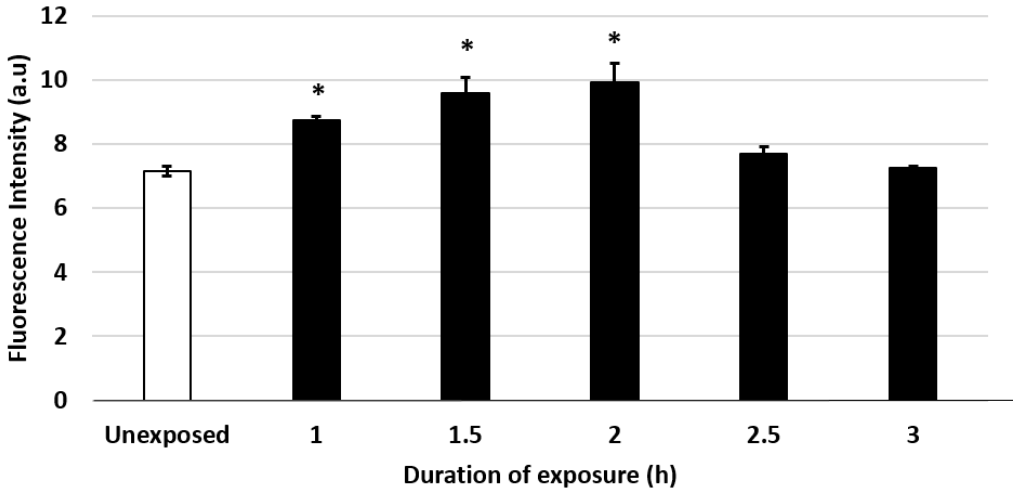

FIG. 4.5: Measurement of ROS fluorescence intensity in immortalised rat osteoblasts upon exposure to 5 mW/cm^2 405 nm light for 1, 1.5, 2, 2.5 and 3 h (18, 27, 36, 45 & 54 J/cm^2 respectively), using carboxy-H_2DCFDA at an excitation wavelength of 495 nm and emission wavelength of 525 nm. Data (Mean ± SEM, n=8) were analysed using one-way ANOVA plus Dunnett's post-hoc test. * indicates a significant difference ($p < 0.05$) between light-exposed and unexposed samples.

4.3.2 Measurement of GSH/GSSG content in mammalian cells

The intracellular GSH content of, and the GSSG efflux from, the mammalian cells were measured post-405 nm light treatment at different doses to find out whether the cells experienced oxidative stress. The GSH and GSSG concentrations of samples were calculated from their respective standard curves (see appendix Fig A.1 & A.2 for standard curves). Data in Fig.4.6 show that there was a significant decrease ($p < 0.05$) in the intracellular GSH content of the light-exposed cells at 3 h (54 J/cm^2) compared with the respective unexposed samples. There was no significant decrease in GSH levels prior to this dose. The extracellular GSSG concentration of the light-exposed samples increased significantly at 3 h exposure (54 J/cm^2) ($p < 0.05$) when compared with their respective unexposed samples (Fig. 4.6). The amount of intracellular GSH lost from the cells (nmol) was accounted for by the gain in extracellular GSSG (nmol). Taking the data from those presented on Fig 4.6, 0.21 ± 0.02 nmoles of GSH lost from the cells were accounted for by a gain of 0.09 ± 0.03 nmoles of GSSG in the extracellular buffer between exposure periods of 2.5 and 3 h (45 and 54 J/cm^2 respectively).

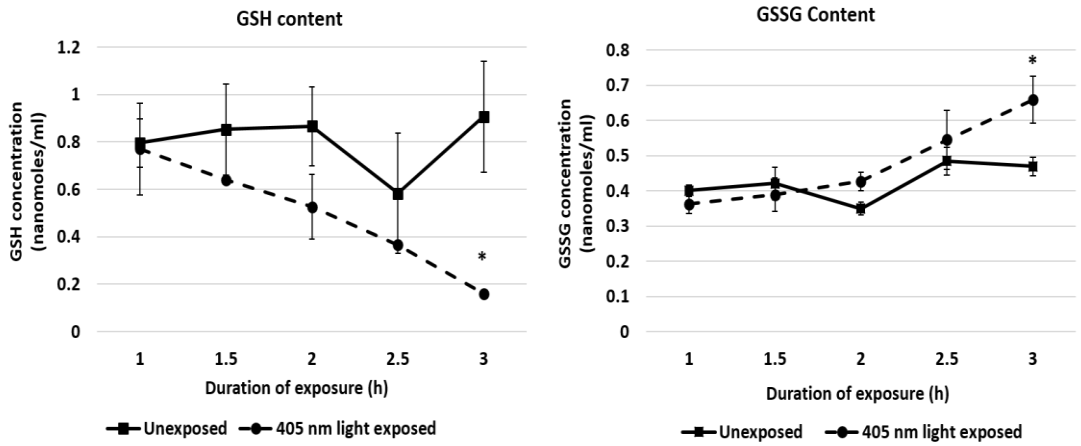

FIG. 4.6: Intracellular GSH concentration and extracellular GSSG concentration of rat osteoblasts exposed to 5 mW/cm^2 405 nm light for 1, 1.5, 2, 2.5 and 3 h (18, 27, 36, 45 & 54 J/cm^2 respectively). Data (Mean ± SEM, n=8) were analysed using unpaired Student's t-test; * indicates a significant difference (*, $p < 0.05$) between light-exposed and unexposed samples.

4.3.3 Mammalian cell viability in the presence and absence of ROS scavengers

Having shown generation of elevated ROS levels in both mammalian and bacterial cells during exposure to 405 nm light, experiments were carried out to find out whether or not cell viability was affected, and whether free radical scavengers could offer cell protection. Data in Figure. 4.7 show significantly decreased attached cell protein content for 405 nm light-treated samples exposed for 3 h (54 J/cm^2) in DPBS alone ($p < 0.001$), compared with the unexposed control. Interestingly, there was no significant decrease in protein content of the samples exposed to the same dose in the presence of sodium pyruvate (1 mM) and catalase (50 U/ml), compared with their respective unexposed controls. This demonstrates that the sodium pyruvate and catalase were able to prevent the loss of protein observed in non-scavenger exposed cells exposed to 405 nm light for 3 h. DMTU did not protect the light exposed cells to the same extent, when compared to the cells exposed in the absence of scavengers ($p > 0.05$).

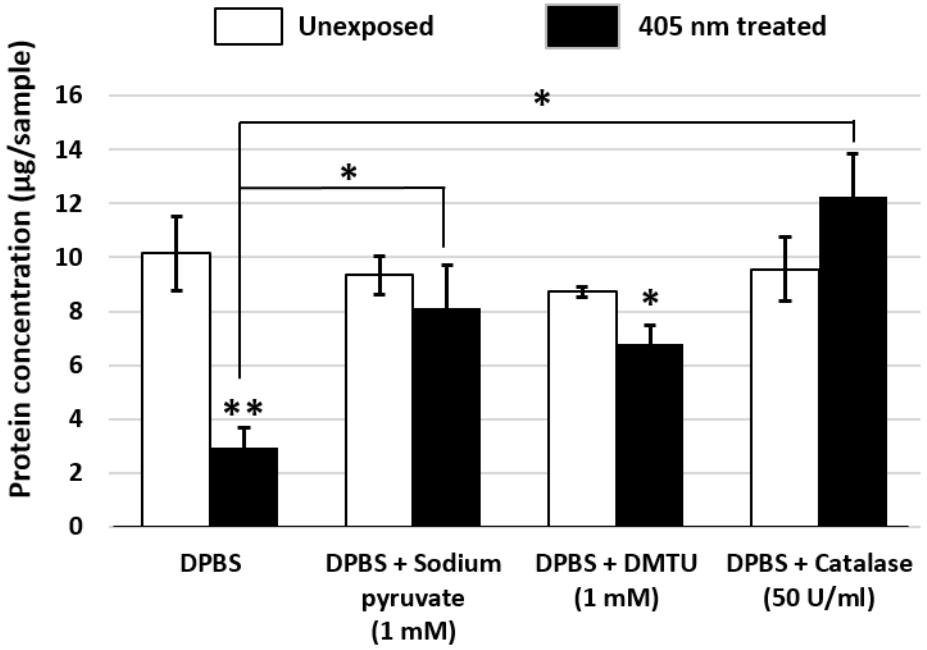

FIG.4.7: Protein concentration of rat osteoblasts exposed to 5 mW/cm^2 405 nm light at a dose of 54 J/cm^2 (3 h exposure), in the absence (DPBS alone) and presence of ROS scavengers: sodium pyruvate (1 mM), DMTU (1 mM) and catalase (50 U/ml). Measurements were made 48 hour post-treatment. Data (Mean ± SEM, n=8 and experiments were quadrupled with 2 samples each experiment) were analysed using an unpaired Student's t-test to detect significant differences between light-exposed and unexposed samples; (*, $p < 0.05$; **, $p < 0.001$) and one-way ANOVA plus Dunnett's post-hoc test to detect significant differences between light-exposed samples in the presence and absence of scavengers (*, $p<0.05$, denoted by line connectors).

When light toxicity was measured in terms of % of cellular metabolic activity (Fig. 4.8), only catalase offered complete protection from the effects of 405 nm light. In the presence of both sodium pyruvate and DMTU the toxicity of the light was evident by the decrease in % of cellular metabolic activity.

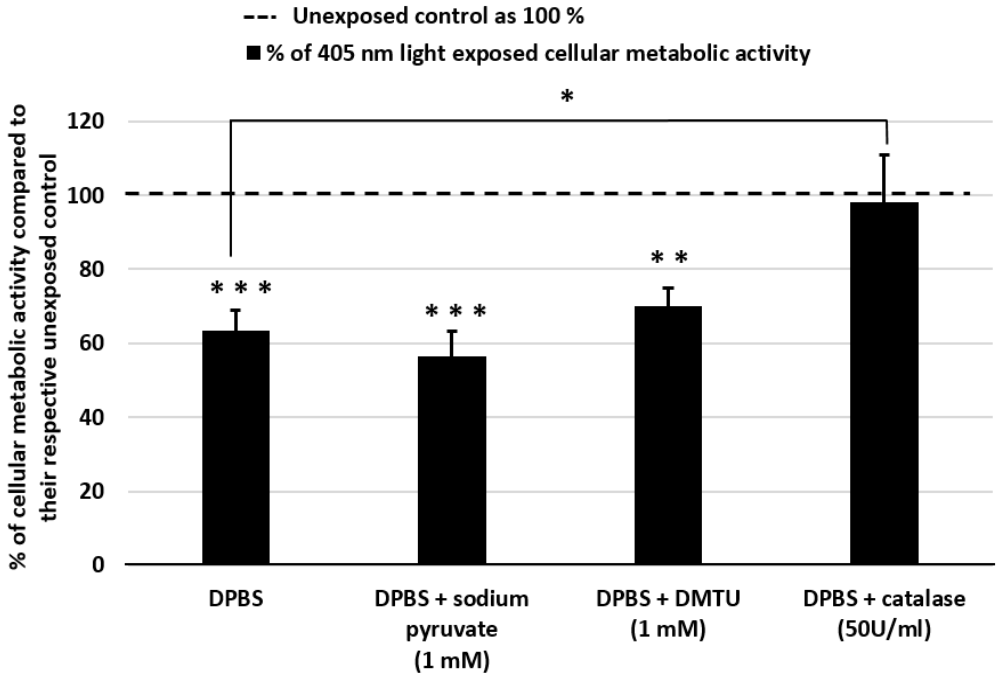

FIG.4.8: % of cellular MTT reduction of rat osteoblasts exposed to 5 mW/cm^2 405 nm light at a dose of 54 J/cm^2 (3 h exposure), in the absence (DPBS alone) and presence of ROS scavengers: sodium pyruvate (1 mM), DMTU (1 mM) and catalase (50 U/ml). Control taken as 100%, is unexposed cells treated with or without individual scavengers. Measurements were made 48 hour post-treatment. Data (Mean ± SEM, n=12) were analysed using an unpaired Student's t-test to detect significant differences between light-exposed and unexposed samples (**, $p<0.01$; ***, $p< 0.001$); and one-way ANOVA plus Dunnett's post-hoc test to detect significant differences between light-exposed samples in the presence and absence of scavengers (*, $p<0.05$, denoted by line connectors).

4.3.4 ROS detection in bacterial cells using carboxy-H_2DCFDA

In the bacteria, the accumulation of fluorescence is also shown both by microscopic images (Fig. 4.9) and by quantitative spectrofluorimetry (Fig. 4.10). The fluorescence intensity measurement for the unexposed bar (Fig. 4.10) was averaged over all exposure time points. This procedure was justified because there was no significant difference between the unexposed samples at all time points ($p > 0.05$), using one-way ANOVA plus Tukey post hoc test. Data in Fig. 4.9 & Fig. 4.10 show a significant increase in green fluorescence in 405 nm light-treated samples at exposure periods of 1 and 3 h (54 J/cm^2 and 162 J/cm^2 respectively) when compared with their respective controls, using one-way ANOVA plus Dunnett's post-hoc test. The green fluorescence of 405 nm treated samples decreased significantly at an exposure period of 6 h (324 J/cm^2) compared to the 3 h (162 J/cm^2) exposed samples ($p < 0.05$).

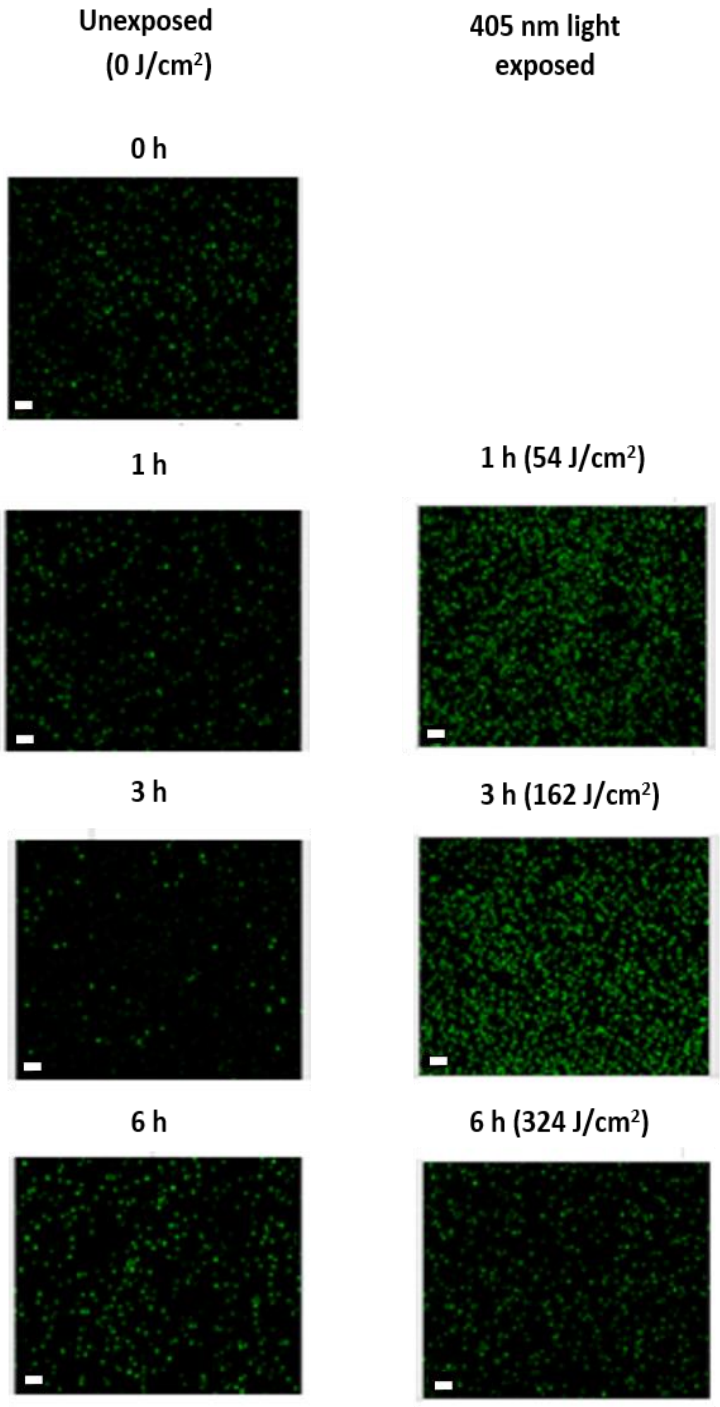

FIG. 4.9: Visual detection of ROS production using carboxy-H_2DCFDA in the bacterium *Staphylococcus epidermidis*, at a population of 10^9 CFU/ml, upon exposure to 15 mW/cm^2 405 nm light for 1, 3 and 6 h (54, 162, 324 J/cm^2 respectively) and using fluorescence microscopy at an excitation wavelength of 450-490 nm and emission wavelength of 515-565 nm. Scale bars are 6 µm.

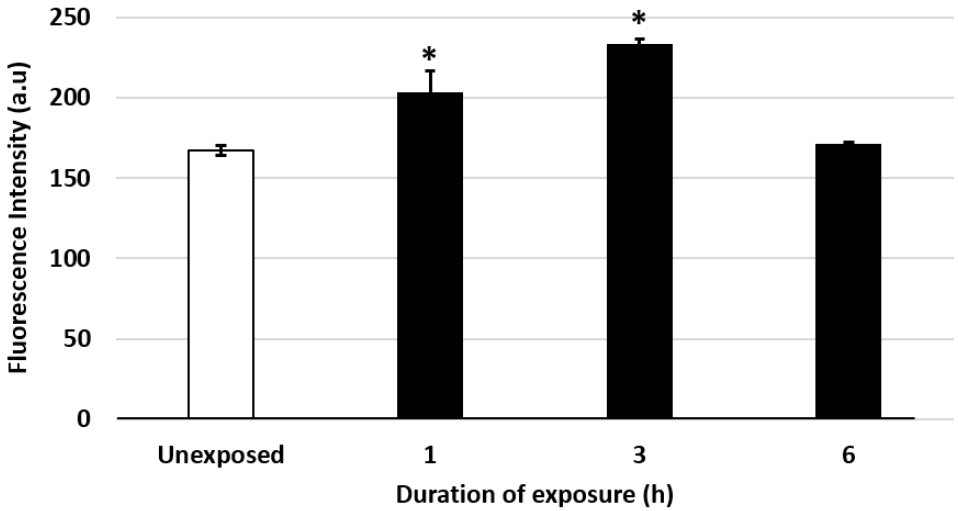

FIG. 4.10: Measurement of ROS fluorescence intensity in the bacterium *Staphylococcus epidermidis*, at a population of 10^9 CFU/ml, upon exposure to 15 mW/cm^2 405 nm light for 1, 3 and 6 h (54, 162, 324 J/cm^2 respectively) at an excitation wavelength of 495 nm and emission wavelength of 525 nm. Data (Mean ± SEM, n=6) were analysed using one-way ANOVA plus Dunnett's post-hoc test. * indicates a significant difference ($p<0.05$) between light-exposed and unexposed samples.

4.3.5 Bacterial cell viability in the presence and absence of ROS scavengers

Exposure of *S. epidermidis* to 405 nm light in the absence of scavengers produced significant population reductions (Fig. 4.11), with a 4.8-$\log_{10}$ reduction at an exposure period of 3 h (162 J/cm^2) ($p<0.001$), increasing to a 7-$\log_{10}$ reduction by 6 h (324 J/cm^2) ($p<0.001$). Due to the high (10^9 CFU/ml) population density used, higher concentrations of ROS scavengers (100 mM sodium pyruvate, 100 mM DMTU, 200 U/ml catalase) than those used for the mammalian cell study, were used to investigate whether they exerted a protective effect on bacterial cells exposed to 405 nm light. Results showed that when cells were exposed in the presence of sodium pyruvate, bacterial inactivation was significantly reduced, with only 2.8-$\log_{10}$ reduction achieved after a 3 h exposure period: 2-$\log_{10}$ less than when in the absence of scavengers. A degree of protection was observed with catalase, with 1.1-$\log_{10}$ less inactivation at 3 h, than in the absence of scavengers ($p<0.05$), however, by 6 h, the bacterial population had decreased to a similar level as measured without scavengers. DMTU appeared to offer no protection to 405 nm light-exposed cells at the concentration used in this study. Interestingly, the greatest protection was afforded by the combined use of the three scavengers, with inactivation at 3 h reduced by 3.5 $\log_{10}$ compared to that in the absence of scavengers ($p<0.05$). By 6 h, protection from the scavenger combination was similar to that exerted by the sodium pyruvate.

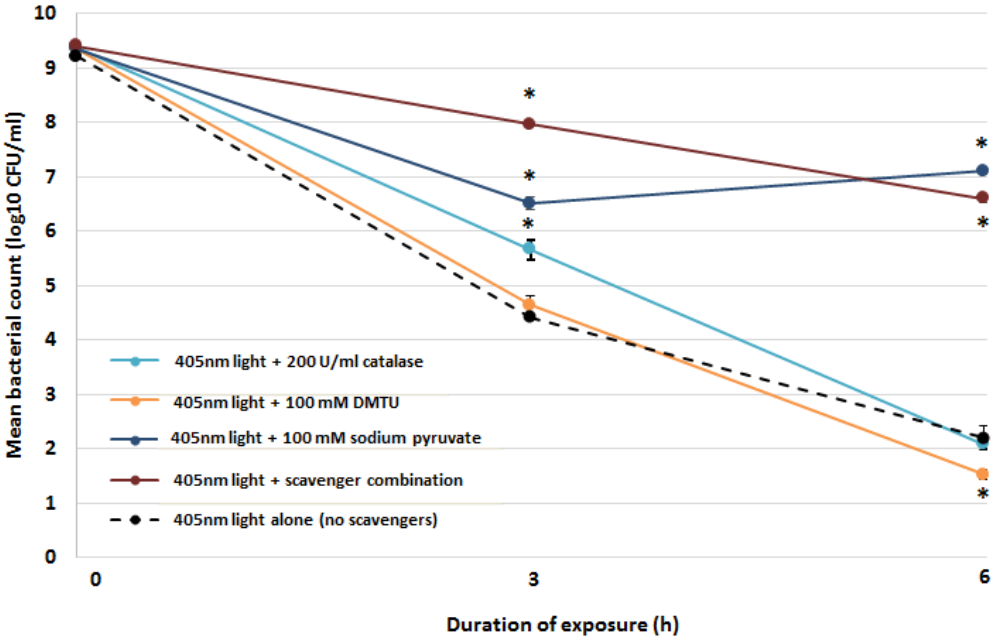

FIG. 4.11: Viability of *Staphylococcus epidermidis* exposed to 15 mW/cm^2 405 nm light for 3 and 6 h (162 & 324 J/cm^2) in the absence (in PBS) and presence of ROS scavengers: 100 mM sodium pyruvate, 100 mM DMTU, 200 U/ml catalase. Bacteria were also exposed to a combination of the scavengers, at the same concentrations. Data (mean $\log_{10}$ CFU/ml ± SEM, n=8) were analysed using a one-way ANOVA plus Dunnett's post-hoc test. * indicates a significant difference ($p<0.05$) between light-exposed samples in the presence and absence of scavengers. No significant change was detected in the non-exposed control samples over the duration of the experiment ($p>0.05$).

4.3.6 ROS detection and measurement in bacterial cells in the presence of scavengers using carboxy-H_2DCFDA

To check for a decrease in ROS production in bacterial cells in the presence of scavengers, carboxy-H_2DCFDA was used. A dose of 162 J/cm^2 (15 mW/cm^2 for 3 h) was selected for use as it was the mid-point on the inactivation curve (Fig. 4.11). Data show, both visually (Fig. 4.12) and spectroscopically (Fig. 4.13), that the least increase in fluorescence is produced with the cells exposed both in the presence of sodium pyruvate alone and the scavenger combination, which correlates well with the cell viability results. More cells survived when the ROS inhibitors were present, compared to non-scavenger treated light exposed cells. However, significant cell inactivation still occurred in the presence of different ROS inhibitors compared to unexposed ROS inhibitor treated control cells.

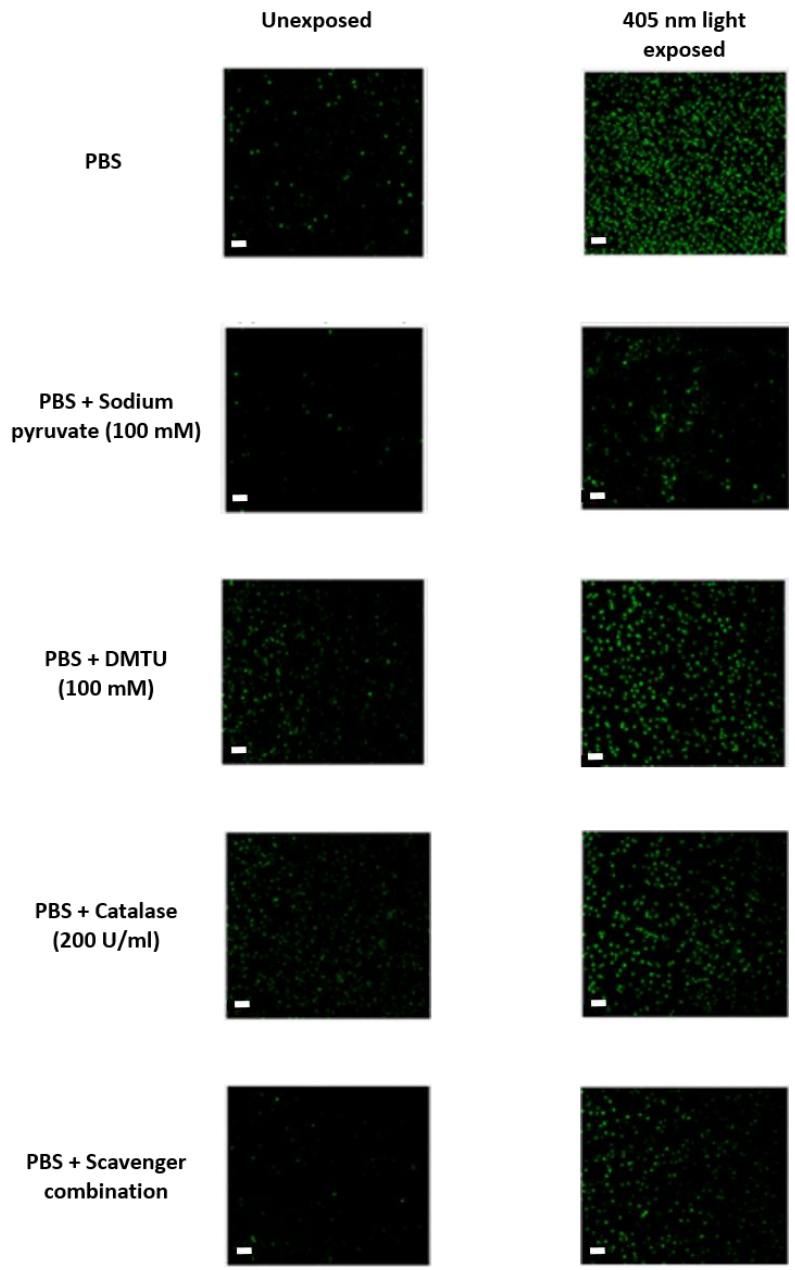

FIG. 4.12: Visual detection of ROS production in *Staphylococcus epidermidis,* at a population of 10^9 CFU/ml, exposed to 162 J/cm^2 405 nm light (15 mW/cm^2 for 3 h) in the absence (in PBS) and presence of ROS scavengers, using carboxy-H_2DCFDA and using fluorescence microscopy at an excitation wavelength of 450-490 nm and emission wavelength of 515-565 nm. The scavengers used were: 100 mM sodium pyruvate, 100 mM DMTU, 200 U/ml catalase, and a combination of the three (at the same concentrations). Scale bars are 8 μm.

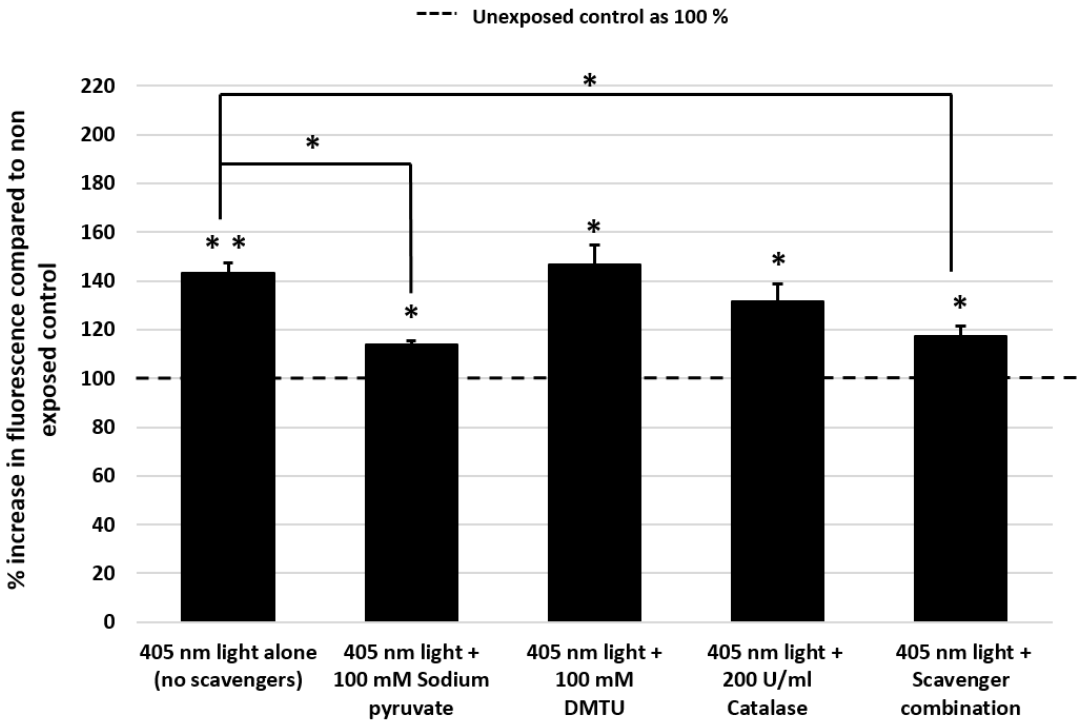

FIG. 4.13: Measurement of % increase in fluorescence intensity in *Staphylococcus epidermidis*, at a population of 10^9 CFU/ml, exposed to 162 J/cm^2 405 nm light (15 mW/cm^2 for 3 h) in the absence (in PBS) and presence of ROS scavengers, using carboxy-H_2DCFDA, compared to non-exposed control, at an excitation wavelength of 495 nm and emission wavelength of 525 nm. Control taken as 100 %, is unexposed cells treated with or without scavengers. Data (mean ± SEM, n=6) were analysed using an unpaired Student's t-test to detect significant differences between light-exposed and unexposed samples (*, $p < 0.05$; **, $p < 0.001$); and using one-way ANOVA plus Dunnett's post-hoc test to detect significant differences between light-exposed sample in the presence and absence of scavengers (*, $p<0.05$, denoted by line connectors).

4.4 Discussion

While investigating the effects of 405 nm light on normal function, proliferation rate and viability of rat osteoblasts, it was found that an exposure period of more than 2 h at an irradiance level of 5 mW/cm^2 (>36 J/cm^2) was toxic to cells leading to an impairment in cell function and cell death (see chapter 3). Hence, the mechanism(s) responsible for cell kill by 405 nm light were sought to find out whether oxidative stress was involved. Glutathione exists in both reduced (GSH) and oxidised (GSSG) states. The ratio of reduced to oxidised glutathione within cells is often used as a marker of cellular toxicity (Castronovo and Locigno, 2001; Foyer and Noctor, 1998; Townsend et al., 2003) and an increase in GSSG concentration has been reported to be an indicator of oxidative stress (Aukrust et al., 1995). The enzyme glutathione reductase which is constitutively active and inducible upon oxidative stress, converts the GSSG back to GSH. In a resting cell, the molar GSH:GSSG ratio exceeds 100:1, while during oxidative stress conditions, this ratio has been shown to drop to values of 10:1 and even 1:1 (Chai et al., 1994). GSSG is expelled from cells rapidly and accumulates extracellularly. GSSG efflux is not mediated by simple diffusion but by active membrane transport. In 1980, the transport of GSSG across the plasma membrane was proven to be an ATP-dependent primary active process in human erythrocytes (Kondo et al., 1980).

Zhang and co-workers (2012) showed that exposure of young and old mice to 20.6 kJ/m^2 of broadband UVB+UVA light resulted in a 17 % and 34 % decrease in lens GSH level respectively, when compared with their untreated controls. In 2014, Wu and co-workers demonstrated that exposure of the HaCaT human keratinocyte cell line to 8 J/cm^2 of UVA light resulted in loss of GSH compared to non-irradiated

cells. They also showed that pre-treatment of cell line with increasing concentrations of α-tocopherol prior to UVA irradiation resulted in a decrease in GSH depletion.

When oxidative stress occurs within a cell, excessive production of ROS overwhelms the cellular antioxidant defence systems. Enhanced production of ROS in the cells leads to lipid peroxidation, protein and nucleic acid oxidation, enzyme inhibition and activation of programmed cell death pathways, ultimately causing cell death (Dubey and Sharma, 2005; Meriga et al., 2004; Mittler, 2002; Shah et al., 2001)**.** During photosensitization of the cell, it is thought that the porphyrin molecules present within the cell absorb light energy and become excited from the singlet ground state, to a singlet excited state, which then undergoes intersystem crossing to the triplet state (Chiaviello et al., 2011). The excited photosensitizer can then react with either ground state triplet oxygen to form excited state singlet oxygen ($^1O_2$), or with cell components to form free radicals and radical ions. The half-life of some of these free radicals is in the range of 10^{-6} (e.g: $O_2^{\cdot -}$ and $^1O_2$) to 10^{-9} seconds ($^{\cdot}OH$) (Table 4.5).

Table 4.5: The half-life periods of various ROS (Jayabalan & Finosh, 2013)

Free radical	Half-life (s)
Superoxide ($O_2^{\cdot -}$)	10^{-6}
Hydroxyl radical ($^{\cdot}OH$)	10^{-9}
Hydrogen peroxide (H_2O_2)	Stable
Peroxyl radical ($RCOO^{\cdot}$)	Seconds
Organic hydroperoxide (RCOOH)	Stable
Singlet oxygen ($^1O_2$)	10^{-6}
Ozone (O_3)	Seconds

A significant increase in green fluorescence for the 405 nm treated osteoblast samples for up to an exposure period of 2 h clearly indicates that there was an overproduction of ROS present (Figure 4.4 & 4.5). One of the reasons for the reduction of green fluorescence within the 405 nm treated cells at 2.5 and 3 h, compared to the 2 h exposed samples, could be due to the cells dying. The dying cells would have damaged membranes, and as a result intracellular esterases would be lower in concentration, resulting in less deacetylation of the non-fluorescent dye molecule, and furthermore the fluorescent dye formed could escape from the cells. Alternatively, there is also a possibility that the cells might have upregulated their intrinsic antioxidant capacities, counteracting the increased ROS formation at high doses of 405 nm light exposure i.e. 2.5 and 3 h. However, from our earlier study on mammalian cell viability post 405 nm light exposure (Ramakrishnan et al., 2014), there was a significant reduction in cell viability, function and proliferation rate in 405 nm light exposed samples at 2.5 and 3 h, after a 48 and 72 h post treatment period. This also suggests that the reduction in green fluorescence observed at higher exposure periods of 405 nm light is likely due to the cells dying.

Experiments measuring the GSH/GSSG concentration of mammalian cells were carried out post 405 nm light treatment at different doses ranging from 1- 3 h. In Figure 4.6, the results showed a significant decrease in intracellular GSH concentration and a significant increase in extracellular GSSG production at 3 h for the 405 nm treated samples, thus indicating oxidative stress in the cells.

Normally, cells defend themselves against ROS damage with enzymes such as catalases, superoxide dismutases (Li et al., 1995 & Didion and Faraci, 2004) and

glutathione peroxidases (Tanaka et al., 2002). Packer *et* al., in 2001, stated that antioxidants such as tocopherols and tocotrienols are part of an interlinking set of antioxidant cycles and tocotrienols which penetrate rapidly through skin, efficiently combat oxidative stress induced by UV light or ozone. A few of the other antioxidants that play a crucial role in preventing cell death owing to oxidative stress conditions include ascorbic acid (Padayatty et al., 2003 & Montecinos V *et* al., 2007), uric acid (Ames et al., 1981) and glutathione (Pompella et al., 2003;). In order to find out whether free radical scavengers, when added externally to cells, limited the toxic effects of ROS and provided cell protection, sodium pyruvate (a H_2O_2 scavenger) (Desagher et al., 1997), DMTU (a $\cdot OH$ scavenger) (Bruck et al., 2001) and catalase (detoxifies H_2O_2) (Bauer and Schimmel, 2002) were added to both mammalian and bacterial cells during 405 nm light treatment.

Figures 4.7 and 4.8 show that after a dose of 54 J/cm^2 (5 mW/cm^2 for 3 h) and a 48 h post treatment period, 50 U/ml catalase offered complete protection to 405 nm treated osteoblasts. It is known that H_2O_2, which is produced from $O_2^{\cdot -}$ by the action of superoxide dismutase, is relatively stable and can last for many seconds within the cell, so it is likely to exert significant effects on the cellular biochemistry in that time. However, it is also highly permeable to cell membranes, and may have been released from the cells, which would explain why extracellular catalase can be cytoprotective although it does not penetrate the cell membrane. Hockberger and co-workers (1999) also showed that light in the violet-blue region led to ROS formation in mammalian cells, especially H_2O_2, and that catalase was protective against this H_2O_2 insult (Hockberger et al., 1999). In this study, sodium pyruvate which is also a H_2O_2 scavenger, did show a protective effect towards 405 nm treated samples when

investigating protein concentration but did not have a cytoprotective effect at 1 mM (or at 10 mM (data not shown)) in terms of % cellular metabolic activity. From the literature it is suggested that pyruvate at similar concentrations causes acidification of cell cytosol. If cytosolic pH is reduced, this will affect the ability of reductase enzymes to reduce MTT, possibly accounting for the decrease in MTT reduction. No such decrease in attached viable cells measured by protein was observed after treatment with pyruvate, indicating that the decrease in pH is sub-lethal (Desagher et al. 1997). DMTU, a ·OH scavenger, did not significantly protect the cells from dying, possibly due to the short half-life (10^{-9} seconds) of ·OH radicals.

As with the damage to mammalian cells, the bactericidal effect of 405 nm light **(**Bache et al., 2012; Maclean et al., 2015, 2013, 2009; McKenzie et al., 2014**)** is also thought to be caused by photoexcitation of endogenous porphyrins within the cell leading to the production of ROS. This study aimed to confirm that a similar cytotoxic mechanism exists in mammalian and bacterial cells. To detect ROS production, the DCFDA dye, which has previously been used to detect ROS in bacteria including *Escherichia coli* and *Staphylococcus aureus* (Hwan et al., 2011; Jung et al., 2003)**,** detected ROS by an increase in green fluorescence in 405 nm treated bacterial samples after 1 and 3 h exposure periods, thus clearly indicating an overproduction of ROS within the 405 nm treated cells (Figure 4.9 & 4.10). The decrease in green fluorescence after a dose exposure of 324 J/cm^2 compared to the 162 J/cm^2 exposed sample is again likely due to dying bacterial cells, as observed with the mammalian osteoblasts.

The effectiveness of scavengers on *S. epidermidis* during 405 nm light treatments was studied by measuring viable bacteria ($\log_{10}$ CFU/ml) after a 24 h post treatment

period and by spectrofluorometric and microscopic measurement of ROS production. Results (Fig. 4.11) showed that bacterial inactivation could be significantly reduced when cells are exposed to the light in the presence of certain scavengers. Sodium pyruvate proved to be the single most effective ROS scavenger, indicating that, as in the case of the mammalian cells, H_2O_2 is one of the key ROS responsible for bacterial cell death. Catalase offered a degree of protection at the mid-point of the inactivation kinetics, however, possibly due to the concentration used not being sufficient to offer protection against large amounts of intracellular H_2O_2, it became ineffective at the later point in the inactivation curve. DMTU did not have an effect on cell viability indicating that either ·OH caused less toxic damage to cells due to its short life span (10^{-9} seconds) or the concentration of DMTU used was not sufficient enough to offer any protection. The combined use of the three scavengers offered most protection to the 405 nm exposed bacteria cells, thus suggesting that the different ROS may each exhibit different levels of toxicity and play a role to some extent.

In order to detect the ROS production using carboxy-H_2DCFDA after exposing the samples in the presence of scavengers to 405 nm light, a dose of 162 J/cm^2 (15 mW/cm^2 for 3 h) was chosen, since 162 J/cm^2 was identified as the mid-point in the bacterial inactivation curve as well as the dose at which the green fluorescence due to ROS production in the absence of scavengers was recorded as highest when compared to 54 and 324 J/cm^2. Results (Fig. 4.12 & 4.13) showed that the samples exposed in the presence of sodium pyruvate and the combined use of all the three scavengers showed significantly less green fluorescence compared to the sample exposed in the absence of scavengers, both qualitatively and quantitatively, thereby proving once again that sodium pyruvate and the combined use of all the three

scavengers are the most effective protection from ROS generation in this study.

Overall, this study has demonstrated that exposure to toxic levels of 405 nm light induces over-production of ROS in both mammalian and bacterial cells, and that oxidative stress plays a key role in cell death. It was not possible to directly compare the ROS generation and viability of the mammalian and bacterial cells, because for spectrofluorometric analysis and fluorescence microscopy visualisation of the bacteria, the use of significantly higher population densities of bacteria was required, making direct comparison of results difficult. These increased bacterial population densities meant that increased doses of 405 nm light needed to be used to exert cell damage, and higher scavenger concentrations were thus needed to investigate any protective effects.

Nonetheless, despite these limitations, results have clearly demonstrated that the cytotoxic mechanism triggered in both mammalian cells and bacterial cells upon exposure to 405 nm light has distinct similarities, with both processes involving oxidative damage via the production of ROS, and H_2O_2 appearing to have a key role in cellular damage in both cases.

Chapter 5

Assessment of light spectra obtained from surgical lights used in operating theatres in hospitals and optical analysis of 405 nm LED arrays

5.1 Introduction

A surgical light, also known as an operating light, is a medical device that aids healthcare staff and doctors in performing a surgical procedure by illuminating the surgical site of the patient for optimal visualization of small, low-contrast objects at varying depths in incisions and body cavities. During an orthopaedic surgery a minimum of two surgical lights are used and a combination of two or more surgical lights is referred to as a surgical light system. Figure 5.1 shows the typical position of a surgical light system in an operating theatre environment.

Fig. 5.1: An operating theatre environment including the operating theatre table and surgical light system. (*Source: http://www.weds.wales.nhs.uk/operating-department-practitioners*)

The distance between the operating theatre table and surgical light system is approximately 1.3 – 1.5 m. The different types of surgical light systems that are currently being used in operating theatres include the conventional gas-filled incandescent lamps, halogen lamps and LED surgical lights. The spectra obtained from a halogen lamp and white LED lamp are shown in figure 5.2A and 5.2B respectively.

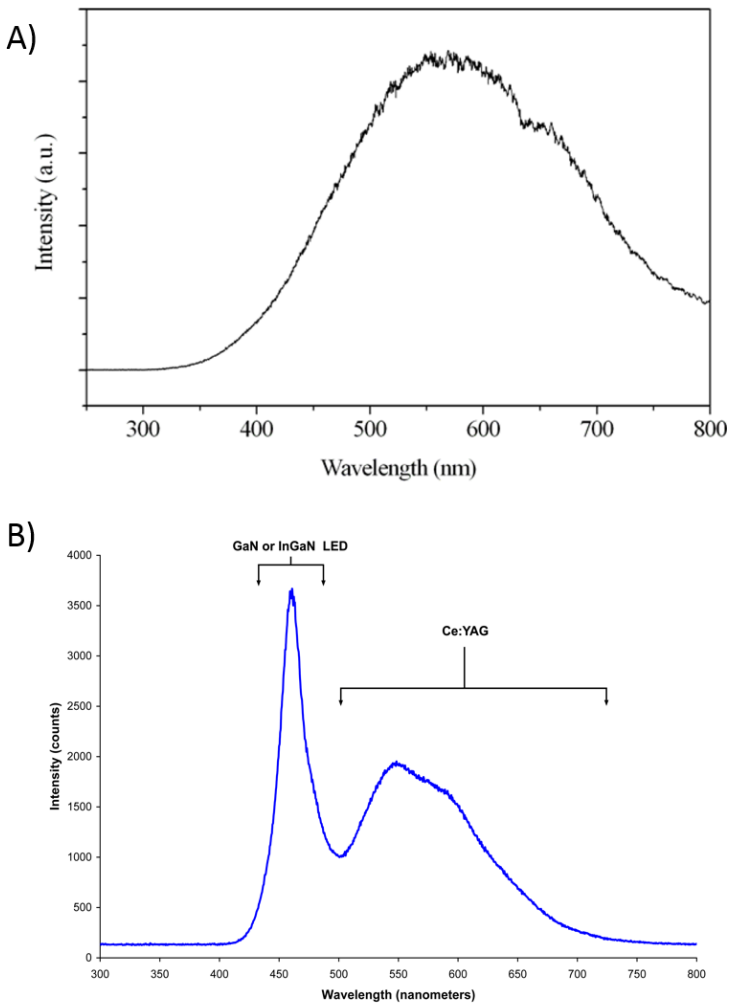

Fig. 5.2: The spectra obtained from A) Halogen lamp (Whang *et al*., 2009), B) White LED lamp (Gallium Nitride (or) Indium Gallium Nitride LEDs peaking at about 465 nm combined with Cerium-doped Yttrium Aluminium Garnet phosphor which emits at about 500-700 nm (Tanabe *et al*., 2005)).

It is clear from the literature that HAI following surgeries, is a serious threat to patients and from earlier studies and current research, it is shown that 405 nm light is safe for mammalian cell exposure whilst still being bactericidal to a variety of medically relevant bacteria. Hence, the use of 405 nm LEDs in an operating environment could reduce the bacterial burden, thereby minimising the incidence of HAI. In order to integrate the 405 nm LEDs with the existing Operating Theatre (OT) lights to facilitate decontamination, it is essential to first study the spectra obtained from existing surgical light systems used in operating theatres. These measurements will help us (i) to identify the amount of 405 nm light currently emitted by the existing surgical lights and (ii) to determine how much of an amplification of the 405 nm component, using external 405 nm LEDs would be required to enable decontamination.

5.2 Existing OT light spectrum measurement in hospitals

5.2.1 Southern General hospital (SGH)

The surgical light system used in the orthopaedic unit in Southern General Hospital, Glasgow, UK is a halogen based light system (ALM Prismalix^{TM}, U.S.A) consisting of 2 surgical lights. The spectra were measured from 1 surgical light and 2 surgical lights combined, at heights of 1.3 m (minimum distance from the surgical table) and 2 m (maximum distance from the surgical table) using a HR4000, Ocean Optics spectrometer. The fluorescent light spectrum (room lights) with the surgical lights turned off at SGH, is also shown in Figure 5.7. The background lighting used in the operating room (fluorescent light) was read and subtracted from the spectra obtained from the OT lights using dark spectrum on the spectrometer, prior to the

measurement of OT light spectra. The power intensities obtained for different components in the spectrum (UV, Visible (400 – 420 nm), Visible (420 -700 nm) and IR) of the surgical lights were calculated using Matlab software (Tables 5.1, 5.2, 5.3, 5.4 and 5.5) and the spectral graphs were created using Microsoft Excel 2013 (Figures 5.3, 5.4, 5.5, 5.6, 5.7).

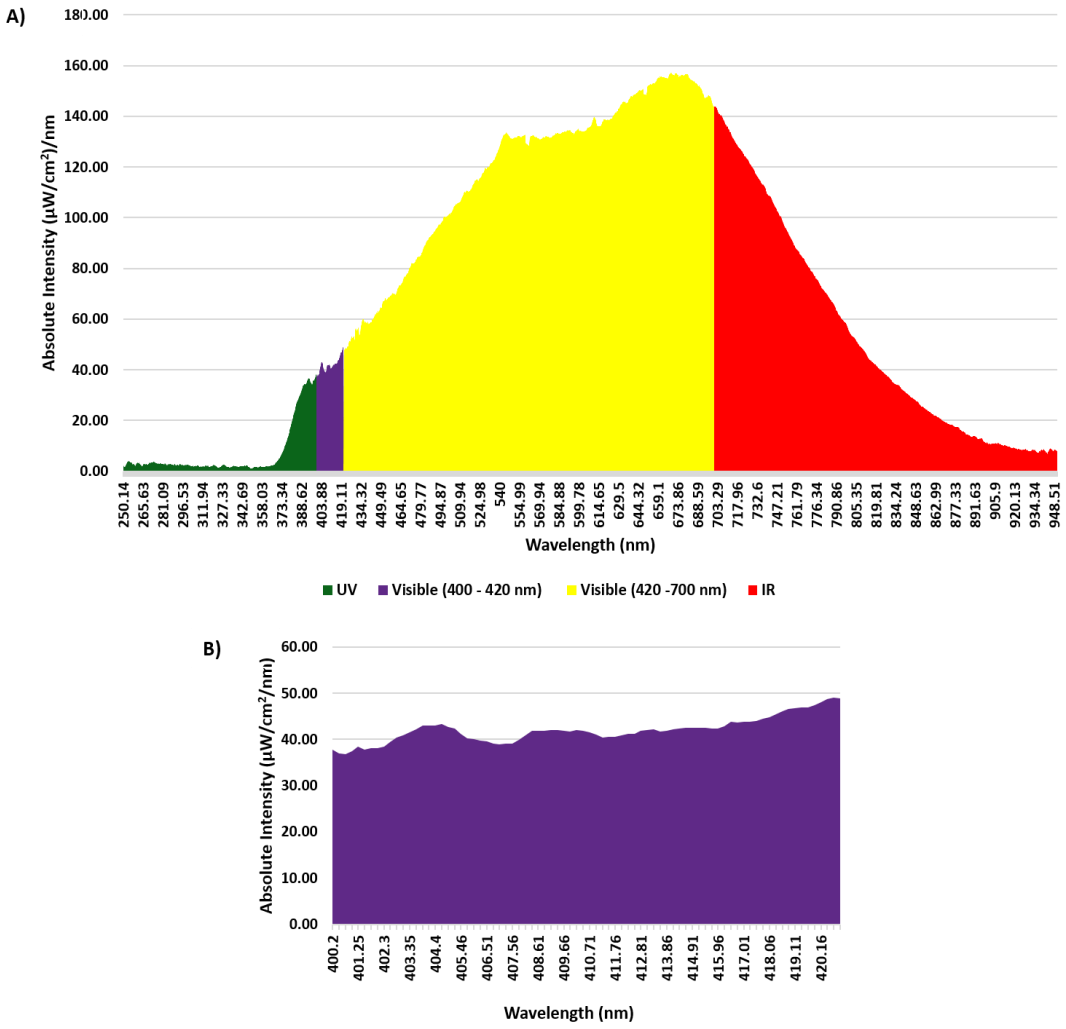

Fig. 5.3: A) The spectrum measured at 1.3 m height from one light source highlighting the UV, Visible-405 nm, Visible and IR components **B)** spectral distribution of Visible -405 nm component between 400 - 420 nm.

Table 5.1: Absolute intensities of different light components present in the spectrum measured at 1.3 m from one light source.

Light component	Wavelength (nm)	Absolute intensity (mW/cm^2)
UV	250 - 400	0.98
Visible	400 - 700	33.87
405	404 - 406	0.088
405	400 - 420	0.83

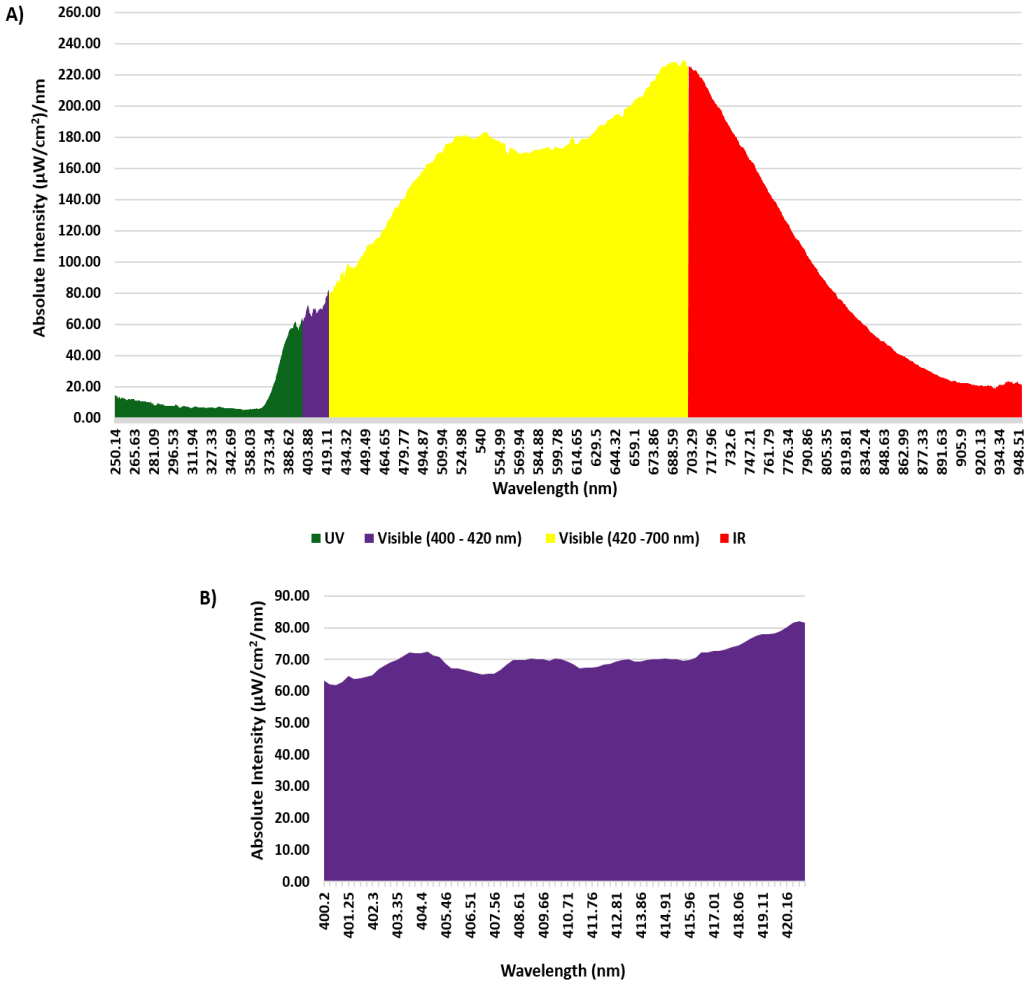

Fig. 5.4: A) The spectrum measured at 1.3 m height from two light sources combined at the focal point (highlighting the UV, Visible-405 nm, Visible and IR components **B)** spectral distribution of Visible-405 nm component between 400 - 420 nm.

Table 5.2: Absolute intensities of different light components present in the spectrum measured at 1.3 m from two light sources combined at the focal point.

Light component	Wavelength (nm)	Absolute intensity (mW/cm^2)
UV	250 - 400	2.18
Visible	400 - 700	48.37
405	404 - 406	0.147
405	400 - 420	1.38

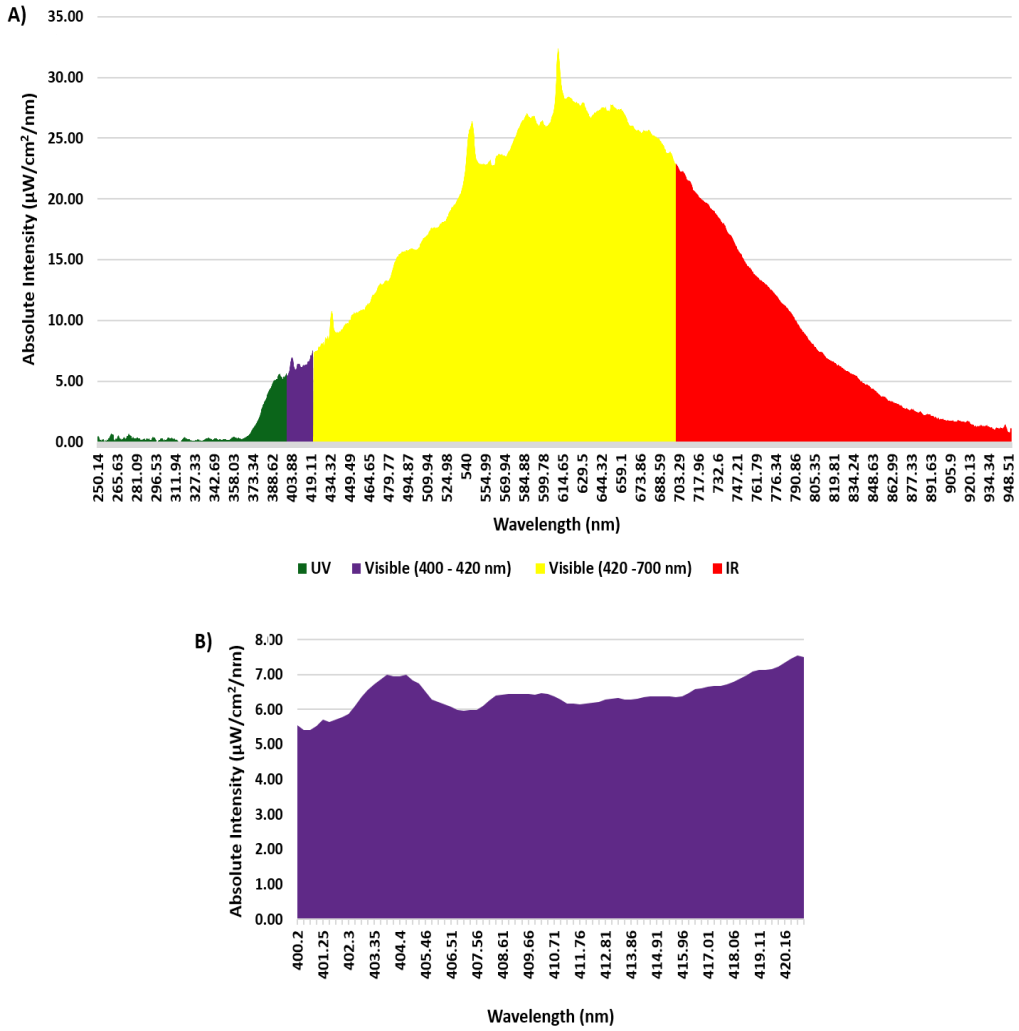

Fig. 5.5: A) The spectrum measured at 2 m height from one light source combined highlighting the UV, Visible-405 nm, Visible and IR components **B)** spectral distribution of Visible-405 nm component between 400 -420 nm.

Table 5.3: Absolute intensities of different light components present in the spectrum measured at 2 m from one light source.

Light component	Wavelength (nm)	Absolute intensity (mW/cm^2)
UV	250 - 400	0.139
Visible	400 - 700	5.9
405	404 - 406	0.014
405	400 - 420	0.127

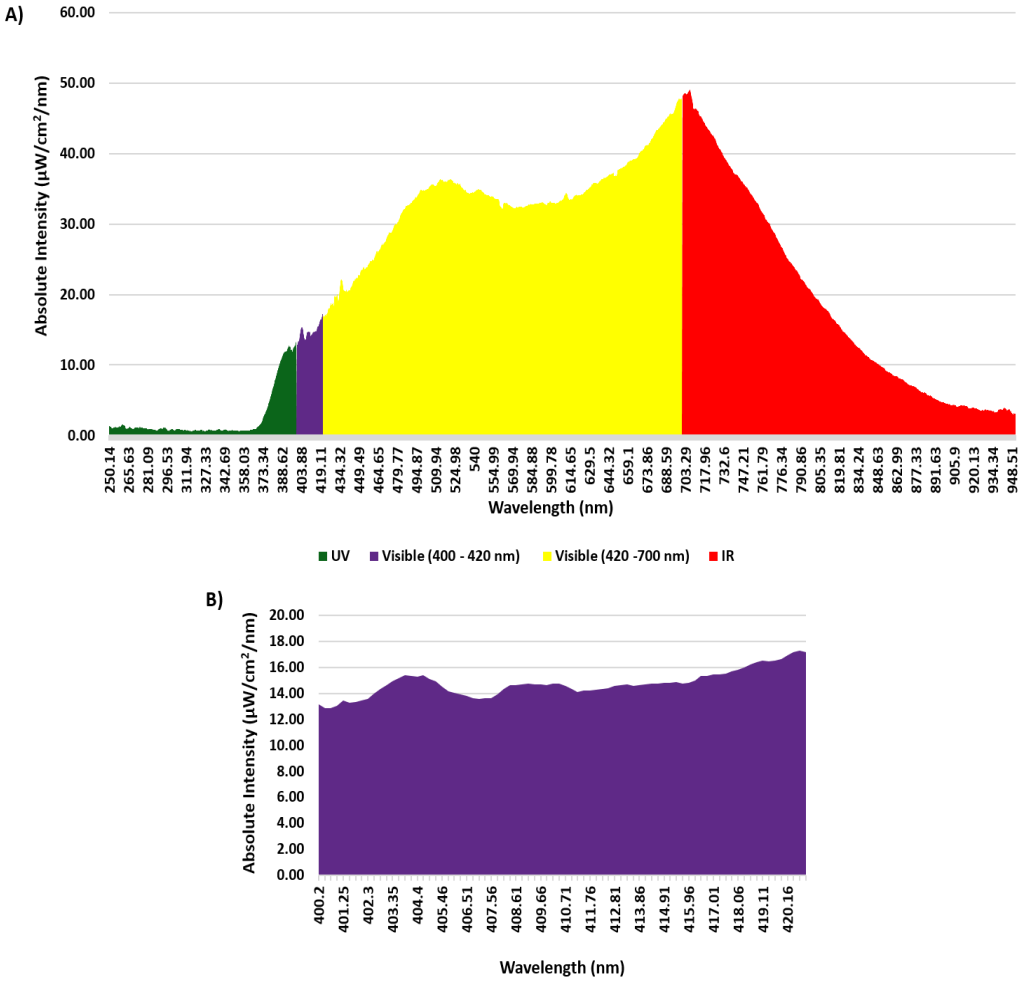

Fig. 5.6: A) The spectrum measured at 2 m height from two light sources combined at the focal point, highlighting the UV, Visible-405 nm, Visible and IR components **B)** spectral distribution of Visible-405 nm component between 400 -420 nm.

Table 5.4: Absolute intensities of different light components present in the spectrum measured at 2 m from two light sources combined at the focal point.

Light component	Wavelength (nm)	Absolute intensity (mW/cm^2)
UV	250 - 400	0.352
Visible	400 - 700	9.59
405	404 - 406	0.031
405	400 - 420	0.292

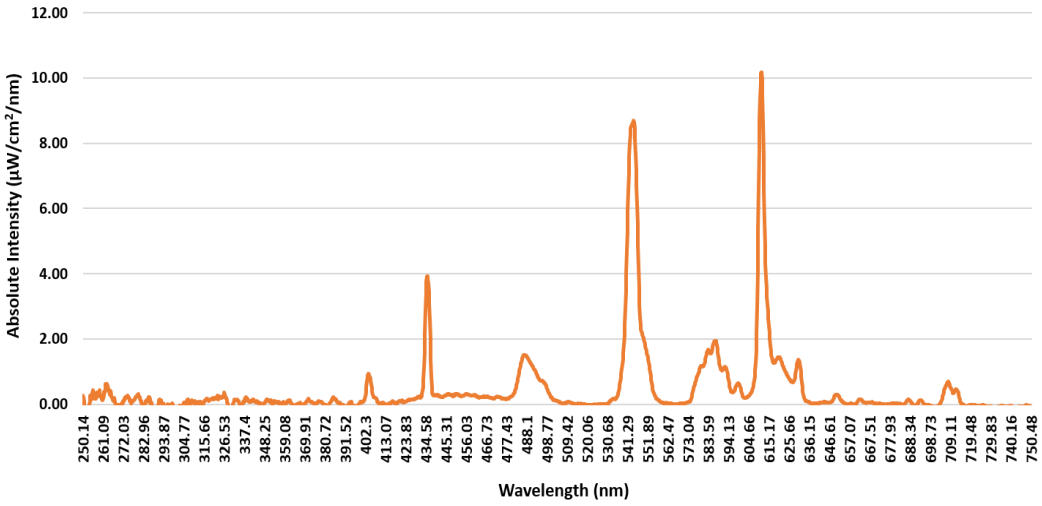

Fig. 5.7: The spectrum measured at ground level at an approximate distance of 2.2 m with surgical lights turned off and room lights ON, highlighting the UV, Visible-405 nm, Visible and IR components

Table 5.5: Absolute intensities of different light components present in the fluorescent spectrum measured at ground level at an approximate distance of 2.2 m from the ceiling.

Light component	Wavelength (nm)	Absolute intensity (mW/cm^2)
UV	250 - 400	0.008
Visible	400 - 700	0.208
405	404 - 406	0.00148
405	400 - 420	0.00366

5.2.2 Golden Jubilee National Hospital (GJNH)

The surgical light system being used in the orthopaedic unit in Golden Jubilee National Hospital, Glasgow, UK is a LED based light system (MAQUET Getinge group - PowerLED, France) consisting of 2 surgical lights. The spectra were measured from 1 surgical light and 2 surgical lights combined at heights 1.3 m (minimum distance from the surgical table) and 2 m (maximum distance from the surgical table) using a HR4000, Ocean Optics spectrometer. The fluorescent light spectrum obtained in the orthopaedic unit in GJNH was similar to the spectrum obtained at SGH. The background lighting used in the operating room (fluorescent light) was read and subtracted from the spectra obtained from the OT lights using dark spectrum on the spectrometer, prior to the measurement of OT light spectra. The power intensities obtained for different components in the spectrum were calculated using Matlab software (Tables 5.6, 5.7, 5.8 and 5.9) and the spectral graphs were created using Microsoft Excel 2013 (Figure 5.8, 5.9, 5.10, 5.11).

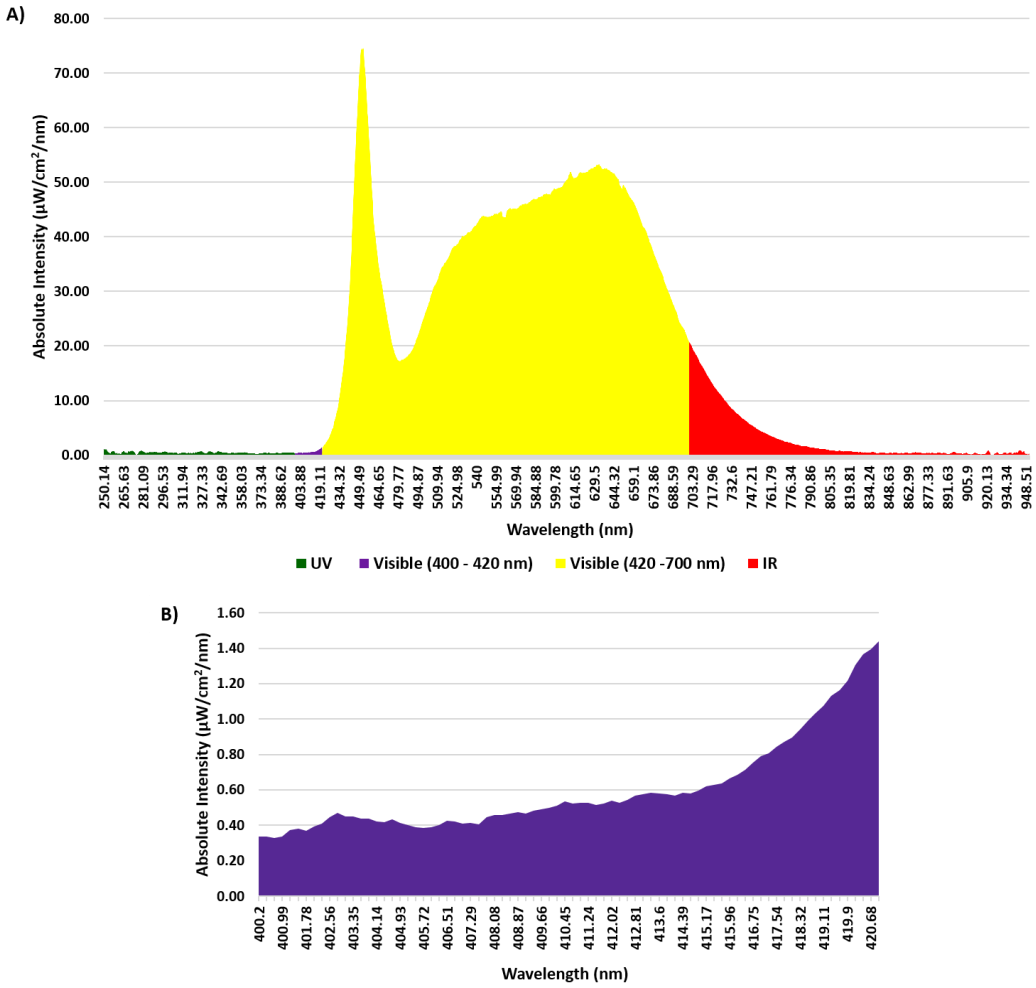

Fig. 5.8: A) The spectrum measured at 1.3 m height from one light source highlighting the UV, Visible-405 nm, Visible and IR components **B)** spectral distribution of Visible-405 nm component between 400 -420 nm.

Table 5.6: Absolute intensities of different light components present in the spectrum measured at 1.3 m from one light source.

Light component	Wavelength (nm)	Absolute intensity (mW/cm^2)
UV	250 - 400	0.07
Visible	400 - 700	10.79
405	404 - 406	0.00086
405	400 - 420	0.01125

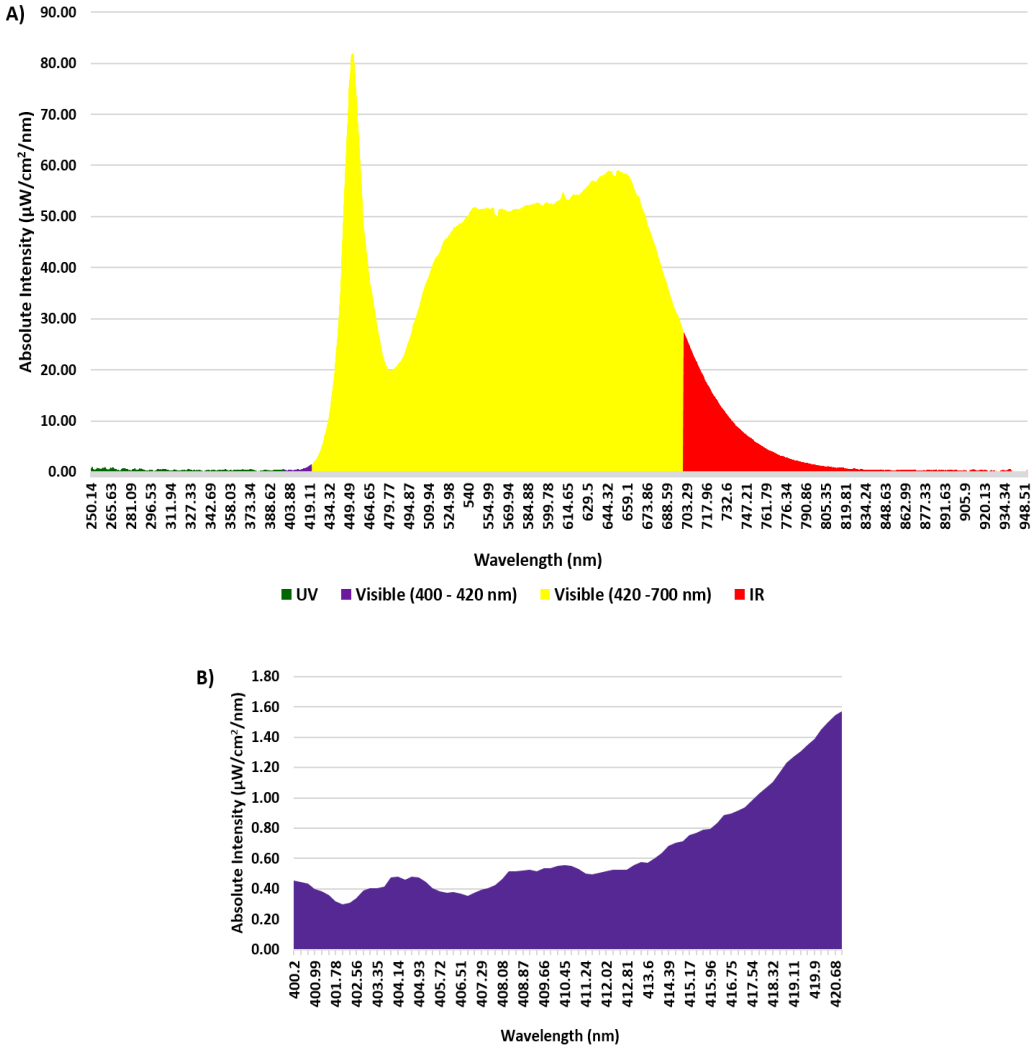

Fig. 5.9: A) The spectrum measured at 1.3 m height from two light sources combined at the focal point highlighting the UV, Visible-405 nm, Visible and IR components **B)** spectral distribution of Visible-405 nm component between 400 -420 nm.

Table 5.7: Absolute intensities of different light components present in the spectrum measured at 1.3 m from two light sources combined at the focal point.

Light component	Wavelength (nm)	Absolute intensity (mW/cm^2)
UV	250 - 400	0.07
Visible	400 - 700	12.43
405	404 - 406	0.00092
405	400 - 420	0.01220

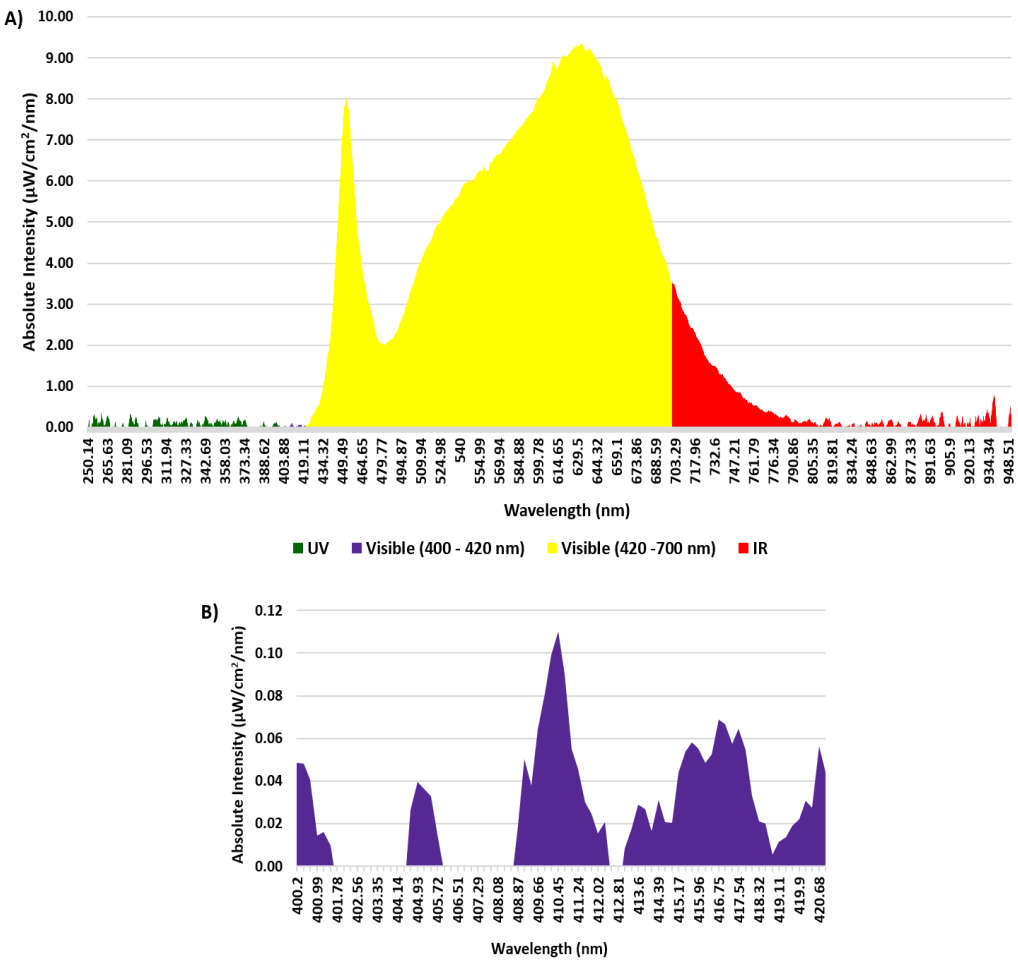

Fig. 5.10: A) The spectrum measured at 2 m height from one light source highlighting the UV, Visible-405 nm, Visible and IR components **B)** spectral distribution of Visible-405 nm component between 400 -420 nm.

Table 5.8: Absolute intensities of different light components present in the spectrum measured at 2 m from one light source.

Light component	Wavelength (nm)	Absolute intensity (mW/cm^2)
UV	250 - 400	0.01
Visible	400 - 700	1.59
405	404 - 406	0.00032
405	400 - 420	0.000341

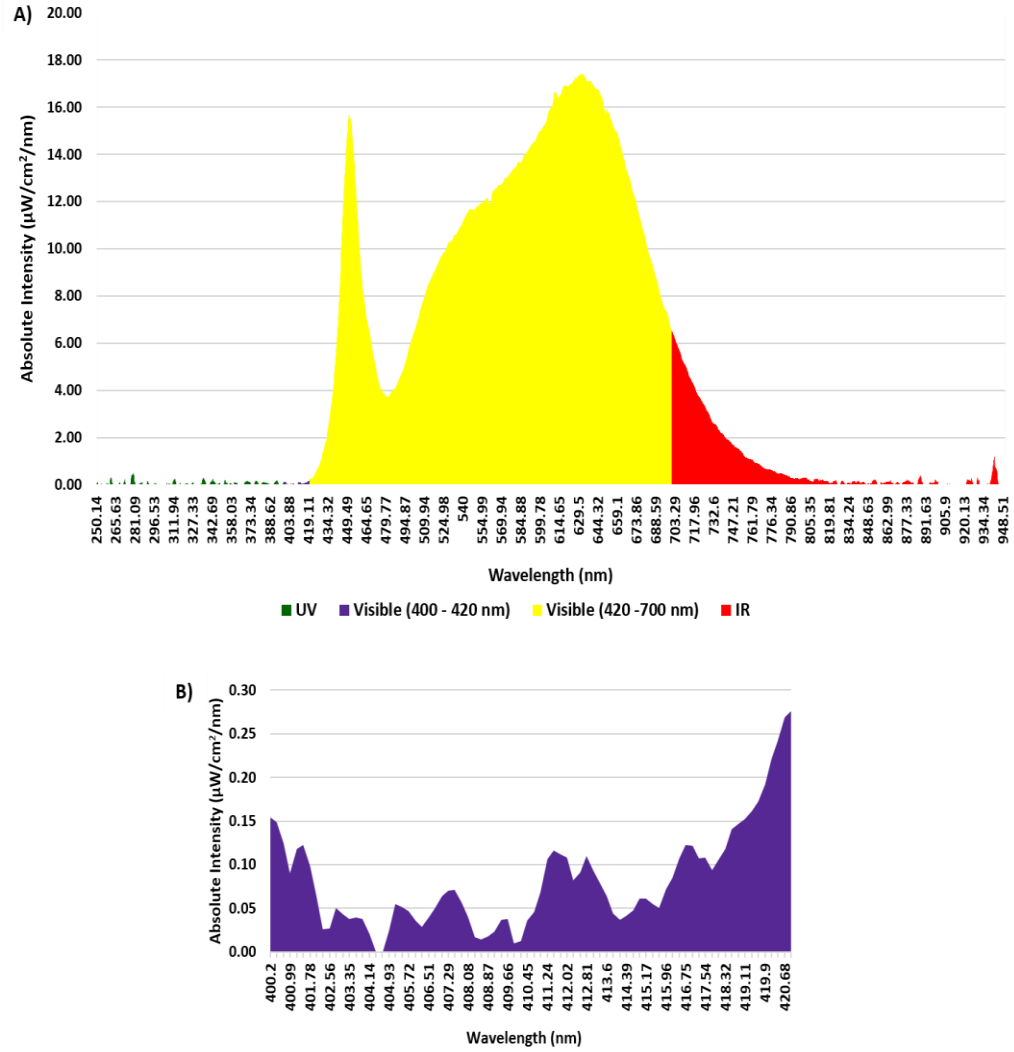

Fig. 5.11: A) The spectrum measured at 2 m height from two light sources combined including the UV, Visible-405 nm, Visible and IR components **B)** spectral distribution of Visible-405 nm component between 400 -420 nm.

Table 5.9: Absolute intensities of different light components present in the spectrum measured at 2 m from two light sources combined at the focal point.

Light component	Wavelength (nm)	Absolute intensity (mW/cm^2)
UV	250 - 400	0.004
Visible	400 - 700	3.02
405	404 - 406	0.00006
405	400 - 420	0.001451

5.3 Optical Analysis of 405 nm LED sources

Three 405 nm light systems were assessed to determine their optical outputs: (i) a 99-DIE LED array (Opto Diode Corp, CA, USA) (ii) High power 405 nm LED array (Photonstar, UK) and (iii) 405 nm LEDs (GE Illumination – Vio GE-VHD-1A-3D8). These were tested to measure the 405 nm light intensities achieved at different distances (25 cm, 50 cm, 75 cm, 100 cm, 125 cm, and 130 cm) from the light source. These different LED arrays were studied in an attempt to find out if any had the appropriate optical output to allow it to be integrated with the existing surgical light systems to amplify the 405 nm component sufficiently to induce bactericidal effects, thereby facilitating decontamination during orthopaedic surgery.

5.3.1 99-DIE LED array

An indium-gallium-nitride 99-DIE - LED array (Opto Diode Corp, CA, USA) powered by a PS 1503SB SMPS was set at 1A and 11.6V. The array measured 20 mm × 16 mm in size and had an emission at 405 nm with a 14 nm FWHM. The LED array was attached to a heat sink and cooling fan to allow thermal management. The intensities obtained at different distances from the light source (Figure 5.12) were recorded using a HR4000, Ocean Optics spectrometer and measured using Matlab software (Table 5.10). The spectral graphs were created using Microsoft Excel 2013 (Figure 5.13). All spectra were recorded with room lights OFF.

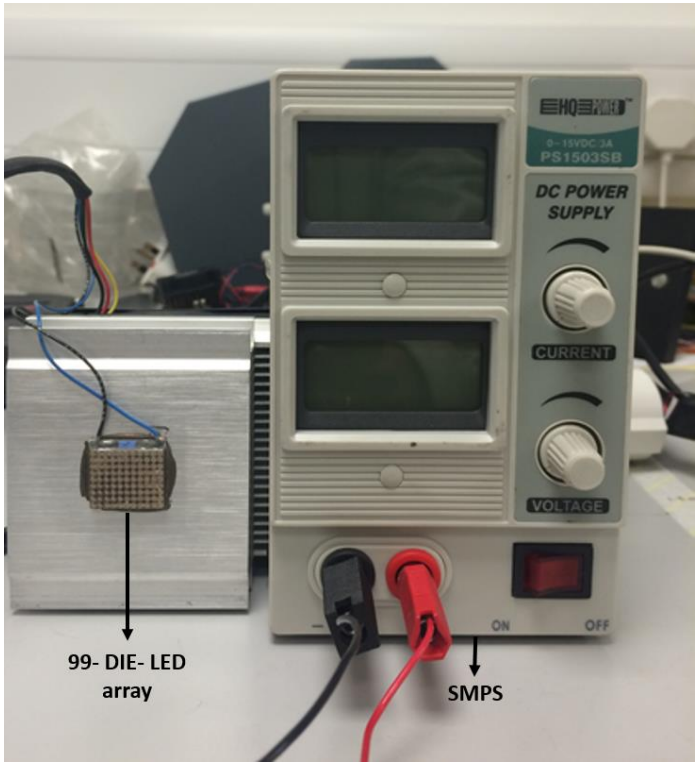

Fig.5.12: The 99 DIE -LED array (Optodiode) powered by a SMPS giving a peak output at 405 nm (14 nm FWHM)

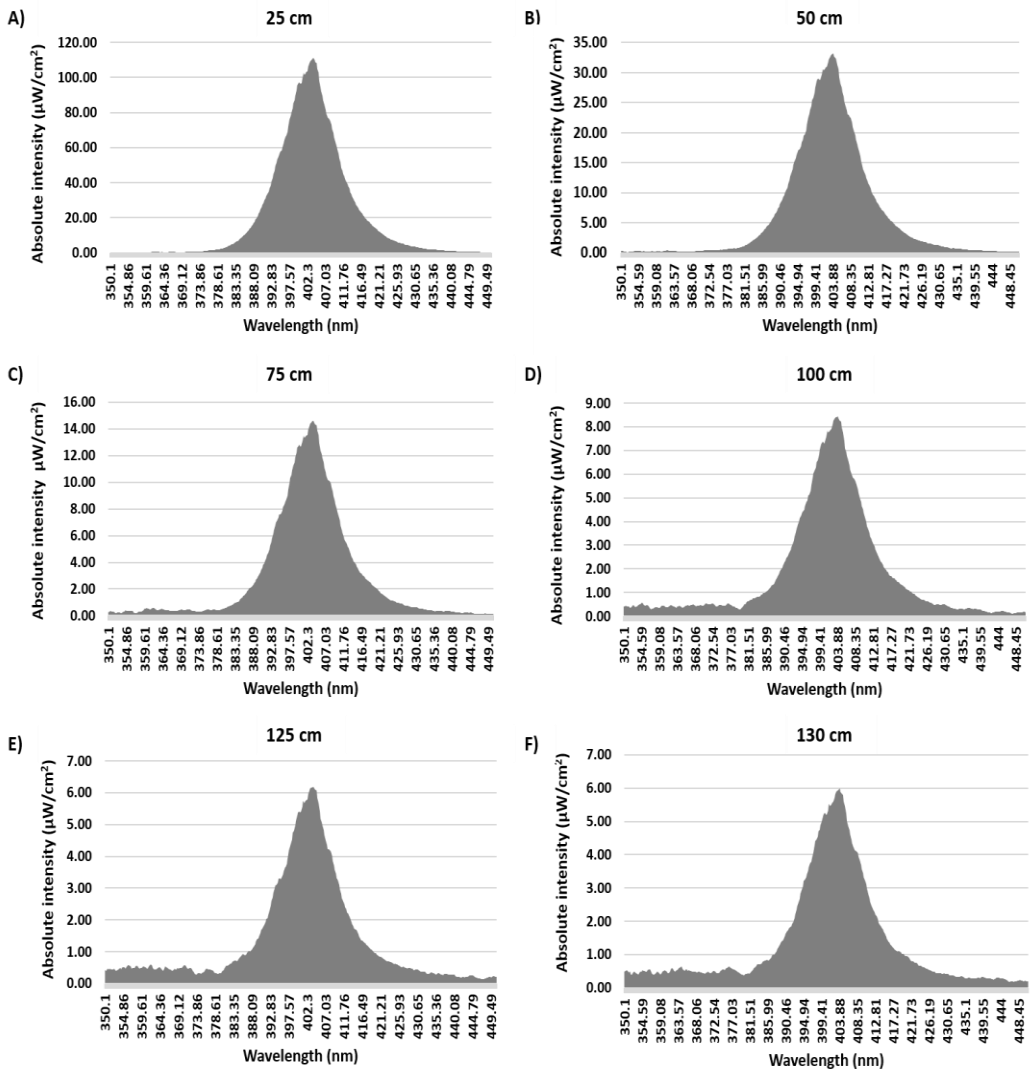

Fig. 5.13: Spectral graphs of absolute intensities (µW/cm^2) obtained from the 99-DIE- LED array (Optodiode) at different distances from the light source (25, 50, 75, 100, 125 and 130 cm) using a HR4000, Ocean Optics spectrometer.

Table 5.10: The absolute intensities (mW/cm^2) measured at different wavelengths and at different distances from the 99-DIE- LED array (Optodiode), using Matlab software.

Distance from the light source (cm)	Wavelength range (nm)	Absolute intensity (mW/cm^2)
25	350 - 450	2.04
	350 - 390	0.123
	390 - 400	0.57
	400 - 420	1.23
	420 - 450	0.104
50	350 - 450	0.615
	350 - 390	0.043
	390 - 400	0.171
	400 - 420	0.366
	420 - 450	0.035
75	350 - 450	0.284
	350 - 390	0.027
	390 - 400	0.076
	400 - 420	0.163
	420 - 450	0.018
100	350 - 450	0.176
	350 - 390	0.023
	390 - 400	0.045
	400 - 420	0.095
	420 - 450	0.012
125	350 - 450	0.135
	350 - 390	0.022
	390 - 400	0.033
	400 - 420	0.069
	420 - 450	0.011
130	350 - 450	0.135
	350 - 390	0.023
	390 - 400	0.032
	400 - 420	0.067
	420 - 450	0.012

5.3.2 High power 405 nm LED array

The high power 405 nm LED array (UNO 24, Photonstar^{TM} Technologies, UK), powered by a 50 W Philips Xitanium ^{TM} power supply, had a bandwidth of approximately 14 nm and a light emitting surface (LES) of 90 mm^2. The LED array was attached to a heat sink and cooling fan for thermal management. The intensities obtained at different distances from the light source (Figure 5.14) were recorded using a HR4000, Ocean Optics spectrometer and measured using Matlab software (Table 5.11). The spectral graphs were created using Microsoft Excel 2013 (Figure 5.15). All spectra were recorded with room lights OFF.

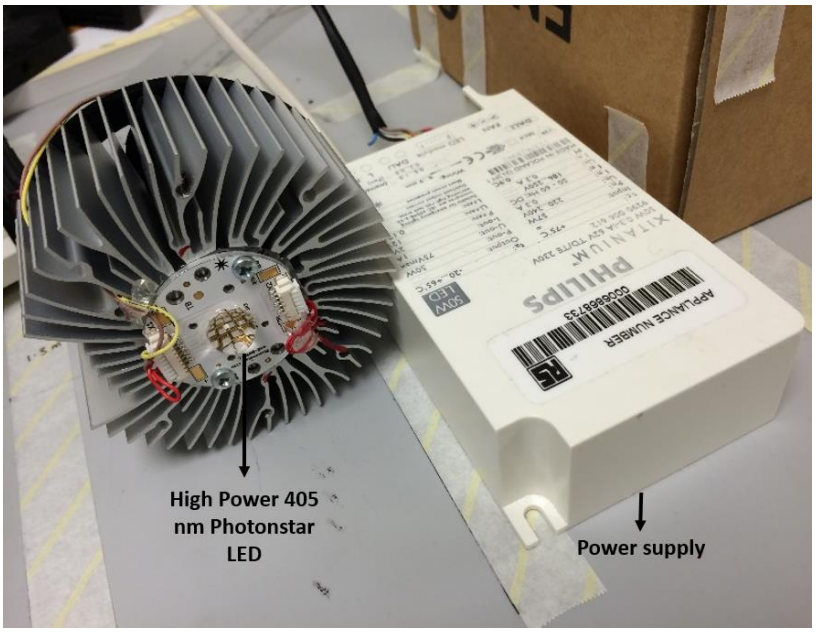

Fig.5.14: The high power 405 nm LED array (Photonstar) giving a peak output at 405 nm (14 nm FWHM).

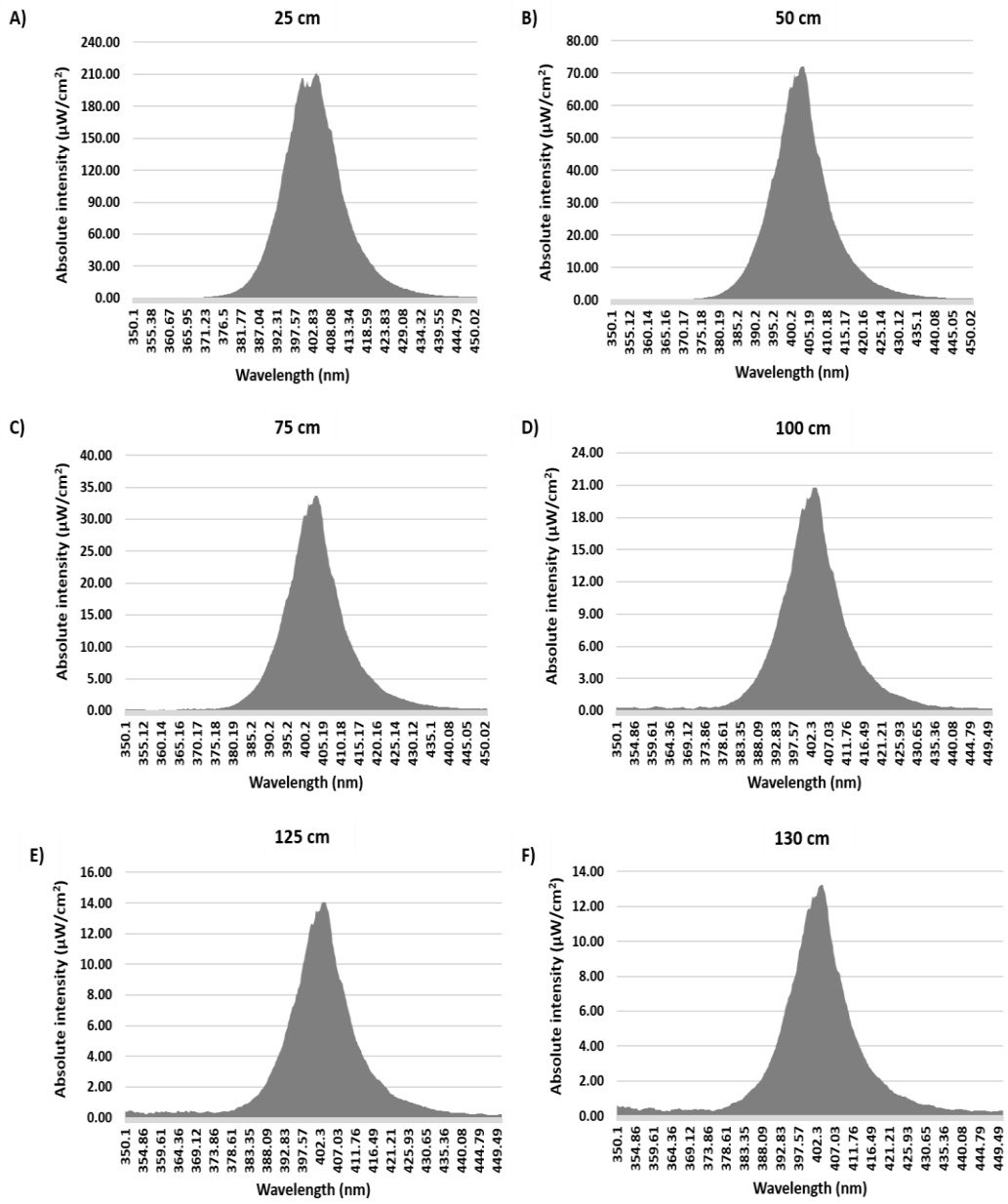

Fig. 5.15: Spectral graphs of absolute intensities (µW/cm^2) obtained from the high power 405 nm LED array (Photonstar) at different distances from the light source (25, 50, 75, 100, 125 and 130 cm) using a HR4000, Ocean Optics spectrometer.

Table 5.11: The absolute intensities (mW/cm^2) measured at different wavelengths and at different distances from the high power 405 nm LED array (Photonstar), using Matlab software.

Distance from the light source (cm)	Wavelength range (nm)	Absolute intensity (mW/cm^2)
25	350 - 450	4.35
	350 - 390	0.28
	390 - 400	1.34
	400 - 420	2.5
	420 - 450	0.23
50	350 - 450	1.29
	350 - 390	0.08
	390 - 400	0.38
	400 - 420	0.76
	420 - 450	0.072
75	350 - 450	0.613
	350 - 390	0.04
	390 - 400	0.17
	400 - 420	0.36
	420 - 450	0.036
100	350 - 450	0.386
	350 - 390	0.03
	390 - 400	0.11
	400 - 420	0.22
	420 - 450	0.03
125	350 - 450	0.271
	350 - 390	0.026
	390 - 400	0.074
	400 - 420	0.151
	420 - 450	0.019
130	350 - 450	0.25
	350 - 390	0.027
	390 - 400	0.07
	400 - 420	0.142
	420 - 450	0.019

5.3.3 405 nm GE LED array

The third light source used was an arrangement of 9 GE 405 nm LEDs (Vio GE-VHD-1A-3D8). This was the source used for mammalian and bacterial cell exposures (Fig 2.1). The arrays were powered using a SMPS set at 10.25 V and 1.56 A. The intensities obtained at different distances from the light source were recorded using a HR4000, Ocean Optics spectrometer and measured using Matlab software (Table 5.12).The spectral graphs were created using Microsoft Excel 2013 (Figure 5.16). All spectra were recorded with room lights OFF.

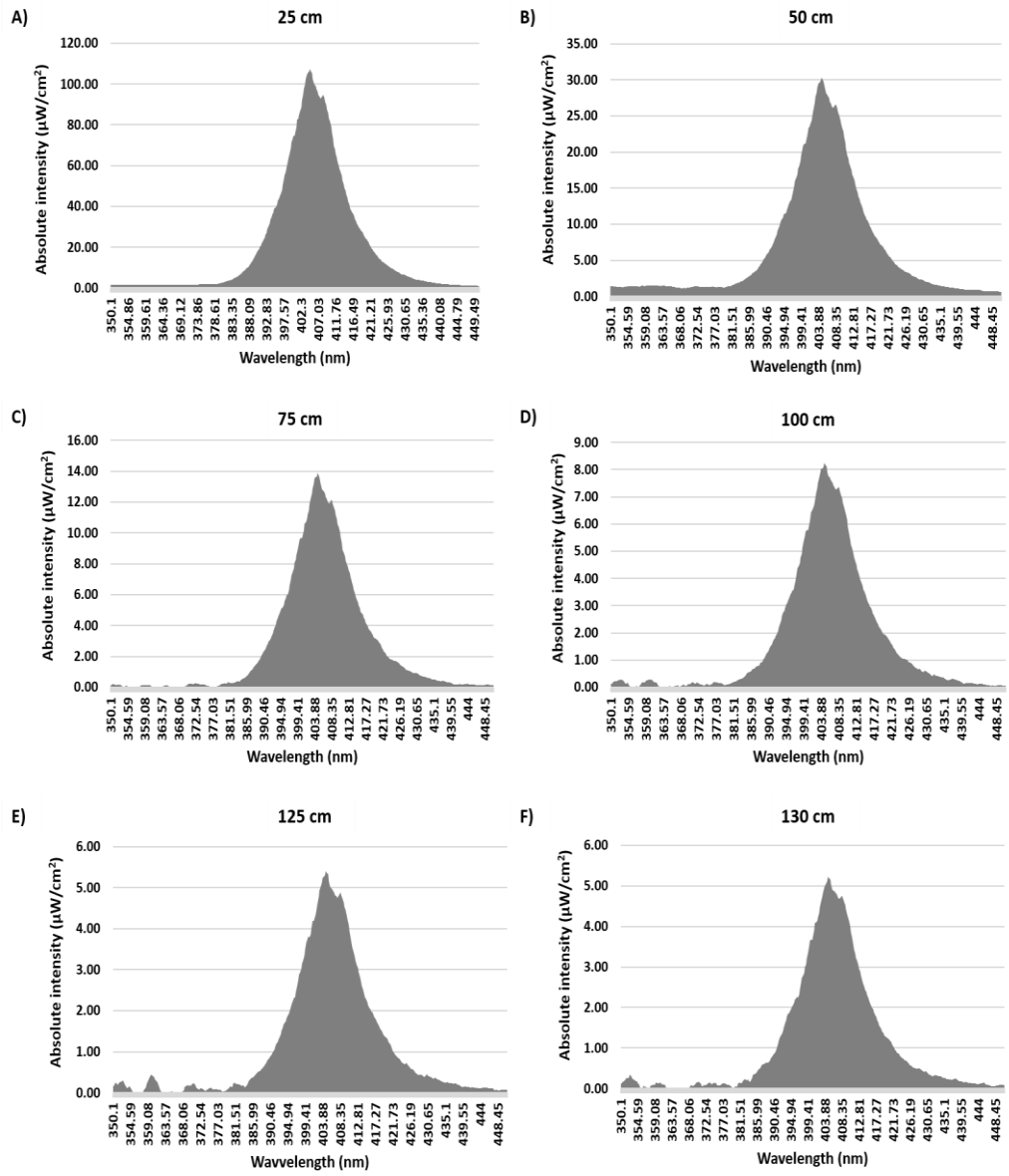

Fig. 5.16: Spectral graphs of absolute intensities (µW/cm^2) obtained from the 405 nm GE LEDs at different distances from the light source (25, 50, 75, 100, 125 and 130 cm) using a HR4000, Ocean Optics spectrometer.

Table 5.12: The absolute intensities (mW/cm^2) measured at different wavelengths and at different distances from the 405 nm GE LEDs, using Matlab software.

Distance from the light source (cm)	Wavelength range (nm)	Absolute intensity (mW/cm^2)
25	350 - 450	2.1
	350 - 390	0.117
	390 - 400	0.4
	400 - 420	1.4
	420 - 450	0.2
50	350 - 450	0.646
	350 - 390	0.067
	390 - 400	0.119
	400 - 420	0.394
	420 - 450	0.066
75	350 - 450	0.283
	350 - 390	0.016
	390 - 400	0.063
	400 - 420	0.179
	420 - 450	0.025
100	350 - 450	0.165
	350 - 390	0.009
	390 - 400	0.032
	400 - 420	0.108
	420 - 450	0.016
125	350 - 450	0.109
	350 - 390	0.007
	390 - 400	0.020
	400 - 420	0.072
	420 - 450	0.011
130	350 - 450	0.107
	350 - 390	0.006
	390 - 400	0.020
	400 - 420	0.070
	420 - 450	0.011

5.4 Combination of surgical light spectra obtained from hospitals with high power 405 nm LED array (Photonstar)

The high power 405 nm LED array (Photonstar) was used to obtain the data, as out of the three 405 nm light systems tested, the Photonstar system produced the highest 405 nm output (400 -420 nm) at a distance of 1.3 m from the light source (0.142 mW/cm^2) (see table 5.11) compared to 99 LED Opto diode (0.07 mW/cm^2) (see table 5.10) and 405 nm GE (0.07 mW/cm^2) (see table 5.12) systems.

5.4.1 Combination of surgical light spectra obtained from Golden Jubilee National Hospital with high power 405 nm LED array (Photonstar)

Figure 5.17A & B show the spectra of the High Power 405 nm Photonstar LED at 1.3 m, combined with the spectrum obtained from one and two surgical light systems respectively, at a distance of 1.3 m from the surgical table, as used in the orthopaedic unit in the Golden Jubilee National Hospital, Glasgow, UK. The intensities achieved at different wavelengths after the integration of two light spectra (405 nm Photonstar LED spectrum and surgical light spectrum), are measured and listed in Table 5.13A and B for one light source and two light sources respectively.

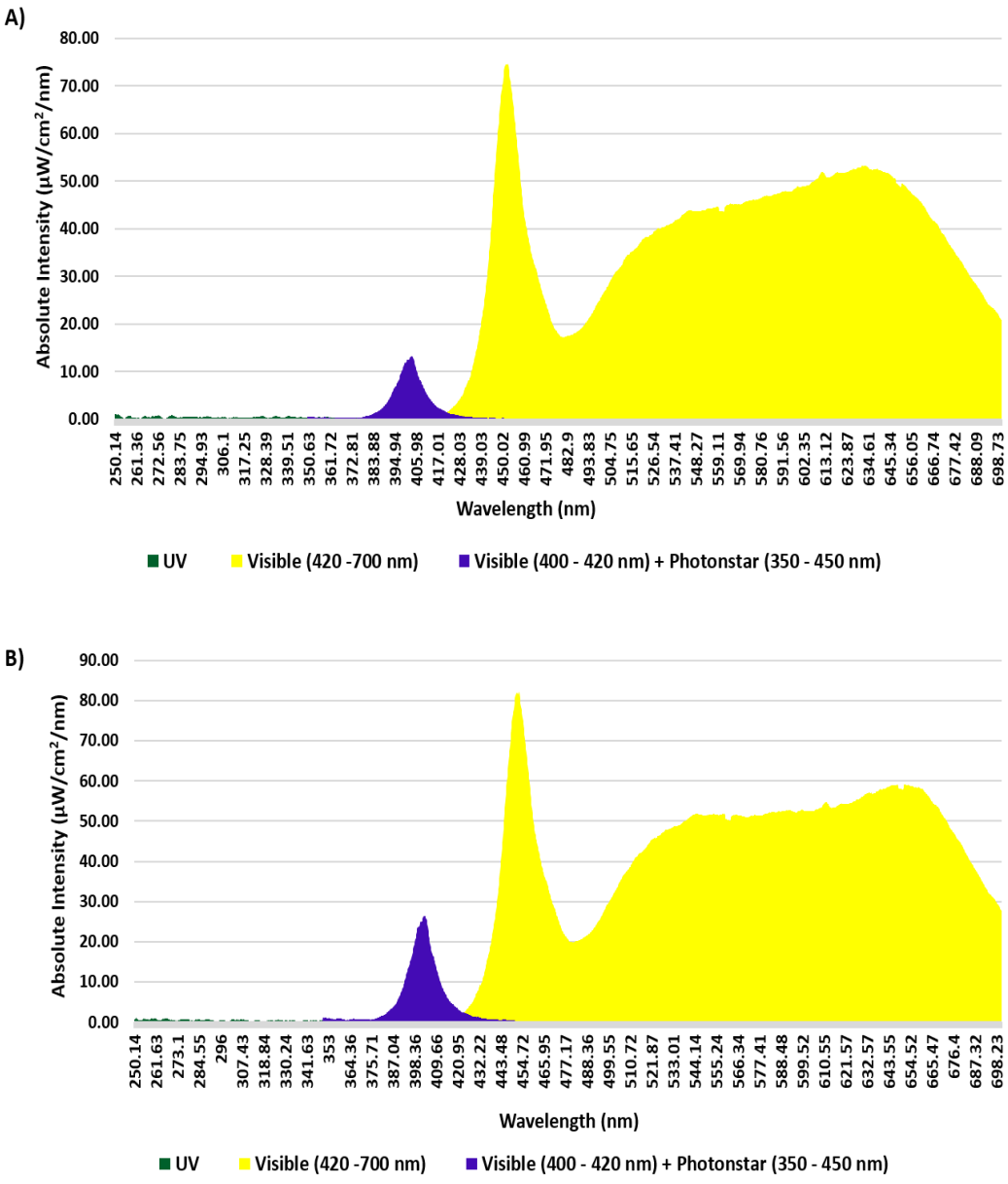

Fig. 5.17: The spectral graphs of 405 nm spectrum obtained from A) one 405 nm Photonstar LED array combined with one surgical light source, B) two 405 nm Photonstar LED array combined with two surgical light sources, measured at 1.3 m height from the light source.

Table 5.13: The absolute intensities (mW/cm^2) of the 405 nm Photonstar LED array, measured for different spectral regions at a distance of 1.3 m from A) one surgical LED light source and B) two surgical LED light sources.

A)

	Component	Wavelength (nm)	Intensity (mW/cm^2) Without Photonstar	With Photonstar (x1)
One surgical light source	UV	250 - 400	0.07	0.167
	Visible	400 -700	10.79	10.951
	405 nm	400 - 420	0.01125	0.153

B)

	Component	Wavelength (nm)	Intensity (mW/cm^2) Without Photonstar	With Photonstar (x2)
Two surgical light sources	UV	250 - 400	0.07	0.264
	Visible	400 -700	12.43	12.752
	405 nm	400 - 420	0.01220	0.2962

From the measurements obtained, if the Photonstar LEDs were to be integrated with the surgical light system, then the 405 nm light intensity achieved at a distance of 1.3 m would be ~ 0.15 mW/cm^2 from one light source and ~ 0.3 mW/cm^2 from the two light sources. Hence, in order to achieve an intensity of 5 mW/cm^2 (as used in bacterial inactivation tests in this study (section 3.3.9)) of 405 nm light using the Photonstar LED array (2.5 mW/cm^2 from each surgical light source combined with Photonstar LED), approximately seventeen 405 nm LED arrays would need to be added to each of the existing light sources: each LED array adding an output of 0.14 mW/cm^2 to the surgical light intensity (0.01 mW/cm^2).

5.4.2 Combination of surgical light spectra obtained from Southern General Hospital with high Power 405 nm LED array (Photonstar)

Figure 5.18A & B show the spectra of the high power 405 nm Photonstar LED array combined with the spectrum obtained from one and two surgical light systems respectively, at a distance of 1.3 m from the surgical table, as used in the orthopaedic unit in the Southern General Hospital. The intensities achieved at different wavelengths after the integration of the two spectra, are measured and listed in Table 5.14A and B for one light source and two light sources, respectively.

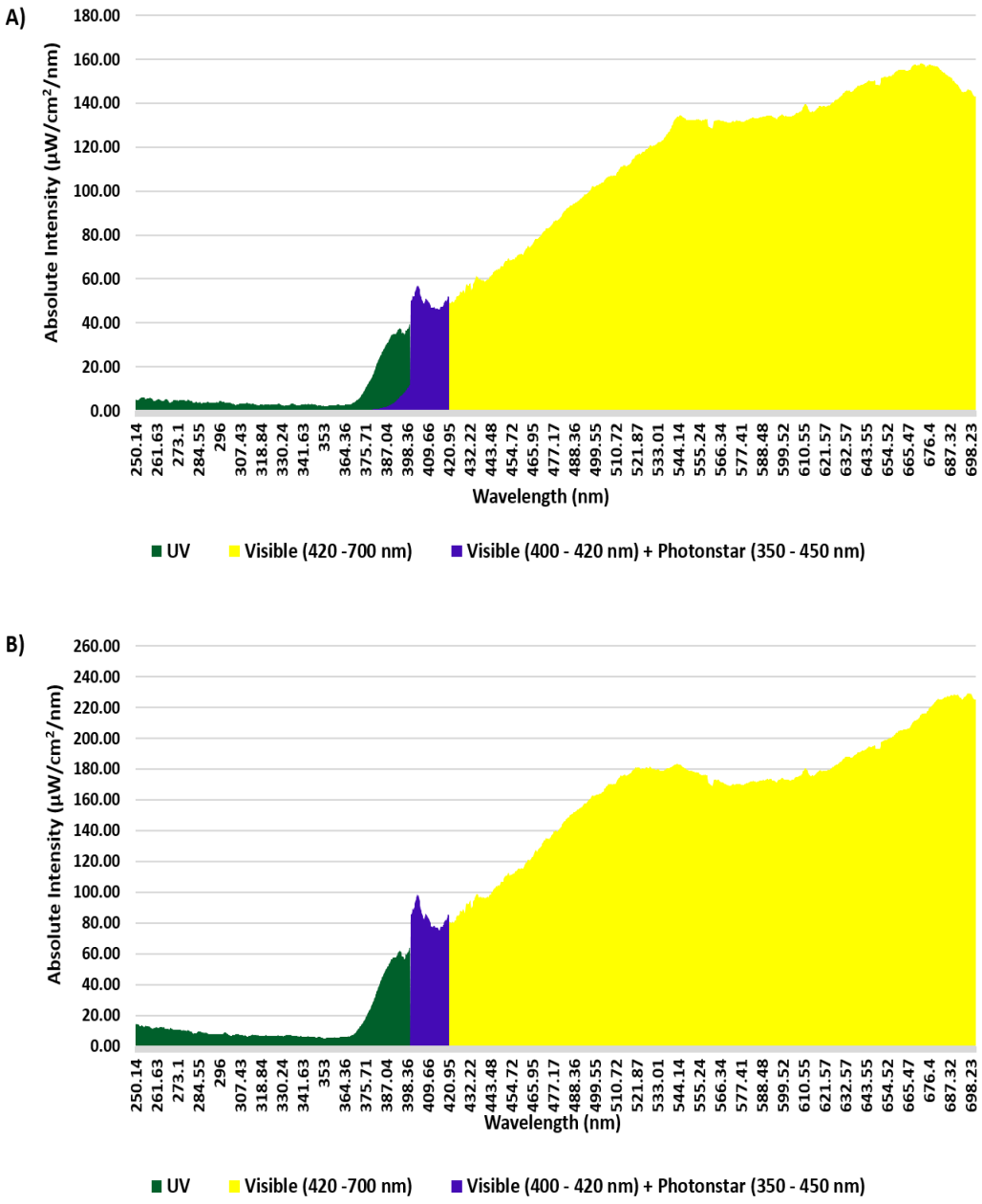

Fig. 5.18: The spectral graphs of 405 nm spectrum obtained from A) one 405 nm Photonstar LED array combined with one surgical light source, B) two 405 nm Photonstar LED array combined with two surgical light sources, measured at 1.3 m height from the light source.

Table 5.14: The absolute intensities (mW/cm^2) of the 405 nm Photonstar LED array, measured for different spectral regions at a distance of 1.3 m from A) one surgical halogen light source and B) two surgical halogen light sources.

A)

	Component	Wavelength (nm)	Intensity (mW/cm^2) Without Photonstar	Intensity (mW/cm^2) With Photonstar (x1)
One surgical light source	UV	250 - 400	0.98	1.077
	Visible	400 -700	33.87	34.031
	405 nm	400 - 420	0.83	0.972

B)

	Component	Wavelength (nm)	Intensity (mW/cm^2) Without Photonstar	Intensity (mW/cm^2) With Photonstar (x2)
Two surgical light sources	UV	250 - 400	2.18	2.374
	Visible	400 -700	48.37	48.692
	405 nm	400 - 420	1.38	1.664

From the measurements obtained, if the Photonstar LED was to be integrated with the surgical light system, then the 405 nm light intensity achieved at a distance of 1.3 m would be ~ 1 mW/cm^2 from one light source and ~ 1.7 mW/cm^2 from two light sources. Hence, in order to achieve an intensity of 5 mW/cm^2 (as used in bacterial inactivation tests in this study (section 3.3.9)) of 405 nm light, using the Photonstar LED array (2.5 mW/cm^2 from each surgical light source combined with Photonstar LED), approximately twelve 405 nm LED arrays would need to be added to each of the existing light sources: each LED adding an output of 0.14 mW/cm^2 to surgical light intensity (0.83 mW/cm^2).

5.5 Proposed 3D models of a 405 nm light system for use in Operating theatres for decontamination during surgery

In earlier studies, two High-intensity narrow spectrum light environmental decontamination systems (HINS- light EDS) were installed in a vascular ward, isolation rooms in the Burns Unit and the Intensive Care Unit in Glasgow Royal Infirmary and its performance was assessed by enumerating the number of bacteria (CFU/plate) before, during and after use of the HINS-light EDS (i.e. PreHINS, HINS and PostHINS). The ceiling-mounted HINS-light EDS emitted 405 nm violet blue light at 0.5 mW/cm^2 with FWHM of 14 nm and white LEDs were incorporated into the systems to make the light appear white. In all the three locations, the use of HINS- light EDS resulted in approximately 30 – 90 % reduction in total viable bacteria (Bache *et al*., 2012; Maclean *et al*., 2010; Booth *et al*., 2010).

Decontamination in an operating theatre environment could be facilitated by enhancing the 405 nm content in a range of situations. The first and main area related to the results of this chapter so far, is the surgical light system, thereby promoting not only surgical site decontamination but also environmental decontamination during cleaning of wounds, thus reducing transfer of bugs to surgical site. Other potential areas which could benefit from having 405 nm light are (i) the laminar flow chamber, thereby promoting environmental decontamination, and (ii) the tray tables, thereby promoting surgical device decontamination. In order to propose these, computer aided 3D simulations were created using Sketchup 2015 software, in order to visualise how the 405 nm light could potentially be utilised in practice

5.5.1 Surgical light system integrated with 405 nm LEDs

Surgical site decontamination could be facilitated by integrating the surgical light system with high power 405 nm LEDs to give a final output of e.g., 36 J/cm^2 (all light systems combined), altering the irradiance level (mW/cm^2) depending on the duration of the surgery. For example, 10 mW/cm^2 for 1 h (or) 5 mW/cm^2 for 2 h etc. A proposed design of the 405 nm LEDs integrated with the surgical light system is shown in Figure 5.19.

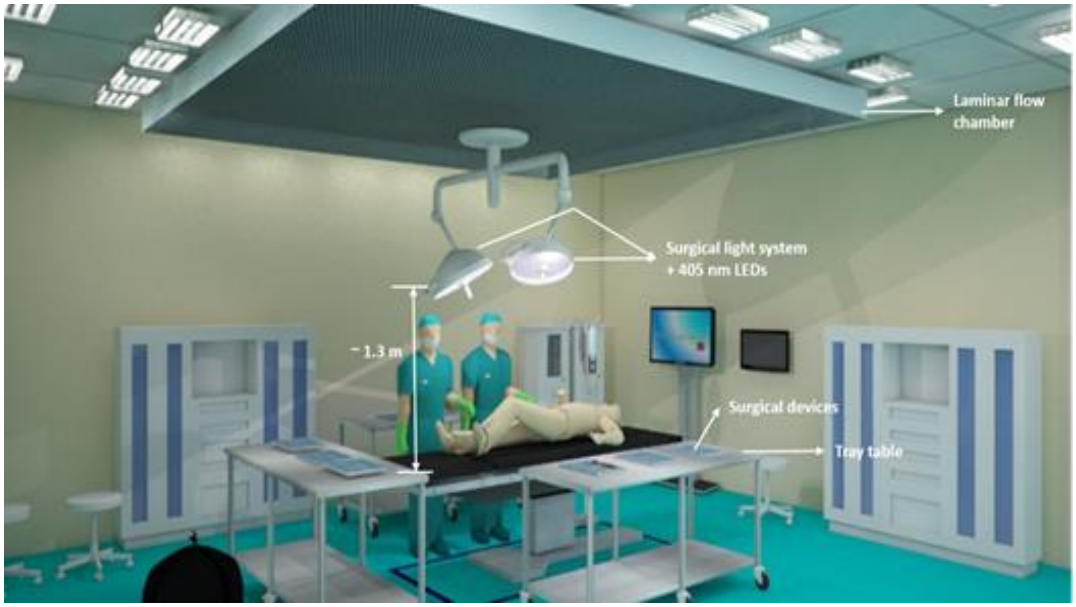

Fig. 5.19: Surgical light system integrated with 405 nm LEDs to promote surgical site decontamination in an operating theatre environment.

5.5.2 Laminar flow chamber integrated with 405 nm LEDs for environmental decontamination

Environmental decontamination can be facilitated by integrating the laminar flow chamber with high power 405 nm LEDs to give a final output of e.g., 36 J/cm^2, altering the irradiance level (mW/cm^2) depending on the duration of the surgery. A proposed design of the 405 nm LEDs integrated with the laminar flow system is shown in Figure 5.20.

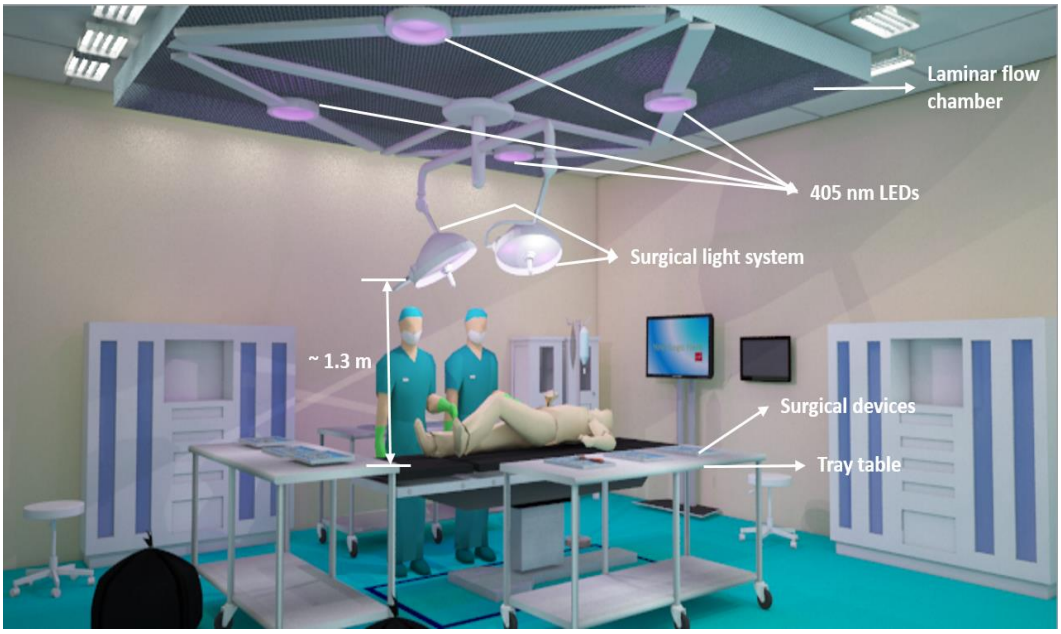

Fig. 5.20: Laminar flow system integrated with 405 nm LEDs to promote environmental decontamination in an operating theatre environment.

5.5.3 Tray tables integrated with 405 nm LEDs for surgical device decontamination

Surgical device decontamination could be facilitated by integrating the tray tables (containing the surgical devices) with high power 405 nm LEDs. Higher doses of 405 nm light could be used in this scenario (> 36J/cm^2) as neither the medical personnel nor the patient will be directly exposed to the light. Proposed designs of 405 nm LEDs integrated with the tray tables are shown in figure 5.21A & B. For easy handling of surgical devices kept on tray tables, the typical distance between equipment and light source (e.g. high power 405 nm LED array (Photonstar)) could be set to 25 cm or 50 cm and in which case an irradiance level of 2.5 mW/cm^2 or 0.76 mW/cm^2 of 405 nm light could be achieved from each LED respectively.

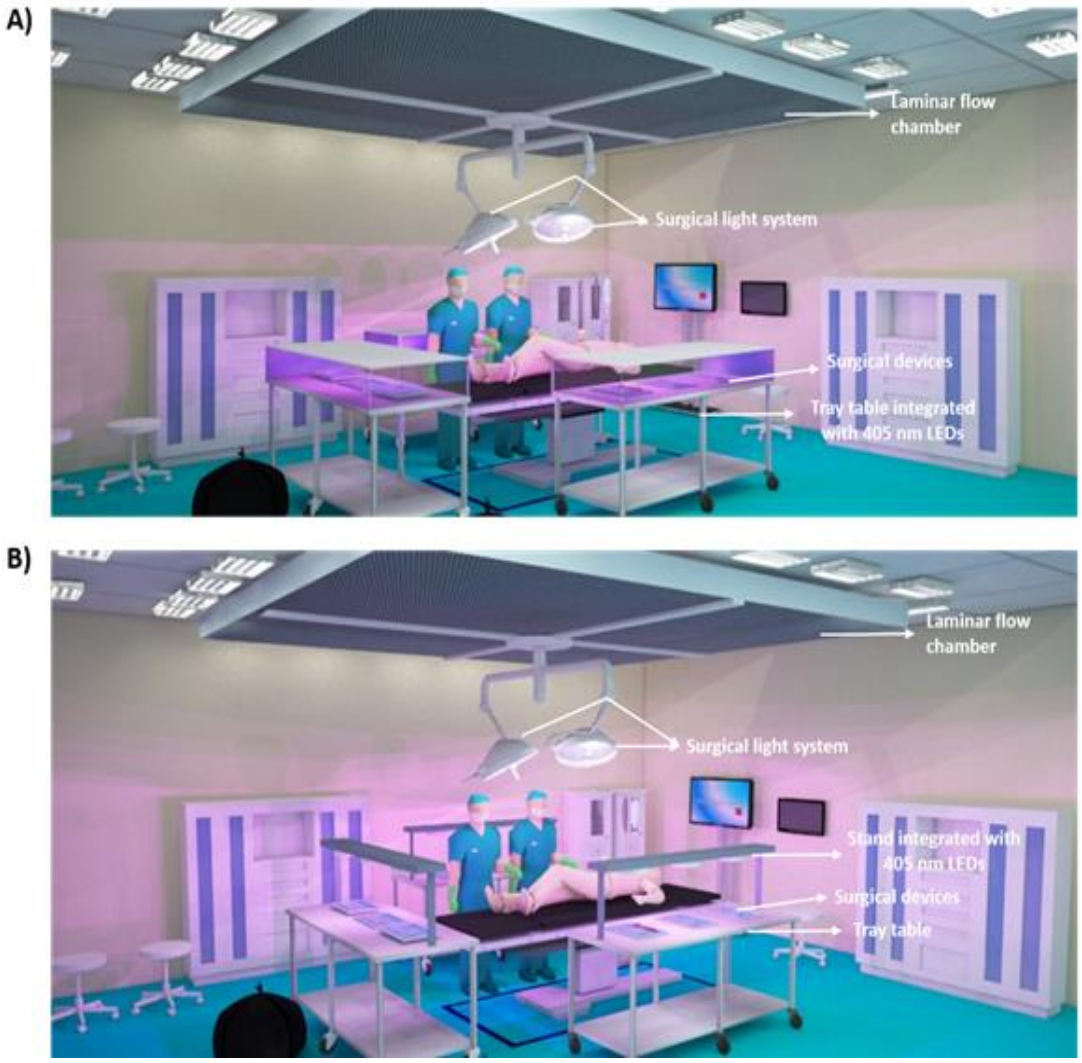

Fig. 5.21: The integration of 405 nm LEDs with tray tables enabling A) complete enclosure of tables B) use of stands on tray tables with 405 nm LEDs to facilitate easy handling of devices, to promote surgical device decontamination in an operating theatre environment.

5.5.4 Conclusion

In summary, in both hospital scenarios studied (GJNH and SGH), if the Photonstar LED array was to be integrated with the surgical light system, the other components in the Photonstar LED spectrum (UV component and wavelengths (420 -450 nm)) may get amplified if multiple LEDs are used. This problem could be solved by filtering the unwanted wavelengths using optical band pass filters/ diffusers, and/or by identifying better and more efficient high power 405 nm LEDs (high power output at greater heights while consuming less current) in which case can the number of LEDs required to be integrated could be decreased.

While integrating the 405 nm LEDs with the surgical light system and/or laminar flow system and/or tray tables in an operating theatre environment has decontamination benefits, it would need to be ensured that the medical personnel do not experience vision problems i.e. difficulty in visualising the patient/ surgical site due to altered lighting colour caused by the violet blue colour of 405 nm light. Hence, lights would need to be developed so that they had the appropriate white colour temperature (~ 3000K – 4000K). This colour temperature problem can be addressed by blending the 405 nm light LEDs with other colours of LEDs (red, yellow, green LEDs) to minimize the brightness of violet blue colour of 405 nm light and make it white in appearance (Zhao *et al*. 2002), while not altering the final 405 nm intensity.

Introducing 405 nm LEDs in an operating environment may increase the temperature of the surrounding which in turn might cause discomfort to medical personnel present in an operating theatre. The 405 nm LEDs may also induce skin burns in

patients exposed to light, during the surgical procedure. This issue can be resolved by using 405 nm LED systems with (i) proper heat sinks, (ii) cooling fans, for thermal management. The temperature of the samples exposed to a dose of 108 J/cm^2 of 405 nm light at an irradiance of 40 mW/cm^2 and at a distance of 2 cm from the light source, was recorded to be 30°C using a digital thermometer and thermocouple (Kane May 340, Comark Instruments, Norwich, UK) (Maclean *et al*., 2013). The 405 nm LED systems used for conducting *in-vitro* studies in this thesis, were provided with heat sinks that maintained the operating temperature of the LEDs constant for the duration of light experiments and removed the impact of temperature on cells.

This study is limited to the LED arrays available in our laboratory. However other configurations/ light sources could be used to integrate with existing operating theatre light systems (e.g. Prizmatix Ultra High Power-Mic- LED – 405, emits > 2.0 W of 405 nm light at FWHM of 15 nm). New light systems could have higher amounts of 405 nm light output incorporated at manufacture. Earlier studies using HINS-light EDS for hospital environmental decontamination, involved the use of lower intensities of 405 nm light i.e. ~ 0.5 mW/cm^2 at ~ 1.5 m distance from the light source and a 48 h exposure period resulted in an approximate 60 % reduction in total viable bacteria in the presence of patient (Maclean *et al*., 2010). 5 mW/cm^2 of 405 nm light at 8 cm distance from light source, has been used in this study to achieve rapid bacterial inactivations (98 – 100%). Hence, the use of 5 mW/cm^2 intensity of 405 nm light achieved at ~ 1.5 m could result in quicker inactivation of bacteria and this could prove to be vital in case of decontaminating the operating environment during orthopaedic surgeries.

Chapter 6

Summary and Future work

From the literature, it is clear that HAI pose a serious threat to patients admitted to hospital and is associated with (i) an increase in length of stay by several days causing pain and discomfort in patients, (Plowman *et al*., 1999),
and (ii) additional hospital costs incurred in treating these infections (Coello *et al*., 1993). It was also found out from the literature that SSIs associated with medical implants still remain a common and serious complication in arthroplasty surgery, contributing to increased rates of patient morbidity and mortality (Jenks *et al*., 2014). The duration of surgery and the movement of medical personnel in an operating environment are noted as some of the risk factors that contribute to the existence of HAI (Howorth, 1985). The movement of staff members in an operating environment is unavoidable, however their movement may disturb the settled down bacterial particles existing in different inanimate surfaces and re-suspend them in the air. The duration of a typical arthroplasty surgery lasts for 1 – 2 h, while a complex revision surgery may last even longer (3 – 4h) and this increases the chances of these resuspended bacterial particles to come in contact with the surgical site. In the UK, despite the use of several disinfectants and other sterilisation procedures (laminar flow system) to maintain sterility in an operating environment, the incidence of infection rates in arthroplasty surgery and revision surgery are quite high for both hips and knees. The use of UV light systems in an operating environment have shown remarkable reductions in airborne bacterial burden and incidence rates of HAI

(Ritter *et al*., 2007). However, the use of UV light for decontamination during surgeries is not widely accepted in the UK due to the requirement of heavy protective clothing and protective eye gear.

Blue light (400 - 450 nm) has also shown to induce photo-inactivation of several medically relevant bacteria without the use of exogenous photosensitisers (Kawada *et al*., 2002; Sigurdsson *et al*., 1990). Unlike UV (ionising radiation), 405 nm light is a non-ionising radiation of the visible spectrum that has been successfully used in enabling inactivation of both gram- positive and gram-negative bacteria (Maclean *et al.*, 2009). 405 nm light systems operating at an intensity of 0.5 mW/cm^2 have been successfully installed in isolation rooms in Glasgow Royal Infirmary for facilitating continual decontamination (Maclean *et al*., 2010). However, to facilitate decontamination during arthroplasty surgeries (1- 2 h), a higher intensity of 405 nm light needs to be used to enable quicker bacterial inactivation within the surgical period. Hence, it is essential to investigate the effects of higher intensity 405 nm light on both mammalian and bacterial cells.

Therefore, the aim of this study was to establish a safe threshold dose of 405 nm light using a higher intensity compared to the intensity used in environmental decontamination systems, that does not induce any significant mammalian cell damage, i.e.; osteoblasts (bone cells), but is still bactericidal to a variety of clinically related bacteria responsible for causing HAI, and hence could have the potential to be developed for continual decontamination during arthroplasty surgery.

6.1. A summary of the research findings

6.1.1. Effect of 405 nm HINS light on osteoblasts cell line and clinically relevant bacteria

HAI acquired by patients following arthroplasty surgeries (hip or knee replacement surgeries) is a serious and an expensive complication. One source of HAI is the environment (air, surfaces), therefore the surgical process would greatly benefit from improved environmental decontamination. Previous studies (Bache *et al*., 2012; Maclean *et al*, 2010; Booth *et al*., 2010) have shown that 405 nm light can be successfully used for continuous environmental decontamination of hospital isolation rooms, therefore there is great potential for 405 nm HINS light to be used for reducing the environmental bacterial burden (bacteria present on surfaces and in the air), during arthroplasty procedures. The employment of 405 nm HINS light during surgeries would involve exposing the bone tissues to light and hence it is essential to study the effects of the light on bone cells. So to ensure the light could be applied safely during surgeries, the effect of 405 nm HINS light on osteoblast function was examined. Immortalised rat osteoblasts were used for studying the effects of 405 nm HINS light, as they are an acceptable in vitro model system mimicking the bone characteristics.

Environmental decontamination systems installed in Glasgow Royal Infirmary uses low intensity (0.5 mW/cm^2) for continual decontamination of hospital isolation rooms (MacLean *et al*., 2010). However, if 405 nm light is to be used for decontamination during arthroplasty surgeries which are carried out for about 1-2 h, quicker bacterial inactivation is required. The present study thus involved exposing

mammalian and bacterial cells to higher intensity of 405 nm light (5mW/cm^2) for 1, 2 and 3 h.

Protein content measurement by Lowry assay and cell staining with Crystal violet were used to quantify the number of viable cells attached to culture dishes post 405 nm HINS light exposure. The results propose that exposure of osteoblasts to 405 nm light for up to a dose of 36 J/cm^2 did not affect cell viability when compared with their respective unexposed controls, after a 48 and 72 h post treatment period. However, a significant difference in cell viability was noted for 405 nm light exposed cells when compared with its respective unexposed control, for a dose of 54 J/cm^2 following a 48 and 72 h post treatment period.

The protein content measurement by Lowry assay and cell staining with Crystal violet were also quantified to find out if the effects of 405 nm light on osteoblasts were dose-dependent, and if the effects remain the same if the dose is administered using different irradiance/exposure regimes. The results suggest that exposure of cells to 18 J/cm^2 of 405 nm HINS light using different irradiance/exposure regimes did not affect cell viability when compared with their respective unexposed controls, while a dose of 54 J/cm^2 induced a statistically significant difference in cell viability of exposed cells irrespective of how the dose was administered, following a 48 and 72 h post treatment period. These results confirmed that the effects of 405 nm HINS light on osteoblasts were dose-dependent.

The cell metabolic activity by MTT reduction, the alkaline phosphatase activity (an established marker of the ability of osteoblasts to form bone) and the proliferation rate of the cells measured by BrdU assay were assessed to establish a safe threshold

of exposure of osteoblasts to 405 nm light. The cells were exposed to 18, 27, 36 and 45 J/cm^2 of 405 nm light. After a 48 and 72 h post treatment period, cells exposed for up to a dose of 36 J/cm^2 of 405 nm light showed no statistically significant difference in any of the above measured parameters when compared with their unexposed controls, while a significant difference was noted in the 405 nm treated cells in all the parameters after an exposure dose of 45 J/cm^2. These results have established that a dose of 36 J/cm^2 is considered to be a safe threshold for osteoblasts exposure to 405 nm light.

Fluorescent microscopy images with Acridine orange & Propidium Iodide staining showed more apoptotic and dead cells for 405 nm light treated samples exposed to a dose of 45 J/cm^2 when compared to 36 J/cm^2 exposed samples, after a 48 and 72 h post treatment period, confirming the findings with MTT reduction. Phalloidin-FITC and DAPI staining of the cells showed the presence of more circular shaped cells (where actin filaments form a ring around the cell membrane, indicative of apoptosis) in samples exposed to 45 J/cm^2 of 405 nm light compared to 36 J/cm^2, following a 48 and 72 h post treatment period.

PARP analysis by western blotting was conducted to confirm the induction of apoptosis by determining if caspases were activated following 405 nm light exposure. Cells were exposed to 405 nm light for 1, 2 and 3 h at 15 mW/cm^2 (54, 108 and 162 J/cm^2 respectively). The results showed that there was no detectable PARP cleavage occurring at any of the applied doses of 405 nm light when compared with the unexposed controls, demonstrating that the applied doses did not activate

caspases or that this method was not sufficiently sensitive to detect the extent of apoptosis.

Fluorescence Activated Cell Sorting (FACS) using annexin-PE and 7-AAD dyes, was performed on 405 nm light treated cells exposed to 1, 2 and 2.5 h of 405 nm light (18, 36 and 45 J/cm^2 respectively) and after a 48 h post treatment period, to obtain further evidence for the occurrence of apoptosis. The results revealed a high % of early apoptotic cells (55 – 65 %) and late apoptotic cells (30 – 40 %) for both the unexposed samples and 405 nm treated samples at 2 h exposure to 405 nm light. For example, 50.6 % of cells were identified in the late apoptotic phase for unexposed samples. Due to the presence of cells in early and late apoptotic stages in the unexposed control samples, the occurrence of apoptosis of cells post 405 nm light treatment could not be confirmed by FACS analysis. This was thought to be due to the damage caused when the adherent osteoblasts were taken into suspension by the use of TrypLE enzyme. FACS is an ideal method for cells in suspension, but not for adherent cells.

Having established that doses up to 36 J/cm^2 of 405 nm light were safe for mammalian cells, different strains of bacteria including Gram-positive (*Staphylococcus aureus*, *Staphylococcus epidermidis*) and Gram-negative (*Pseudomonas aeruginosa*, *Acinetobacter baumannii*, *Escherichia coli*, *Klebsiella pneumoniae*) bacteria were exposed to doses ranging from 4.5 – 36 J/cm^2. The present study used light doses and surface- seeded bacterial cells at population densities ($\sim 10^2$ CFU/plate) that are more relevant to practical clinical environmental decontamination applications, (MacLean *et al*., 2010) as has been demonstrated in a

previous work (McDonald *et al*., 2013).The bacterial inactivation results demonstrated that significant inactivation of all strains tested was achieved at 18 J/cm^2 while 99.5 – 100 % inactivation was achieved at 36 J/cm^2, with *Acinetobacter baumannii* being the most susceptible of the strains measured (> 98% kill achieved at 4.5 J/cm^2). Therefore, doses up to 36 J/cm^2 of 405 nm light being safe for mammalian cell exposure, were found to be bactericidal to a variety of clinically relevant bacteria.

McDonald, 2011 conducted 1 h exposure studies to 405 nm light at different intensities (e.g. 0.5, 1.8, 5 and 15 mW/cm^2) and established that no detrimental effects were observed in the viability of osteoblasts upon exposure to 5 mW/cm^2 for 1 h compared to 15 mW/cm^2 for 1 h. However, the experiments conducted in this present study determined the viability of osteoblasts upon exposure to 5 mW/cm^2 for different time periods (1, 2 & 3 h) and a safe threshold dose of 36 J/cm^2 (5 mW/cm^2 for 2 h) for mammalian cell exposure, yet bactericidal for a variety of clinically relevant bacteria was identified. The safe threshold dose of 405 nm light thus obtained could potentially be used for facilitating patient-safe decontamination for the duration of arthroplasty surgery.

6.1.2. Cytotoxic responses to 405 nm light exposure in mammalian and bacterial cells

The cytotoxicity experiments were carried out to investigate and compare the inactivation mechanisms occurring in mammalian and bacterial cells upon exposure to 405 nm light. It was anticipated that the results would help to identify the mechanisms of cell kill and identify ways to minimise damage to mammalian cells.

ROS production in mammalian cells was detected and quantified by fluorescent microscopy and spectrofluorimetry respectively, using carboxy-H_2DCFDA staining of cells, immediately post 405 nm light exposure. The results revealed that there was a statistically significant increase in the production of green fluorescence from carboxy- H_2DCFDA for up to a period of 2 h (36 J/cm^2) of 405 nm light exposure when compared with their respective unexposed controls, and a decrease in the fluorescence was observed at 2.5 and 3 h exposures (45 and 54 J/cm^2 respectively) when compared to 36 J/cm^2 exposed samples. These results demonstrated that excess ROS production was involved in mammalian cell kill at higher doses of light (45 and 54 J/cm^2 (i) rendering cellular esterases inactive to convert the dye, failing to produce fluorescence upon reacting with ROS, (ii) inducing membrane damage that resulted in the failure to retain the intracellularly accumulated fluorescence within cells.

The intracellular reduced glutathione (GSH) content and the oxidised glutathione (GSSG) efflux from cells were assessed immediately after exposure to 405 nm light at 5 mW/cm^2 for 0, 1, 1.5, 2, 2.5 and 3 h (18, 27, 36, 45 and 54 J/cm^2). The results showed a statistically significant decrease in the GSH intracellular content and a statistically significant increase in the GSSG content of extracellular medium at 3 h exposure (54 J/cm^2) when compared with their respective unexposed controls, indicating that the cells were experiencing oxidative stress when exposed to high doses of light.

Experiments involving the introduction of reactive oxygen species scavengers (1 mM sodium pyruvate, 1 mM DMTU and 50 U/ml catalase) in mammalian samples during 405 nm light exposure were carried out to find out if these scavengers

offered any cell protection. 405 nm light treated samples at 54 J/cm^2 (5 mW/cm^2 for 3 h) in the absence of scavengers, and after a 48 h post treatment period, showed a significant decrease in the Lowry protein content of cells when compared with its unexposed control. However, after a 48 h post treatment period, no statistically significant decrease in the Lowry protein content of cells exposed to 54 J/cm^2 of 405 nm light in the presence of 1 mM sodium pyruvate and 50 U/ml catalase was observed when compared with their respective unexposed controls. This demonstrates that the sodium pyruvate and catalase were able to prevent the loss of protein observed in non-scavenger exposed cells exposed to 405 nm light for 3 h (54 J/cm^2). DMTU did not protect the light exposed cells when compared to the cells exposed in the absence of scavengers and this could be due to short half-life of ·OH radicals.

MTT reduction activity of the osteoblasts exposed to 405 nm light at 54 J/cm^2 (5 mW/cm^2 for 3 h) in the presence of 1 mM sodium pyruvate, 1 mM DMTU and 50 U/ml catalase, was also carried out after a 48 h post treatment period to assess the metabolic activity of cells post light exposure. The results showed that only catalase offered complete cell protection from the effects of 405 nm light compared to cells exposed to the light in the absence of scavengers. This is unlike cells in the presence of sodium pyruvate and DMTU where the light toxicity induced by the light was still evident, shown by a statistically significant decrease in MTT reduction. Hence, these results suggested that H_2O_2, which is relatively stable with a half-life of many seconds and is highly permeable to cell membranes, exerts significant effects on the cellular biochemistry, and may have also been released from the cells, enabling the extracellular catalase to offer cytoprotection. In this study, sodium pyruvate, which is also a H_2O_2 scavenger, did not have a

cytoprotective effect on 405 nm treated samples at 1 mM in terms of % cellular metabolic activity, because it causes an acidic environment inducing sub-lethal damage in cells, which influences MTT reduction.

ROS production in the bacterium *Staphylococcus epidermidis* was also detected and quantified by the same techniques using carboxy-H_2DCFDA, immediately post 405 nm light exposure. The results showed a statistically significant increase in green fluorescence in 405 nm light-treated samples at exposure periods of 1 and 3 h (54 J/cm^2 and 162 J/cm^2 respectively) when compared with their respective unexposed controls. A decrease in fluorescence in the 405 nm light-treated samples at an exposure period of 6 h (324 J/cm^2) was also observed when compared to the 3 h (162 J/cm^2) exposed samples. These results demonstrated that excess ROS production was also involved in bacterial cell kill.

The survival of *Staphylococcus epidermidis* in the presence of scavengers including 100 mM sodium pyruvate, 100 mM DMTU, 200 U/ml catalase, against the toxic effects of 405 nm light was also studied. In the absence of scavengers, a 4.8-log$_{10}$ reduction at 3 h (162 J/cm^2) increasing to a 7- log$_{10}$ reduction by 6 h (324 J/cm^2) was recorded. However, in the presence of sodium pyruvate, only 2.8- log$_{10}$ reduction was achieved after an exposure period of 3 h (162 J/cm^2). In the presence of catalase, 1.1-log$_{10}$ less inactivation at 3 h was achieved compared to that in the absence of catalase, however, after 6 h, similar reductions in bacterial populations were measured for both light exposed samples (in the presence and absence of catalase). DMTU results revealed that it did not offer any protection to cells at any concentrations tested in this study. The combined use of all the three scavengers offered the highest protection, with inactivation reduced by 3.5-log$_{10}$ compared to

that in the absence of scavengers, at 3 h (162 J/cm^2) with similar protective effects as exerted by sodium pyruvate, at 6 h (324 J/cm^2). These results showed that sodium pyruvate was the most effective ROS scavenger, and that, H_2O_2 was one of the key ROS responsible for cell death in bacteria, as in the case of mammalian cells. Although catalase offered a degree of protection at the mid-point of the inactivation kinetics, it became ineffective at the later point, possibly due to the use of insufficient concentration to offer protection against large amounts of intracellular H_2O_2. DMTU did not alter the cell viability demonstrating that either the concentration used was insufficient to offer any cell protection or the ·OH radicals induced less toxic damage to cells due to its short life span (10^{-9} seconds). The most protection to the 405 nm light exposed bacteria cells was offered by the combined use of the three scavengers, thus suggesting that each of the different ROS species produced may individually exhibit different levels of toxicity and play a role to some extent.

The ROS production in 405 nm light exposed *Staphylococcus epidermidis* cells in the presence of scavengers was detected and quantified immediately post 405 nm light exposure by fluorescent microscopy and spectrofluorimetry. The results demonstrated that there was a significant decrease in green fluorescence in samples exposed to 405 nm light at 162 J/cm^2 in the presence of 100 mM sodium pyruvate and in the presence of the combination of the three scavengers (100 mM sodium pyruvate, 100 mM DMTU, 200 U/ml catalase), correlating well with the cell viability results. Thus, ROS production is involved in the toxicity of 405 nm light in both mammalian and bacterial cells.

6.1.3. Assessment of light spectra obtained from surgical lights used in operating theatres in hospitals and optical analysis of 405 nm LED arrays

Having established a safe threshold dose of 405 nm HINS light for mammalian cell exposure, which is effectively bactericidal, it was essential to investigate ways to incorporate 405 nm LEDs into the operating room lights in order to develop a continuous decontamination method that could be used during arthroplasty surgery. This could potentially decrease the incidence of HAI. Before the incorporation of 405 nm LEDs into the theatre light system, it is vital to study the optical output of existing operating theatre light systems.

The surgical light systems used in the orthopaedic surgery theatres in the Southern General Hospital and the Golden Jubilee National Hospital were characterised to identify the overall optical output, and the existing content of 405 nm light within their optical spectra. In the Southern General Hospital, the 405 nm (400 - 420 nm) component obtained from one of the operating theatre lights (halogen light) at a distance of 1.3 m from the operating room floor, was measured to be 0.83 mW/cm^2 increasing to 1.38 mW/cm^2 from two light sources. At a distance of 2 m from the operating room floor, the 405 nm component (400 - 420 nm) received from one light source was calculated to be 0.127 mW/cm^2 increasing to 0.292 mW/cm^2 from two light sources.

In the Golden Jubilee National Hospital, the 405 nm (400 - 420 nm) component obtained from one of the operating theatre lights (white LED light) at a distance of 1.3 m from the operating room floor, was measured to be 0.01125 mW/cm^2 increasing to 0.01220 mW/cm^2 from two light sources. At a distance of 2 m from the

operating room floor, the 405 nm component (400 - 420 nm) received from one light source was calculated to be 0.000341 mW/cm^2 increasing to 0.001451 mW/cm^2 from two light sources.

Irrespective of the type of light systems used in Southern General hospital (halogen) and Golden Jubilee National hospital (LED), the 405 nm component present in the existing operating theatre light spectra is negligible and that external 405 nm LEDs needs to be integrated with the operating lights to provide antibacterial lighting during surgeries.

Three 405 nm light systems currently available in the laboratory were evaluated to determine their optical outputs: (i) 99-DIE LED array (Opto Diode) (ii) High Power 405 nm LED array (Photonstar) and (iii) 405 nm LEDs (GE). These were tested to measure the 405 nm component obtained from these light systems at different distances from the light source. The 405 nm component obtained at 25, 50, 75, 100, 125 and 130 cm distances from the 99-DIE LED array (Opto diode system) set at 1A and 11.6 V, were 1.23, 0.366. 0.163, 0.095, 0.069 and 0.067 mW/cm^2 respectively. The 405 nm component obtained at 25, 50, 75, 100, 125 and 130 cm distances from the high power 405 nm LED array (Photonstar) system powered by a Philips (Xitanium ^{TM}) power supply having a peak output of 50W, were 2.5, 0.76. 0.36, 0.033, 0.151 and 0.142 mW/cm^2 respectively. The 405 nm component obtained at 25, 50, 75, 100, 125 and 130 cm distances from the 405 nm GE system set at 10.25V and 1.568 A, were 1.4, 0.394, 0.179, 0.108, 0.072 and 0.070 mW/cm^2 respectively. Since, the highest 405 nm output (0.142 mW/cm^2) was obtained from the high power 405 nm LED array (Photonstar) at a 1.3 m distance from the light source, compared

to the 99-DIE LED array (Opto Diode) (0.07 mW/cm^2) and the 405 nm GE system (0.07 mW/cm^2), spectral graphs of the 405 nm spectrum obtained from the high power 405 nm LED array (Photonstar) were combined with the spectra obtained from one and/or two surgical light systems used in the two hospitals. Using the spectra from the LED surgical lights in the Golden Jubilee National Hospital, if the high power 405 nm LED array (Photonstar) was to be integrated with one surgical light system, the combined 405 nm output was calculated to be 0.153 mW/cm^2 increasing to 0.2962 mW/cm^2 with two light sources. In this case, to achieve an intensity of 5 mW/cm^2 of 405 nm light at a distance of 1.3 m from the light source, approximately seventeen, 405 nm LEDs would need to be added to each of the existing light sources.

Using the spectra from the halogen surgical lights in the Southern General Hospital, if the high power 405 nm LED array (Photonstar) was to be integrated with one surgical light system, the combined 405 nm output was calculated to be 0.972 mW/cm^2 increasing to 1.664 mW/cm^2 with two light sources. In this case, to achieve an intensity of 5 mW/cm^2 of 405 nm light at a distance of 1.3 m from the light source, approximately twelve, 405 nm LEDs would need to be added to each of the existing light sources.

Decontamination in an operating theatre during arthroplasty surgeries can be facilitated by integrating the 405 nm LEDs with (i) the surgical light systems (ii) the laminar flow chamber, and (iii) the tray tables, thereby promoting surgical site, environmental and surgical device decontamination, respectively. In order to overcome the vision problems that may arise among medical personnel during

orthopaedic surgeries, owing to the use of 405 nm violet blue light, the 405 nm light LEDs can be blended with red, yellow and green LEDs to make them appear as white light without altering the 405 nm output. The issue of rise in temperature of the operating environment and induction of skin burns in patients, when exposed to 405 nm light during surgeries can be resolved by using the 405 nm light systems with (i) proper heat sinks, (ii) cooling fans, for thermal management.

Any 405 nm light system developed for use during orthopaedic surgeries would also need to be safety tested (as was the case with the existing 405 nm HINS- EDS). The different 405 nm light systems mentioned earlier would need to be assessed against safety standards for eye safety, photoretinitis and photokeratitis. The content of 405 nm light in our proposed system for surgery would need to have much higher 405 nm output than the standard EDS (~0.5 mW/cm^2 at a height of 1.5 m) in order to facilitate a faster decontamination effect within the operation time-frame. Therefore, in addition to having looked at the effects of 405 nm light on mammalian cells earlier, any lighting fixture would need to be assessed against standards to ensure user safety (International Commission on Non-Ionizing Radiation Protection (ICNIRP), 2013; ICNIRP, 2004; ICNIRP, 1997; American Conference of Governmental Industrial Hygienists (ACGIH), 2015; ACGIH, 2007).

6.2 Limitations, future work and conclusions

6.2.1 Study of the effects of 405 nm light on primary cell types and on *in-vivo* animal models

Although a safe threshold dose of 405 nm HINS light which is effectively bactericidal has been established for mammalian cell exposure *in vitro*, there is still a

lot of work to be carried out before proving that 405 nm HINS light is completely safe for environmental decontamination during arthroplasty surgeries.

The 405 nm light exposure experiments in this study were carried out using immortalised rat foetal osteoblast cells *in vitro*, to identify the sensitivity of the cells to the light. The light exposure studies were performed on rat derived cell lines, indicating that results have to be extrapolated to primary cells in situ in the patient, and also to humans rather than rat. These cell lines can have marginal variations in their characteristics, but cannot replicate inter-individual differences between patients. They can also lose tissue-specific functions and not always replicate the properties of the cell type they are derived from (Olschlager *et al*., 2009; Pan *et al*., 2009). The next stages of development of this light technology for decontamination purposes, would include investigating the safe threshold dose in mammalian cells by measuring the cell viability parameters on primary cell types post exposure to 405 nm light. The effects seen at higher doses of 405 nm light on mammalian cell viability in this study, are also likely to be 'worst case scenario' as cells in the real environment are likely to have much more protection due to the presence of skin, blood etc. Hence, the effects of 405 nm light on mammalian cell viability in the presence of skin and blood also needs to be investigated.

In the current study, the response of only one cell type (osteoblasts) to 405 nm light was evaluated. However, in real time surgery if 405 nm light technology is to be implemented for facilitating patient safe decontamination, different cell types including keratinocytes, red blood cells, leukocytes, endothelial cells, epithelial cells and osteoblasts will be exposed to light. Hence, the responses of cell types other than osteoblasts to 405 nm light should be established. With the help of an *in vivo* model,

a better understanding of how 405 nm light may affect mammalian cell processes, can be achieved.

Mouse models are relatively inexpensive and easy to maintain (Jilka, 2013). These have been previously used in several studies. For example, models have been used, (i) to evaluate the effects of 415 nm light on skin, burns infected with *Pseudomonas aeruginosa* (Dai *et al*., 2013), (ii) to investigate age-related bone loss in humans (Jilka, 2013), (iii) to detect the effects of low level laser therapy (Demidova-Rice *et al*., 2007) and (iv) to investigate exposure to LEDs (Whelan *et al*., 2001). These *in vivo* models will provide stronger evidence about the effects of 405 nm light on primary cells, compared to *in vitro* studies.

6.2.2 Study of the effects of 405 nm light on implant materials

During an orthopaedic surgery, different implant materials such as titanium alloy, cobalt chrome alloy, stainless steel, polyethylene and ceramic, could also be exposed to 405 nm light. It will therefore be important to assess whether light exposure would have any effects on the implant materials. In general, light exposure, depending on the wavelength and exposure time, may have effects including:

- reducing the durability,
- increasing the wear rate of these materials,
- causing release of ions when in situ in the patients, which would in turn cause metallosis,
- implant loosening and systemic metal toxicity.

It is however, unlikely that 405 nm light would have any effects on the implant materials as any exposure time of the material will be short (operation time frame)

and the intensity used will be low. Moreover, photo degradation of the material occurs over long periods of exposure and is commonly associated with UV light (Irving *et al*., 2014).

One study has investigated the effects of 405 nm light on implant material. McDonald and co-workers (2011) exposed polyethylene terephthalate (PET) vascular graft materials (Vascutek Ltd., Inchinnan, Glasgow, UK) to 5 mW/cm^2 of 405 nm HINS light for 1 h and obtained SEM images of material samples immediately before exposure, shortly following exposure and at 3 months following exposure. They found that 1 h exposure did not cause any detectable difference in fibre structure and integrity. After conducting mechanical testing of materials immediately following exposure and at 3 months post exposure, it was found that there was no significant decrease in stress, strain and breaking load properties (McDonald, 2011). Orthopaedic surgeries may last longer than 1 h and in our study 2 h at 5 mW/cm^2 (36 J/cm^2) has been established as a safe threshold for mammalian cell exposure. Hence, the effects of 405 nm light on the above mentioned implant material properties should be investigated after an exposure period of 2 h to 5 mW/cm^2 of light, both immediately and after a post exposure period.

6.2.3 Study of the effects of 405 nm light on different bacterial species

Exposure of different bacterial strains responsible for causing HAI including *Staphylococcus aureus*, *Staphylococcus epidermidis*, *Escherichia coli*, *Pseudomonas aeruginosa*, *Klebsiella pneumoniae*, and *Acinetobacter baumannii* to 405 nm light at 5 mW/cm^2 resulted in a 99.5 – 100 % kill at 2 h (36 J/cm^2). However, there are also several bacteria other than those assessed in this research work, that are known to cause HAI, and hence exposing a wider range of bacteria to 405 nm light at the

intensities used in this study would be essential. There are also light resistant bacteria as suggested in the literature (Maclean et al., 2009; Ashkenazi et al., 2003; Henry et al., 1996). Bacterial species used in this research were obtained from National Collection of Type Cultures (NCTC), Collindale, UK and Laboratorium voor Microbiologie, Universiteit Gent, Belgium (LMG) which offers bacterial cultures with defined properties and definite source. However, similar to the differences between primary cell lines and established cell lines, clinical isolates may respond differently to 405 nm light compared to established cultures. McDonald and co-workers (2013) exposed clinical bacterial isolates including *Staphylococcus aureus*, *Staphylococcus epidermidis*, *Corynebacterium striatum*, *Enterococcus faecalis*, *Micrococcus* sp, *Escherichia coli*, *Klebsiella pneumoniae*, *Serratia marcescens* and *Pseudomonas aeruginosa*. These clinical isolates were isolated from infected hip and knee arthroplasties, and were acquired from the Southern General Hospital Microbiology Department (Glasgow, UK). They showed that 405 nm light has a non-selective bactericidal effect with successful inactivation achieved across a wide range of Gram-positive and Gram-negative species.

Gupta and co-workers (2015) also demonstrated that complete inactivation of a wide range of clinical bacterial isolates and the yeast, *Candida albicans* isolated from infected hip and knee arthroplasties at the Southern General Hospital Microbiology Department (Glasgow, UK), was achieved after exposure to 405 nm light at 123 mW/cm^2. Murdoch and co-workers (2013) assessed the effects of 405 nm light on yeast and mould fungi including *Saccharomyces cerevisiae*, *Candida albicans*, and dormant and germinating spores (conidia) of the mould *Aspergillus niger*. They found that all three fungal species were inactivated by the 405 nm light involving

ROS generated oxidative damage, without a requirement for addition of exogenous photosensitiser chemicals. Tomb and co-workers (2014) studied the effects of 405 nm light on bacteriophage ϕC_{31}, a surrogate for non-enveloped doubled-stranded DNA viruses, to establish whether 405 nm light can induce virucidal effects. They found that ~ 3, 5 and 7- $\log_{10}$ reductions in phage titer occurred when exposed in nutrient-rich media and after exposure to doses of 0.3, 0.5 and 1.4 KJ/cm^2 demonstrating that viral susceptibility to 405 nm light can be significantly enhanced in the presence of exogenous photosensitive components.

In this research work, all bacterial exposures were performed in PBS buffer. McDonald and co-workers (2011) found that bacterial inactivation rates were significantly reduced when the cells were exposed to 405 nm light on nutritious surfaces, compared to PBS suspension, or on less nutritious agar surfaces. During a surgical procedure, loss of skin integrity will expose the subcutaneous tissue which in turn provides a warm, moist and nutrient rich environment for proliferation of microbes (Bowler et al., 2001). Hence, bacterial exposures to 405 nm light on surfaces closely resembling a surgical wound will be required. *In vivo* mouse models as described by Dai et al (2013) involving mouse skin burns infected with *Pseudomonas aeruginosa* and those described by Jawhara and Mordon (2004) involving cutaneous wounds in rats contaminated with bioluminescent *Escherichia coli* (Jawhara & Mordon, 2004), could be used.

6.2.4 Study of the effects of 405 nm light on mammalian-bacterial cell in-vitro co-culture models

Another limitation in this research is that, the effects of 405 nm light were studied on mammalian and bacterial cells separately. However, during a surgical procedure, as described earlier, bacteria will come into contact with mammalian cells which might as a result reduce the bactericidal effects of 405 nm HINS light. In 2009, Smith and co-workers established that exposing 3T3 cells separately to 405 nm light at 10 mW/cm^2 for 2.5 h (90 J/cm^2) resulted in only a small reduction in cell viability, but the same irradiance/exposure regime resulted in a near complete inactivation of *Staphylococcus epidermidis*. From their preliminary co-culture experiments (exposure of 3T3 cells to 405 nm light in the presence of bacteria), they observed a significant decrease in mammalian cell viability whilst the bacterial colony count remained unaffected. The group later concluded that the mammalian cells could have released a factor into the suspending media which may have provided a protective barrier against the effects of 405 nm light exposure in bacteria, while increasing mammalian cell death (Smith, 2009). Freestone and co-workers (2008) observed that the microbes that were infecting cells, initiated their growth and pathogenic process by intercepting neurohormonal products of the stress response of the host cell. In the case of 3T3 cells, there is a possibility that the mammalian cells may have experienced oxidative stress on exposure to 405 nm HINS light and/or by the bacterial presence, and thus may have triggered the host 3T3 cells to release a chemical signal, leading to increased bacterial survival.

Interestingly, Dai and co-workers (2013) showed that an approximate 1 h exposure of mouse skin burns infected with *Pseudomonas aeruginosa* to 14.6 mW/cm^2 415 nm

blue light (52.5 J/cm^2) completely eliminated the bacterial luminescence without causing any significant damage to mouse skin. In another study conducted by Zhang and co-workers (2014), they demonstrated that a 62 minute exposure period of mouse skin burns infected with *Acinetobacter baumannii* to 14.6 mW/cm^2 415 nm blue light (54.3 J/cm^2) significantly reduced the bacterial burden without damaging the mouse skin DNA. Hence it is vital to conduct *in vivo* wound environment studies involving the inoculation of bacteria on mouse skin and bone cells before exposure of patients to 5 mW/cm^2 for 120 minutes 405 nm light (36 J/cm^2) during surgery (established safe threshold dose for mammalian cell exposure and less) and study the viability of both bacterial cells and mammalian cells. The *in vivo* wound environment studies will utilise low intensity (5 mW/cm^2) of 405 nm light but longer duration of exposure (2 h) compared to earlier studies (Dai *et al*., 2013 & Zhang *et al*., 2014). Another limitation with regard to the use of 405 nm light for decontamination during an orthopaedic surgery is that, once the bacteria come into contact with the surgical site, the light can only cause bacterial inactivation on the skin surface. This is due to the fact that violet blue light cannot penetrate > 2 mm into the human tissue (Moan *et al*., 1996), thereby limiting the bactericidal applications of 405 nm HINS light to surface treatments.

6.2.5 Designing a 405 nm light system for continual decontamination during arthroplasty surgery

In order to implement the 405 nm light technology in an operating theatre (OT) for continual decontamination during arthroplasty surgeries, it is vital to approach operating theatre light manufacturers and find out ways of integrating the 405 nm

LEDs with the OT lights thereby achieving the desired 405 nm output, while not altering the white colour temperature (~ 3000K – 4000K) of the OT lights.
Hence it is clear that although 405 nm HINS light technology has the prospect of reducing bacterial burden without affecting mammalian cell function, the light on its own cannot completely eliminate the incidence of HAI in patients. However, a substantial decrease of certain bacterial populations responsible for causing these infections could be accomplished by using the 405 nm HINS light in combination with the existing safety practices followed by medical personnel. Further development of this 405 nm HINS-light is encouraged for use in high-risk operative procedures such as arthroplasty surgeries.

6.2.6 Other areas of 405 nm light application

6.2.6.1 Endoscope storage

The use of UV-C light in the decontamination of flexible endoscopes between procedures has been associated with material degradation, thereby leading to device failure and increased risk to patients. 405 nm light may offer a possible alternative, potentially causing bacterial inactivation without inducing any material damage. Irving and co-workers investigated the endoscope polymer chemistry, endoscope material roughness (R_a /nm) and bacterial adhesion to endoscope material after exposure to 400 h 405 nm light and 400 h UVC light. They found that 405 nm light exposed samples showed little to no change in the polymer structure unlike UVC exposed material which showed bond scission within the polymer and breakdown of material, when compared to unexposed material. Atomic Force Microscopy (AFM) results revealed that the roughness of unexposed and 400 h 405 nm light exposed

endoscope materials were similar (2.34 ± 1.20 compared with 2.32 ± 1.41 nm), while for the 400 h UVC exposed sample, roughness was measured to be 68.70 ± 51.08 nm. Confocal microscopy studies indicated significant surface cracking after exposure to UVC light. They also demonstrated that the UVC exposed samples showed a significant increase (87 %) in bacterial adhesion compared to unexposed samples and the 405 nm treated samples (Irving *et al*., 2014). These results suggest that 405 nm light has the potential to provide improved endoscope infection control without compromising the device lifespan and it shows increased patient safety compared to UVC light sterilised endoscopes as the 405 nm light does not increase bacterial adhesion.

6.2.6.2 Food and drinks industry

Since 405 nm light lies within the visible light range and can be used safely in the presence of people (unlike UV light), and from the results obtained by Murdoch and co-workers (2012) which show the efficacy of 405 nm light for inactivating food-related pathogens, it is clear that 405 nm light also has the potential to be used for continuous decontamination of food contact areas in the presence of operator personnel thereby preventing contamination by bacteria (Murdoch et al., 2012).

Hence, 405 nm light has the potential of widespread use in healthcare, food industry and other situations e.g. public toilets where decontamination of surfaces is essential.

LIST OF PUBLICATIONS

JOURNAL PAPERS

Ramakrishnan, P., Maclean, M., MacGregor, S. J., Anderson, J. G., Grant, M. H., 2016. Cytotoxic responses to 405 nm light exposure in mammalian and bacterial cells: involvement of reactive oxygen species. Toxicol In Vitro. **33**:54-62. doi: 10.1016/j.tiv.2016.02.011.

Ramakrishnan, P., Maclean, M., MacGregor, S. J., Anderson, J. G., Grant, M. H., 2014. Differential sensitivity of osteoblasts and bacterial pathogens to 405-nm light highlighting potential for decontamination applications in orthopedic surgery. J Biomed Opt, **19**(10): 105001.

McDonald, R. S., Gupta, S., Maclean, M., Ramakrishnan, P., Anderson, J. G., MacGregor, S. J., Meek, R. M. D., Grant, M. H., 2013. 405 nm light exposure of osteoblasts and inactivation of bacterial isolates from arthroplasty patients: potential for new disinfection applications? Eur. Cell Mater. **25**: 204–214.

CONFERENCE PROCEEDINGS

Ramakrishnan, P., Maclean, M., MacGregor, S. J., Anderson, J. G., Grant, M. H., 2015. 405 nm light technology shows potential for patient safe decontamination during orthopaedic surgery. eCM XVI Bone and Implant Infection, Davos, European Cells and Materials Vol. 30. Suppl. 2, p 25

Ramakrishnan P., Maclean M., MacGregor, S.J., Anderson, J.G, Grant, M.H., 2014. Optimising 405 nm hins-light technology for patient safe decontamination during arthroplasty surgery. Tissue and Cell Engineering Society Conference, Newcastle, European Cells and Materials, Vol. 28. Suppl. 4, p 36.

REFERENCES

10th Annual Report National Joint Registry for England and Wales 2013. Accessed October 2013 from http://www.njrcentre.org.uk/njrcentre/Portals/0/Documents/England/Reports/10th_annual_report/NJR%2010th%20Annual%20Report%202013%20B.pdf.

Ahn, W. S., Bae, S. M., Huh, S. W., Lee, J. M., Namkoong, S. E., Han, S. J., et al. (2004). Necrosis-like death with plasma membrane damage against cervical cancer cells by photodynamic therapy. *International Journal of Gynecological Cancer, 14*(3), 475-482.

Albrecht, V., Gitter, B. (2005). Antimicrobial photodynamic therapy compound and method of use. WO2005021094A2.

Albrecht, M., Gauthier, R., Leaper, D. (2009). Forced-air warming: a source of airborne contamination in the operating room? *Orthop. Rev. (Pavia) 1*(2), 85–89.

Alexakis, P. G., Feldon, P. G., Wellisch, M., Richter, R. E., Finegold, S. M. (1976). Airborne bacterial contamination of operative wounds. *The Western Journal of Medicine, 124*(5), 361-369.

Alexander, H., Anderson, J.M., Bianco, R.W., Brunski, J.B., Chang, T.M.S., Colas, A. (2004). Host Reactions to Biomaterials and Their Evaluation. In: Ratner, B.D., Hoffman, A.S., Schoen, F.J., Lemons, J.E. (eds.). *Biomaterials Science: An Introduction to Materials in Medicine.* 2nd Edition. London, UK: Elsevier Academic Press,:293-345.

Alnemri, E.S., Livingston, D.J., Nicholson, D.W., Salvesen, G., Thornberry, N.A., Wong, W.W. (1996). Human ICE/CED-3 protease nomenclature. *Yuan J. Cell, 87*(2):171.

American Conference of Governmental Industrial Hygienists (ACGIH) (2007). Threshold Limit Values (TLVs) & Biological Exposure Indices. Signature Publications, Cincinnati.

American Conference of Governmental Industrial Hygienists (ACGIH) (2015). Threshold Limit Values and Biological Exposure Indices, 7th Edition. Signature publications.

Ames, B. N., Cathcart, R., Schwiers, E., Hochstein, P. (1981). Uric acid provides an antioxidant defense in humans against oxidant- and radical-caused aging and cancer: a hypothesis. *Proc Natl Acad Sci U S A. 78*(11):6858-62.

An, Y.H., Friedman, R.J. (1996). Prevention of sepsis in total joint arthroplasty. *J Hosp Infect, 33*(2):93-108.

Ansari, B., Coates, P.J., Greenstein, B.D., Hall, P.A. (1993). In situ end-labelling detects DNA strand breaks in apoptosis and other physiological and pathological states, *J Pathol. 170* (1): 1-8.

Archana, M., Bastian, Yogesh, T.L., Kumaraswamy, K.L. (2013). Various methods available for detection of apoptotic cells- A review. *Indian J Cancer, 50*(3):274-83.

Ashkenazi, H., Malik, Z., Harth, Y., Nitzan, Y. (2003). Eradication of Propionibacterium acnes by its endogenic porphyrins after illumination with high intensity blue light. *FEMS Immunol Med Microbiol; 35*(1):17-24.

Aukrust, P., Svardal, A. M., Muller, F., Lunden, B., Berge, R. K., Ueland, P. M., Froland, S. S. (1995). Increased levels of oxidized glutathione in CD4+ lymphocytes associated with disturbed intracellular redox balance in human immunodeficiency virus type 1 infection. *Blood 86*: 258–267.

Ayliffe, G. A. J., Collins, B. J. (1967). Wound infections acquired from a disperser of an unusual strain of Staphylococcus aureus. *Journal of Clinical Pathology, 20*(2), 195-198.

Bache, S. E., Maclean, M., MacGregor, S. J., Anderson, J. G., Gettinby, G., Coia, J. E., Taggart, I. (2012). Clinical studies of the HINS-light Environmental Decontamination System (HINS-light EDS), for continuous disinfection in the burn unit inpatient and outpatient settings. *Burns. 38*(1):69-76. doi: 10.1016/j.burns.2011.03.008. Epub 2011 Nov 21.

Bendy, R. H., Jr., Nuccio, P. A., Wolfe, E., Collins, B., Tamburro, C., Glass, W., et al. (1964). Relationship of Quantitative Wound Bacterial Counts to Healing of Decubiti: Effect of Topical Gentamicin. *Antimicrobial Agents and Chemotherapy, 10*, 147-155.

Benediktsdóttir, E., Hambraeus, A. (1982). Dispersal of non-sporeforming anaerobic bacteria from the skin. *J Hyg (Lond); 88*(3):487-500.

Berg, M., Bergman, B.R., Hoborn, J. (1991). Ultraviolet radiation compared to an ultra-clean air enclosure. Comparison of air bacteria counts in operating rooms. *J Bone Joint Surg Br,73*(5):811-5.

Berns, M.W., Rettenmaier, M., McCullough, J., Coffey, J., Wile, A., Berman, M., DiSaia, P., Weinstein, G. (1984). Response of psoriasis to red laser light (630 nm) following systemic injection of hematoporphyrin derivative. *Lasers Surg Med.;4*(1):73-7.

Bilski, P., Belanger, A.G., Chignell, C.F. (2002). Photosensitized oxidation of 2',7'-dichlorofluorescin: singlet oxygen does not contribute to the formation of fluorescent oxidation product 2',7'-dichlorofluorescein. *Free Radic Biol Med.; 33*(7):938-46.

Bisland, S.K., Burch, S. (2006). Photodynamic therapy of diseased bone, *Photodiagn. Photodyn. Therapy 3*(3), 147–155.

Bohm, F., Edge, R., Foley, S., Lange, L., Truscott, T. G. (2001). Antioxidant inhibition of porphyrin-induced cellular phototoxicity. *Journal of Photochemistry and Photobiology B: Biology, 65*(2-3), 177-183.

Booth, M., Maclean, M., MacGregor, S.J., Anderson, J.G., Woolsey, G.A., Coia, J.E., Hamilton, K., Gettinby, G. (2010). Use of a novel light technology for environmental disinfection within an Intensive Care Unit, *Euroanaesthesia 2010, conference of the European Society of Anaesthesiology*, Helsinki, Finland, 12-15 June 2010.

Bouillaguet, S., Owen, B., Wataha, J. C., Campo, M. A., Lange, N., Schrenzel, J. (2008). Intracellular reactive oxygen species in monocytes generated by photosensitive chromophores activated with blue light. *Dental materials*, *24*(8), 1070-1076.

Bowers, G. N., Jr., McComb, R. B. (1966). A Continuous Spectrophotometric Method for Measuring the Activity of Serum Alkaline Phosphatase. *Clinical Chemistry*, *12*(2), 70-89.

Bowler, P. G., Duerden, B. I., & Armstrong, D. G. (2001). Wound Microbiology and Associated Approaches to Wound Management. *Clinical Microbiology Reviews*, *14*(2), 244-269.

Bozic, K.J., Kurtz, S.M., Lau, E., Ong, K., Chiu, V., Vail, T.P., Rubash, H.E., Berry, D.J. (2010). The epidemiology of revision total knee arthroplasty in the United States. *Clin Orthop Relat Res.* 468:45–51.

Brandt C, Hott U, Sohr D, Daschner F, Gastmeier P, Ruden H. (2008). Operating room ventilation with laminar airflow shows no protective effect on the surgical site infection rate in orthopedic and abdominal surgery. Ann Surg.; 248:695–700.

Brubacher, J. L., Bols, N. C. (2001). Chemically de-acetylated 2′,7′-dichlorodihydrofluorescein diacetate as a probe of respiratory burst activity in mononuclear phagocytes, *J Immunol Methods, 251*(1-2): 81-91.

Bruck, R., Shirin, H., Aeed, H., Matas, Z., Hochman, A., Pines, M., Avni, Y. (2001). Prevention of hepatic cirrhosis in rats by hydroxyl radical scavengers. *J Hepatol. 35*(4):457-64.

Cahill, J.L., Shadbolt, B., Scarvell, J.M., Smith, P.N. (2008). Quality of life after infection in total joint replacement. *J Orthop Surg (Hong Kong), 16*(1):58-65.

Campoccia, D., Montanaro, L., Arciola, C.R. (2006). The significance of infection related to orthopaedic devices and issues of antibiotic resistance. *Biomaterials.* (11):2331-9.

Cao, L. Q., Xue, P., Lu, H. W., Zheng, Q., Wen, Z. L., & Shao, Z. J. (2009). Hematoporphyrin derivative-mediated photodynamic therapy inhibits tumor growth in human cholangiocarcinoma in vitro and in vivo. *Hepatology Research, 39*(12), 1190-1197.

Chai, Y.C., Ashraf, S.S., Rokutan, K., Johnston, R.B. Jr, Thomas, J.A. (1994). S-thiolation of individual human neutrophil proteins including actin by stimulation of the respiratory burst: evidence against a role for glutathione disulfide. *Arch Biochem Biophys. 310*(1):273-81.

Charnley, J., Eftekhar, N. (1969). Postoperative infection in total prosthetic replacement arthroplasty of the hip-joint with special reference to the bacterial content of the air of the operating room. *British Journal of Surgery, 56*(9), 641-649.

Chiaviello, A., Postiglione, I., Palumbo, G. (2011). Targets and Mechanisms of Photodynamic Therapy in Lung Cancer cells: A Brief Overview. *Cancers. 3*(1), 1014-1041.

Chow, T.T., Yang, X.Y (2005). Ventilation performance in the operating theatre against airborne infection: numerical study on an ultra-clean system. *J Hosp Infect; 59*:138–147.

Chow, T.T., Zhang, L., Bai, W. (2006). The integrated effect of medical lamp position and diffuser discharge velocity on ultra-clean ventilation performance in an operating theatre. *Indoor Built Environ, 15*:315–331.

Clark, R.P., de Calcina-Goff, M.L. (2009). Some aspects of the airborne transmission of infection. *J R Soc Interface. 6*:S767-82.

Clark, R. P., Reed, P. J., Seal, D. V., Stephenson, M. L. (1985). Ventilation conditions and air-borne bacteria and particles in operating theatres: proposed safe economies. *Journal of Hygiene (London), 95*(2), 325-335.

Coello, R., Glenister, H., Fereres, J., Bartlett, C., Leigh, D., Sedgwick, J., Cooke, E. (1993). The cost of infection in surgical patients: A case control study, *Journal of Hospital Infection, 25*, 239-250.

Cogen, A. L., Nizet, V., Gallo, R. L. (2008). Skin microbiota: a source of disease or defence? *Br J Dermatol. 158* (3): 442–55.

Collins, A.R. (2002). Comet assay—principles, applications, and limitations. *Methods Mol Biol*; 203:163-77.

Cooper, J.A. (1987). Effects of cytochalasin and phalloidin on actin. *J.Cell Biol. 105*(4): 1473-8.

Couto, N., Malys, N., Gaskell, S., Barber, J. (2013). "Partition and Turnover of Glutathione Reductase from Saccharomyces cerevisiae: a Proteomic Approach". *Journal of Proteome Research, 12* (6): 2885–94

Crabtree, J.H., Burchette, R.J., Siddiqi, R.A., Huen, I.T., Hadnott, L.L., Fishman, A. (2003). The efficacy of silver-ion implanted catheters in reducing peritoneal dialysis-related infections. *Perit Dial Int, 23*:368–74

Cruse, P.J.E., Foord, R. (1973). A five-year prospective study of 23,649 surgical wounds. *Archives of Surgery. 107* (2): 206.

Cummings, M.C., Winterford, C.M., Walker, N.I. (1997). Apoptosis. *Am J Surg Pathol, 21*: 88-101.

Dai, T., Tegos, G.P., Lu, Z., Huang, L., Zhiyentayev, T., Franklin, M.J., Baer, D.G., Hamblin, M.R. (2009). Photodynamic therapy for Acinetobacter baumannii burn infections in mice. *Antimicrob Agents Chemother, 53*:3929–34.

Dai, T., Gupta, A., Huang, Y.Y., Yin, R., Murray, C.K., Vrahas, M.S., Sherwood, M.E., Tegos, G.P., Hamblin, M.R. (2013). Blue light rescues mice from potentially fatal Pseudomonas aeruginosa burn infection: efficacy, safety, and mechanism of action. *Antimicrob Agents Chemother; 57*(3):1238-45. doi: 10.1128/AAC.01652-12.

Dai, T., Gupta, A., Huang, Y.-Y., Sherwood, M. E., Murray, C. K., Vrahas, M. S., … Hamblin, M. R. (2013). Blue Light Eliminates Community-Acquired Methicillin-Resistant *Staphylococcus aureus* in Infected Mouse Skin Abrasions. *Photomed Laser Surg*, *31*(11), 531–538. http://doi.org/10.1089/pho.2012.3365

Dai, T., Fuchs, B.B., Coleman, J.J., Prates, R.A., Astrakas, C., St Denis, T.G., Ribeiro, M.S., Mylonakis, E., Hamblin, M.R., Tegos, G.P. (2012). Concepts and principles of photodynamic therapy as an alternative antifungal discovery platform. *Front Microbiol. 10*; 3:120

Darouiche, R.O. (2004). Treatment of infections associated with surgical implants. *N Engl J Med, 350*(14):1422-9.

Daud-Gallotti, R.M., Costa, S.F., Guimarães, T., Padilha, K.G., Inoue, E.N., Vasconcelos, T.N., da Silva Cunha Rodrigues, F., Barbosa, E.V., Figueiredo, W.B., Levin, A.S. (2012). Nursing workload as a risk factor for healthcare associated infections in ICU: a prospective study. *PLoS One, 7*(12):e52342.

Davis, N., Curry, A., Gambhir, A.K., Panigrahi, H., Walker, C.R.C., Wilkins, E.G.L., Worsley, M.A., Kay, P.R. (1999). Intraoperative bacterial contamination in operations for joint replacement. *J Bone Joint Surg; 81*-B: 886-9

Demidova-Rice, T. N., Salomatina, E. V., Yaroslavsky, A. N., Herman, I. M., & Hamblin, M. R. (2007). Low-level light stimulates excisional wound healing in mice. *Lasers in Surgery and Medicine, 39*(9), 706-715.

Department of Health, UK. Hospital infection control: guidance on the control of infections in hospitals. HSG (95)10. London, UK: Department of Health, 1995.

Desagher, S., Glowinski, J., Prémont, J. (1997). Pyruvate protects neurons against hydrogen peroxide-induced toxicity. *J Neurosci, 17*(23):9060-7.

Desouza, M., Gunning, P. W., Stehn, J. R. (2012). The actin cytoskeleton as a sensor and mediator of apoptosis. *Bioarchitecture*, *2*(3), 75–87. http://doi.org/10.4161/bioa.20975.

Devasagayam, T. P. A., Tilak, J. C., Boloor, K. K., Sane K. S., Ghaskadbi S. S., Lele R. D. (2004). Free Radicals and Antioxidants in Human Health: Current Status and Future Prospects. *J Assoc Physicians India*, 52: 796.

Digiovine, B., Chenoweth, C., Watts, C., Higgins, M. (1999).The attributable mortality and costs of primary nosocomial bloodstream infections in the intensive care unit. *Am J Respir Crit Care Med*, *160*: 976–981.

Dougherty, T.J., Gomer, C.J., Henderson, B.W., Jori, G., Kessel, D., Korbelik, M., Moan, J., Peng, Q. (1998). Photodynamic therapy. *J Natl Cancer Inst.; 90*(12):889-905

Drago, L., Boot, W., Dimas, K., Malizos, K., Hänsch, G.M., Stuyck,, J., Gawlitta, D., Romanò, C.L. (2014). Does Implant Coating With Antibacterial-Loaded Hydrogel Reduce Bacterial Colonization and Biofilm Formation in Vitro? *Clin Orthop Relat Res; 472*(11): 3311–3323.

Elek, S. D. (1956). Experimental Staphylococcal Infections in the Skin of Man. *Annals of the New York Academy of Sciences*, *65*(3), 85-90.

Elmore, S. (2007). Apoptosis: A Review of Programmed Cell Death. *Toxicol Pathol. 35*(4): 495–516.

Embil, J. M., McLeod, J. A., Al-Barrak, A. M., Thompson, G. M., Aoki, F. Y., Witwicki, E. J., et al. (2001). An outbreak of methicillin resistant Staphylococcus aureus on a burn unit: potential role of contaminated hydrotherapy equipment. *Burns*, *27*(7), 681-688.

Engelmann, J., Volk, J., Leyhausen, G., Geurtsen, W. (2005). ROS formation and glutathione levels in human oral fibroblasts exposed to TEGDMA and camphorquinone. *J Biomed Mater Res B Appl Biomater. 75*(2):272-6.

Ennever, J.F., Sobel, M., McDonagh, A.F., Speck, W.T. (1984). "Phototherapy for neonatal jaundice: in vitro comparison of light sources". *Pediatr. Res. 18* (7): 667–70.

Eron, L.J., Lipsky, B.A. (2006). Use of cultures in cellulitis: when, how, and why? *Eur J clinical Microbiol Infect Dis, 25*: 615–617.

European Centre for Disease Prevention and Control. Antimicrobial resistance surveillance in Europe 2010. Annual report of the European Antimicrobial Resistance Surveillance Network (EARS-Net). Stockholm: ECDC; 2011.

Evans, R.P. (2011). Current concepts for clean air and total joint arthroplasty: laminar airflow and ultraviolet radiation: a systematic review. *Clin Orthop Relat Res; 469*:945–953

Evensen, J. F. (1995). The use of porphyrins and non-ionizing radiation for treatment of cancer. *Acta Oncologica, 34*(8), 1103-1110

Fadeel, B., Gleiss, B., Hogstrand, K., Chandra, J., Wiedmer, T., Sims, P.J., Henter, J.I., Orrenius, S., Samali, A. (1999). Phosphatidylserine exposure during apoptosis is a cell-type specific event and does not correlate with plasma membrane phospholipid scramblase expression. *Biochem Biophys Res Commun; 266*:504-611.

Fan, C., Wang, W., Zhao, B., Zhang, S., Miao, J. (2006). Chloroquine inhibits cell growth and induces cell death in A549 lung cancer cells. *Bioorg Med Chem. 14*(9):3218-22.

Faraci, F. M., Didion, S. P. (2004). Vascular protection: superoxide dismutase isoforms in the vessel wall. *Arterioscler Thromb Vasc Biol. 24*(8):1367-73.

Feuerstein, O., Ginsburg, I., Dayan, E., Veler, D., Weiss, E. I. (2005). Mechanism of Visible Light Phototoxicity on Porphyromonas gingivalis and Fusobacterium nucleatum. *Photochemistry and Photobiology, 81*(5), 1186-1189.

Freestone, P. P. E., Sandrini, S. M., Haigh, R. D., & Lyte, M. (2008). Microbial endocrinology: how stress influences susceptibility to infection. *Trends in Microbiology, 16*(2), 55-64.

Fuchs, J., Thiele, J. (1998). The Role of Oxygen in Cutaneous Photodynamic Therapy. *Free Radical Biology and Medicine, 24*(5), 835-847.

Ganz, R. A., Viveiros, J., Ahmad, A., Ahmadi, A., Khalil, A., Tolkoff, M. J., et al. (2005). Helicobacter pylori in patients can be killed by visible light. *Lasers in Surgery and Medicine*, *36*(4), 260-265.

Gastmeier, P., Breier, A.C., Brandt, C. (2012). Influence of laminar airflow on prosthetic joint infections: a systematic review. *J Hosp Infect, 81*(2):73-8.

Gayl, S.V. (2001). Photofrin-mediated photodynamic therapy for treatment of aggressive head and neck nonmelanomatous skin tumors in elderly patients. *Laryngoscope, 111*(6):1091-8.

Geipel, U. (2009). Pathogenic organisms in hip joint infections. *International Journal of Medical Sciences, 6* (5):234-240.

Glickman, G., Byrne, B., Pineda, C., Hauck, W.W., Brainard, G.C. (2006). Light therapy for seasonal affective disorder with blue narrow-band light-emitting diodes (LEDs). *Biol Psychiatry, 59*(6):502-7.

Godley, B.F., Shamsi, F.A., Liang, F.Q., Jarrett, S.G., Davies, S., Boulton, M. (2005). Blue light induces mitochondrial DNA damage and free radical production in epithelial cells. *J Biol Chem, 280*(22):21061-6.

Goldoni, A. (2002). Porphyrins: fascinating molecules with biological significance. ELETTRA Laboratory, Research Highlights 2001-2002: *Atomic, Molecular and Supramolecular Studies,* 64-65.

Gosden, P.E., MacGowan, A.P., Bannister, G.C. (1998). Importance of air quality and related factors in the prevention of infection in orthopaedic implant surgery, *J. Hosp. Infect. 39*(3), 173–180.

Gould, I.M. (2006). Costs of hospital-acquired methicillin-resistant Staphylococcus aureus (MRSA) and its control. *Int J Antimicrob Agents.28*(5):379-84.

Graves, N., Weinhold, D., Tong, E., Birrell, F., Doidge, S., Ramritu, P., Halton, K., Lairson, D., Whitby, M. (2007). Effect of healthcare-acquired infection on length of hospital stay and cost. *Infect Control Hosp Epidemiol.*(3):280-92.

Grzelak, A., Rychlik, B., & Bartosz, G. (2001). Light-dependent generation of reactive oxygen species in cell culture media. *Free Radical Biology and Medicine, 30*(12), 1418-1425.

Guffey, J.S., Wilborn, J. (2006). In vitro bactericidal effects of 405-nm and 470-nm blue light. *Photomed Laser Surg. 24*(6):684-8.

Gupta, S., Maclean, M., Anderson, J.G., MacGregor, S.J., Meek, R.M., Grant, M.H. (2015). Inactivation of micro-organisms isolated from infected lower limb arthroplasties using high-intensity narrow-spectrum (HINS) light. *Bone Joint J, 97-B* (2):283-8. doi: 10.1302/0301-620X.97B2.35154.

Halliwell, B., Gutteridge, J.M.C. (2001). Antioxidant defences, Chapter 3 in Free Radicals in Biology and Medicine, pp. 105–245, Oxford University Press, Oxford.

Hamblin, M.R., Demidova, T.N. (2006). Photodynamic inactivation of bacterial spores. 20060223729.

Hamblin, M.R., Viveiros, J., Yang, C., Ahmadi, A., Ganz, R.A., Tolkoff, M.J. (2005). Helicobacter pylori accumulates photoactive porphyrins and is killed by visible light. Antimicrob Agents Chemother. ; 49(7):2822-7.

Hamblin, M.R., Hasan, T. (2004). Photodynamic therapy: a new antimicrobial approach to infectious disease? *Photochem Photobiol Sci*, *3*(5): 436–450.

Hambraeus, A. (1988). Aerobiology in the operating room—a review. *J Hosp Infect, 11*:68–76

Hamilton, H., Jamieson, J. (2008). Deep infection in total hip arthroplasty. *Canadian Journal of Surgery. 51*(2), 111-117.

Hart, D. (1960). Bactericidal ultraviolet radiation in the operating room. Twenty-nine-year study for control of infections. *J Am Med Assoc; 172*:1019-28.

Haupt, S., Berger, M., Goldberg, Z., Haupt, Y. (2003). Apoptosis – the p53 network. *J Cell Sci; 116*:4077-85.

Henry, C. A., Dyer, B., Wagner, M., Judy, M., & Matthews, J. L. (1996). Phototoxicity of argon laser irradiation on biofilms of Porphyromonas and Prevotella species. *Journal of Photochemisty and Photobiology B, 34*(2-3), 123-128.

Herceg, Z., Wang, Z.Q. (2001). Functions of poly (ADP-ribose) polymerase (PARP) in DNA repair, genomic integrity and cell death. *Mutat Res. 477*(1-2):97-110.

Hetrick, E.M., Schoenfisch, M.H. (2006). Reducing implant-related infections: active release strategies. *Chem Soc Rev. 35* (9):780-9. Epub 2006 May 5.

Hissin, P. J., Hilf, P. R. (1976). A fluorometric method for determination of oxidized and reduced glutathione in tissues. *Anal Biochem.74*(1):214-26.

Ho, G., Grant, M. H., Barbenel, J. C., Henderson, C. J. (2004). Low-level laser therapy on tissue-engineered skin substitutes: effect on the proliferation rate of 3T3 mouse fibroblast cells, Proc. SPIE 5610, 124–134.

Hockberger, P. E., Skimina, T. A., Centonze, V. E., Lavin, C., Chu, S., Dadras, S., Reddy, J. K., White, J.G. (1999). Activation of flavin-containing oxidases underlies light-induced production of H_2O_2 in mammalian cells. *Proc Natl Acad Sci U S A*, 96(11):6255-60.

Howorth, F.H. (1985). Prevention of airborne infection during surgery. *Lancet.16*; 1(8425):386-8.

Hunter, G., Dandy, D. (1977). The natural history of the patient with an infected total hip replacement. *J Bone Joint Surg Br, 59*:293-297.

Hwan, K. S., Lee, H. S., Ryu, D. S., Choi, S. J., Lee, D. S. (2011). Antibacterial Activity of Silver-nanoparticles Against Staphylococcus aureus and Escherichia coli. *Korean J. Microbiol. Biotechnol. 39*(1): 77–85.

International Commission on Non-Ionizing Radiation Protection (ICNIRP). Guidelines on limits of exposure to optical radiation from 0.38 to 3 μm. *Health Physics*, 73 (1997), pp. 539–554

International Commission on Non-Ionizing Radiation Protection (ICNIRP). Guidelines on Limits of Exposure to Incoherent Visible and Infrared Radiation. *Health Physics*, 105(1):74-96; 2013.

International Commission on Non-Ionizing Radiation Protection (ICNIRP). Guidelines on limits of exposure to ultraviolet radiation of wavelengths between 180nm and 400nm (incoherent radiation). *Health Physics*, 87 (2004), pp. 171–186.

Irving, D., Grant, M.H., Maclean, M., Lamprou, D., Anderson, J.G., MacGregor, S.J. (2014). The degradative effects of germicidal light on flexible endoscope material: the safety and suitability of UVC and 405nm light sources. The 9th Healthcare Infection Society International Conference 2014.

Jabłoński, A. (1933)."Efficiency of Anti-Stokes Fluorescence in Dyes" *Nature, 131,* pp. 839-840.

Jämsen, E., Furnes, O., Engesaeter, L.B., Konttinen, Y.T., Odgaard, A., Stefánsdóttir, A., Lidgren, L. (2010). Prevention of deep infection in joint replacement surgery. *ActaOrthop, 81*:660–666.

Jawhara, S., Mordon, S. (2004). In vivo imaging of bioluminescent Escherichia coli in a cutaneous wound infection model for evaluation of an antibiotic therapy. *Antimicrobial Agents and Chemotherapy, 48*(9), 3436-3441.

Jayabalan, M., Finosh, G.T. (2013). Reactive oxygen species—Control and management using amphiphilic biosynthetic hydrogels for cardiac applications. *Advances in Bioscience and Biotechnology. 4*: 1134-1146.

Jenks, P.J., Laurent, M., McQuarry, S., Watkins, R. (2014). Clinical and economic burden of surgical site infection (SSI) and predicted financial consequences of elimination of SSI from an English hospital. *J Hosp Infect, 86*:24–33.

Jilka, R. L., Weinstein, R. S., Bellido, T., Parfitt, A. M., & Manolagas, S. C. (1998). Osteoblast programmed cell death (apoptosis): Modulation by growth factors and cytokines. *Journal of bone and mineral research, 13*(5), 793-802.

Jilka, R.L. (2013).The relevance of mouse models for investigating age-related bone loss in humans. *J Gerontol A Biol Sci Med Sci; 68*(10):1209-17.

Johnson, V.L., Ko, S.C., Holmstrom, T.H., Eriksson, J.E., Chow, S.C. (2000). Effector caspases are dispensable for the early nuclear morphological changes during chemical-induced apoptosis. *J Cell Sci, 113*:2941-53.

Johnson, I., Spence, M.T.Z. (2010). Molecular Probes Handbook, A Guide to Fluorescent Probes and Labeling Technologies, Chapter 18 – Probes for Reactive Oxygen Species, Including Nitric Oxide, 11th Edition, 815 – 817.

Joshi, G.P., Chung, F., Vann, M.A., Ahmad, S., Gan, T.J., Goulson, D.T., Merrill, D.G., Twersky, R. (2010). Society for Ambulatory Anesthesia. Society for Ambulatory Anesthesia consensus statement on perioperative blood glucose management in diabetic patients undergoing ambulatory surgery. *Anesth Analg; 111:*1378–1387.

Jung, I. L., Oh, T. J., Kim, I. G. (2003). Abnormal growth of polyamine-deficient Escherichia coli mutant is partially caused by oxidative stress-induced damage. *Arch Biochem Biophys. 418*(2):125-32.

Kapuscinski, J. (1995). "DAPI: a DNA-specific fluorescent probe". *Biotech Histochem, 70*(5): 220-33.

Kaufmann, S.H., Desnoyers, S., Ottaviano, Y., Davidson, N.E., Poirier, G.G. (1993). Specific proteolytic cleavage of poly (ADP-ribose) polymerase: an early marker of chemotherapy-induced apoptosis. *Cancer Res.; 53*(17):3976-85.

Kawada, A., Aragane, Y., Kameyama, H., Sangen, Y., Tezuka, T. (2002). Acne phototherapy with a high-intensity, enhanced, narrow-band, blue light source: an open study and in vitro investigation. *J Dermatol Sci.*(2):129-35.

Kerr, J.F., Winterford, C.M, Harmon, B.V. (1994). Apoptosis: Its significance in cancer and cancer therapy. *Cancer;* 73:2013-026.

Kessel, D. (1982). Components of Hematoporphyrin Derivatives and Their Tumor-localizing Capacity. *Cancer Research, 42*(5), 1703-1706.

Kim, J.S., Kuk, E., Yu, K.N., Kim, J.H., Park, S.J., Lee, H.J., Kim, S.H., Park, Y.K., Park, Y.H., Hwang, C.Y., Kim, Y.K., Lee, Y.S., Jeong, D.H., Cho, M.H. (2007). Antimicrobial effects of silver nanoparticles. *Nanomedicine. 3*(1):95-101.

Kluck, R.M., Bossy-Wetzel, E., Green, D.R., Newmeyer, D.D. (1997). The release of cytochrome c from mitochondria: a primary site for Bcl-2 regulation of apoptosis. *Science. 275* (5303): 1132-6.

Kotelevets, L. M., Babenko, Iu. S., Lukoianova, M. A. (1988). Spectral properties of cytochromes from Staphylococcus aureus. *Prikl Biokhim Mikrobiol. 24*(1):68–75.

Kowalski, W.J., Bahnfleth, W.P., Witham, D.L., Severin, B.F., Whittam, T.S. (2000). "Mathematical modeling of ultraviolet germicidal irradiation for air disinfection". *Quantitative Microbiology (Springer) 2* (3): 249–270.

Kraft, C.N., Hansis, M., Arens, S., Menger, M.D., Vollmar, B. (2000). Striated muscle microvascular response to silver implants: a comparative in vivo study with titanium and stainless steel. *J Biomed Mater Res.; 49*:192–9. 15.

Kramer, A., Schwebke, I., & Kampf, G. (2006). How long do nosocomial pathogens persist on inanimate surfaces? A systematic review. *BMC Infectious Diseases, 6*(1), 130.

Krasnovskii, A. A., Jr., Venediktov, E. A., & Chernenko, O. M. (1982). Quenching of singlet oxygen with chlorophylls and porphyrins. *Biofizika., 27*(6), 966-972.

Krizek, T. J., Davis, J. H. (1966). Endogenous Wound Infection. *The Journal of Trauma, 6*(2), 239-248.

Kuehl, R., Brunetto, P., Woischnig, A-K., Rajacic, Z., Fromm, K., Khanna, N. (2015). Preventing implant associated infections by silver coating. *European Cells and Materials* Vol. 30. Suppl. 2, (page 8).

Kurtz, S., Ong, K., Lau, E., Mowat, F., Halpern, M. (2007). Projections of primary and revision hip and knee arthroplasty in the United States from 2005 to 2030. *J Bone Joint Surg Am.; 89*(4):780-5.

Kvitek, L., Panacek, A., Soukupova, J., Kolar, M., Vecerova, R., Prucek, R., Holecova, M., Zboril, R. (2008). Effect of Surfactants and Polymers on Stability and Antibacterial Activity of Silver Nanoparticles (NPs). *J Phys Chem C 112*: 5825–5834

Landis, S. (2008). Chronic Wound Infection and Antimicrobial Use. *Advances of Skin & Wound Care, 21*(1), 531-540.

Larson, E.L., Cimiotti, J.P., Stone, P.W. (2004). A cost comparison of hand hygiene regimens. *Nursing Economic$; 22*:196–199. 204, 175.

Whang, T.J., Huang, H.Y., Hsieh, M.T., Chen, J.J. (2009). Laser-Induced Silver Nanoparticles on Titanium Oxide for Photocatalytic Degradation of Methylene Blue. *Int. J. Mol. Sci, 10*(11), 4707-4718; doi:10.3390/ijms10114707

Lavi, R., Sinyakov, M., Samuni, A., Shatz, S., Friedmann, H., Shainberg, A., Breitbart, H., Lubart, R. (2004). ESR detection of $_1O^2$ reveals enhanced redox activity in illuminated cell cultures. *Free Radic Res. 38*(9):893–902.

Lazebnik, Y.A., Kaufmann, S.H., Desnoyers, S., Poirier, G.G., Earnshaw, W.C. (1994). Cleavage of poly (ADP-ribose) polymerase by a proteinase with properties like ICE. *Nature, 22*; 371(6495):346-7.

Leong, G., Wilson, J., Charlett, A. (2006). Duration of operation as a risk factor for surgical site infection: comparison of English and US data. *J Hosp Infect.; 63*(3):255-62.

Li, Y., Huang, T. T., Carlson, E. J., Melov, S., Ursell, P. C., Olson, J. L., Noble L. J., Yoshimura, M. P., Berger, C., Chan, P. H., Wallace, D. C., Epstein, C. J. (1995). Dilated cardiomyopathy and neonatal lethality in mutant mice lacking manganese superoxide dismutase. *Nat. Genet. 11* (4): 376–81.

Lidwell, O. M. (1994). Ultraviolet radiation and the control of airborne contamination in the operating room. *Journal of Hospital Infection, 28*(4), 245-248.

Lidwell, O. M., Lowbury, E. J. L., Whyte, W., Blowers, R., Stanley, S. J., & Lowe, D. (1983). Airborne contamination of wounds in joint replacement operations: the relationship to sepsis rates. *Journal of Hospital Infection, 4(*2), 111-131.

Lidwell, O. M., Lowbury, E. J. L., Whyte, W., Blowers, R., Stanley, S. J., & Lowe, D. (1982). Effect of ultraclean air in operating rooms on deep sepsis in the joint after total hip or knee replacement: a randomised study. *British Medical Journal (Clinical Research Ed.), 285*(6334), 10-14.

Lipovsky, A., Nitzan, Y., Gedanken, A., Lubart, R. (2010).Visible light-induced killing of bacteria as a function of wavelength: implication for wound healing. *Lasers Surg Med, 42*(6):467-72.

Lipovsky, A., Nitzan, Y., Friedmann, H., & Lubart, R. (2009). Sensitivity of Staphylococcus aureus Strains to Broadband Visible Light. *Photochemistry and Photobiology, 85*(1), 255-260.

Locigno, R., Castronovo, V. (2001). Reduced glutathione system: role in cancer development, prevention and treatment (review). *Int J Oncol; 19*:221–236.

Loftus, R.W., Muffly, M.K., Brown, J.R., Beach, M.L., Koff, M.D., Corwin, H.L., Surgenor, S.D., Kirkland, K.B., Yeager, M.P. (2011). Hand contamination of anesthesia providers is an important risk factor for intraoperative bacterial transmission, *Anesth. Analg. 112*(1), 98–105.

Logoluso, N., Malizos, K., Blauth, M., Danita, A., Simon, K., Romanò, C.L. (2015). Anti-bacterial hydrogel coating of osteosynthesis implants. Early clinical results

from a multi-center prospective trial. *European Cells and Materials Vol. 30.* Suppl. 2, (page 35).

Logue, S.E., Martin, S.J. (2008). Caspase activation cascades in apoptosis. *Biochem Soc Trans*, *36*:1-9.

Lowell, J.D., Kundsin, R.B., Schwartz, C.M., Pozin, D. (1980). Ultraviolet radiation and reduction of deep wound infection following hip and knee arthroplasty. *Ann N Y Acad Sci.; 353*:285–93.

Lowry, O.H., Rosebrough, N.J., Farr, A.L., Randall, R.J. (1951). Protein measurement with the folin phenol reagent, *J. Biol. Chem. 193*(1), 265–275.

Lubart, R., Lipovski, A., Nitzan, Y., Friedmann, H. (2011). A possible mechanism for the bactericidal effect of visible light, *Laser Ther. 20*(1), 17–22.

Lynch, M.J., Raphael, S.S., Mellor, L.D., Spare, P.D. Inwood, M.J. (1969). Medical Laboratory Technology and Clinical Pathology, 2nd edition, WB Saunders Co., Philadelphia London Toronto LG Luna, Manual of Histologic Staining Methods of the Armed Forces Institute of Pathology, third edition, McGraw Hill.

Maclean, M., Macgregor, S.J., Anderson, J.G., Woolsey, G.A., Coia, J.E., Hamilton, K., Taggart, I., Watson, S.B., Thakker, B., Gettinby, G. (2010). Environmental decontamination of a hospital isolation room using high-intensity narrow-spectrum light. *J Hosp Infect.76*(3):247-51. doi: 10.1016/j.jhin.2010.07.010.

Maclean, M., MacGregor, S. J., Anderson, J. G., Woolsey, G. A. (2009). Inactivation of bacterial pathogens following exposure to light from a 405-nanometer light-emitting diode array. *Appl Environ Microbiol. 75* (7): 1932-1937.

Maclean, M., MacGregor, S.J., Anderson, J.G., Woolsey, G.A. (2008). The role of oxygen in the visible-light inactivation of Staphylococcus aureus. *J Photochem Photobio*; B. 92 (3), 180-184.

Maclean, M., McKenzie, K., Anderson, J. A., Gettinby, G., MacGregor, S. J. (2015). 405nm light technology for the inactivation of pathogens and its potential role for environmental disinfection and infection control. *J Hosp Infect. 88*(1):1-11.

Maclean, M., Murdoch, L. E., MacGregor, S. J., Anderson, J. G. (2013). Sporicidal effects of high intensity 405 nm visible light on endospore-forming bacteria. *Photochem Photobiol 89*:120-126.

Mahan, J., Selgison, D., Henry, S.L., Hynes, P., Dobbins, J. (1991). Factors in pin tract infections. *Orthopedics, 14*:305–8.

Majno, G., Joris, I. (1995). Apoptosis, oncosis, and necrosis. An overview of cell death. *Am J Pathol*; 146:3-15.

Maki, D.G., Tambyah, P.A. (2001). Engineering out the risk for infection with urinary catheters. *Emerg Infect Dis. 7*(2):342-7.

Malawer, M.M., Chou, L.B. (1995). Prosthetic survival and clinical results with use of large-segment replacements in the treatment of highgrade bone sarcomas. *J Bone Joint Surg Am. 77*: 1154–65.

Malik, Z., Lugaci, H. (1987). Destruction of erythroleukaemic cells by photoactivation of endogenous porphyrins. *British Journal of Cancer, 56*(5), 589-595.

Marin-Garcia, J. (2005). ROS Generation, Antioxidants, and Cell Death, in Mitochondria and the Heart. Developments in Cardiovascular Medicine, Vol. 256, pp. 99-122: Springer US.

Masse, A., Bruno, A., Bosetti, M., Biasibetti, A., Cannas, M., Gallinaro, P. (2000). Prevention of pin track infection in external fixation with silver coated pins: clinical and microbiological results. *J Biomed Mater Res; 53*:600–4.

McDonald, R., Macgregor, S.J., Anderson, J.G., Maclean, M., Grant, M.H. (2011). Effect of 405-nm high-intensity narrow-spectrum light on fibroblast-populated collagen lattices: an in vitro model of wound healing. *J Biomed Opt. 16*(4):048003.

McDonald, R. (2011). Effects of 405nm HINS-Light on Mammalian Cells and Potential Biomedical Disinfection Applications. Glasgow, Scotland, University of Strathclyde.

McDonald, R., Gupta, S., Maclean, M., Ramakrishnan, P., Anderson, J. G., MacGregor, S. J., Meek, R. M., Grant, M. H. (2013). 405 nm light exposure of osteoblasts and inactivation of bacterial isolates from arthroplasty patients: potential for new disinfection applications? *Eur. Cell Mater. 25*: 204–214.

McIlwain, D.R., Berger, T., Mak, T.W. (2013). Caspase functions in cell death and disease. *Cold Spring Harb Perspect Biol. 5*(4):a008656.

McIntyre, F.J., McCloy R. (1994). Shaving patients before surgery a dangerous myth? *Annals Royal College of Surgeons of England. 76*: 3-4.

McKenzie, K., Maclean, M., Timoshkin, I. V., MacGregor, S. J., Anderson, J. G. (2014). Enhanced 311 inactivation of Escherishia coli and Listeria monocytogenes by exposure to 405 nm light under sub lethal temperature, salt and acid stress conditions. *Int J Food Microbiol. 170*: 91-98.

Meddings, J., Rogers, M.A.M., Krein, S.L., Fakih, M.G., Olmsted, R.N., Saint, S. (2013). Reducing unnecessary urinary catheter use and other strategies to prevent catheter-associated urinary tract infection: an integrative review. *BMJ Qual Saf.* 23(4):277-89. doi: 10.1136/bmjqs-2012-001774. Epub 2013 Sep 27.

Meehan, J., Jamali, A.A., Nguyen, H. (2009). Prophylactic antibiotics in hip and knee arthroplasty. *J Bone Joint Surg Am; 91*:2480–2490.

Memarzadeh, F., Manning, A. (2002). Comparison of operating room ventilation systems in the protection of the surgical site. *ASHRAE Trans; 2*:3–15.

Meriga, B., Reddy, B. K., Rao, K. R., Reddy, L. A., Kishor, P. B. K. (2004). Aluminium-induced production of oxygen radicals, lipid peroxidation and DNA damage in seedlings of rice (Oryza sativa). *J Plant Physiol, 161*(1): 63–68.

Mishell, B.B., Shiiqi, S.M., Henry, C. (1980). Selected methods, in Cellular Immunology, Eds., pp. 21–22, Freeman, San Francisco, Calif, USA.

Misteli, H., Widmer, A.F., Rosenthal, R., Oertli, D., Marti, W.R., Weber, W.P. (2011). Spectrum of pathogens in surgical site infections at a Swiss university hospital. *Swiss Med Wkly;140*: w13146.

Mittler, R. (2002). Oxidative stress, antioxidants and stress tolerance. *Trends Plant Sci,7*(9), 405–410.

Moan, J., Iani, V., Ma, L. (1996). Choice of the proper wavelength for photochemotherapy. *Photochemotherapy: Photodynamic Therapy and Other Modalities*, Proceedings 2625, 544-549.

Montanaro, L., Speziale, P., Campoccia, D., Ravaioli, S., Cangini, I., Pietrocola, G., Giannini, S., Arciola,C.R. (2011). Scenery of Staphylococcus implant infections in orthopedics. *Future Microbiol; 6*(11):1329-49.

Montecinos, V., Guzman, P., Barra, V., Villagran, M., Munoz-Montesino, C., Sotomayor, K., Escobar, E., Godoy, A., Mardones, L., Sotomayor, P., Guzman,

C., Vasquez, O., Gallardo, V., van Zundert, B., Bono, M.R., Onate, S.A., Bustamante, M., Carcamo, J.G, Rivas, C.I., Vera, J.C. (2007). Vitamin C is an essential antioxidant that enhances survival of oxidatively stressed human vascular endothelial cells in the presence of a vast molar excess of glutathione. *J Biol Chem. 25; 282*(21):15506-15.

Murdoch, L.E., Maclean, M., Endarko, E., MacGregor, S.J., Anderson, J.G. (2012). Bactericidal Effects of 405 nm Light Exposure Demonstrated by Inactivation of Escherichia, Salmonella, Shigella, Listeria, and Mycobacterium Species in Liquid Suspensions and on Exposed Surfaces. *ScientificWorldJournal,* 137805.

Murdoch, L.E., McKenzie, K., Maclean, M., Macgregor, S.J., Anderson, J.G. (2013). Lethal effects of high-intensity violet 405-nm light on Saccharomyces cerevisiae, Candida albicans, and on dormant and germinating spores of Aspergillus niger. *Fungal Biol.; 117* (7-8):519-27. doi: 10.1016/ j.funbio. 2013.05.004. Epub 2013 May 30.

Murphy, R. C., Robson, M. C., Heggers, J. P., & Kadowaki, M. (1986). The effect of microbial contamination on musculocutaneous and random flaps. *Journal of Surgical Research, 41*(1), 75-80.

Nablo, B.J., Prichard, H.L., Butler, R.D., Klitzman, B., Schoenfisch, M.H. (2005). Inhibition of implant-associated infections via nitric oxide release. *Biomaterials; 26*(34):6984-90.

Nakanishi-Ueda, T., Majima, H.J., Watanabe, K., Ueda, T., Indo, H.P., Suenaga, S., Hisamitsu, T., Ozawa, T., Yasuhara, H., Koide, R. (2013). Blue LED light exposure develops intracellular reactive oxygen species, lipid peroxidation, and subsequent cellular injuries in cultured bovine retinal pigment epithelial cells. *Free Radic Res.; 47*(10):774-80.

Namdari, S., Voleti, P.B., Baldwin, K.D., Lee, G.C. (2011). Primary total joint arthroplasty performed in operating rooms following cases of known infection. *Orthopedics ; 34*:e541–e545.

Nitzan, Y., Ashkenazi, H. (1999). Photoinactivation of Deinococcus radiodurans: An Unusual Gram-Positive Microorganism. *Photochemistry and Photobiology, 69*(4): 505-510.

Nitzan, Y., Ashkenazi, H. (2001). Photoinactivation of Acinetobacter baumannii and Escherichia coli B by a cationic hydrophilic porphyrin at various light wavelengths. *Curr Microbiol. 42*(6):408-14.

Nitzan, Y., Salmon-Divon, M., Shporen, E., Malik, Z. (2004). ALA induced photodynamic effects on Gram positive and negative bacteria, *Photochem. Photobiol. Sci. 3*(5), 430–435.

Nitzan, Y., Kauffman, M. (1999). Endogenous porphyrin production in bacteria by δ-aminolaevulinic acid and subsequent bacterial photoeradication, *Lasers Med. Sci. 14*(4), 269–277.

Noctor, G., Foyer, C. H. (1998). Ascorbate and glutathione: keeping active oxygen under control. *Annu Rev Plant Physiol Mol Biol; 49*:249–279.

Nussbaum, E. L., Lilge, L., & Mazzulli, T. (2003). Effects of low-level laser therapy (LLLT) of 810 nm upon in vitro growth of bacteria: relevance of irradiance and radiant exposure. *Journal of Clinical Laser Medicine and Surgery, 21*(5), 283-290.

Oberhammer, F., Wilson, J.W., Dive, C., Morris, I.D., Hickman, J.A., Wakeling, A.E. (1993). Apoptotic death in epithelial cells: Cleavage of DNA to 300 and/or 50 kb fragments prior to or in the absence of internucleosomal fragmentation. *EMBO J; 12*:3679-84.

Oguma, K., Katayama, H., Mitani, H., Morita, S., Hirata, T., Ohgaki, S. K. (2001). Determination of pyrimidine dimmers in Escherichia coli and Cryptosporidium parvum during UV light inactivation, photoreactivation, and dark repair, *Appl. Environ. Microbiol. 67*(10), 4630–4637.

Olschlager, V., Schrader, A., & Hockertz, S. (2009). Comparison of primary human fibroblasts and keratinocytes with immortalized cell lines regarding their sensitivity to sodium dodecyl sulfate in a neutral red uptake cytotoxicity assay. *Arzneimittelforschung; 59*(3), 146-152.

Olsen, M.A., Nepple, J.J., Riew, K.D., Lenke, L.G., Bridwell, K.H., Mayfield, J., Fraser, V.J. (2008). Risk factors for surgical site infection following orthopaedic spinal operations. *J Bone Joint Surg Am.; 90*:62–9.

Otto, M. (2009). Staphylococcus epidermidis--the 'accidental' pathogen. *Nat Rev Microbiol. 7*(8):555-67.

Owens, C. D., Stoessel, K. (2008). Surgical site infections: epidemiology, microbiology and prevention. *J Hosp Infect.;70* (2): 3–10

Owers, K. L., James, E., & Bannister, G. C. (2004). Source of bacterial shedding in laminar flow theatres. *Journal of Hospital Infection*, *58*(3), 230-232.

Packer, L., Weber, S. U., Rimbach, G. (2001). Molecular aspects of α-tocotrienol antioxidant action and cell signalling. *J Nutr. 131*(2): 369S–73S.

Padayatty, S. J., Katz, A., Wang, Y., Eck, P., Kwon, O., Lee, J. H., Chen, S., Corpe, C., Dutta, A., Dutta, S. K., Levine, M. (2003). Vitamin C as an antioxidant: evaluation of its role in disease prevention. *J Am Coll Nutr. 22*(1):18-35.

Pan, C., Kumar, C., Bohl, S., Klingmueller, U., & Mann, M. (2009). Comparative Proteomic Phenotyping of Cell Lines and Primary Cells to Assess Preservation of Cell Type-specific Functions. *Molecular & Cellular Proteomics*, *8*(3), 443-450.

Pastuszka, J., Marchwinska-Wyrwal, E., & Wlazlo, A. (2005). Bacterial Aerosol in Silesian Hospitals: Preliminary Results. *Polish Journal of Environmental Studies*, *14*(6), 883-890.

Pattison, D. I., Davies, M. (2006). Actions of ultraviolet light on cellular structures, *EXS.* (96):131–157.

Perun, S., Tatchen, J., & Marian, C. M. (2008). Singlet and triplet excited states and intersystem crossing in free-base porphyrin: TDDFT and DFT/MRCI study. *ChemPhysChem (A European Journal of Chemical Physics and Physical Chemistry)*, *9*(2), 282-292.

Peter, H.P., Edward, S.R. (1984). Free Radicals And Disease In Man. *Physiological Chemistry and Physics and Medical NMR, 16*,175-195

Petrovsky, A., Schellenberger, E., Josephson, L., Weissleder, R., Bogdanov, A. Jr. (2003). Near-infrared fluorescent imaging of tumor apoptosis. *Cancer Res; 63*:1936-42.

Pflaum, M., Kielbassa, C., Garmyn, M., & Epe, B. (1998). Oxidative DNA damage induced by visible light in mammalian cells: extent, inhibition by antioxidants and genotoxic effects. *Mutation Research/DNA Repair*, *408*(2), 137-146.

Pittet, D., Hugonnet, S., Harbarth, S., Mourouga, P., Sauvan, V., Touveneau, S., Perneger,T.V. (2000). Effectiveness of a hospital-wide programme to improve compliance with hand hygiene. Infection Control Programme. *Lancet; 356*(9238):1307-12.

Plowman, R. (2000).The socioeconomic burden of hospital acquired infection. *Euro Surveill, 5*(4):49-50.

Plowman, R.P., Graves, N., Griffin, M., Roberts, J.A., Swan, A.V., Cookson, B.C. and Taylor, L. (1999). The Socioecomic Burden of Hospital Acquired Infection, Public Health Laboratory Service, London.

Plowman, R., Graves, N., Griffin, M.A.S., Roberts, J.A., Swan, A.V., Cookson, B., Taylor, L. (2001) The rate and cost of hospital-acquired infections occurring in patients admitted to selected specialties of a district general hospital in England and the national burden imposed. *The Journal of hospital infection, 47* (3). pp. 198-209.

Pompella, A., Visvikis, A., Paolicchi, A., Tata, V., Casini, A. F. (2003). The changing faces of glutathione, a cellular protagonist. *Biochem Pharmacol.66* (8): 1499–503.

Pulido, L., Ghanem, E., Joshi, A., Purtill, J.J., Parvizi, J. (2008). Periprosthetic joint infection: the incidence, timing, and predisposing factors. *Clin Orthop Relat Res;* 466:1710–1715.

Qudiesat, K., Abu-Elteen, K., Elkarmi, A., Hamad, M., Abussaud, M. (2009). Assessment of airborne pathogens in healthcare settings. *African Journal of Microbiology Research, 3*(2), 66-76.

Ramakrishnan, P., Maclean, M., MacGregor, S. J., Anderson, J. G., Grant, M. H. (2014). Differential sensitivity of osteoblasts and bacterial pathogens to 405-nm light highlighting potential for decontamination applications in orthopedic surgery. *J Biomed Opt, 19*(10): 105001.

Reilly, J., Stewart, S., Allardice, G., Noone, A., Robertson, C., Walker, A., Coubrough, S. (2007). NHS Scotland national HAI prevalence survey. Final Report 2007, Health Protection Scotland.

Ridgeway, S., Wilson, J., Charlet, A., Kafatos, G., Pearson, A., Coello, R. (2005). Infection of the surgical site after arthroplasty of the hip. *J Bone Joint Surg Br, 87*:844–50.

Riley, D.K., Classen, D.C., Stevens, L.E., Burke, J.P. (1995). A large randomised clinical trial of a silver-impregnated urinary catheter: lack of efficacy and staphylococcal superinfection. *Am J Med; 98*:349–56.

Rimington, C. (1960). Spectral-absorption coefficients of some porphyrins in the Soret-band region. *Biochemical Journal, 75*(3), 620-623.

Ritter, M.A., Olberding, E.M., Malinzak, R.A. (2007). Ultraviolet lighting during orthopaedic surgery and the rate of infection. *J Bone Joint Surg Am.; 89*(9):1935-40.

Rosenblatt, J., Raff, M. C., Cramer, L.P. (2001). An epithelial cell destined for apoptosis signals its neighbors to extrude it by an actin- and myosin-dependent mechanism. *Curr Biol*: 11(23):1847-57.

Sadrizadeh, S., Tammelin, A., Nielsen, P.V., Holmberg, S. (2014). Does a mobile laminar airflow screen reduce bacterial contamination in the operating room? A numerical study using computational fluid dynamics technique. *Patient Saf Surg; 8*: 27.

Salgame, P., Varadhachary, A.S., Primiano, L.L., Fincke, J.E., Muller, S., Monestier, M. (1997). An ELISA for detection of apoptosis. *Nucleic Acids Res.; 25*(3):680-1.

Schafer, F. Q., Buettner, G. R. (1999). Singlet Oxygen Toxicity Is Cell Line-dependent: A Study of Lipid Peroxidation in Nine Leukemia Cell Lines. *Photochemistry and Photobiology, 70*(6), 858-867.

Schimmel, M., Bauer, G. (2002). Proapoptotic and redox state-related signalling of reactive oxygen species generated by transformed fibroblasts. *Oncogene, 21*(38):5886-96.

Sculco, T.P. (1993). The economic impact of infected total joint arthroplasty. *Instr. Course Lect. 42*, 349–351.

Shah, K., Kumar, R. G., Verma, S., Dubey, R. S. (2001). Effect of cadmium on lipid peroxidation, superoxide anion generation and activities of antioxidant enzymes in growing rice seedlings. *Plant Sci. 161*(6):1135–1144.

Sharma, P., Dubey, R. S. (2005). Drought induces oxidative stress and enhances the activities of antioxidant enzymes in growing rice seedlings. *Plant Growth Regul. 46* (3):209–221.

Shiraishi, H., Okamoto, H., Yoshimura, A., Yoshida, H. (2006). ER stress induced apoptosis and caspase-12 activation occurs downstream of mitochondrial apoptosis involving Apaf-1. *J Cell Sci; 119*:3958- 66.

Sies, H. (1997). Oxidative stress: Oxidants and antioxidants. *Exp Physiol. 82* (2): 291–5.

Sigurdsson, V., Knulst, A.C., van Weelden, H. (1990). Phototherapy of acne vulgaris with visible light correlates with localized protoporphyrin IX fluorescence. *Am J Pathol; 136*:891–897.

Smith, M. D., Barbenel, J. C., Courtney, J. M., Grant, M. H. (1992). Novel quantitative methods for the determination of biomaterial cytotoxicity. *Internat. J. Artif. Org.15*:73-76.

Smith, S. (2009). Effect of novel electronic sterilisation methods on the components of hybrid collagen-based biomaterials. Glasgow, Scotland, University of Strathclyde.

Smith, S., Maclean, M., MacGregor, S.J., Anderson, J.G., Grant, M.H. (2009). Exposure of 3T3 mouse fibroblasts and collagen to high intensity blue light, in IFMBE Proc. 13th Int. Conf. on Biomedical Engineering, Vol. 23, pp. 1352–1355, Springer, Berlin Heidelberg.

Smyth, E.T., McIlvenny, G., Enstone, J.E., Emmerson, A.M., Humphreys, H., Fitzpatrick, F., Davies, E., Newcombe, R.G., Spencer, R.C. Hospital Infection Society Prevalence Survey Steering Group. (2008). Four country healthcare associated infection prevalence survey 2006: overview of the results. *J Hosp Infect*, *69*(3): 230-48.

Sondi, I., Goia, D.V., Matijević, E. (2003). Preparation of highly concentrated stable dispersions of uniform silver nanoparticles. *J Colloid Interface Sci. 260*(1):75-81.

Soukos, N.S., Som, S., Abernethy, A.D., Ruggiero, K., Dunham, J., Lee, C., Doukas, A.G., Goodson, J.M. (2005). Phototargeting oral black-pigmented bacteria. Antimicrob Agents Chemother. ; 49(4):1391-6.

Sternberg, E., Dolphin, D. (1998). Porphyrin-based photosensitizers for use in photodynamic therapy, *Tetrahedron 54*(17), 4151–4202.

Stokowski, L.A. (2006). Fundamentals of phototherapy for neonatal jaundice..*Adv Neonatal Care, 6* (6): 303–12.

Strausbaugh, L.J. (2001). Emerging health care-associated infections in the geriatric population. *Emerg Infect Dis, 7*(2):268-71.

Tanabe, S., Fujita, S., Yoshihara, S., Sakamoto, A., Yamamoto, S. (2005). YAG glass-ceramic phosphor for white LED (II): luminescence characteristics (PDF). Proc. Of SPIE. Fifth International Conference on Solid State Lighting 5941: 594112. doi: 10.1117/12.614681.

Tanaka, Y., Tran, P. O., Harmon, J., Robertson, R. P. (2002). A role for glutathione peroxidase in protecting pancreatic beta cells against oxidative stress in a model of glucose toxicity. *Proc Natl Acad Sci U S A. 99*(19):12363-8.

Taoufik, K., Mavrogonatou, E., Eliades, T., Papagiannoulis, L., Eliades, G., Kletsas, D. (2008). Effect of blue light on the proliferation of human gingival fibroblasts. *Dent Mater.24*(7):895-900.

Taylor, G.J.S., Bannister, G.C., Leeming, J.P. (1995). Wound disinfection with ultraviolet radiation, *J. Hosp. Infect. 30*(2), 85–93.

Tegos, G.P., Dai, T., Fuchs, B.B., Coleman, J.J., Prates, R.A., Astrakas, C., St. Denis, T.G., Ribeiro, M.S., Mylonakis, E., Hamblin, M.R. (2012). Concepts and Principles of Photodynamic Therapy as an Alternative Antifungal Discovery Platform. *Front Microbiol; 3*: 120.

Testa, M. P., Alvarado, O., Wournell, A., Lee, J., Guilford, F. T., Henriksen, S. H., Phillips, T. R. (2011). Screening assay for oxidative stress in a feline astrocyte cell line, G355-5. *J Vis Exp* (53): e2841.

Thomas, J. P., & Girotti, A. W. (1989). Role of Lipid Peroxidation in Hematoporphyrin Derivative-sensitized Photokilling of Tumor Cells: Protective Effects of Glutathione Peroxidase. *Cancer Research, 49*(7), 1682-1686.

Tkach, J.R., Shannon, A.M., Beastrom, R. (1979). Pseudofolliculitis due to pre-operative shaving. *AORN Journal. 30* (5): 881-884.

Tomb, R.M., Maclean, M., Herron, P.R., Hoskisson, P.A., MacGregor, S.J., Anderson, J.G.· (2014). Inactivation of Streptomyces phage ϕC31 by 405

nm light: Requirement for exogenous photosensitizers? *Bacteriophage.28*; 4:e32129.

Townsend, D. M., Tew, K. D., Tapiero, H. (2003). The importance of glutathione in human disease. *Biomed Pharmacother. 57*:145–155.

Trifunovic, A., Hansson, A., Wredenberg, A., Rovio, A. T., Dufour, E., Khvorostov, I., Spelbrink, J. N., Wibom, R., Jacobs, H. T., Larsson, N. G. (2005). Somatic mtDNA mutations cause aging phenotypes without affecting reactive oxygen species production. *Proc Natl Acad Sci U S A. 102*(50):17993-8.

Vermes, I., Haanen, C., Steffens-Nakken, H., Reutelingsperger, C. (1995). A novel assay for apoptosis. Flow cytometric detection of phosphatidylserine expression on early apoptotic cells using fluorescein labelled Annexin V. *J Immunol Methods. 184* (1):39-51.

von Eiff, C., Jansen, B., Kohnen, W., Becker, K. (2005). Infections associated with medical devices: pathogenesis, management and prophylaxis. *Drugs. 65*(2):179-214.

Walder, B., Pittet, D., Trame`r, M.R. (2002). Prevention of bloodstream infections with central venous catheters treated with antiinfective agents depends on catheter type and insertion time: evidence from a meta-analysis. *Infect Control Hosp Epidemiol; 23*:748–56. 16.

Wang, H., Cheng, M., Hu, J., Wang, C., Xu, S., Han, C.C. (2013). Preparation and optimization of silver nanoparticles embedded electrospun membrane for implant associated infections prevention. *ACS Appl Mater Interfaces; 5*(21):11014-21.

Wang, H. P., Qian, S. Y., Schafer, F. Q., Domann, F. E., Oberley, L. W., & Buettner, G. R. (2001). Phospholipid hydroperoxide glutathione peroxidase protects against singlet oxygen-induced cell damage of photodynamic therapy. *Free Radical Biology & Medicine*, *30*(8), 825-835.

Waugh, D. G., Lawrence, J. (2013). Laser surface treatment of a polymeric biomaterial: wettability characteristics and osteoblast cell response modulation, p 216, vol 1. Old city publishing, Philadelphia, PA.

Weinstein, R. A. (1998). Nosocomial infection update. *Emerging Infectious Diseases*, *4*(3), 416–419.

Wells, W.F., Fair, G.M. (1935).Viability of B. coli exposed to ultra-violet radiation in air. *Science; 82*(2125):280-1.

Whelan, H. T., Smits, R. L., Jr., Buchman, E. V., Whelan, N. T., Turner, S. G., Margolis, D. A., et al. (2001). Effect of NASA light-emitting diode irradiation on wound healing. *Journal of Clinical Laser Medicine and Surgery, 19*(6), 305-314.

Whyte, W., Hodgson, R., & Tinkler, J. (1982). The importance of airborne bacterial contamination of wounds. *Journal of Hospital Infection, 3*(2), 123-135.

Wijesekera, T. P., Dolphin, D. (1985). Some preparations and properties of porphyrins. *Advances in Experimental Medicine and Biology, 193*, 229-266.

Wilson, J. (2006). Preventing wound infection. In: Infection Control in Clinical Practice. 3rd ed. Bailliere Tindall Elsevier, London: 179-198.

Wilson, J., Charlett, A., Leong, G., McDougall, C., & Duckworth, G. (2008). Rates of surgical site infection after hip replacement as a hospital performance indicator: analysis of data from the English mandatory surveillance system. *Infection Control and Hospital Epidemiology, 29*(3), 219-226

Wilson, M. (2004). Lethal photosensitisation of oral bacteria and its potential application in the photodynamic therapy of oral infections. *Photochemical & Photobiological Sciences, 3*(5), 412-418.

Wong, K.C., Leung, K.S. (2004). Transmission and prevention of occupational infections in orthopaedic surgeons. *J Bone Joint Surg Am.; 86*-A(5):1065-76.

Wu, C.M., Cheng, Y.L., Dai, Y.H., Chen, M.F., Wang, C.C. (2014). α-Tocopherol protects keratinocytes against ultraviolet A irradiation by suppressing glutathione depletion, lipid peroxidation and reactive oxygen species generation. *Biomed Rep, 2*(3):419-423.

Wu, D., Yotnda, P. (2011). Production and Detection of Reactive Oxygen Species (ROS) in Cancers. *J Vis Exp,* (57): 3357.

Wulf Droge. (2002). Free Radicals in the Physiological Control of Cell Function. *Physiological Reviews, 82* (1): 47-95.

Zhang, J., Yan, H., Löfgren, S., Tian, X., Lou, M.F. (2012). Ultraviolet radiation-induced cataract in mice: the effect of age and the potential biochemical mechanism. *Invest Ophthalmol Vis Sci.; 53*(11):7276-85.

Zhang, Y., Zhu, Y., Gupta, A., Huang, Y., Murray, C.K., Vrahas, M.S., Sherwood, M.E., Baer, D.G, Hamblin, M.R., Dai, T. (2014). Antimicrobial Blue Light Therapy for Multidrug-Resistant Acinetobacter baumannii Infection in a Mouse Burn Model: Implications for Prophylaxis and Treatment of Combat-related Wound Infections. *J Infect Dis; 209*(12): 1963–1971.

Zhao, F., Narendran, N., Van Derlofske, J.F. (2002). Optical elements for mixing colored LEDs to create white light. SPIE Proceedings 4776: 207-214.

Ziegler, U., Groscurth, P. (2004). Morphological features of cell death. *News Physiol Sci;19*:124-8.

Zou, H., Henzel, W. J., Liu, X., Lutschg, A., Wang, X. (1997). Apaf-1, a human protein homologous to C. elegans CED-4, participates in cytochrome c-dependent activation of caspase 3. *Cell, 90*: 405–413

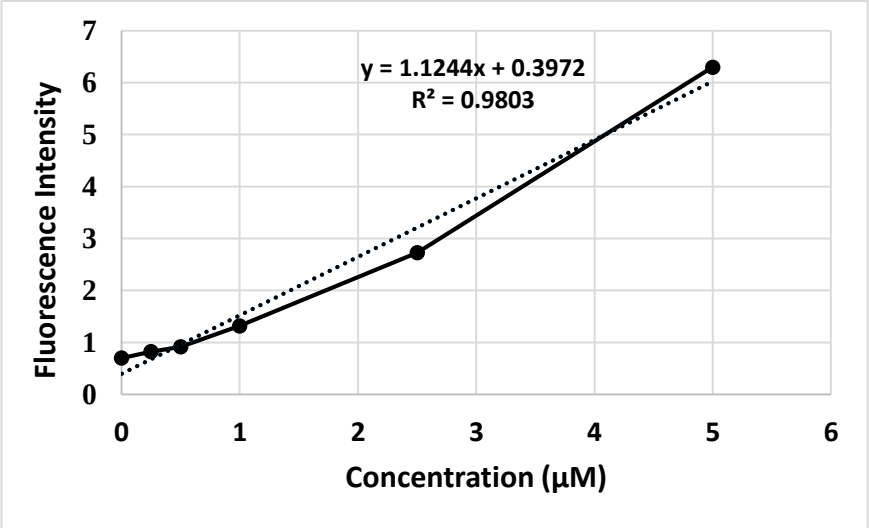

Fig.A.1: GSH standard curve.

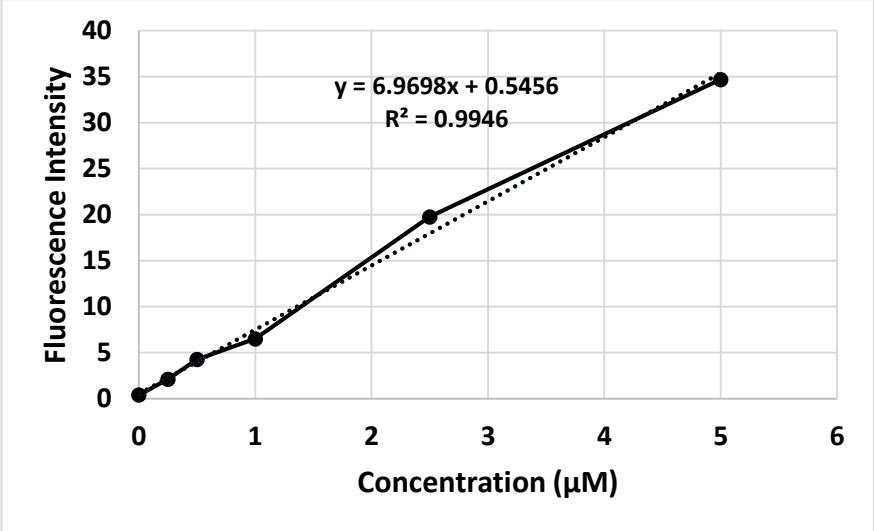

Fig.A.2: GSSG standard curve.

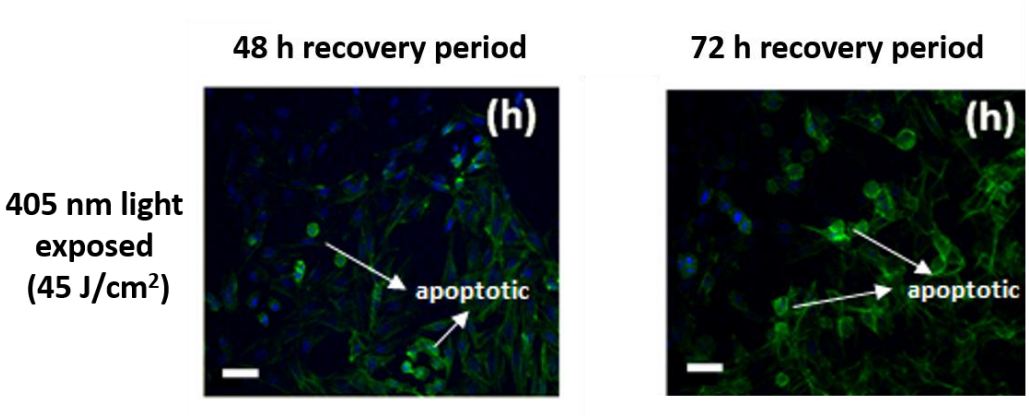

Fig.A.3: Enlarged images of actin rings formed in samples exposed to 405 nm light at 45 J/cm^2 following a 48 h and 72 h recovery period. Scale bars are 40 μm.